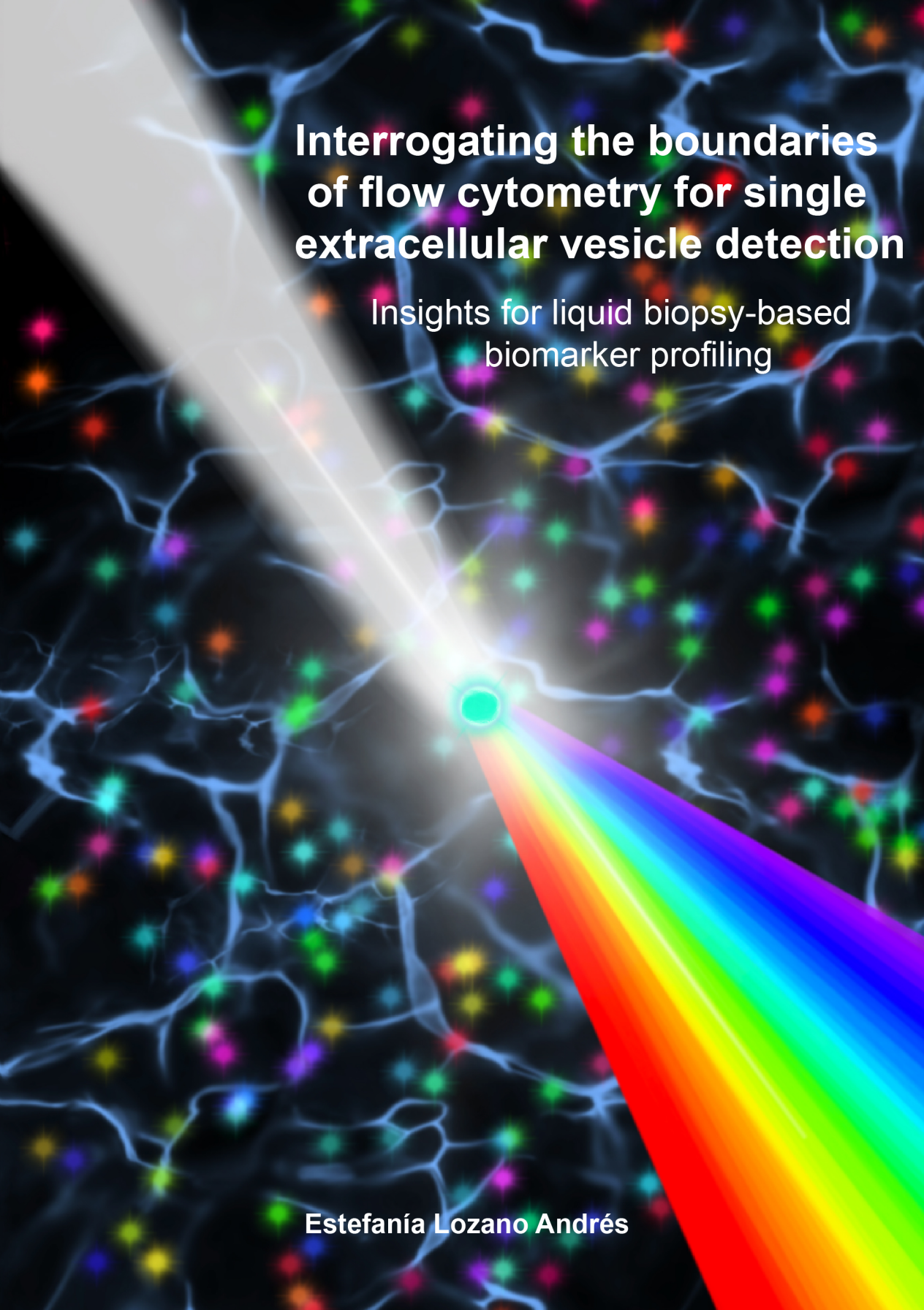

Interrogating the boundaries of flow cytometry for single extracellular vesicle detection

Insights for liquid biopsy-based biomarker profiling

Estefanía Lozano Andrés

Interrogating the boundaries of flow cytometry for single extracellular vesicle detection:

Insights for liquid biopsy-based biomarker profiling

Estefanía Lozano Andrés

Colofon
ISBN: 978-94-6483-157-3
DOI: https://doi.org/10.33540/705

Cover and interior chapter designs © 2023 Cristina Lozano Andrés
Printing: thesis specialist ridderprint.nl
Lay-out & design: Robin Weijland, persoonlijkproefschrift.nl

Printing of this thesis was financially supported by Infection & Immunity Utrecht and by the Department of Biomolecular Health Sciences, Faculty of Veterinary Medicine, Utrecht University.

Interrogating the boundaries of flow cytometry for single extracellular vesicle detection:

Insights for liquid biopsy–based biomarker profiling

Onderzoek naar de grenzen van flow cytometrie voor de detectie van individuele extracellulaire blaasjes:

Inzichten voor biomarkerprofilering in vloeibare biopsieën

(met een samenvatting in het Nederlands)

Proefschrift

ter verkrijging van de graad van doctor aan de
Universiteit Utrecht
op gezag van de
rector magnificus, prof.dr. H.R.B.M. Kummeling,
ingevolge het besluit van het college voor promoties
in het openbaar te verdedigen op dinsdag 30 mei 2023 des ochtends te 10.15 uur

door

Estefanía Lozano Andrés

geboren op 12 juni 1991
te Guadalajara, Spanje

Promotor:
Prof. dr. M.H.M. Wauben

Copromotor:
Dr. G.J.A. Arkesteijn

Beoordelingscommissie:
Prof. dr. E. I. Buzas
Prof. dr. G.W. Jenster
Dr. R. Nieuwland
Prof. dr. R.M. Schiffelers
Prof. dr. M.A. Tryfonidou

This research was supported by the European Union's Horizon 2020 research and innovation programme under the Marie Skłodowska-Curie grant agreement No. 722148 (TRAIN-EV).

“What would life be if we had no courage to attempt anything? ”

Vincent van Gogh

TABLE OF CONTENTS

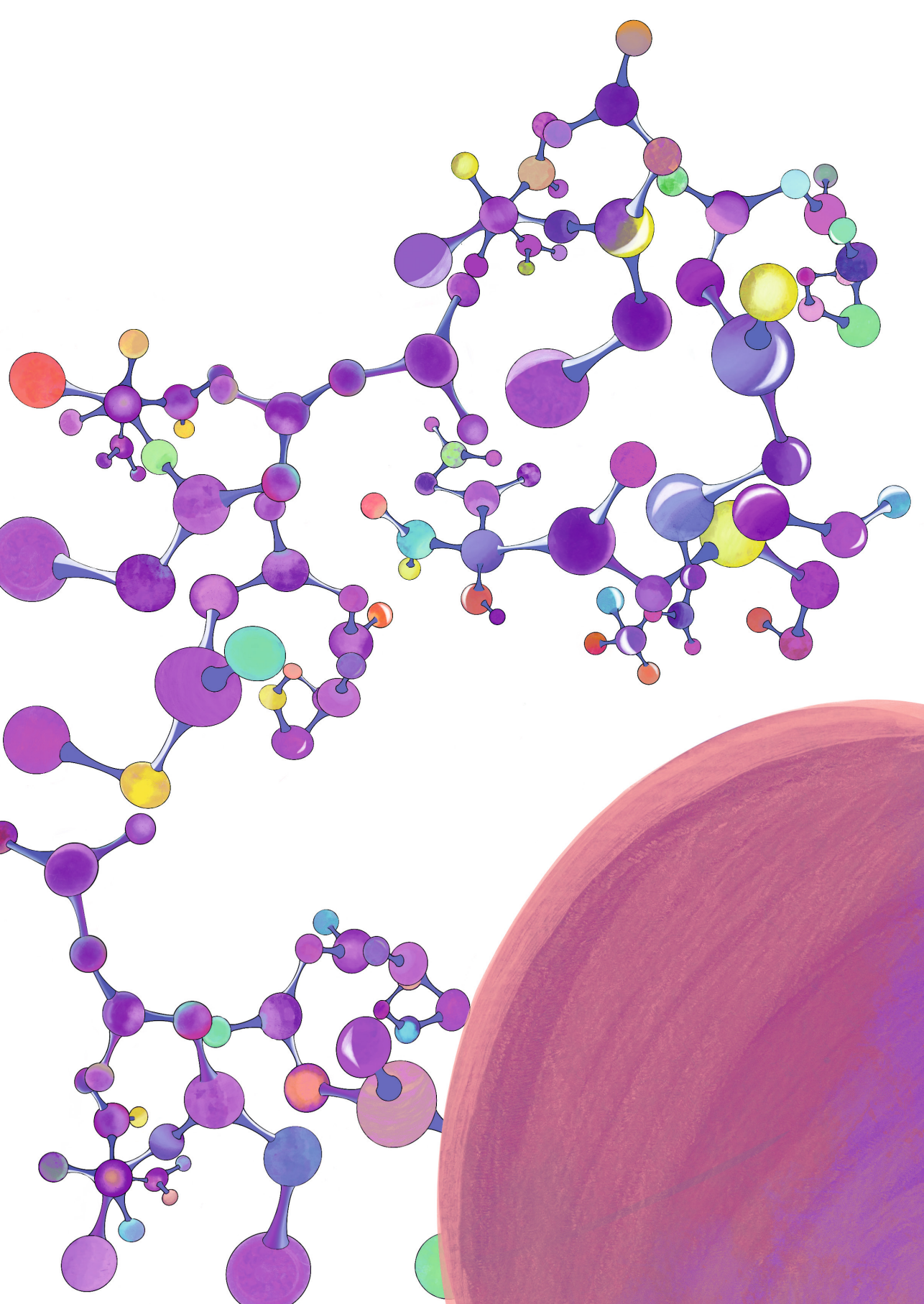

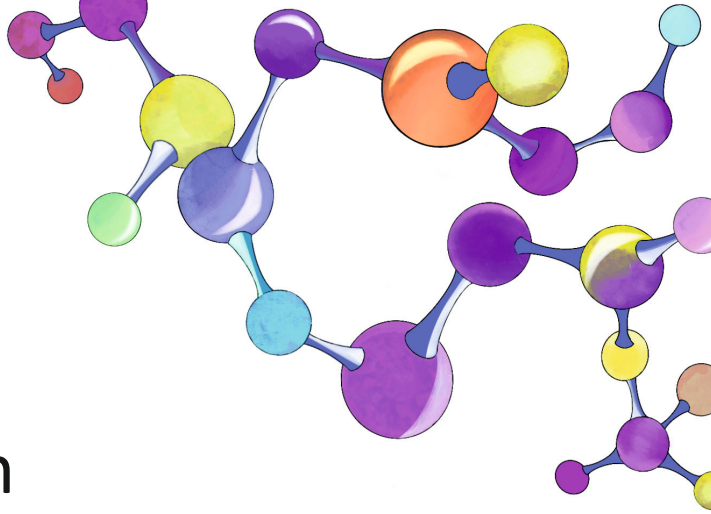

CHAPTER 1

Introduction

Estefanía Lozano-Andrés[1]
Division of Cell Biology, Metabolism & Cancer, Department of Biomolecular Health Sciences, Faculty of Veterinary Medicine, Utrecht University, Utrecht, The Netherlands

Part of section 1.5 is adapted from:
Welsh J. et al., (2023). A compendium of single extracellular vesicle flow cytometry. Journal of Extracellular Vesicles, 12, e12299.
https://doi.org/10.1002/jev2.12299

1.1. THESIS MOTIVATION

Emerging landscape: In recent years, extracellular vesicles (EVs) have attracted the attention of scientists from many different biological fields. EVs are lipid enclosed vesicles released by cells that contain biomolecular cargo from the cell of origin. The role of EVs as multicomponent messengers during intercellular communication is recognized in several cellular processes such as immune modulation, cell survival, metastatic processes and proliferation [1, 2]. Therefore, the detection and characterization of these released biological vesicles is a fundamental step towards the understanding of physiological and pathological processes.

Challenges in EV research: The investigation of EVs is complicated due to their small size, heterogeneity and complexity, which resulted in a plethora of isolation and detection methods [3]. Consequently, concerns about the reproducibility have been raised, encouraging transparency and comprehensive reporting in the EV field [4, 5]. To address these concerns, efforts have been initiated to establish guidelines, reference materials and reporting frameworks that will fuel robustness in EV research [6-11]. At the same time, the EV community is looking for technological solutions for the detection of single EVs. Such technologies would ideally be high-throughput while providing quantitative and qualitative information. Flow cytometry (FCM) was originally designed for cells, whose signals are well above the detection limit of flow cytometric instruments, in sharp contrast to the dim signals of EVs. Despite this limitation, FCM is a promising technology and currently one of the methods of choice for EV characterization [12, 13]. EVs, however, are orders of magnitude smaller than cells and their signals are often below or close to the detection limit of the instruments, which causes a number of limitations and challenges that need to be accounted for [14].

Tackling the challenges: To address the lack of reproducibility in the EV field and to advance the use of FCM towards the exploitation of EVs for biomedical applications, I present in this PhD thesis a sequence of chapters that cover: (1) the development and characterization of EV reference materials, (2) the development of a reporting framework for flow cytometric EV analysis, (3) the evaluation of the legitimacy for the use of fluorescence calibration materials in EV research, (4) the reduction of optical background signals to improve flow cytometric EV analysis and (5) the description of interactions between EVs and other particles present in biofluids that impact single EV analysis. The work presented in this thesis follows the current guidelines of reporting and applies advanced technologies for EV analysis. Overall this work contributes to the standardization of EV measurements and reporting of EV analysis and shed light on the complexity of single EV analysis in biofluids, which will ultimately contribute to a successful clinical translation.

1.2. EXTRACELLULAR VESICLES

1.2.1. A brief history of extracellular vesicles

One of the first scientific reports of EVs dates back in the 1940s, when Chargaff & West subjected plasma samples to centrifugation and observed a particulate fraction with thromboplastic properties [15]. Twenty years after this publication, another research study lead by Wolf reported sub-micrometer structures being released from activated platelets. These released small vesicles (20-50 nm) that were shed from the plasma membrane were named 'platelet-dust' [16]. In the early 1970s, landmark studies by Anderson and Bonucci identified heterogeneous membranous vesicles embedded in the cartilage matrix with a defined function related to bone mineralization [17-19]. Along the same time, Aaronson et al. referred to these released membranous vesicles as 'extracellular vesicles' [20]. Significant discoveries followed and took place in the 1980s, when Pan & Johnstone and Stahl were working on plasma membrane biochemistry and membrane trafficking. Their work referred to 'exosomes' as small EVs (30-100 nm) of endosomal origin derived from multivesicular bodies (MVB) that were released in the extracellular environment upon fusion of the MVB with the cell plasma membrane [21, 22].

Several seminal findings followed, where EV functions began to unfold [23]. An important study in this period showed that B cells release exosomes bearing molecules from the major histocompatibility complex class II (MHC-II), suggesting a role in the induction of antigen-specific immune responses [24]. Besides a role of EVs in intercellular communication processes, EVs also play a role as 'waste bin' to dispose obsolete cell products in order to keep cellular homeostasis [25]. Altogether, in the late 1990s EV research gained momentum with several studies that unveiled a multitude of biological roles for EVs during blood coagulation, inflammation and cell survival and proliferation [26-28].

Ever since the first observations, EVs have attracted the attention from scientists working in all biological fields. The exploitation of EVs for biomedical applications has an enormous potential, including their putative benefit as disease biomarkers [29, 30] and their prospective administration to elicit a protective immune response against cancer [31, 32], which advanced into phase I clinical trials [33]. In addition, the growing interest in EVs is stimulating the development of EV-tailored technology [3]. However, this accelerating growth rhythm gave rise to a body of literature that partially shows controversial communications [23]. Thus, awareness about robustness and reproducibility, dissemination of good practices and educative tools have become priorities to advance the field into a good direction.

1.2.2. Extracellular vesicles, heterogeneity and current nomenclature

The current definition of EVs refers to lipid membrane bilayer enclosed vesicles that are released by cells [6]. Thus, EVs can contain biological information from the cell of origin, i.e. lipids, nucleic acids, proteins and metabolites (figure 1). Historically, EVs have received

a variety of names depending on the cell of origin (e.g. prostasomes from prostate cells, oncosomes from tumor cells, etc.) or the biogenesis route (e.g. exosomes when derived from MVB or ectosomes or microvesicles when released via direct budding from the plasma membrane of eukaryotic cells, or outer membrane vesicles (OMV) when derived from the outer membrane of gram-negative bacteria) [1, 34]. Hence, the diversity in nomenclature can be partially explained due to fact that 1) vesiculation is evolutionary conserved and observed in a wide variety of different cell types and organisms and 2) different biogenesis routes for EVs have been described [1, 34].

Biogenesis processes of EVs have been studied and described extensively in reviews [2, 34-36]. As shown in figure 1, for eukaryotic cells often roughly three different routes are indicated, i.e. the fusion of multivesicular bodies (MVB) with the plasma membrane at the end of the endocytic recycling pathway (exosomes), the direct budding from the plasma membrane (ectosomes or microvesicles) and the formation of apoptotic bodies via membrane blebbing [1, 34, 37]. The endosomal sorting complex required for transport (ESCRT) machinery is key for the formation of EVs within the MVB but other ESCRT-independent mechanisms and intracellular processes (e.g. autophagy) have also been identified [34, 35]. In addition, the intersection of different pathways can result in EV release but how this takes place is less understood.

Intrinsic EV features such as size ,buoyant density or expression of a protein are often used in literature to describe the EV types. EV size distribution typically ranges from 30 nm up to 1 mm in diameter [37], while buoyant density has been reported to be in the range of 1.13 to 1.19 g ml^{-1} for the majority of EVs when subjected to a sucrose gradient [3, 24]. Furthermore, EVs can be described by the expression of certain markers, such as tetraspanins CD9, CD63 and CD81, but not all EV subpopulations express the same markers [36, 38].

Since EVs are highly heterogeneous in origin, function, composition and size, their classification is still evolving [1]. The International Society for Extracellular Vesicles (ISEV), encourages the term EVs as a catchall term, which might be accompanied by other characteristics, such as size range. A sharpened EV nomenclature is expected to arise as knowledge is built upon EV biology and the clear description of EV subpopulations based on unique markers and intrinsic features will progress [39, 40]. In the meantime, it is important to create awareness of these challenges and to draft guidelines and recommendations for robust and reproducible EV research [7, 39].

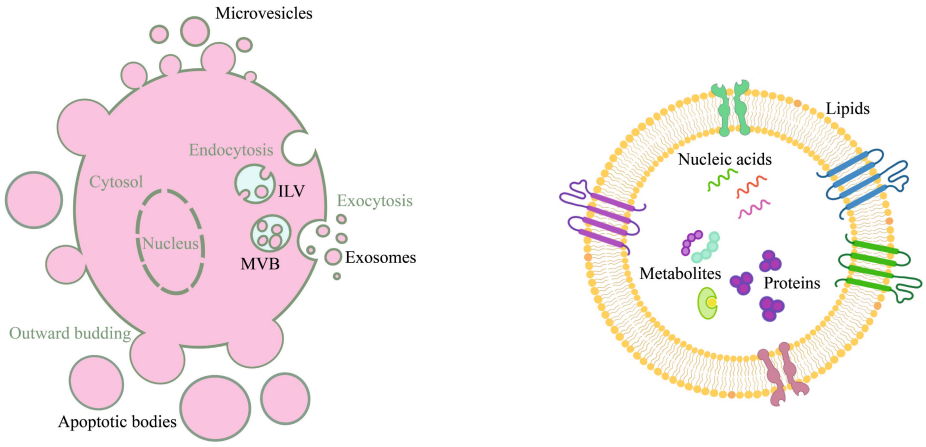

Figure 1. Schematic representation of EV biogenesis, heterogeneity and composition. Eukaryotic cell releasing different types of EVs via outward budding of the plasma membrane(i.e., ectosomes or microvesicles and apoptotic bodies) or via fusion of MVB with the plasma membrane resulting in the release of intraluminal vesicles (ILV), so-called exosomes (left). Content of an EV composed of nucleic acids, proteins, lipids, metabolites, the delimiting lipid membrane and inner compartment with cargo are shown (right).

1.2.3. Isolation methods for extracellular vesicles

The tailored composition of EVs released in the extracellular space during health and disease processes together with cell type specific signatures opened new possibilities for their clinical translation as disease biomarkers [41, 42]. For the analysis of EVs in the circulation, EVs need to be isolated from complex biofluids. The EV enrichment or isolation strategy of choice is a critical aspect for any EV related study, since it directly affects the obtained EV subset(s) in the preparation and the co-isolated factors. Widely used techniques that effectively separate EVs from other colloidal components present in body fluids or tissue culture supernatant are based on combined biochemical and biophysical properties of EVs [1, 3, 43]. Albeit isolation by differential ultracentrifugation (UC) has been a 'gold standard' method in the field [44, 45], concerns about reproducibility, aggregation, purity and integrity have been raised [46, 47]. Other available methods are based on ultrafiltration [48], immune-affinity [49], precipitation [50], size exclusion chromatography (SEC) [51, 52] and density gradient centrifugation (DGC) [49]. Therefore, several methods have been used to obtain EV preparations from different sources [3, 13, 45] but no stand-alone isolation method is perfect. Rather, a combination of methods has been useful to obtain EV preparations with higher purity, especially when working with complex biofluids such as plasma [47, 53, 54]. In addition, comparison studies assessing the obtained EV preparations show that the isolation method has an impact on the quality of EV samples [55]. Newer developments are also arising, including promising methods such as asymmetric flow field fractionation (AF4) and the use of microfluidic chips [56, 57].

Importantly, the unique and complex composition of different biofluids in which EVs reside, poses additional and biofluid-specific challenges for EV isolation that must be acknowledge [8, 58]. Blood plasma is one of the most used body fluids for EV analysis, but it requires careful handling because a number of pre-clinical variables have been identified as a source of discrepancy [3, 58, 59]. Besides EVs, plasma also contains high numbers of protein complexes (i.e. albumin, fibrinogen) and lipoprotein particles (LPPs). LPPs have partially overlapping biophysical properties with EVs, such as size and density and outnumber EVs in order of magnitudes. Isolation methods solely based on size or density separation result in the co-isolation of EVs and LPPs [47, 60]. Efforts to find alternatives that can increase the purity of EV preparations have resulted in the combination of isolation methods based on size and density [53]. The drawback is that some EV subpopulations might be lost and heterogeneity be compromised, as elaborate isolation and purification strategies select for certain EV subpopulations.

Overall, the selection of a certain isolation method requires careful consideration due to the high impact it will have on the downstream application [3, 4]. Finding the right balance between purity, integrity and yield is a key aspect, next to the understanding that certain isolation methods might induce biases in the isolation of EVs by selecting for certain subpopulations or might compromise certain downstream applications.

1.2.4. Emerging scenery of EV biomarkers

The field of liquid biopsy (LB) refers to the use of body fluids as specimen for diagnosis rather than a fragment of tissue. EVs released into the cell environment have been detected in the surrounding tissue and body fluids (i.e. blood, urine, etc.). Thus, the easy access to certain body fluids, enormously increased the interest in EVs to be used as LB biomarkers [41, 61]. Analysis of circulating EVs in blood from healthy and diseased subjects, showed examples in which the overall EV concentration in blood was increased in the disease state, e.g. in cancer and thrombosis [62, 63]. Moreover, qualitative EV-analysis based on the presence of certain tumor markers and specific subpopulations of plasma EVs has been shown to aid in the prognosis of gastric cancer patients [63]. Among the benefits of exploiting LB for EV-biomarker analysis are: minimally invasive, early detection of disease and the ease to monitor real-time treatment response [42]. In addition, LB EVs can facilitate the diagnosis of diseases for which clinical assessment is difficult or even lacking, such as pediatric solid tumors [64].

1.3. REPRODUCIBILITY AND ROBUSTNESS IN EV RESEARCH

1.3.1. About guidelines, reporting and transparency

The rapid expansion of the EV field in the last years has been accompanied by a general and growing realization of the challenges that the field is still facing, with raised concerns about reproducibility [4, 65]. ISEV has made great efforts to publish guidelines and position papers that aim to improve reproducibility, robustness and standardiza-

tion. Firstly, guidelines for the minimal information for studies of extracellular vesicles (MISEV) were initially developed in 2014 and are still being regularly updated [6-8]. Secondly, an important step towards reproducibility entails adequate reporting and transparency. To this end, the EV-TRACK knowledge-base was generated [11]. The realization of the high number of unique EV isolation protocols reported in literature and their impact on downstream analysis [4] motivated and re-enforced the implementation of EV-TRACK, as recommended by ISEV [8]. As the field evolves, future updates are also expected to be added [66] and tailored guidelines for specific EV samples, applications and technology are in progress, e.g. urine derived EVs or plant derived EVs [64, 67, 68].

1.3.2. Reference materials in the making

Tailored reference materials (RM) are an important element to improve reproducibility and robustness in the EV field [65]. A RM can be defined as any material with consistent and stable properties that have been characterized for a validated measurement procedure [69].

RM can provide precision and/or trueness, being two components of the accuracy for a given measurement. Thus, an ideal RM will provide a high precision that is low random error, and a high trueness or low systematic error [9]. In fact, RM can fit into different categories as they can serve different purposes. For example, a RM for calibration will require a higher level of characterization, while a RM for quality control or to track instrument performance might allow a more broad uncertainty range [9]. Additional valuable properties for RM are (i) commutability, that is the ability of a reference to behave as the unknown sample, and (ii) quality assurance, which assesses the comparability and validation of a RM [69]. In addition, traceability is desired, as it ensures that a certain measurement result can be related to a reference that has been well documented. To achieve a certain recognized status (i.e. traceable), metrology institutions such as the National Institute of Standards and Technology (NIST) are often involved in both production and measurement procedure development [65, 70].

Only in the last five years a few studies aiming to develop RM for EV research have been published [71, 72]. Yet, the heterogeneity and diversity of EVs possess significant challenges towards a ‘one size fits all’ RM for EVs. Rather than that, a ‘fit for purpose’ strategy is most likely to be successful, as dedicated RM are developed and validated for different EV types and selected downstream applications [73, 74].

1.3.3. Approaching standardization

While RM are definitely useful for several applications, the standardization of measurements is the ultimate goal towards reproducibility of results. Standardization allows to express the measurement result in standards units rather than arbitrary or relative units that cannot be compared across instruments and laboratories. Thus, it is a process that compares the relationship between a certain measurement and the assigned

measurement standards [75]. It is important to realize that because no measurement is ever perfect, a given standard will always have an uncertainty value next to the assigned standardized value [70]. The characterization of the level of uncertainty and the definition of an acceptable uncertainty range is therefore essential to generate consensus on calibration methods and the recognition of useful materials [76]. Note that a certain calibrated RM might not simultaneously provide both trueness and precision. But when high trueness is not available due to technical limitations or unknown values, a high precision can still be useful for the harmonization of results. Harmonization is a first step towards standardization. Thus, albeit the ideal scenario is striving for standardization, if that is not possible, harmonizing results across instruments and laboratories is very useful [70, 77]. Furthermore, it is important to acknowledge that each calibration method has its limitations. Since harmonized results might not align with the true values, data should not be interpreted as absolute to avoid misinterpretations and future inconsistencies [75]. Consensus and advice on good quality RM and calibration methods needs to be taken as a first step towards harmonization and standardization of results.

1.4. METHODOLOGIES TO DETECT AND CHARACTERIZE EVS

1.4.1. Current methods for EV characterization

A variety of methods is currently used to analyze EVs, which can be categorized into bulk-based or single particle-based methods. Bulk-based methods provide average population phenotyping and can assess biochemical characteristics of the EVs present in a preparation. Commonly used methods such as immunoblotting and enzyme-linked immunosorbent assay (ELISA) make use of specific antibodies against the protein of interest for detection [13, 45, 78]. While the average presence of markers will continue to be useful, bulk-based methods cannot discern between EV subsets within the bulk, give no information on the distribution of the marker of interest per EV, and cannot provide a reliable particle count, which are all parameters desired for EV biomarker profiling. Furthermore, bulk-based analysis often requires a large amount of input material, which can become a hurdle when working with patient samples.

Single particle-based analysis methods are therefore, as they allow to unveil EV heterogeneity by differentiating between EV (sub)populations [3]. Single particle-based methods for biomarker profiling would ideally provide both quantitative and qualitative information, while being high-throughput. Technical knowledge is often required, as EVs tend to be at the detection limit. While the unknown and/or non-reported technical specifications make results difficult to compare across instruments and laboratories and standardized protocols and recommendations for each method are underdeveloped, a positive shift happened in the last five years [5, 11, 13].

Peer-reviewed publications providing further details about working principles and the classification of the different methods are available in literature [3, 8]. Single particle methods that are commonly used can be divided into non-optical and optical technologies. These include electron microscopy (EM), atomic force microscopy (AFM), tunable resistive pulse sensing (TRPS), nanoparticle tracking analysis (NTA), super-resolution microscopy (SRM), Optically trapped-Raman spectroscopy (OT-RS) and flow cytometry (FCM). A comparison of qualitative and quantitative capabilities is shown in Table 1.

		Quantitative		Qualitative	
		Concentration determination	High-throughput measurements	Heterogeneity, size distribution	Multiple phenotyping
NON-OPTICAL	EM	+	-	+	-
	AFM	-	-	+	-
	TRPS	+	+	+	-
OTPICAL	NTA	+	+	+	-
	SRM	+	-	+	+
	OT-RS	-	-	-	+
	FCM	+	+	+	+

Table 1. Evaluation of quantitative and qualitative capabilities of detection methods for the analysis of EVs. Plotted on the top row are the desired characteristics and on the left column the evaluated equipment, a '+' symbol was used when the characteristic is matched and a '–' symbol was used for limited and/or absent capability.

1.4.2. Non-optical technologies

Electron microscopy (EM). First used in 1930 for the first observations of EVs [79]. Advances in recent years allowed the detection and characterization of single EVs, providing size distribution and morphology information with a resolution down to 2 nm for biological structures [80]. In addition, immunolabelling by using gold nanoparticles conjugated to antibodies provides phenotypic information to decipher EV composition, which has made significant contributions to the field over the years [16, 21, 44]. Weaknesses are lengthy sample preparation, the need of expensive equipment, limited high-throughput and the fact that phenotyping of multiple markers simultaneously is cumbersome. Also, artifacts can be introduced during sample preparation, affecting concentration measurements. Protocols that address some of these challenges are available [81] and newer adaptations such as cryogenic EM (cryo-EM) can offer insights into the native structure of EVs [79].

Atomic force microscopy (AFM). Provides size and shape information by imaging EVs with a high resolution scanning probe. Samples are added to a coverslip that is placed inside the AFM chamber for the acquisition of the deflection of the cantilever with a laser and photodiode. Through imaging, the mechanical properties from the analyzed particles are obtained and their topography can be reconstructed [82]. AFM has been proved useful to provide insights on the mechanical properties of EVs, which have also been shown to be altered during disease [83]. Weaknesses are the sample attachment to the coverslip, lengthy measurements with relatively low-throughput and limited multiple phenotyping [84]. Standardized procedures are starting to become available for the community [84].

Tunable resistive pulse sensing (TRPS). Determines the diameter of particles in a solution from 50 nm up to 10 mm when they pass through a non-conductive membrane [85]. When particles are passing through the fixed sized pore an electric current is applied and a signal relatively proportional to the particle volume is generated. Weaknesses are that for robust measurements of heterogeneous samples, different pore sizes need to be applied, which can reduce the reproducibility and induce pore clogging. These factors can limit the sample throughput, which is expected to be worsened when other non-EV particles are also present in the sample [86]. Also, phenotypic information is very limited. Nevertheless, newer adaptations and standardized protocols of this technology are being developed. An example is microfluidic resistive pulse sensing (MRPS), which uses disposable microfluidic cartridges and pre-calibrated pores to provide more reproducible particle size distribution and concentration data [87] but further research is needed to validate the precision and accuracy of this technology on EV samples.

1.4.3. Optical technologies

Nanoparticle tracking analysis (NTA). Allows to measure the light scattering and size distribution of individual particles according to their Brownian motion. After laser illumination, the random motion generated by the particles is collected through a microscope objective and detected by a camera [88]. The diameter of the particles, usually ranging from 50 nm up to 1 mm is then calculated with the Stokes-Einstein equation, which includes a known temperature and viscosity of the suspension [89]. The particle count is also determined to provide a particle concentration. Weaknesses include the limited resolution to represent heterogeneous populations, high input yield and high variability [90]. Recent standardized procedures aim to address some of the concerns about reproducibility [88].

Super-resolution microscopy (SRM). While traditional optical microscopy has enormously contributed to the understanding of biology, its resolution for single EV detection is limited in the nanometric scale due to aberration and diffraction [91]. Newer promising adaptations include stochastic optical reconstructive microscopy (STORM), stimulated emission depletion microscopy (STED) and single-molecule localization mi-

croscopy (SMLM) [91, 92], which can provide multiple phenotyping and co-localization data [93]. Weaknesses include sample preparation time, high cost of the equipment and relatively low throughput. The use of high-speed imaging can be useful [94, 95] but the road for the implementation of this technology to detect EVs still needs to be built and standardized.

Optical trapping-Raman Spectroscopy (OT-RS). By using optical tweezers, particles can be trapped in a focal spot and resolution improved, making it possible to perform single EV analysis [96-98] and provide information on the molecular composition and the structure of biological particles by means of inelastic light-scattering. The particles are illuminated by a monochromatic laser, which induces a change in the detected scattered light. These vibrations and scattering changes are molecule-specific. Consequently each biomolecule can be identified by its own Raman spectra [97]. The combination of OT-RS with Rayleigh scattering comprises a promising tool to unravel the composition of EVs [96]. This label-free method allows quantification although its throughput is limited as time measurements are usually lengthy.

Flow cytometry (FCM). Developed to detect and separate cells in the 1970s [99] [100], which became possible because of the break throughs made in: the use of dyes for the staining of cell components in the 1860s [101], the development of a cell counter in 1930s [102], fluorescently conjugated antibodies [103], a method for counting particles [104] and the conceptualization of hydrodynamic focusing [105]. Since then, the technology evolved to what we know today as conventional FCM (cFCM) which is composed of three integral systems: fluidics, optics and electronics. When a cell or particle in suspension meets the illuminating beam in the 'interrogation spot', light scattering originates into different directions. Forward scatter (FSC) and side scatter (SSC, 90° degree from the laser source) signals, as well as emitted fluorescence signals, are then collected by detectors, processed in the electronics to be finally displayed in the computer (Figure 2). Light scattering signals from FSC and SSC are often used to inquire cell size and complexity, respectively. But this approach is not an universal rule, but rather the result of oversimplified assumptions that not always hold truth [14, 106]. FCM has certainly been fundamental to our current understanding of cell biology and immunology by providing multiparameter phenotypic information used to decipher biological heterogeneity and characterize cell subsets [106]. While the technology effectively has evolved, the lack of sensitivity of cFCM is a major hurdle for single EV detection. However, efforts made to push the limits of detection resulted in the development of high-sensitivity FCM (hFCM). Because hFCM is an essential element of this PhD thesis, a dedicated section follows.

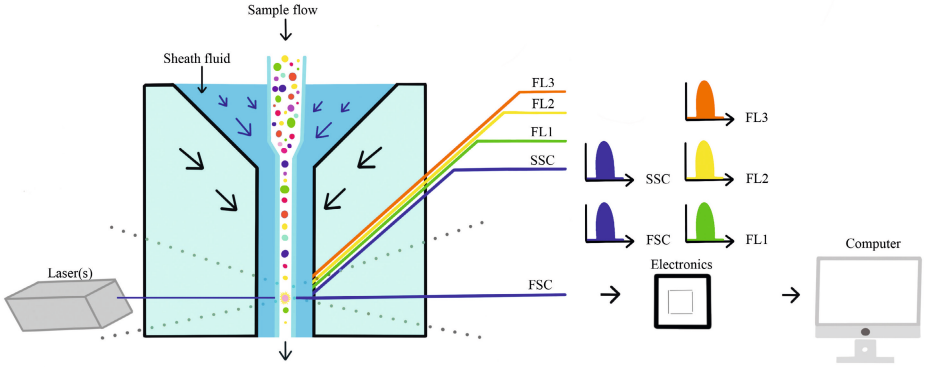

Figure 2. Schematic representation of a flow cytometer. Particles in suspension are forced into a single file by hydrodynamic forces of a sheath fluid before being illuminated by the laser beam. The zone where the illuminating beam meets the particle is known as the 'interrogation spot'. Light scatter is sent into different directions and collected by the forward scatter (FSC) and side scatter (SSC) detectors. Emitted fluorescence can also be collected by different detectors (FL1, FL2, FL3). Signals are then processed in the electronics and generated data is finally displayed and stored in the computer.

1.5. OVERTURE TO HIGH SENSITIVITY FLOW CYTOMETRY

High-sensitivity flow cytometry (hFCM) makes it possible to detect single EVs in a high-throughput manner, while providing phenotypic information. At present, technologies that can provide both quantitative and qualitative information on single EVs present in heterogenous EV-bulk samples in a high-throughput fashion are scarce (table 1). Although, hFCM fulfills these criteria, the technology evolved from working at the limit of resolution. Peer-reviewed reports have shown that most conventional instruments have a limit of detection at ~200 nm for polystyrene particles based on light scattering [107, 108]. These studies date back from a decade ago but they set an important starting point for the development of hFCM. Importantly, simply because of the RI differences between a polystyrene particle and biological EVs can account for a 10-fold more light scattering [14, 107], such instruments are not the most suited for EV detection as signals of interest will be below the detection limit and/or overlap with background signals. Alternative strategies have been developed over the years, where a fluorescent-based detection pushed the limit of detection from 200 nm to 100 nm for polystyrene particles [109, 110]. Recent innovations have circumvented the limitations of cFCM allowing for unprecedented light scatter-based sensitivity, such as the laboratory-built nanofcm platform [111] or by using alternative trigger threshold strategies such as the 405 nm laser [112]. Next, three key elements that impact hFCM EV detection will be introduced. These being (i) the relationship between the particle and light, (ii) the use of a trigger threshold and (iii) the impact of background signals [14, 113].

1.5.1. Light scattering

Due to EV intrinsic features such as small size and low refractive index, most EVs generate weak light scattering signals, that end up being close to and below the limit of detection.

Light scattering occurs when the illuminating beam hits a particle in suspension, as electromagnetic radiation is released in the form of oscillating charges. The re-emitted light goes into different directions that depend on both the illuminating beam and the particle. Thus, all illuminated particles scatter light. Light scattering is a complex function that highly depends on (i) wavelength of the illuminating beam, (ii) particle diameter and (iii) refractive index (RI). Therefore, changes in either of these parameters will translate into different light scattering levels. Besides, other factors that can influence efficiency of light scattering collection, such as the collection angle, have also been identified [113]. Firstly, regarding the wavelength of the illuminating beam, 488 nm is the standard choice for most FCM. Secondly, particle diameter is intrinsic to the sample, in the case of EVs it can go from 30 nm up to 1 mm. Thirdly, the RI is the ratio of the speed of light in vacuum compared to the speed of light in a material, and defines how efficiently a particle scatters light. Simplified, light passing higher RI material travels more slowly and can scatter more light compared to lower RI materials in an identical surrounding medium. Because the RI is also a complex intrinsic property, it can vary with factors such as the wavelength of the light source and the temperature. Reference values are available for solid particles, for example when illuminated by a 488 nm light source polystyrene particles have a RI of 1.604 while silica particles have a RI of 1.463 [114]. In practical terms we can translate the RI differences into, polystyrene particles scattering light much more efficiently than silica particles. For biological EVs that are not solid particles but rather have a core-shell morphology with varying compositions, it is technically difficult to define a RI value. Very few studies tried to assess this parameter and reported RI values between 1.36-1.41 based on NTA [115]. While this calculated RI value is useful to estimate EV size etc., it is important to take into consideration that an EV population is heterogeneous in composition which might be reflected in RI variations between different EVs.

1.5.2. Trigger threshold

FCM works with setting trigger thresholds. Particles whose signals are below the trigger threshold value will remain ‘unseen’ by the instrument, while only the signals that are above the set trigger threshold will be processed as an event. Therefor the selection and level of the trigger threshold determines what an event is. In cFCM, light scattering is often the signal where the trigger threshold is imposed on. This decision is a traditional practice that sufficiently holds for the purpose of cell measurements. Since cells are much bigger than EVs, they also scatter much light that easily surpass the limit of detection of the instrument. Therefore, as long as cells of interest can be discriminated from signals of non-interest, including the background, this threshold suffice. In con-

trast, for hFCM it becomes a critical element as a trigger threshold that is set too high will, impairs detection of dim EVs (figure 3a). Lower the triggering threshold can result in the detection of a dim EV but background signals will become detected as events, resulting in the loss of discrimination between EVs and background.

Alternatively, fluorescence has been reported to display lower background interference when working at the limit of detection [109, 116]. Therefore, when EVs emit brightly enough fluorescent signals, the detection of EVs can be improved (figure 3b). As such, fluorescence-based threshold triggering improves hFCM, especially when EVs generate weak light scattering that will always remain very close to, at or even below the background levels (particle 1, figure 3a). A number of strategies have been developed to improve detection in this way [109, 116, 117]. However, a sufficiently bright fluorescence signal is required to efficiently apply a fluorescent threshold that can detect all or most of the EVs present in the sample.

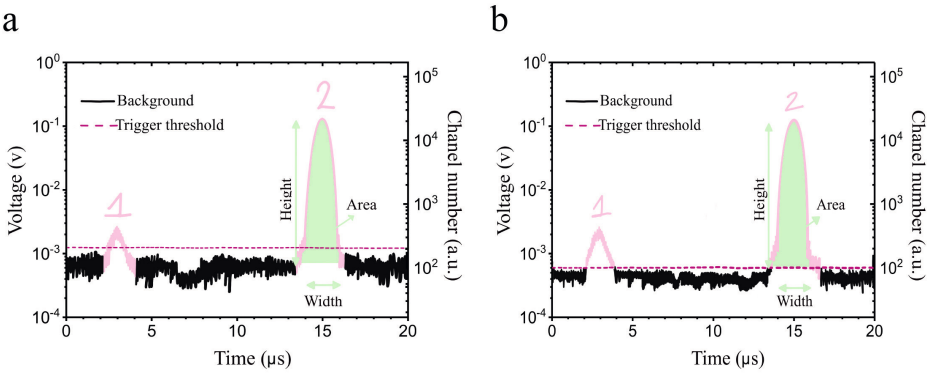

Figure 3. Representation of a signal pulse. Simulated voltage from electrical signals from a detector (left axis) and digitalized channel number in arbitrary units (a.u., right axis) by the electronics versus time (X axis). The signal background level fluctuates along time while particle 1 (at 3 ms) and particle 2 (at 15 ms) pass the interrogation point producing a Gaussian pulse. The trigger threshold is used to identify the particle signal while keeping most of the background noise below the threshold level (dotted line). A particle will be represented as the area under the pulse (green). Pulse height is the amplitude while pulse width is the time taken for the particle to pass through the interrogation point. Signals from (a) light scatter or (b) fluorescence can be suitable for triggering. Fluorescence triggering can provide a better choice, especially for smaller particles (such as particle 1) whose light scatter intensities are closer to background noise.

1.5.3. Dancing with the background

While most background signals often remain below the trigger threshold and are disregarded in cFCM, the background severely impacts the detection of EVs [118]. There are different sources and types of background that have to be considered [14]. Note that even when no EV or particle of interest is present in the interrogation point, the electronic system will continuously receive signals arising from background. Background

signals can originate from the instrument (1) fluidic, (2) optic and (3) electronic systems but also from the sheath fluid or sample (e.g. debris) and its preparation (e.g. colloidal structures).

Some workarounds can help to deal with background signals. Fluidic background is known to increase due to the presence of particulate matter in the sheath fluid and buffers, so cleaning procedures and buffers have to be consider. Optical background is typically higher than background noise and dominated by light scattering and/or autofluorescence but hardware components, such as the size of the obscuration bar that blocks direct laser light can minimize its interference. Electronic background is a complex function that varies within instruments, mainly due to differences in detectors and settings. In addition, the trigger threshold acts as a filter to define only signals from the particles of interest as events (figure 3, dashed line), while leaving out the background (figure 3, continuous black line).

In the ideal situation,, a particle will pass through the interrogation point generating a gaussian pulse distribution with a peak. The peak of the pulse then corresponds to the maximum height of the signal, which will be well above the background level (figure 3, particle 2). But when it comes to EVs and particles that generate weak signals they inevitably end up closer to the background floor and peaks and gaussian pulse distributions are less pronounced (figure 3, particle 1). Hence, background matters and finding ways to reduce it stay important.

1.5.4. Navigating within the premises of high-sensitivity flow cytometry

To exploit the potential of hFCM and reveal EV heterogeneity, there are a number of premises that have to be followed. Firstly, light scattering signals do not directly indicate size and/or complexity, but they can be used to infer biophysical properties such as relative RI and size when other variables have been accounted for. Secondly, generic and/or specific fluorescent reagents can aid to decipher EV molecular composition. Dyes that are (1) lipophilic and intercalate in the lipid bilayer, such as Paul Karl Horan dyes (PKH26 or PKH67) and 4-(2-[6-(dioctylamino)-2-naphthalenyl]ethenyl)-1-(3-sulfopropyl) pyridinium (di-8-ANEPPS), or (2) amine-reactive, such as 5-(and-6)-Carboxyfluorescein Diacetate Succinimidyl Ester (CFDA-SE, often referred to as CFSE) can be used for generic EV staining [109, 117, 119]. Furthermore, phenotypic information can be obtained by using antibodies that are fluorescently conjugated [109, 117]. However, compared to cells that have thousands of epitopes on their surface, the copy number that is present on a single EV should be reduced by one or two orders of magnitude [14]. To detect these low copy numbers generating dim fluorescent signals, highly sensitive instruments are required and the selection of bright fluorescent conjugates is preferred [109, 113]. In addition, certain generic dyes and antibodies can form aggregates and introduce artifacts during sample preparation, which can be monitored by using the appropriate buffer and procedural controls. Importantly, post-staining methods such as DGU or SEC

(Chapter 1, section 1.2.3) can be used to remove these unbound reagents effectively before analyzing samples by hFCM [109, 117, 119].

Another known pitfall in the hFCM field is the coincident detection of more than one particle simultaneously (figure 4). When multiple particles are passing through the interrogation point, the instrument becomes unable to discriminate them, integrating signals as one event [107]. This phenomenon is often referred to as 'swarm detection' rather than single EV detection and has been observed when measuring samples with a high concentration but simply diluting samples helps to reveal this potential artifact [107, 120, 121]. When a linear relationship is observed between the number of events and the dilution factor (figure 4b), while event light scattering and fluorescent signal intensities are kept linear (figure 4c) swarm detection can be excluded [14, 113]. The upper and lower ends of a particle concentration range need to be determined on each instrument, to define the optimal dynamic range for the detection of single EVs. Differences in fluidics, pressure settings and flow rates between instruments can impact the dynamic range, so testing different particle concentrations to validate single EV detection is good practice for every instrument.

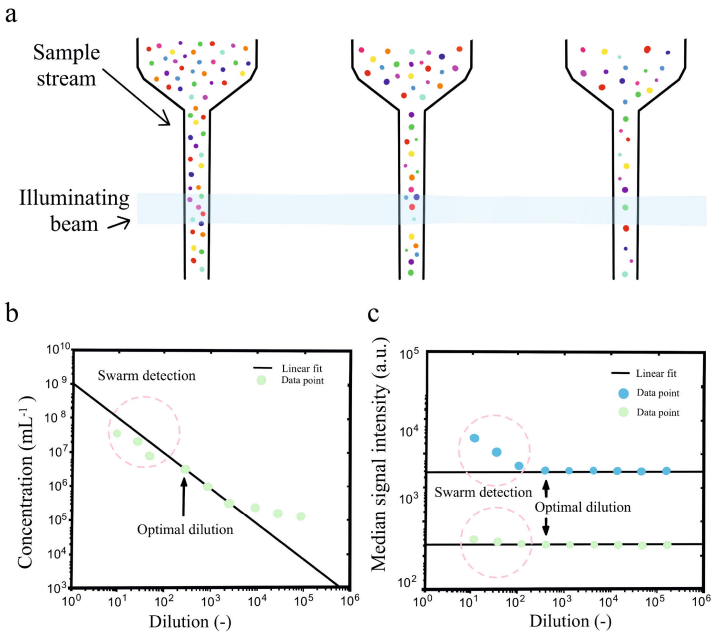

Figure 4. Graphic representation of the effect of serial dilution to prevent swarm detection. (a) Higher sample concentrations (left panel) can result in swarm detection of multiple particles and erroneously be integrated as a single event as compared to more diluted samples (right panel). (b) Simulated concentration (number of events per mL) versus dilution. (c) Simulated median light scatter (blue) or fluorescence (green) intensities versus dilution. Linear fitting is showed. The dashed circles indicate dilutions for which swarm detection occurs. The optimal dilution is the lowest dilution for which swarm detection does not occur (arrows).

Although EV FCM holds the promise to revolutionize the field, technical limitations together with the biological complexity of EV samples generate a challenging scenario for its implementation and interpretation. In my research I have been working on several aspects to move hFCM to the next level.

1.6. OUTLINE OF THESIS CHAPTERS

In **Chapter 2** I describe the development and characterization of an adaptable synthetic reference material for EV research that can be used for broad applications, including high-sensitivity FCM, to enhance the reproducibility of EV measurements.

Chapter 3 consists of a reporting framework for single EV flow cytometry experiments. This chapter is the result of a joint effort of the EV FCM working group (https://www.evflowcytometry.org) and was published as an ISEV position manuscript. By joining forces between the International Society for Extracellular Vesicles (ISEV), International Society for Advancement of Cytometry (ISAC), and the International Society on Thrombosis and Haemostasis (ISTH), this framework was developed to assist researchers with the reporting of critical information related to EV sample preparation, experimental design and EV detection. This chapter lands as a groundwork towards the added value of implementing fluorescence calibration into EV experiments (further investigated in Chapter 4 of this thesis and consequently implemented in Chapters 5 and 6).

In **Chapter 4** I explored the use of different fluorescence calibrators for small particle flow cytometry. In this collaborative study with industry (BD Biosciences and NanoFCM) and NIST, we provide insights into the precision and accuracy of currently available calibrators, such as Molecules of equivalent soluble fluorophores (MESF) beads, for the measurement of nanoparticles and EVs by flow cytometry.

Chapter 5 describes the improvement of flow cytometric EV detection due to the reduction of optical background signals by implementing different hardware adaptations. This proof-of- concept study shows the improvement of light scatter based detection of nanoparticles and EVs, which is often limited by background signals. This strategy has recently been implemented in new generation of flow cytometers with improved capabilities for EV analysis .

In **Chapter 6** we investigated the detection of tumor derived EVs in the presence of other non-EV particles, i.e., lipoprotein particles (LPPs). Lipoprotein particles are known to partially share biophysical properties and to outnumber EVs in complex biofluids such as blood plasma. Here, we used a variety of complementary single particle detection techniques to investigate if and how LPPs can influence EV analysis in blood.

Chapter 7 is the general discussion of this thesis in which I evaluated and connected the key elements presented in the thesis and indicated suggestions for follow-up studies and research lines.

REFERENCES

1. Yanez-Mo, M., et al., *Biological properties of extracellular vesicles and their physiological functions.* J Extracell Vesicles, 2015. **4**: p. 27066.
2. Colombo, M., G. Raposo, and C. Thery, *Biogenesis, secretion, and intercellular interactions of exosomes and other extracellular vesicles.* Annu Rev Cell Dev Biol, 2014. **30**: p. 255-89.
3. Coumans, F.A.W., et al., *Methodological Guidelines to Study Extracellular Vesicles.* Circ Res, 2017. **120**(10): p. 1632-1648.
4. Van Deun, J., et al., *The impact of disparate isolation methods for extracellular vesicles on downstream RNA profiling.* J Extracell Vesicles, 2014. **3**.
5. Nieuwland, R., et al., *Reproducibility of extracellular vesicle research.* Eur J Cell Biol, 2022. **101**(3): p. 151226.
6. Lotvall, J., et al., *Minimal experimental requirements for definition of extracellular vesicles and their functions: a position statement from the International Society for Extracellular Vesicles.* J Extracell Vesicles, 2014. **3**: p. 26913.
7. Witwer, K.W., et al., *Updating the MISEV minimal requirements for extracellular vesicle studies: building bridges to reproducibility.* J Extracell Vesicles, 2017. **6**(1): p. 1396823.
8. Thery, C., et al., *Minimal information for studies of extracellular vesicles 2018 (MISEV2018): a position statement of the International Society for Extracellular Vesicles and update of the MISEV2014 guidelines.* J Extracell Vesicles, 2018. **7**(1): p. 1535750.
9. Welsh, J.A., et al., *Towards defining reference materials for measuring extracellular vesicle refractive index, epitope abundance, size and concentration.* J Extracell Vesicles, 2020. **9**(1): p. 1816641.
10. Welsh, J.A., et al., *MIFlowCyt-EV: a framework for standardized reporting of extracellular vesicle flow cytometry experiments.* J Extracell Vesicles, 2020. **9**(1): p. 1713526.
11. Consortium, E.-T., et al., *EV-TRACK: transparent reporting and centralizing knowledge in extracellular vesicle research.* Nat Methods, 2017. **14**(3): p. 228-232.
12. Valkonen, S., et al., *Biological reference materials for extracellular vesicle studies.* Eur J Pharm Sci, 2017. **98**: p. 4-16.
13. Gardiner, C., et al., *Techniques used for the isolation and characterization of extracellular vesicles: results of a worldwide survey.* J Extracell Vesicles, 2016. **5**: p. 32945.
14. Nolan, J.P., *Flow Cytometry of Extracellular Vesicles: Potential, Pitfalls, and Prospects.* Curr Protoc Cytom, 2015. **73**: p. 13 14 1-16.
15. Chargaff, E. and R. West, *The biological significance of the thromboplastic protein of blood.* J Biol Chem, 1946. **166**(1): p. 189-97.
16. Wolf, P., *The nature and significance of platelet products in human plasma.* Br J Haematol, 1967. **13**(3): p. 269-88.
17. Anderson, H.C., *Vesicles associated with calcification in the matrix of epiphyseal cartilage.* J Cell Biol, 1969. **41**(1): p. 59-72.
18. Ali, S.Y., S.W. Sajdera, and H.C. Anderson, *Isolation and characterization of calcifying matrix vesicles from epiphyseal cartilage.* Proc Natl Acad Sci U S A, 1970. **67**(3): p. 1513-20.
19. Bonucci, E., *Fine structure of early cartilage calcification.* J Ultrastruct Res, 1967. **20**(1): p. 33-50.
20. Aaronson, S., et al., *Ultrastructure of intracellular and extracellular vesicles, membranes, and myelin figures produced by Ochromonas danica.* J Ultrastruct Res, 1971. **35**(5): p. 418-30.

21. Pan, B.T. and R.M. Johnstone, *Fate of the transferrin receptor during maturation of sheep reticulocytes in vitro: selective externalization of the receptor.* Cell, 1983. **33**(3): p. 967-78.
22. Harding, C., J. Heuser, and P. Stahl, *Receptor-mediated endocytosis of transferrin and recycling of the transferrin receptor in rat reticulocytes.* J Cell Biol, 1983. **97**(2): p. 329-39.
23. Couch, Y., et al., *A brief history of nearly EV-erything - The rise and rise of extracellular vesicles.* J Extracell Vesicles, 2021. **10**(14): p. e12144.
24. Raposo, G., et al., *B lymphocytes secrete antigen-presenting vesicles.* J Exp Med, 1996. **183**(3): p. 1161-72.
25. Johnstone, R.M., et al., *Exosome formation during maturation of mammalian and avian reticulocytes: evidence that exosome release is a major route for externalization of obsolete membrane proteins.* J Cell Physiol, 1991. **147**(1): p. 27-36.
26. Sims, P.J., et al., *Assembly of the platelet prothrombinase complex is linked to vesiculation of the platelet plasma membrane. Studies in Scott syndrome: an isolated defect in platelet procoagulant activity.* J Biol Chem, 1989. **264**(29): p. 17049-57.
27. Gasser, O. and J.A. Schifferli, *Activated polymorphonuclear neutrophils disseminate anti-inflammatory microparticles by ectocytosis.* Blood, 2004. **104**(8): p. 2543-8.
28. Baj-Krzyworzeka, M., et al., *Platelet-derived microparticles stimulate proliferation, survival, adhesion, and chemotaxis of hematopoietic cells.* Exp Hematol, 2002. **30**(5): p. 450-9.
29. Hoshino, A., et al., *Tumour exosome integrins determine organotropic metastasis.* Nature, 2015. **527**(7578): p. 329-35.
30. Stevic, I., et al., *Specific microRNA signatures in exosomes of triple-negative and HER2-positive breast cancer patients undergoing neoadjuvant therapy within the GeparSixto trial.* BMC Med, 2018. **16**(1): p. 179.
31. Zitvogel, L., et al., *Eradication of established murine tumors using a novel cell-free vaccine: dendritic cell-derived exosomes.* Nat Med, 1998. **4**(5): p. 594-600.
32. Andre, F., et al., *Exosomes in cancer immunotherapy: preclinical data.* Adv Exp Med Biol, 2001. **495**: p. 349-54.
33. Escudier, B., et al., *Vaccination of metastatic melanoma patients with autologous dendritic cell (DC) derived-exosomes: results of thefirst phase I clinical trial.* J Transl Med, 2005. **3**(1): p. 10.
34. van Niel, G., G. D'Angelo, and G. Raposo, *Shedding light on the cell biology of extracellular vesicles.* Nat Rev Mol Cell Biol, 2018. **19**(4): p. 213-228.
35. Kowal, J., M. Tkach, and C. Thery, *Biogenesis and secretion of exosomes.* Curr Opin Cell Biol, 2014. **29**: p. 116-25.
36. Buzas, E.I., *The roles of extracellular vesicles in the immune system.* Nat Rev Immunol, 2022: p. 1-15.
37. Thery, C., L. Zitvogel, and S. Amigorena, *Exosomes: composition, biogenesis and function.* Nat Rev Immunol, 2002. **2**(8): p. 569-79.
38. Andreu, Z. and M. Yanez-Mo, *Tetraspanins in extracellular vesicle formation and function.* Front Immunol, 2014. **5**: p. 442.
39. Witwer, K.W. and C. Thery, *Extracellular vesicles or exosomes? On primacy, precision, and popularity influencing a choice of nomenclature.* J Extracell Vesicles, 2019. **8**(1): p. 1648167.
40. Gyorgy, B., et al., *Membrane vesicles, current state-of-the-art: emerging role of extracellular vesicles.* Cell Mol Life Sci, 2011. **68**(16): p. 2667-88.
41. Boukouris, S. and S. Mathivanan, *Exosomes in bodily fluids are a highly stable resource of disease biomarkers.* Proteomics Clin Appl, 2015. **9**(3-4): p. 358-67.

42. Fais, S., et al., *Evidence-Based Clinical Use of Nanoscale Extracellular Vesicles in Nanomedicine.* ACS Nano, 2016. **10**(4): p. 3886-99.
43. Konoshenko, M.Y., et al., *Isolation of Extracellular Vesicles: General Methodologies and Latest Trends.* Biomed Res Int, 2018. **2018**: p. 8545347.
44. Thery, C., et al., *Isolation and characterization of exosomes from cell culture supernatants and biological fluids.* Curr Protoc Cell Biol, 2006. **Chapter 3**: p. Unit 3 22.
45. Royo, F., et al., *Methods for Separation and Characterization of Extracellular Vesicles: Results of a Worldwide Survey Performed by the ISEV Rigor and Standardization Subcommittee.* Cells, 2020. **9**(9).
46. Cvjetkovic, A., J. Lotvall, and C. Lasser, *The influence of rotor type and centrifugation time on the yield and purity of extracellular vesicles.* J Extracell Vesicles, 2014. **3**.
47. Sodar, B.W., et al., *Low-density lipoprotein mimics blood plasma-derived exosomes and microvesicles during isolation and detection.* Sci Rep, 2016. **6**: p. 24316.
48. Nordin, J.Z., et al., *Ultrafiltration with size-exclusion liquid chromatography for high yield isolation of extracellular vesicles preserving intact biophysical and functional properties.* Nanomedicine, 2015. **11**(4): p. 879-83.
49. Greening, D.W., et al., *A protocol for exosome isolation and characterization: evaluation of ultracentrifugation, density-gradient separation, and immunoaffinity capture methods.* Methods Mol Biol, 2015. **1295**: p. 179-209.
50. Royo, F., et al., *Comparative miRNA Analysis of Urine Extracellular Vesicles Isolated through Five Different Methods.* Cancers (Basel), 2016. **8**(12).
51. Boing, A.N., et al., *Single-step isolation of extracellular vesicles by size-exclusion chromatography.* J Extracell Vesicles, 2014. **3**.
52. Ronquist, G. and I. Brody, *The prostasome: its secretion and function in man.* Biochim Biophys Acta, 1985. **822**(2): p. 203-18.
53. Karimi, N., et al., *Detailed analysis of the plasma extracellular vesicle proteome after separation from lipoproteins.* Cell Mol Life Sci, 2018. **75**(15): p. 2873-2886.
54. Onodi, Z., et al., *Isolation of High-Purity Extracellular Vesicles by the Combination of Iodixanol Density Gradient Ultracentrifugation and Bind-Elute Chromatography From Blood Plasma.* Front Physiol, 2018. **9**: p. 1479.
55. Tian, Y., et al., *Quality and efficiency assessment of six extracellular vesicle isolation methods by nano-flow cytometry.* J Extracell Vesicles, 2020. **9**(1): p. 1697028.
56. Zhang, H. and D. Lyden, *Asymmetric-flow field-flow fractionation technology for exomere and small extracellular vesicle separation and characterization.* Nat Protoc, 2019. **14**(4): p. 1027-1053.
57. Reategui, E., et al., *Engineered nanointerfaces for microfluidic isolation and molecular profiling of tumor-specific extracellular vesicles.* Nat Commun, 2018. **9**(1): p. 175.
58. Clayton, A., et al., *Considerations towards a roadmap for collection, handling and storage of blood extracellular vesicles.* J Extracell Vesicles, 2019. **8**(1): p. 1647027.
59. Vergauwen, G., et al., *Confounding factors of ultrafiltration and protein analysis in extracellular vesicle research.* Sci Rep, 2017. **7**(1): p. 2704.
60. Yuana, Y., et al., *Co-isolation of extracellular vesicles and high-density lipoproteins using density gradient ultracentrifugation.* J Extracell Vesicles, 2014. **3**.
61. Killingsworth, B., J.A. Welsh, and J.C. Jones, *EV Translational Horizons as Viewed Across the Complex Landscape of Liquid Biopsies.* Front Cell Dev Biol, 2021. **9**: p. 556837.
62. Biro, E., et al., *Human cell-derived microparticles promote thrombus formation in vivo in a tissue factor-dependent manner.* J Thromb Haemost, 2003. **1**(12): p. 2561-8.

63. Zhang, C., et al., *Plasma extracellular vesicle derived protein profile predicting and monitoring immunotherapeutic outcomes of gastric cancer.* J Extracell Vesicles, 2022. **11**(4): p. e12209.
64. Lak, N.S.M., et al., *Extracellular Vesicles: A New Source of Biomarkers in Pediatric Solid Tumors? A Systematic Review.* Front Oncol, 2022. **12**: p. 887210.
65. Plant, A.L., et al., *Improved reproducibility by assuring confidence in measurements in biomedical research.* Nat Methods, 2014. **11**(9): p. 895-8.
66. Roux, Q., et al., *The EV-TRACK summary add-on: integration of experimental information in databases to ensure comprehensive interpretation of biological knowledge on extracellular vesicles.* J Extracell Vesicles, 2020. **9**(1): p. 1699367.
67. Pinedo, M., L. de la Canal, and C. de Marcos Lousa, *A call for Rigor and standardization in plant extracellular vesicle research.* J Extracell Vesicles, 2021. **10**(6): p. e12048.
68. Erdbrugger, U., et al., *Urinary extracellular vesicles: A position paper by the Urine Task Force of the International Society for Extracellular Vesicles.* J Extracell Vesicles, 2021. **10**(7): p. e12093.
69. Bunk, D.M., *Reference materials and reference measurement procedures: an overview from a national metrology institute.* Clin Biochem Rev, 2007. **28**(4): p. 131-7.
70. Coxon, C.H., C. Longstaff, and C. Burns, *Applying the science of measurement to biology: Why bother?* PLoS Biol, 2019. **17**(6): p. e3000338.
71. Geeurickx, E., et al., *The generation and use of recombinant extracellular vesicles as biological reference material.* Nat Commun, 2019. **10**(1): p. 3288.
72. Varga, Z., et al., *Hollow organosilica beads as reference particles for optical detection of extracellular vesicles.* J Thromb Haemost, 2018.
73. Garcia-Manrique, P., et al., *Selected Tetraspanins Functionalized Niosomes as Potential Standards for Exosome Immunoassays.* Nanomaterials (Basel), 2020. **10**(5).
74. Gorgens, A., et al., *Optimisation of imaging flow cytometry for the analysis of single extracellular vesicles by using fluorescence-tagged vesicles as biological reference material.* J Extracell Vesicles, 2019. **8**(1): p. 1587567.
75. Choquette, S.J., D.L. Duewer, and K.E. Sharpless, *NIST Reference Materials: Utility and Future.* Annu Rev Anal Chem (Palo Alto Calif), 2020. **13**(1): p. 453-474.
76. *Better research through metrology.* Nat Methods, 2018. **15**(6): p. 395.
77. Humphrey, J.H. and I. Batty, *Letter: International units and standards in immunology.* Br Med J, 1976. **1**(6014): p. 898.
78. Coumans, F.A.W., E.L. Gool, and R. Nieuwland, *Bulk immunoassays for analysis of extracellular vesicles.* Platelets, 2017. **28**(3): p. 242-248.
79. Cizmar, P. and Y. Yuana, *Detection and Characterization of Extracellular Vesicles by Transmission and Cryo-Transmission Electron Microscopy.* Methods Mol Biol, 2017. **1660**: p. 221-232.
80. Diebolder, C.A., A.J. Koster, and R.I. Koning, *Pushing the resolution limits in cryo electron tomography of biological structures.* J Microsc, 2012. **248**(1): p. 1-5.
81. Linares, R., et al., *Imaging and Quantification of Extracellular Vesicles by Transmission Electron Microscopy.* Methods Mol Biol, 2017. **1545**: p. 43-54.
82. Piontek, M.C. and W.H. Roos, *Atomic Force Microscopy: An Introduction.* Methods Mol Biol, 2018. **1665**: p. 243-258.
83. Vorselen, D., et al., *The fluid membrane determines mechanics of erythrocyte extracellular vesicles and is softened in hereditary spherocytosis.* Nat Commun, 2018. **9**(1): p. 4960.
84. Vorselen, D., et al., *Mechanical Characterization of Liposomes and Extracellular Vesicles, a Protocol.* Front Mol Biosci, 2020. **7**: p. 139.

85. Roberts, G.S., et al., *Tunable pores for measuring concentrations of synthetic and biological nanoparticle dispersions.* Biosens Bioelectron, 2012. **31**(1): p. 17-25.
86. Coumans, F.A., et al., *Reproducible extracellular vesicle size and concentration determination with tunable resistive pulse sensing.* J Extracell Vesicles, 2014. **3**: p. 25922.
87. Cimorelli, M., et al., *Standardized procedure to measure the size distribution of extracellular vesicles together with other particles in biofluids with microfluidic resistive pulse sensing.* PLoS One, 2021. **16**(4): p. e0249603.
88. Gardiner, C., et al., *Extracellular vesicle sizing and enumeration by nanoparticle tracking analysis.* J Extracell Vesicles, 2013. **2**.
89. Filipe, V., A. Hawe, and W. Jiskoot, *Critical evaluation of Nanoparticle Tracking Analysis (NTA) by NanoSight for the measurement of nanoparticles and protein aggregates.* Pharm Res, 2010. **27**(5): p. 796-810.
90. Bachurski, D., et al., *Extracellular vesicle measurements with nanoparticle tracking analysis - An accuracy and repeatability comparison between NanoSight NS300 and ZetaView.* J Extracell Vesicles, 2019. **8**(1): p. 1596016.
91. Schermelleh, L., et al., *Super-resolution microscopy demystified.* Nat Cell Biol, 2019. **21**(1): p. 72-84.
92. Tam, J. and D. Merino, *Stochastic optical reconstruction microscopy (STORM) in comparison with stimulated emission depletion (STED) and other imaging methods.* J Neurochem, 2015. **135**(4): p. 643-58.
93. Koliha, N., et al., *A novel multiplex bead-based platform highlights the diversity of extracellular vesicles.* J Extracell Vesicles, 2016. **5**: p. 29975.
94. Chen, C., et al., *Imaging and Intracellular Tracking of Cancer-Derived Exosomes Using Single-Molecule Localization-Based Super-Resolution Microscope.* ACS Appl Mater Interfaces, 2016. **8**(39): p. 25825-25833.
95. Nizamudeen, Z., et al., *Rapid and accurate analysis of stem cell-derived extracellular vesicles with super resolution microscopy and live imaging.* Biochim Biophys Acta Mol Cell Res, 2018. **1865**(12): p. 1891-1900.
96. Enciso-Martinez, A., et al., *Synchronized Rayleigh and Raman scattering for the characterization of single optically trapped extracellular vesicles.* Nanomedicine, 2020. **24**: p. 102109.
97. Rkiouak, L., et al., *Optical trapping and Raman spectroscopy of solid particles.* Phys Chem Chem Phys, 2014. **16**(23): p. 11426-34.
98. Gong, Z., et al., *Optical trapping-Raman spectroscopy (OT-RS) with embedded microscopy imaging for concurrent characterization and monitoring of physical and chemical properties of single particles.* Anal Chim Acta, 2018. **1020**: p. 86-94.
99. Fulwyler, M.J., *Electronic separation of biological cells by volume.* Science, 1965. **150**(3698): p. 910-1.
100. Shapiro, H.M., *The evolution of cytometers.* Cytometry A, 2004. **58**(1): p. 13-20.
101. Ehrlich P, L.A., *Histology of the Blood: Normal and Pathological.* CJ Clay and Sons, PA, USA, 1900.
102. Moldavan, A., *Photo-Electric Technique for the Counting of Microscopical Cells.* Science, 1934. **80**(2069): p. 188-9.
103. Coons, A.H., *The beginnings of immunofluorescence.* J Immunol, 1961. **87**: p. 499-503.
104. Gucker, F.T., Jr. and C.T. O'Konski, *Electronic methods of counting aerosol particles.* Chem Rev, 1949. **44**(2): p. 373-88.
105. Crosland-Taylor, P.J., *A device for counting small particles suspended in a fluid through a tube.* Nature, 1953. **171**(4340): p. 37-8.

106. Shapiro, H.M., *Practical flow cytometry*. 4th ed. 2003, New York: Wiley-Liss. l, 681 p.
107. van der Pol, E., et al., *Single vs. swarm detection of microparticles and exosomes by flow cytometry.* J Thromb Haemost, 2012. **10**(5): p. 919-30.
108. Lacroix, R., et al., *Standardization of platelet-derived microparticle enumeration by flow cytometry with calibrated beads: results of the International Society on Thrombosis and Haemostasis SSC Collaborative workshop.* J Thromb Haemost, 2010. **8**(11): p. 2571-4.
109. van der Vlist, E.J., et al., *Fluorescent labeling of nano-sized vesicles released by cells and subsequent quantitative and qualitative analysis by high-resolution flow cytometry.* Nat Protoc, 2012. **7**(7): p. 1311-26.
110. Nolte-'t Hoen, E.N., et al., *Quantitative and qualitative flow cytometric analysis of nanosized cell-derived membrane vesicles.* Nanomedicine, 2012. **8**(5): p. 712-20.
111. Zhang, W., et al., *Light-Scattering Sizing of Single Submicron Particles by High-Sensitivity Flow Cytometry.* Anal Chem, 2018. **90**(21): p. 12768-12775.
112. McVey, M.J., C.M. Spring, and W.M. Kuebler, *Improved resolution in extracellular vesicle populations using 405 instead of 488 nm side scatter.* J Extracell Vesicles, 2018. **7**(1): p. 1454776.
113. Welsh, J.A., et al., *Extracellular Vesicle Flow Cytometry Analysis and Standardization.* Front Cell Dev Biol, 2017. **5**: p. 78.
114. Welsh, J.A., et al., *FCMPASS Software Aids Extracellular Vesicle Light Scatter Standardization.* Cytometry A, 2019.
115. van der Pol, E., et al., *Refractive index determination of nanoparticles in suspension using nanoparticle tracking analysis.* Nano Lett, 2014. **14**(11): p. 6195-201.
116. Arraud, N., et al., *Fluorescence triggering: A general strategy for enumerating and phenotyping extracellular vesicles by flow cytometry.* Cytometry A, 2016. **89**(2): p. 184-95.
117. Stoner, S.A., et al., *High sensitivity flow cytometry of membrane vesicles.* Cytometry A, 2016. **89**(2): p. 196-206.
118. Nolan, J.P. and E. Duggan, *Analysis of Individual Extracellular Vesicles by Flow Cytometry.* Methods Mol Biol, 2018. **1678**: p. 79-92.
119. Morales-Kastresana, A., et al., *Labeling Extracellular Vesicles for Nanoscale Flow Cytometry.* Sci Rep, 2017. **7**(1): p. 1878.
120. Groot Kormelink, T., et al., *Prerequisites for the analysis and sorting of extracellular vesicle subpopulations by high-resolution flow cytometry.* Cytometry A, 2016. **89**(2): p. 135-47.
121. Libregts, S., et al., *Flow cytometric analysis of extracellular vesicle subsets in plasma: impact of swarm by particles of non-interest.* J Thromb Haemost, 2018.

"You cannot hope to build a better world without improving the individuals. To that end, each of us must work for our own improvement."

Marie Curie

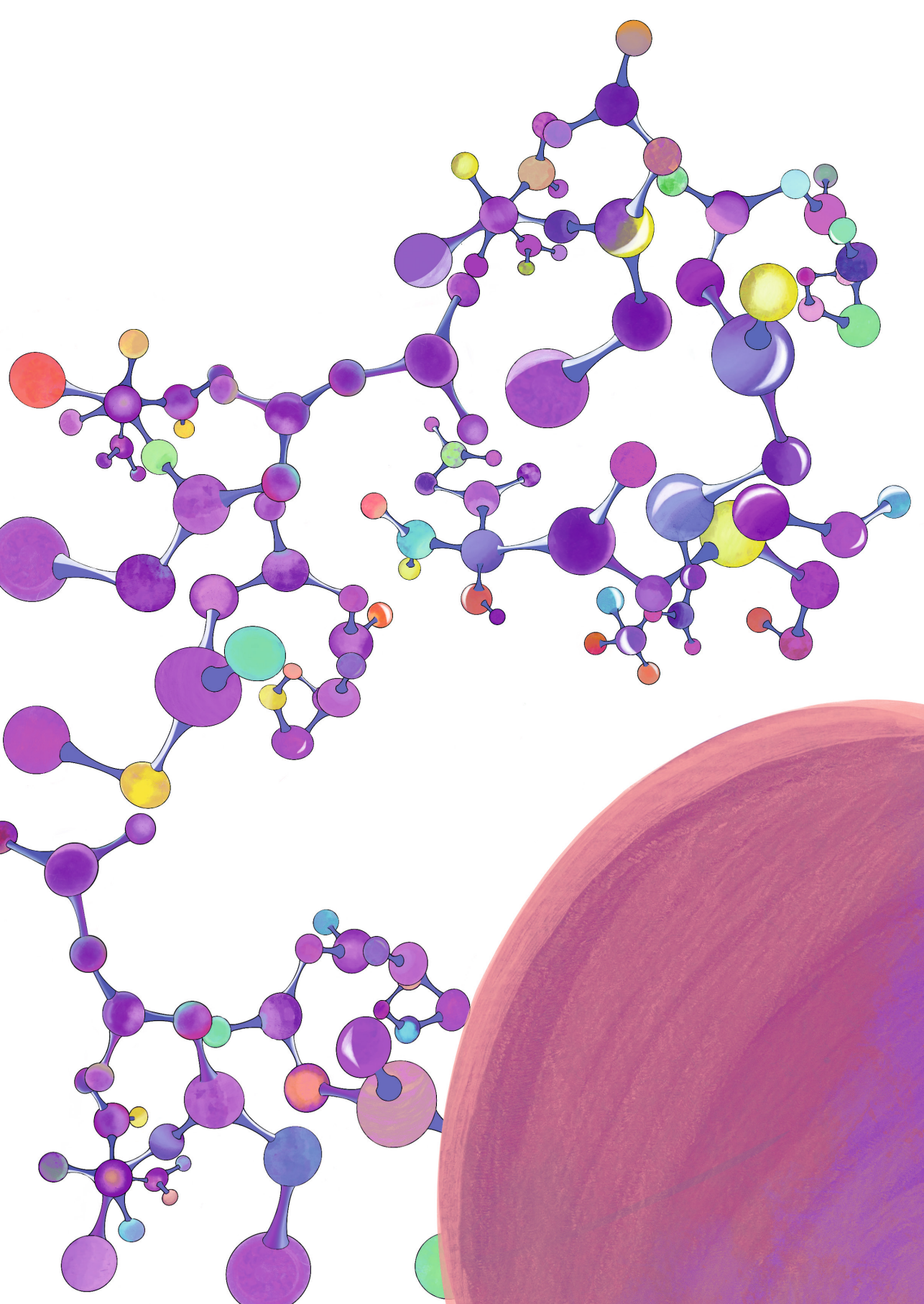

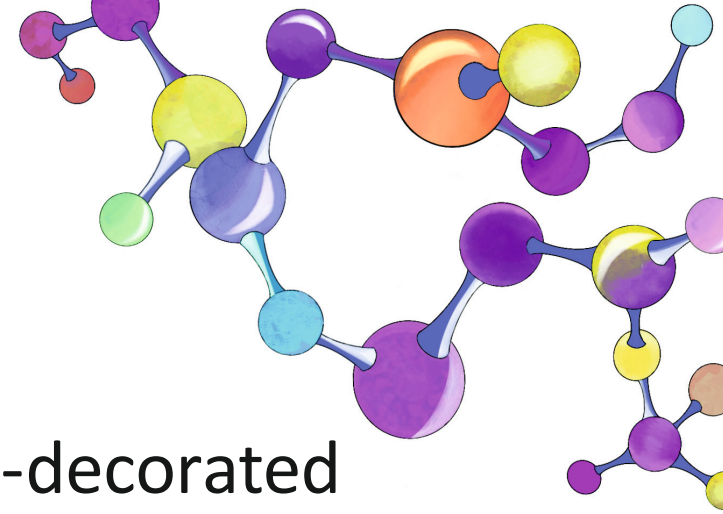

CHAPTER 2

Tetraspanin-decorated extracellular vesicle mimetics as a novel adaptable reference material

Estefanía Lozano-Andrés [a,b], Sten F. Libregts [b], Victor Toribio [a], Félix Royo [c], Sara Morales [d], Soraya López-Martín [a,d], Mar Valés-Gómez [e], Hugh T. Reyburn [e], Juan Manuel Falcón-Pérez [c,f], Marca H. Wauben [b], Manuel Soto [a] and María Yáñez-Mó [a,d]

a Centro de Biología Molecular Severo Ochoa (CSIC-UAM) Departamento de Biología Molecular, Universidad Autónoma de Madrid (UAM), Madrid, Spain;
b Department of Biochemistry and Cell Biology Faculty of Veterinary Medicine, Utrecht University, Utrecht, The Netherlands;
c Exosomes Lab, CIC bioGUNE, CIBERehd, Bizkaia Science and Technology Park, Derio, Bizkaia, Spain;
d Centro de Biología Molecular Severo Ochoa (CBM-SO) and Unidad de Investigación Hospital Santa Cristina, Instituto de Investigación Sanitaria Princesa (IIS-IP), Madrid, Spain; e Immunology and Oncology Department, National Center for Biotechnology (CNB-CSIC), Madrid, Spain;
f IKERBASQUE, Basque Foundation for Science, Bilbao, Spain

Published:
Lozano-Andrés E. et al., (2019). Journal of Extracellular Vesicles, VOL. 8, 1573052
https://doi.org/10.1080/20013078.2019.1573052

ABSTRACT

Features like small size, low refractive index and polydispersity pose challenges to the currently available detection methods for Extracellular Vesicles (EVs). In addition, the lack of appropriate standards to set up the experimental conditions makes it difficult to compare analyses obtained by different technical approaches. By modifying synthetic nanovesicles with recombinant antigenic regions of EV-enriched tetraspanins, we aimed to construct an EV-mimetic that can be used as a suitable standard for EV analyses.

To this end, the sequences of the large extracellular loops of the tetraspanins CD9, CD63 and CD81 were tagged with a target sequence for the biotin ligase BirA, and co-transformed with a BirA expression plasmid into Escherichia coli. GST fusion proteins were then isolated by affinity chromatography and released using thrombin. Biotinylated recombinant tetraspanin-loops were then coupled to (strept)avidin-coated synthetic nanovesicles and analysed and characterized by Dot-blot, Western-blot, Nanoparticle Tracking Analysis, Flow Cytometry and Transmission Electron Microscopy.

With this method, we were able to efficiently produce tetraspanin-domain decorated nanovesicles that share biophysical properties with natural EVs, can be detected using specific antibodies against common EV markers such as tetraspanins, and can be used as robust reference materials for detection techniques that are often used in the EV field.

Keywords: extracellular vesicles, tetraspanins, nanovesicles, niosomes, mimetic, standardization, flow cytometry

INTRODUCTION

Extracellular Vesicles (EVs) are released by most cell types, either by fusion of multivesicular bodies with the plasma membrane at the end of the endocytic recycling pathway (usually named exosomes), or by direct budding form the plasma membrane (commonly called microvesicles or ectosomes)(1). EVs are emerging as a potent mechanism of intercellular communication because of their ability to act as a vehicle for the exchange of genetic and protein material between cells (1). In the last two decades, EVs have become the focus of many studies because of their putative use as non-invasive biomarkers and their potential in bioengineering and clinical applications (2). However, current quantitative and qualitative detection methods for EVs are hindered by intrinsic features of EVs, such as small size, low refractive index and polydispersity. These factors, together with the lack of well-characterised and reproducible Reference Materials (RM) makes it difficult to compare results between samples and different laboratories (3,4).

We therefor aimed to design an Extracellular Vesicle-Mimetic (EVMs) based on the use of niosomes as a scaffold of self-assembled nanovesicles. This strategy can thus be considered either a fully synthetic-bottom-up EV, or a semi-synthetic artificial EV with surface modifications following a classification recently proposed (5). Niosomes are obtained by hydration of non-ionic surface-active agents with appropriate amounts of cholesterol and other amphiphilic molecules (6). Niosomes, similarly to liposomes, display a bilayer structure, nanometric scale size, a refractive index comparable to that of EVs (7,8). Additionally, niosomes can be modified through bioconjugation processes with proteins and fluorescent dyes (5). Furthermore, niosomes have lower production costs and are stable for longer periods of time when compared to liposomes, two characteristics of special importance for a RM development (6,9). The use of synthetic rather natural EVs can offer advantages like a higher and more controllable production yield important for scale-up applications (10).

The tetraspanins CD9, CD63 and CD81 are among the most abundant membrane proteins on natural EVs and are routinely used as markers for their characterization. Within the tetraspanin protein structure, the large extracellular loop (LEL) is the most antigenic region, and is where the majority of available anti-tetraspanin antibodies bind (11,12). Since the production of recombinant transmembrane domains is highly complex, we took the alternative approach of using only the immunogenic LEL domain of the tetraspanins for the construction of the EVMs. In addition, we decided to take advantage of the high-affinity interaction between (strept)avidin-biotin molecules to decorate the surface of the niosomes with these recombinant large extracellular tetraspanin loops. This strategy shows that these nanovesicles can serve as adaptable EVMs and can be successfully used as a novel RM for EV research. They can be isolated and purified by various EV-isolation methods and analysed on multiple platforms used within the EV research field, including Nanoparticle Tracking Analysis (NTA), Electron Microscopy (EM) and Flow Cytometry (FC).

MATERIALS AND METHODS

Antibodies. Primary antibodies anti-CD9 (clones VJ 1/10 and VJ1/20), anti-CD63 (clones TEA 3/10 and TEA 3/18 and H5C6), anti-CD81 (clone Eat2) mAbs have been previously described (13) and were purchased from Immunostep or BD Bioscience either unconjugated or as PE-conjugates. Anti-CD81 (clone 5A6) mAb was kindly provided by Dr Shoshana Levy (Stanford, USA).

Synthetic nanovesicles. Commercially available niosomes (Nio-N-GF-MAL) were purchased from Nanovex Biotechnologies (Asturias, Spain). According to the manufacturer´s description, these niosomes are composed of a formulation of lipids and non-ionic surfactants (Span 60 (Sorbitane monostearate), Tween 60 (Polyoxyethylenesorbitan monolaurate), Cholesterol and DSPE-2000-MAL (1,2-distearoyl-sn-glycero-3-phosphoethanolamine-N-[maleimide(polyethylene glycol)-2000] (ammonium salt)) with the following molar ratios: 0.5:0.5:1:0.01) that were hydrated with 2 ml PBS 20 mM pH 7 at 60ºC. To generate fluorescent niosomes, 1,2 dioleoyl-sn-glycerol phosphoethanolamine modified with carboxyfluorescein molecules was included in the formulation. The mixture is then shaken for two minutes and sonicated using a bath sonicator for 15 minutes to produce nanovesicles with a size range between 50-300 nm.

Surface modification of niosomes was also performed by Nanovex Biotechnologies. The bioconjugation with streptavidin or avidin was performed through thiol activated groups within the molecules of the bilayer, thereby generating a covalent bond between (strept)avidin molecules and the niosomes. 1 mg of a sulfhydryl-containing protein (streptavidin or avidin) was dissolved in a 4 ml niosome solution and incubated for 2h after previous deprotection of the reactive groups of the SATA activated strept(avidin) with hydroxylamine-HCL. To remove residual hydroxylamine and deacylation products, samples were desalted by gel filtration using Sephadex G-75. The bioconjugated niosomes were purified using a column of Agarose 6%. The amount of unbound (strep) avidin was measured by a Bradford assay in the filtrated fraction. Final niosome solutions were analysed using Dynamic Light Scattering (DLS) and NTA to determine their size and concentration, respectively. The change in the Z potential of the bioconjugated niosomes confirmed the presence of (strep)avidin on the surface of niosomes. In the niosome stocks used in the manuscript the amount of (strept)avidin conjugated to the surface was reported to be 232 mg/ml of avidin in the fluorescent niosomes and 224 mg/ml of streptavidin in non-fluorescent niosomes.

Construction of recombinant biotinylated tetraspanin LEL expression plasmids. AviCD9LELAvi, AviCD63LELAvi and AviCD81LELAvi sequences were cloned into the pGEX-4T2 expression vector. DNAs sequences corresponding to the LEL of CD9, CD63 and CD81 tetraspanins were amplified by PCR using master mix solution 2X (Promega), 100 ng of template DNA (CD9-, CD63- or CD81-GFP constructs (14) (15) and the primers (**Table**

1) that included the recognition sequences for BirA and restriction sites for XhoI and BamHI. Products of PCR amplification were inserted in the TOPO® TA vector (Invitrogen) and transformed into supercompetent bacteria by heat shock. Ampicillin-resistant clones were expanded and sequenced. Validated clones were digested with XhoI and BamHI and ligated in the reading frame of GST in the final vector pGEX-4T2. Products of ligation were verified by restriction pattern with XhoI and BamHI.

Oligonucleotides	Sequences (5' to 3`)
CD9LEL AviTag Forward	GATGGATCCTCCGGCCTGAACGACATCTTCGAGGCTCAGAAAATCGAATGGCACGAATCCCACAAGGATGAGGTGATTAAG
CD9LEL AviTag Reverse	GATCCTCGAGTTATTCGTGCCATTCGATTTTCTGAGCCTCGAAGATGTCGTTCAGACCGCCACCTTTATTGTCGAAGACCTCTTTGATG
CD63LEL AviTag Forward	GATGGATCCTCCGGCCTGAACGACATCTTCGAGGCTCAGAAAATCGAATGGCACGAAGGCTATGTGTTTAGAGATAAGGTG
CD63LEL AviTag Reverse	GATCCTCGAGTTATTCGTGCCATTCGATTTTCTGAGCCTCGAAGATGTCGTTCAGACCGCCACCATTTTTCCTCAGCCAGCCCCC
CD81LEL AviTag Forward	GATGGATCCTCCGGCCTGAACGACATCTTCGAGGCTCAGAAAATCGAATGGCACGAAGGCTTTGTCAACAAGGACCAG
CD81LEL AviTag Reverse	GATCCTCGAGTTATTCGTGCCATTCGATTTTCTGAGCCTCGAAGATGTCGTTCAGACCGCCACCCTTCCCGGAGAAGAGGTCATC

Table 1. Oligonucleotides used for PCR amplification of different human tetraspanin LELs. The restriction sites for XhoI (green) and BamHI (blue) as well as the recognition sites for the biotin ligase enzyme or AviTag (red) were inserted at N- and C-terminus during the PCR amplification.

Expression and purification of recombinant tetraspanins. Protease deficient- supercompetent *Escherichia coli* BL21 cells were co-transformed with AviCD9 LELAvi-pGEX-4T2, AviCD63 LELAvi-pGEX-4T2 or AviCD81 LELAvi-pGEX-4T2 constructs together with a pBirAcm, an engineered pACYC184 plasmid with an IPTG inducible BirA gene to over-express the biotin ligase (isolated from the K12 E. coli strain AVB99, Avidity LLC). Colonies were selected and grown overnight in 50 ml of Luria-Bertani (LB) medium containing 0.1 mg/ml ampicillin (Normon) and 0,1 mg/ml chloramphenicol (Sigma). The seed culture was then transferred into 200 ml of fresh LB medium with antibiotics and the indicated concentration of D-Biotin (Thermo Scientific) and cultured for 3 h at 37°C and 200 rpm. Isopropyl-beta-D-thiogalactopyranoside (IPTG, Sigma) was then added to a final concentration of 0.3 mM and bacterial culture continued for 2h at 37 °C and 200 rpm.
Cells were harvested by centrifugation at 4700 g for 15 min at 4 °C. The bacterial pellet was resuspended in 10 ml of the indicated lysis buffers (**Table 2**), supplemented with protease inhibitors cocktail (Roche) and sonicated as indicated. Bacterial lysates were centrifuged at 18000 g for 30 min at 4 °C. Supernatant was collected and GST fusion proteins were purified by affinity chromatography using glutathione-sepharose 4B (GE Healthcare). Proteins were cleaved and eluted from GST using site specific protease thrombin (GE Healthcare). Benzamidine-sepharose (Sigma-Aldrich) was used for the

removal of thrombin as previously described in detail (16). Protein concentration of the preparations was measured with Micro BCA Protein Assay Kit (Pierce Company) following the manufacturer´s instructions.
Samples along the purification process were boiled in Laemmli buffer and resolved by 10 or 12% SDS-PAGE. Gels were incubated with Coomassie Brilliant Blue for 5 minutes, followed by de-stain solution for 10 minutes.
For generation of non-biotinylated CD9LEL similar procedures were followed using CD9EC2-GST construct (15).

Number	Lysis conditions used in cell lysis optimisation
1	Addition of 1% triton and 70% amplitude sonication of 5 pulses of 10 s each pulse with pauses of 10 s between pulses.
2	Incubation of suspension samples with lysozyme (10 mg/mL) and DNase I (1 µg/mL) during 1 h at 4°C followed by 10% sarkosyl and 70% amplitude sonication of 5 pulses of 10 s each with pauses of 10 s between pulses.
3	Incubation of suspension samples with lysozyme (10 mg/mL) and DNase I (1 µg/mL) during 1 h at 4°C followed by 70% amplitude sonication of 5 pulses of 10 s each with pauses of 10 s between pulses.
4	Addition of 1% triton + 0,1% SDS and 70% amplitude sonication of 5 pulses of 10 s each with pauses of 10 s between pulses.
5	Incubation of suspension samples with lysozyme (10 mg/mL) and DNase I (1 µg/mL) during 1 h at 4°C followed by 10% sarkosyl + 0,1% SDS and 70% amplitude sonication of 5 pulses of 10 s each with pauses of 10 s between pulses.
6	Addition of lysozyme (10 mg/mL) and DNase I (1 µg/mL) and 0,1% SDS to the suspension of samples, followed by 70% amplitude sonication of 5 pulses of 10 s each with pauses of 10 s between pulses.
7	Incubation of suspension samples with lysozyme (10 mg/mL) and DNase I (1ug/mL) during 1 h at 4°C followed by 20% sarkosyl and 70% amplitude sonication of 7 pulses of 10 s each with pauses of 10 s between pulses.

Table 2. Different cell lysis conditions used in the optimization of the production of recombinant tetraspanin LELs.

Western blot and Dot blot Analysis. For western blot analysis, samples were loaded onto 10% or 12% polyacrylamide gels.
Where indicated, AviCD9LELAvi, as well as a CD9LEL constructs that were not tagged with the Avi sequence were produced and 6 ml of each recombinant peptide was incubated with streptavidin (Nanovex Biotechnologies) for 15 minutes at RT using two different ratios (3-fold molar excess and 10-fold molar excess of streptavidin/tetraspanin LEL). Samples were boiled in Laemmli buffer and resolved in a polyacrylamide gel. After electrophoresis, the proteins were transferred to a PVDF membrane (Biorad).
For dot blot analysis, samples were spotted onto a 0,22 mm pore size nitrocellulose membrane (GE Healthcare) and let to dry.

Membranes were subsequently blocked with 5% non-fat dry milk and blotted with ABC Peroxidase Standard Staining Kit (Thermo Fisher Scientific) for 30 minutes at RT or incubated overnight with primary antibodies at 4ºC in a humidified chamber. After washing, membranes were probed with secondary antibody anti-mouse horseradish peroxidase (Thermo Fisher Scientific) and Enhanced chemiluminescent (ECL) HRP substrate (Thermo Scientific). Chemiluminescence signal was detected using the LAS4000 mini Image System analyzer from Fujifilm and software ImageQuant-TL (GE Healthcare).

Immunofluorescent analysis. 100 ml of biotinylated CD9, CD63 and CD81 LELs were incubated with 5 ml of streptavidin-sepharose beads (GE Healthcare) for 30 min. Primary antibodies against the three different tetraspanins (hybridoma supernatants) were added and incubated overnight at 4°C. Next, samples were washed three times with TBS-T and incubated for 30 min at 4°C with an AlexaFluor 488 goat anti-mouse IgG secondary antibody (Invitrogen). Samples were washed three times with TBS-T and mounted on coverslips with fluoromount (Thermo Fisher). Confocal images were obtained with a Leica TCS-SP5 confocal scanning laser microscope and Leica confocal LAS software.

Coupling of recombinant tetraspanins to nanovesicles. CD9, CD63 and CD81 biotinylated recombinant tetraspanin-LEL were incubated with (strept)avidin-coupled niosomes. Incubation of recombinant tetraspanins and nanovesicles was performed ON in a tube rotator at RT. Unbound LEL peptide was removed by Size Exclusion Chromatography. Sepharose CL-2B (GE Healthcare) was stacked in a 1 ml syringe (BD, Plastipak) and equilibrated using 0.22 mm filtered PBS, thereby allowing the Sepharose to reach a final matrix length of 6 cm at a diameter of 0,75 cm . Gravity elution was next performed and 20 sequential fractions of two drops (approximately 100 ml) were collected for each sample.

Natural EVs. Human breast carcinoma cell-derived EVs were isolated by SEC from conditioned media of MCF7 cell cultures as described previously (17). Mouse dendritic-cell derived EVs were isolated from conditioned cell culture medium by differential ultracentrifugation as detailed in (18).

Nanoparticle Tracking Analysis (NTA). Size distribution and concentration of nanovesicles was determined by measuring the rate of Brownian motion using a NanoSight LM10 system (Malvern) equipped with 405 nm laser. For each sample, at least 2 videos of 30 s were recorded and analysed with a detection threshold 10. Data was obtained using a shutter speed of 345 and a camera gain of 1.00. The measurements were performed and monitored at ambient temperature. Recorded videos were analysed with NTA Software version 2.2. Samples were diluted in PBS until particle concentration was within the dynamic range of NTA Software.

Electron Microscopy (EM). For cryo-EM, niosome samples were directly adsorbed onto glow-discharged holey carbon grids (QUANTIFOIL). For vitrification, grids were blotted

at 95% humidity and rapidly plunged into liquid ethane with VITROBOT (Maastricht Instruments BV).
For immuno-EM, samples were fixed in 2% paraformaldehyde in PBS and deposited onto Formvar/carbon-coated EM grids, previously pre-coated with Poly-L-lysine (MW of 15,000-30,000 kDa, Sigma Aldrich) as described before (19). The niosome-coated grids were washed with PBS and finally blocked with PBS/1% BSA for 15 min. Blocked grids were transferred to a drop of PBS/0.1% BSA containing primary antibody and incubated ON at 4°C in a humidified chamber. The grids were washed on a drop of PBS, transferred to a drop of PBS/0.1% BSA containing secondary antibodies conjugated to 15 nm gold-particles (Aurion) and incubated for 2 hours at RT in a humidified chamber. Grids were washed with dH_2O and fixed with 1% glutaraldehyde, washed with H_2O and stained with 2% uranyl acetate for 1 min at RT. Afterwards, samples were vitrified as described above and visualized using a JEM-2200FS Field Emission TEM equipped with a digital camera (JEOL).

Bead-assisted flow cytometry. Bead-assisted bulk flow cytometry analysis of niosome or EV samples was performed as previously described (17). Briefly, samples were incubated with aldehyde/sulfate-latex beads (4 µm from Invitrogen) and sequentially incubated with primary antibodies (hybridoma supernatants) and secondary anti-mouse IgG conjugated to Alexa 647 (Life Technologies). Samples were analysed using a FACS Canto II (Becton Dickinson) and FlowJo software (version X Tree Star).

High-resolution flow cytometry. For immunocharacterization of decorated niosomes, samples were incubated for 1h at RT with phycoerythrin (PE)-conjugated monoclonal antibodies. Antibodies used were: anti-CD9PE (clone VJ 1/20, Immunostep) and anti-CD63PE (Clone H5C6, BD Bioscience) at concentrations suggested by the manufacturer. Sucrose density gradient were used for the removal of free unbound dye (20). Briefly, bottom-up density gradient floatation was performed by mixing samples with 1.5 mL 2.5 M sucrose. Samples were next overlaid in SW40 tubes (Beckman-Coulter) with fifteen 700 µL sucrose fractions of decreasing molarity (2.0 M until 0.4 M). Gradients were then subjected to ultracentrifugation for 16 hours at 200,000g (SW40 rotor; 4°C; 39,000 rpm; RCF average 192,072g; RCF max 270,519g; κ-factor 144.5). Twelve fractions of 1 mL were collected from which the density was determined by refractometry using an Atago Illuminator (Japan). Prior to acquisition, sucrose samples were diluted 20 times in PBS. As described previously, qualitative and quantitative analysis of niosome-containing samples were then performed using a jet-in-air-based BD Influx™ flow cytometer (Becton Dickinson) optimized for the detection of submicron-sized particles (20,21). Data obtained was analysed using FlowJo Software version X.

Statistical analysis. Data analysis was performed using GraphPad Prism version 6.0 (GraphPad Software Inc). Error bars represent the standard deviation (SD).

RESULTS AND DISCUSSION

Production of recombinant AviLELAvi proteins

For the production of recombinant human tetraspanin large extracellular loop (LEL) domains we chose three members that are widely employed in EV research, namely CD9, CD63 and CD81. Sequences corresponding to their LELs were amplified by PCR. The 15 aminoacid sequence of the AviTag peptide, that allows recognition and site-specific biotinylation by the highly-specific *Escherichia Coli (E. coli)* biotin ligase A enzyme (BirA) (16), was then introduced at both N- and C-term ends (**Table 1**) together with restriction sites for subcloning into pGEX-4T2 vector in reading frame with the glutathione-S-transferase (GST). The plasmids coding for the Avi-tagged LEL of either CD9, CD63 or CD81 (Avi*CD9 LELAvi-pGEX-4T2*, Avi*CD63 LELAvi-pGEX-4T2* or Avi*CD81 LELAvi-pGEX-4T2)* were co-transformed into *E. coli* (BL21 DE3) cells, together with a plasmid encoding for BirA enzyme. Cells were grown and selected in the presence of antibiotics (ampicillin and chloramphenicol). Cultures were supplemented with D-Biotin and IPTG, to induce both GST and biotinylation.

Bacterial lysis was optimized by testing six different conditions (**Table 2**). These supernatants were affinity-purified with glutathione-sepharose and analysed by SDS-PAGE and Coomassie Blue staining (**Fig. 1A-B**). Fusion protein recovery was greatly improved by increasing Sarkosyl concentration to 20% (lysis condition 7 in **Table 2 Fig. 1C**). To determine biotin concentration for maximal biotinylation of the recombinant tetraspanin, AviCD63LELAvi transformed *E. coli* were cultured in the presence of different concentrations of D-biotin. Total bacterial lysates were analysed by dot-blot to assess recombinant tetraspanin production, as well as biotinylation. When normalized to the total load of protein detected with anti-CD63 mAb, we found that biotinylation efficiency (as detected with ABC Peroxidase) slightly increased with 20 µM of biotin when compared to the 5 µM condition (ratio of ABC signal/anti-CD63 signal was 1.4 when 5 µM was set to 1). 20 µM of D-biotin was the concentration of choice for all further experiments, since no major differences were observed when the biotin concentration was increased to either 75 µM (ratio of 1.5) or 200 µM (ratio of 1.3) (**Fig. 1D**).

Purification of the biotinylated GST fusion recombinant LEL-tetraspanins was then performed by affinity chromatography. First, the highly-specific interaction between GST and glutathione was employed to capture proteins of interest on sepharose beads. In a second step, proteins were cleaved and eluted from GST using the site-specific protease thrombin. Next, thrombin was removed using benzamidine-sepharose beads (**Fig. 2A**). Each sequential step of the production of the recombinant AviLELAvi peptides was evaluated by SDS-PAGE analysis and Coomassie Blue staining. These analyses clearly showed that the recombinant GST-LEL is greatly enriched after affinity purification with glutathione-sepharose beads (bands at 37 kDa in lanes 1-3 and 2-4, respectively (**Fig. 2B** and **C**). Cleavage with thrombin was complete, as only the 23 kDa band of GST could be detected in lanes 5-7 (**Fig. 2B**). Because the cleaved tetraspanin-LELs are difficult to

detect by Coomassie Blue staining due to their small size (a faint band can be appreciated for CD9LEL in lane 8, red arrow in **Fig. 2B**), Western Blot analyses were used to confirm both the biotinylation and purity of the final recombinant CD9, CD63 and CD81 products (**Fig. 2C**). The molecular weight detected for these peptides corresponds to the 12-15 kDa expected for the LEL of tetraspanins plus the two AviTags (**Fig. 2C**, red arrows, lanes 5-7).

Dot Blot analysis, performed using tetraspanin specific monoclonal antibodies or the Avidin-Biotin HRP Complex (ABC Peroxidase), showed strong positive reactions, indicating that the recombinant LEL-tetraspanins were biotinylated and maintained immunogenicity by proper folding (**Fig. 2D**). Within the final product, MicroBCA assays revealed a higher yield for CD9 and CD81 (112.3 ± 16.4 and 106.2 ± 14.3 mg/ml) recombinant peptides than for CD63 (53.8 ± 14.8 mg/ml mean ± SD from 5 independent determinations). Since the LEL of CD63 contains two sites for N-glycosylation, the absence of this post-translational modification may be affecting the protein stability and final yield, although it does not seem to impair antibody recognition.

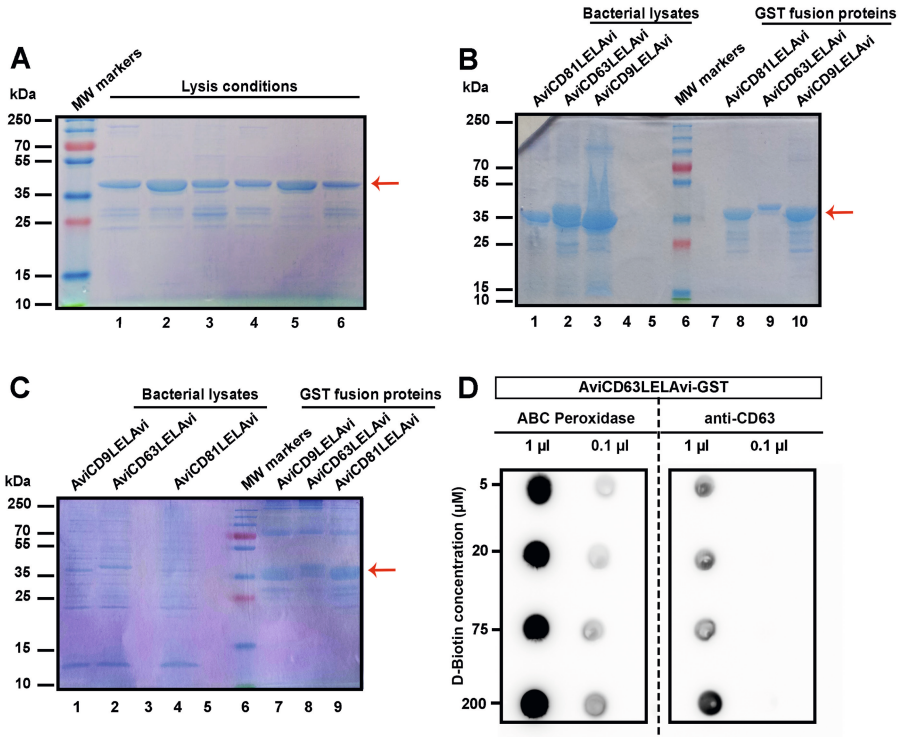

Figure 1. Optimization of the purification process of the recombinant biotinylated tetraspanin-LEL peptides. (A) Cell lysis optimization. Six different lysis conditions (indicated in Table 2) were tested. 10 µl of the obtained AviCD63LELAvi-GST coupled to Glutathione-sepharose beads were lysed in Laemmli buffer, subjected to SDS-PAGE and analysed by Coomassie Blue staining. **(B)** Efficiency of recombinant protein recovery. Non-soluble fraction of the bacterial lysates lysates obtained with lysis condition 2, as well as the recombinant affinity purified AviLELAvi-GST proteins,

were tested by SDS-PAGE to check the recovery of GST fusion proteins from *E.coli*. Lanes 1-3: Bacterial lysates. Lanes 8-10: 10 µl of LELs-GST-Glutathione-sepharose. **(C)** Final optimization of lysis conditions. Total bacterial lysates obtained using condition 7, as well as the recombinant affinity purified AviLELAvi-GST proteins were analysed by SDS-PAGE. Lanes 1,2,4: Non-soluble bacterial lysates. Lanes 7-9: 10 µl of LELs-GST-Glutathione-sepharose obtained. Red arrows indicate the expected molecular weight for the recombinant fusion tetraspanins, which is 37 kDa. **(D)** Optimization of D-biotin labelling. Dot Blot analysis using an ABC Peroxidase Standard Kit and anti-CD63 specific antibody (clone *TEA 3/10*) for detection of the indicated volumes of bacterial cell lysates from AviCD63LELAvi-GST-transformed cultures grown in the presence of the indicated biotin concentrations.

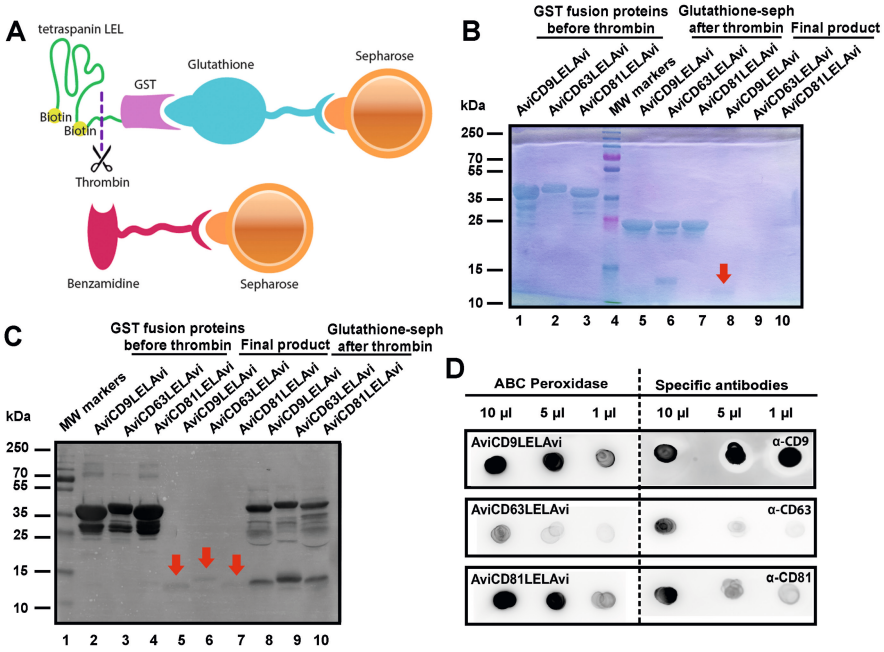

Figure 2. Production of recombinant tetraspanin-LELs. (A) Schematic illustration of the affinity chromatography method used for recombinant tetraspanin LELs purification using glutathione-sepharose beads, thrombin and benzamidine-sepharose beads. **(B)** Follow up of recombinant tetraspanin LELs production. The purification process was followed by Coomassie Blue staining after SDS-PAGE separation. Lanes 1-3: Samples of 10 µl Glutathione-sepharose beads before Thrombin treatment. Lanes 5-7: 10 µl of Glutathione-sepharose beads after treatment with Thrombin. Lanes 8-10: 20 µl of each supernatant after benzamidine-sepharose removal of Thrombin. Red arrows indicate the final LEL biotinylated product. **(C)** Western blot analysis of recombinant tetraspanin LELs. Samples were subjected to SDS-PAGE and detected by chemiluminiscence using Avidin-Biotin-HRP Complexes. Lanes 2-4: Samples of 10 µl of AviLELAvi-GST of CD9, CD63 and CD81 coupled to Glutathione-sepharose. Lanes 5-7: Samples of 20 µl of AviCD9LELAvi, AviCD63LELAvi and AviCD81LELAvi. Lanes 8-10 Samples of 10 µl of Glutathione-sepharose beads after Thrombin treatment. Red arrows indicate the final LEL biotinylated product. **(D)** Dot blot immunodetection of recombinant tetraspanin LELs. The final products, biotinylated CD9, CD63 and CD81 LELs, were detected by Dot-blot using ABC Peroxidase Standard Staining Kit and monoclonal antibodies directed against CD9 (clone VJ 1/20), CD63 (TEA 3/10) and CD81 (5A6).

To assess the degree of biotinylation of the recombinant tetraspanin LELs, we produced and purified AviCD9LELAvi, as well as an untagged CD9LEL protein. Recombinant LELs were incubated with streptavidin (SA) and analysed by Western blot using an anti-CD9 antibody (**Fig. 3A**). When the Avi-tagged biotinylated CD9 LEL was incubated with SA, the majority of CD9 signal was found at higher molecular weights (**Fig. 3A,** lanes 3-4), due to the binding of one or two LEL peptides to the 52.8 kDa SA molecule. As expected, no binding between SA and the untagged CD9LEL could be observed (Fig. 3A, lanes 5-6), proving that the interaction between the tetraspanin LEL and SA molecules was mediated by biotin. Different amounts of SA (3-fold molar and 10-fold molar excess) were tested but showed no improved binding of CD9LEL to SA (**Fig. 3A**, lane 4). However, a small amount of Avi-tagged LEL peptide remained unbound (**Fig. 3A,** lanes 3-4), suggesting that, although highly efficient, complete biotinylation was not achieved. Interestingly, the signal of the SA-bound recombinant peptide was much stronger when compared to the signal obtained when only the soluble peptide was analysed (**Fig. 3A**, lane 2). This suggests that, even though the soluble peptide can be recognized by the CD9 antibody, the recognition is greatly enhanced upon binding to SA. Since the LEL domain is biotinylated at both its C- and N-terminus, binding to the tetrameric streptavidin may help to acquire a three-dimensional conformation that more closely resembles that of the native tetraspanin molecule. Indeed, binding of most anti-tetraspanin mAbs seems to be conformation-dependent since reactivity is lost under reducing conditions.

As a proof of concept to show that our biotinylated recombinant proteins bind to streptavidin and can be detected by a variety of immunoassays, we incubated biotinylated recombinant tetraspanins with streptavidin-coated sepharose beads, and stained these beads for immunofluorescence analysis using confocal microscopy. A bright specific signal could be observed on the beads when biotinylated recombinant CD9-, CD63- and CD81-LELs were incubated with SA-beads and detected with their corresponding specific antibodies (**Fig. 3B, lower panels**). No signal was observed when uncoated SA-beads were stained or when AviCD9LELAvi-coated microspheres were stained with a primary antibody against CD63 tetraspanin (**Fig. 3B, upper panels**).

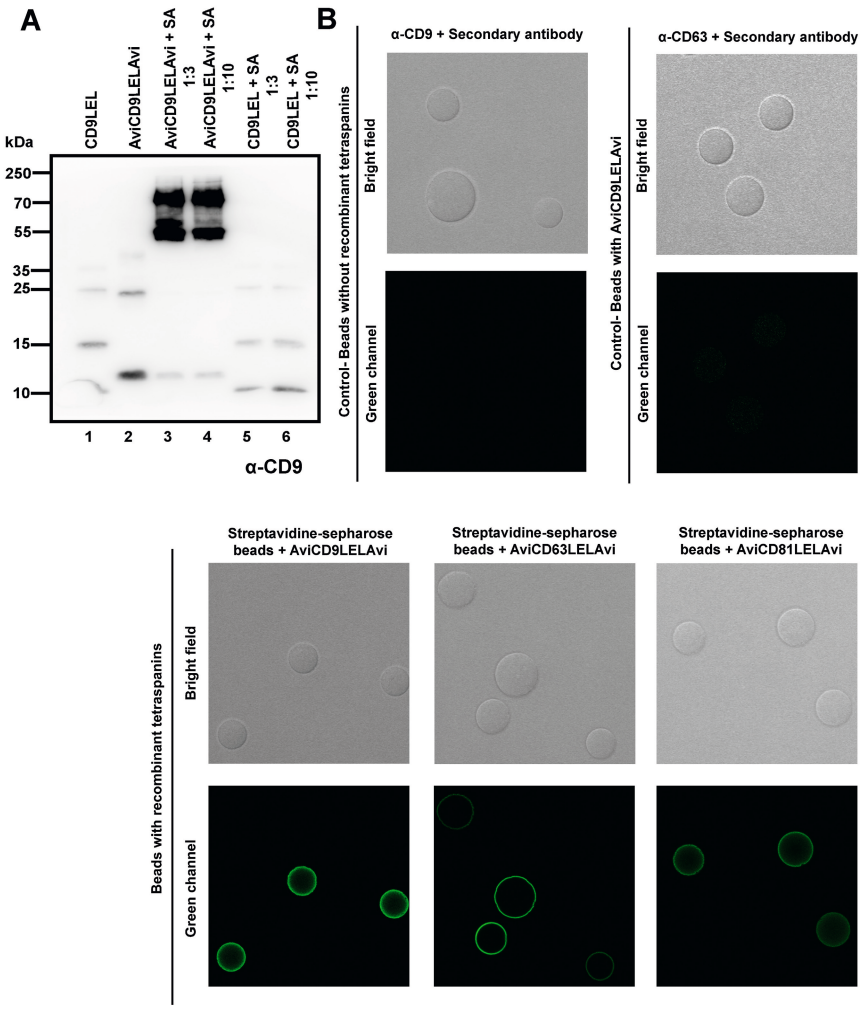

Figure 3. Biotinylation efficiency of recombinant tetraspanins. (A) Samples were run on 12% SDS-PAGE and CD9 was visualised using a specific monoclonal antibody (clone VJ 1/10) followed by a secondary goat anti-mouse antibody conjugated to HRP. Lane 1: 20 µl of non-biotinylated CD9LEL. Lane 3: 20 µl of AviCD9LELAvi. Lanes 3-4: 20 µl of AviCD9LELAvi and Streptavidin with a 3-fold molar excess and 10-fold molar excess, respectively. Lanes 5-6: 20 µl CD9LEL and Streptavidin with a 3-fold molar excess and 10-fold molar excess, respectively. (**B**) Representative images of streptavidin beads incubated with recombinant tetraspanins (lower panels) and stained with specific mAbs and secondary antibodies. Primary antibodies used were anti-CD9 (VJ 1/20), -CD63 (TEA 3/10) and -CD81 (5A6). Upper panels show negative controls obtained either by staining streptavidin beads not loaded with recombinant tetraspanins with both primary and secondary antibodies (upper pannel, right) or streptavidin beads incubated with AviCD9LELAvi recombinant tetraspanin and stained with unmatched anti-CD63 (TEA3/10) primary antibody. An optical section acquired with a Leica TCS-SP5 confocal microscope is shown.

Decoration of synthetic nanovesicles with biotinylated recombinant tetraspanins. Synthetic niosomes, surface-bioconjugated to (strept)avidin molecules, and either fluorescently labelled or not, were incubated with the biotinylated recombinant tetraspanin LEL peptides. Although the binding of biotin to (strep)avidin is known to be a fast process in solution, after immobilization onto a surface the kinetics of the process can be more complex and therefore longer incubation times may be necessary for optimal coupling (22-24). The coupling process was therefore performed with an estimation of two AviLE-LAvi molecules (containing two biotin molecules each) per (strept)avidin molecule, (that have four potential biotin binding-sites available) during an overnight incubation in a tube rotator at RT. Size Exclusion Chromatography (SEC) was used to remove the unbound LEL tetraspanins. After SEC, 20 fractions were collected from each sample and analysed by dot blot to determine in which fractions the decorated nanovesicles eluted. Avidin-Biotin-HRP Complex (ABC peroxidase) would bind to both the free biotin-binding sites on the (strept)avidin as well as to free biotin molecules on the tetraspanin LEL. So, to unequivocally evaluate the presence of recombinant tetraspanins on the niosome-containing fractions, the dot blots were also developed using specific monoclonal antibodies against each tetraspanin. Dot-blot analyses demonstrated that the decorated nanovesicles typically eluted between fractions 6 and 10 (**Fig. 4A**). The small variability in the elution of the positive decorated niosomes-containing fractions between different SEC columns may be due to the variability in collecting the fractions from the SEC process. Dot blot analysis, a fast and simple technique, is useful to precisely determine the nanovesicle-containing fractions after SEC and could aid to the standardization of this isolation protocol.

To further determine the presence of nanovesicles in the dot blot fractions, different SEC-fractions of CD9-decorated niosomes were tested by Nanoparticle Tracking Analysis (NTA). Data shows that the majority of niosomes eluted in fractions 6-8 (**Fig. 4B, upper plot**), thereby confirming the elution profile previously obtained by dot blot analysis. For further analyses, decorated niosomes-containing fractions were pooled and their size distribution and concentration were determined by NTA. The vast majority of decorated niosomes appeared to be between 100 and 300 nm in size diameter, as displayed in a representative size distribution profile of CD63-niosomes (**Fig. 4B, lower plot**). Concentration of pooled positive fractions, for both CD9 and CD63 decorated nanovesicles, was determined to be around 1 x 10^{11} particles/ml.

Bulk analysis of the presence of recombinant CD9 and CD63 on artificial nanovesicles was carried out by bead-assisted flow cytometry (17) (**Fig. 4C**). Here, the pooled positive fractions of decorated niosomes were adsorbed onto 4 μm diameter aldehyde/sulfate latex beads, incubated with antibodies directed against CD9 or CD63 and stained with a secondary antibody conjugated to Alexa Fluor 647. Bright positivity was observed for beads that had been previously incubated with CD9 or CD63 decorated niosomes when compared to uncoated beads incubated with both primary and secondary antibodies (**Fig. 4C**).

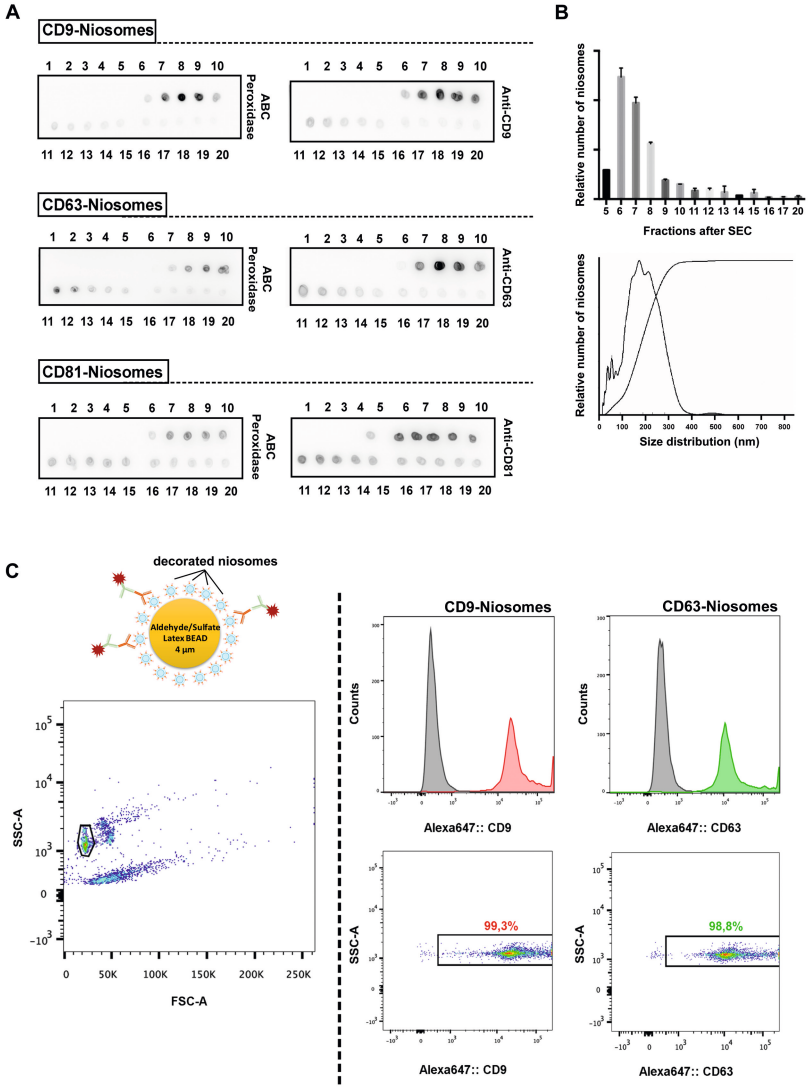

Figure 4. Characterization of tetraspanin-LEL-decorated niosomes. (**A**) Evaluation of SEC elution profile of decorated niosomes by dot blot. Niosomes were coupled to biotinylated recombinant tetraspanins (CD9, CD63 and CD81LEL proteins). 1 ml of each of the 20 fractions collected after SEC was spotted onto a nitrocellulose membrane for dot-blot analysis using ABC-peroxidase and specific monoclonal antibodies against tetraspanins CD9, CD63 and CD81 (clones VJ 1/10, TEA 3/10 and 5A6, respectively). (**B**) NTA-based size determination and quantification. SEC elution profile was confirmed by quantitative NTA analyses of different SEC fractions collected from CD9-niosome samples (upper plot). Particle concentration and mean size distribution of the pooled positive SEC fractions were also measured. A representative size distribution profile is shown for CD63-decorated niosomes (lower graph). (**C**) Bead-assisted flow cytometry of decorated niosomes. 4 µm latex beads were coated with decorated niosomes (pool of positive fractions recovered after SEC) and labeled with primary anti-CD9 (VJ 1/20) and anti-CD63 (TEA 3/10) mAb

followed by Alexa647-labeled anti-mouse secondary antibody. Single beads were selected in the side scatter (SSC) / forward scatter (FSC) dot plot for all samples (left panel). Alexa647-positivity was evaluated in histograms (upper panels) or in a SSC/Alexa647 dot plot (lower panels). Geo-Mean values for both CD9- and CD63-decorated niosomes is indicated in the histogram plots, showing high positivity when compared to the negative controls. Uncoated beads incubated with primary and secondary antibodies were used as negative control (filled grey histograms). The percentage of Alexa647-positive beads is indicated in the dot plots. Experiment shown is representative for n= 3.

Cryo-electron microscopy of tetraspanin-decorated niosomes.

Cryo-electron microscopy (cryo-EM) allows visualization of samples in their native frozen-hydrated state. Cryo-EM analyses of niosome-samples revealed the presence of single nanovesicles with a spherical morphology, similar to the one observed for EVs (25). A bilayer membrane could be clearly appreciated at higher magnification (**Fig. 5C, lower panel**). Interestingly, some lamellar and multilamellar structures were also visualized (**Fig. 5A**). Although rare, the presence of these multilamellar structures has been reported with various EV samples isolated from biological fluids (26). The size range of these nanovesicles coincided with the size distribution profile that we previously determined by NTA. The majority of nanovesicles were between 100 and 200 nm, but a few smaller (50 nm) and bigger (>200 nm) niosomes were also detected. Thus, our bioengineered niosomes reproduce the heterogeneity observed with natural EVs.

To further characterize the presence of recombinant tetraspanins on the surface of these nanovesicles in their native state, cryo-EM was combined with immunogold labelling. To this end, an incubation step with specific antibodies directed against CD9 or CD63 was followed by incubation with secondary antibodies conjugated to 15 nm gold particles. Niosomes positively decorated with CD9 and CD63 were observed (**Fig. 5B**), although the number of gold-particles associated to the niosome-surface was lower than expected. Due to the small size of niosomes steric hindrance interactions between antibodies (with an average size of around 10 nm and coupled to gold nanoparticles of 15 nm) are likely to affect labelling-intensity. Another important consideration when performing immunolabeling is the chemical fixation process, which might alter the ultrastructure of samples (27).

Because of the perspective of view in 2-D images, a gold nanoparticle may seem to be close to the membrane of nanovesicles whereas it is actually not. Thus, to confirm the specificity of the attachment of the gold nanoparticles to the membrane of decorated niosomes we performed a cryo-Electron Tomography (cryo-ET) approach. Cryo-ET offers the possibility to observe samples from different tilt angles, thereby avoiding the ambiguity derived from 2-D projection images (28). By observing a positively stained CD63-decorated niosome under two different tilt angles, -57° and +43° (Fig. 5C, left and right, respectively) we confirmed that the position of the gold nanoparticles was the same as observed for the untilted CD63-decorated niosome (**Fig. 5C**).

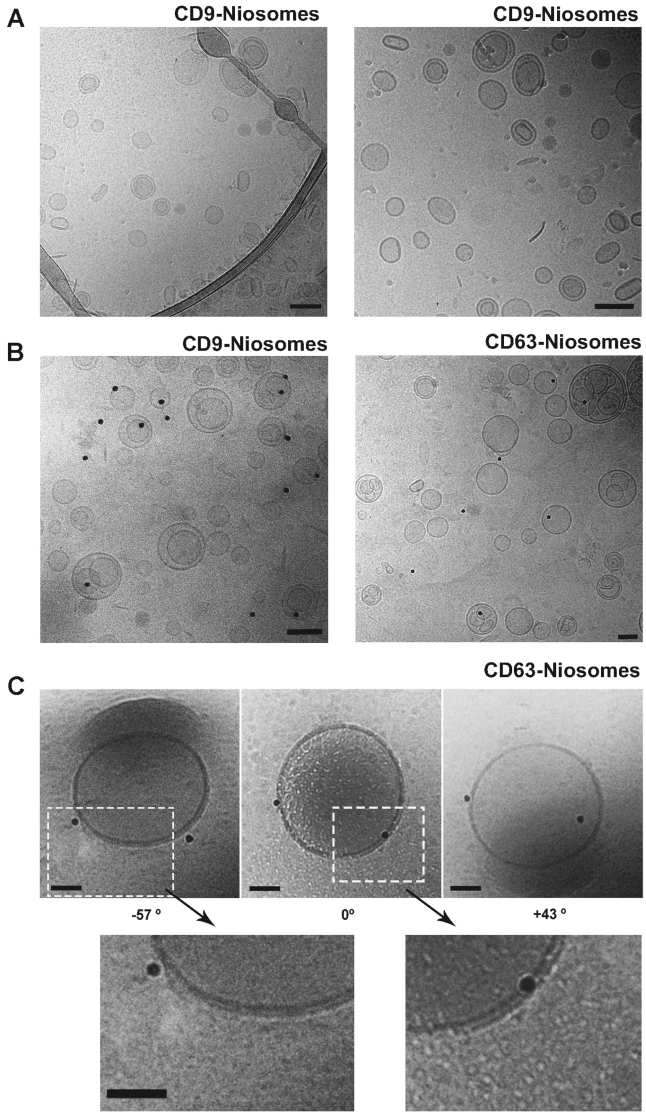

Figure 5. Cryo-Electron Microscopy of decorated niosomes. (A) Cryo-EM of CD9-Niosomes. **(B)** Immunogold staining of CD9 and CD63-decorated niosomes. Antibodies used were anti-CD9 (clone VJ 1/10) on AviCD9LELAvi-decorated niosomes and anti-CD63 (clone TEA 3/18) on AviCD63LELAvi decorated niosomes. **(C)** Cryo-Electron Tomography analysis of a CD63-decorated niosome. CD63-decorated niosome observed without any inclination (0º), or after tilting the sample either -57º or +43º. Magnification of bilayer membrane structure is shown. Bars = 100 nm for all images.

Side by side comparison of tetraspanin-decorated niosomes and natural EVs.
So far, we have provided evidence that most techniques employed for the characterization of naturally occurring EVs can be easily applied to tetraspanin-decorated niosomes. To provide a side by side comparison, we isolated EVs from conditioned media of the breast cancer carcinoma cell line MCF7 by SEC. We measured particle concentration of these EV samples and of niosomes decorated with CD9 peptide (both regular and fluorescent) and we loaded serial dilutions of equal amounts of particles on a nitrocellulose membrane that was developed with anti-CD9 mAb in a dot-blot. A very similar signal was obtained with natural EVs and CD9-decorated niosomes (**Fig.6A**), whereas fluorescent-CD9 niosomes showed a brighter CD9 signal. When matching number of EV and niosome particles were incubated with sulphate-aldehyde latex beads, and analysed by flow cytometry, same results were generated (**Fig. 6B**). Although different sources of naturally occurring EVs may present different quantities of tetraspanins on their surface, these data show that we are able to produce niosomes with immunoreactive tetraspanin regions with similar antigen-densities as those found on naturally occurring EVs.

High-resolution flow cytometric analyses of tetraspanin-decorated niosomes.
To obtain further evidence for the presence of recombinant tetraspanins on the surface of niosomes at a single particle level, and to test the suitability of these decorated niosomes as standards for flow cytometric analysis of EVs, the bioengineered niosomes were analysed by high-resolution flow cytometry (21).

Again, a side by side comparison was performed with CD9-decorated niosomes and natural EVs, in this case derived from DC-conditioned media and enriched by differential ultracentrifugation. The scatter plot of both samples was very similar, in both fluorescence vs FSC and SSC vs FSC dot plots (green dots for EVs and red dots for niosomes, **Fig 6C**). For comparison, calibration polystyrene beads of 200 nm in diameter (dark grey) or 100 nm in diameter (light grey) were also included, clearly highlighting a very different scattering behaviour of this reference material (**Fig 6C**).

For high-resolution flow cytometry detection fluorescence threshold triggering was performed (20). To this end, we first assessed whether the fluorescent signal derived from the carboxyfluorescein labelled 1,2 dioleoyl-sn-glycerol phosphoethanolamine incorporated within the bilayer of the niosomes was enough to resolve them above the threshold and background noise (**Fig. 7A**). Again, decorated niosomes were compared in side by side measurements on the same day with natural EVs isolated from BMDCs and stained with PKH67, as described before (29). The scatter pattern observed within the fluorescein vs rw-FSC dot plots of CD9-niosomes resembles the pattern found in EV samples. The scatter plots displaying SSC vs rw-FSC also show similar scatter characteristics, although the natural BMDC-derived EVs preparations displayed a slightly more complex pattern than the decorated niosomes (**Fig. 7A**). These results thus show that niosomes decorated with fluorescein-molecules display enough fluorescence to

be resolved by fluorescence-based high-resolution flow cytometric analysis and do not need further generic labelling to perform fluorescence-threshold triggering.

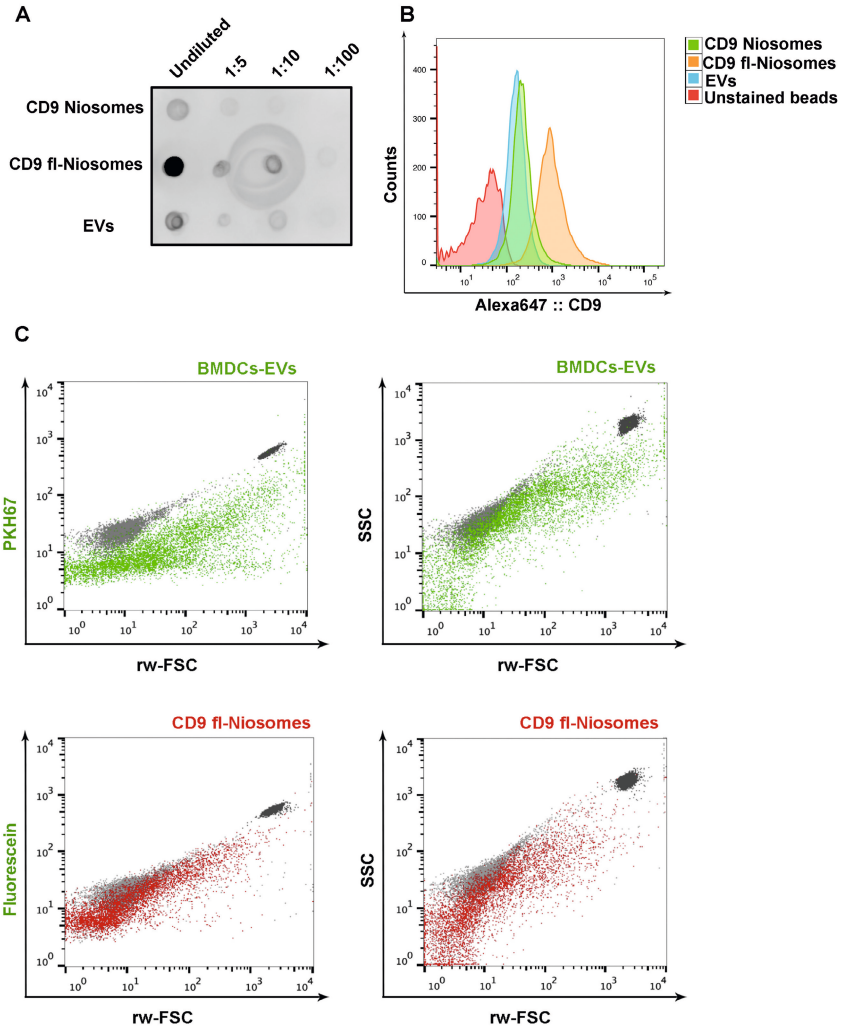

Figure 6. Side by side comparison of CD9-decorated niosomes and natural EVs. (A) Dot blot analysis of serial dilutions of CD9-niosomes, CD9-fluorescent niosomes and EVs isolated by SEC from MCF7 conditioned media. Number of particles were previously matched by NTA quantification of the three samples. **(B)** Bead-assisted flow cytometry of CD9-decorated niosomes and EVs isolated from MCF7 cell culture supernatant. Upon capture, beads were incubated with anti-CD9 VJ1/20 mAb and stained with secondary anti-mouse-Alexa 647**.** Negative control corresponds to beads coated with EVs in the absence of primary antibody. **(C)** High-resolution flow cytometry. Dot plots of fluorescence vs FSC or SSC vs FSC of EVs from DC conditioned media (green) or CD9-decorated fluorescent niosomes (red). As a reference 200 nm and 100 nm yellow-green fluorescent (505/515) FluoSphere Carboxylate-Modified Microspheres (ThermoFisher) are plotted alongside (light and dark grey populations, respectively).

To confirm that that nanovesicles were individually measured samples were serially diluted and acquired. Upon dilution of fluorescein-labelled niosomes, the reduction in event rate displayed a linear correlation and both light scatter and fluorescent signals remained unaltered (**Fig. 7B**), thereby ruling out swarm detection (28-30).

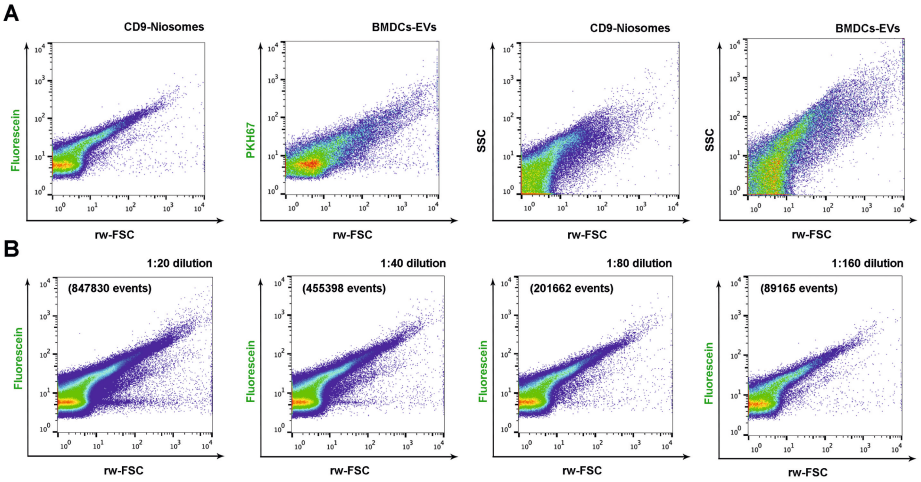

Figure 7. High-resolution flow cytometric analysis of decorated fluorescent niosomes. (A) Dot plots displaying fluorescence from fluorescein or PKH67 vs reduced wide-angle FSC (rw-FSC) and SSC vs rw-FSC of fluorescein containing CD9-niosomes and mouse BMDC-derived PKH67-stained EVs. **(B)** Serial dilutions of the CD9-niosome sample were analysed. Fluorescence vs rw-FCS dot plots for serial dilutions (1:20, 1:40, 1:80, 1:160 from left to right) are shown. Number of events for each dilution plots are indicated. Plots are representative for n= 3.

The next step was to determine tetraspanin expression at the single niosome-level. Here, niosome-samples were stained with PE-conjugated anti-tetraspanin antibodies and floated into a sucrose density gradient to separate them from unbound dye. Interestingly, when performing density gradient floatation to separate niosomes from unbound antibodies, we observed that niosomes migrated to the lowest density fraction of the gradient (density = 1.10-1.06 g/mL) (**Fig. 8C**). Depending on the cellular origin, naturally occurring EVs usually float to a buoyant density of 1.13-1.19 g/mL, (30). This difference in buoyant density likely reflects differences in the content of the vesicles. The difference in buoyant density of both types of nanovesicles, could be of specific interest for spike-in experiments, since niosomes could then be easily separated from EVs by density fractionation.

Stained niosomes were thereafter analysed by high-resolution flow cytometry using fluorescent threshold triggering. 11.8% of CD9-niosomes stained with anti-CD9-PE displayed specific positive signal when compared to a CD9-niosome sample that was

stained with CD81-PE (**Fig. 8A, upper right panel**). For CD63-niosomes, 11.3% of events were found positive (**Fig. 8A, lower right panel)**. Interestingly, when PE-fluorescence was displayed in histograms overlaid with their respective controls, it was clear that the mean fluorescence intensity (MFI) of the entire population of niosomes was shifted (**Fig. 8B**). This indicates that the majority of the niosomes are labelled with tetraspanins, but not all of them could be resolved from the background due to the low number of epitopes on the surface. Indeed, when compared to the control sample there was a 1.5-fold change in the Geo-Mean of the total decorated niosome-population for both CD9 and CD63-niosomes. This range of positive events over the background is comparable to that observed when analyzing antibody-stained natural EVs (31). These data further show that the size of the EV imposes an enormous handicap when being analyzed by techniques relying on staining or labeling. Smaller and brighter probes are therefore urgently needed to achieve more quantitative results.

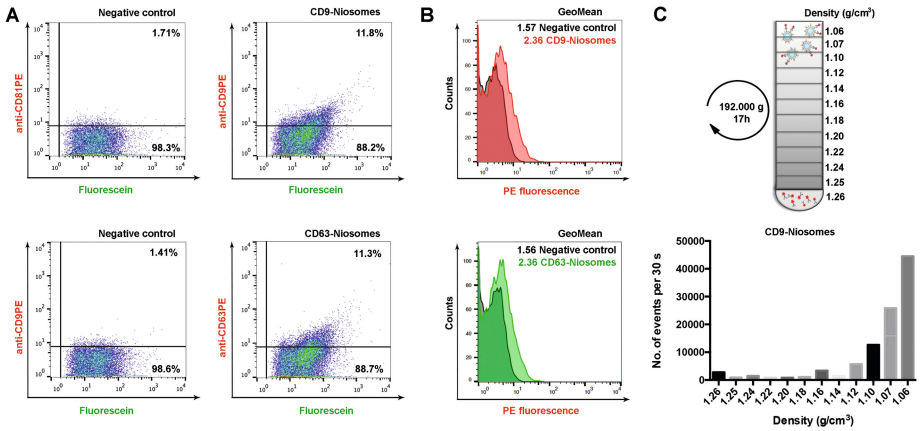

Figure 8. Immunocharacterization of CD9 and CD63 decorated niosomes by high-resolution flow cytometry. (A) Flow cytometric dot plots displaying CD9 and CD63 signal of fluorescein-containing CD9 and CD63-niosomes after staining with either anti-CD9-PE (clone VJ 1/20) or anti-CD63-PE (Clone H5C6) or matched PE-conjugated negative controls (CD9-niosomes stained with anti-CD81-PE or CD63-niosomes stained with anti-CD9-PE). Percentages of gated events are shown. **(B)** Histogram overlays for both CD9 and CD63-niosomes and their respective negative controls (darker histograms). GeoMean Fluorescence Intensities of the total populations are indicated. **(C)** Schematic representation of density gradient flotation performed on antibody-labeled decorated niosomes. Bar graph displaying the fractionation profile of CD9 and CD63-niosomes after sucrose density gradient flotation. The number of events in each fraction is determined using quantitative time-based flow cytometric analysis (number of fluorescein-positive events in 30 seconds).

Single vesicle characterization of EVs is highly challenging due to intrinsic features of the sample, including the limited number of antigens on the surface, which is directly limited by the size of the vesicle. Assuming a similar antigen distribution as the one of the cell of origin, it has been described that, even for high density antigens, the

number of molecules that might be present on the surface of EVs can go down to 10 molecules (32). For our design, we decided to use niosomes because of their similar size range and refractive index when compared to naturally occurring EVs. The use of particles with similar features to natural EVs allows good comparison, also for immunodetection, since analogous restrictions due to number of antigenic molecules and fluorescence intensity or gold labelling efficacy will occur. It is important to mention that antibody-labeling strategies for single EV-detection, such as the ones used along this manuscript for high-resolution flow cytometry and cryo-electron microscopy, have been proved useful for characterization of EV-subsets. They however carry their own limitations, like the already mentioned effects of antigen density distribution and steric hindrance of antibodies. Further improvements for the application of flow cytometry to the EV field are needed to obtain small sized but very bright fluorochromes to overcome these limitations. Yet, despite the fact that single-vesicle flow cytometry is still highly challenging, the high-throughput characterization of small vesicles with specific markers is one of the most powerful techniques available at this moment. The availability of proper standards suitable for immunolabeling would therefore greatly benefit the advances in the optimization of this technique. Moreover, the EVM here described have proven to also be suited for other isolation and characterization techniques currently employed in the EV field, such as SEC, density gradients, NTA, western-blot, bead-based flow cytometry and EM.

In addition, EV Mimetics may offer new possibilities as drug delivery systems and vaccines (33,34). Among the numerous nanotechnology-based therapies, lipid-based nanoparticles and niosomes have interesting biological properties, which include extensive biocompatibility, biodegradability and the ability to entrap both hydrophilic and hydrophobic drugs (34-36). These EVM may be able to increase the half-life in circulation of the cargo, minimize toxicity and increase the therapeutic effect (33-37).

Thus, here we describe for the first time a nanobiotechnological approach to generate an EVM. These bioengineered nanovesicles open up new possibilities for optimisation, cross-standardization and comparison of EV-measurements between laboratories and techniques.

The requirement for suitable standards for EV isolation, characterization and analysis methods in the fast developing EV-field is obvious (38), particularly since the techniques for EV isolation and characterization are constantly evolving, and their applicability is exponentially increasing. Appealing features such as size distribution, morphology and particle concentration make these bioengineered nanovesicles suitable for different EV isolation and detection procedures. We have chosen to initiate the development of EVMs with tetraspanin LELs, but the technology that we describe here is adaptable to the incorporation of different protein markers. By taking advantage of the high-affinity interaction between (strept)avidin and biotin molecules it is possible to perform sur-

face-decoration with any potential protein of interest, which make these nanovesicles tuneable. In addition, they can be generically stained with fluorescent dyes. Since the here-described surface-decorated niosomes display similar biophysical properties as naturally occurring EVs, and are suited for staining with antibodies directed against the most widely used tetraspanins within the EV-field, they can be powerful intrinsic controls for EV characterization platforms like NTA, Electron Microscopy and flow cytometry. Additionally, they are detectable by different bulk-based analysis techniques such as dot blot, western blot and bead-based flow cytometry. Moreover, because of their specific density properties, they could be easily adapted as spike-ins for robust assessment in all these techniques.

ACKNOWLEDGMENTS

The authors would like to thank Dr. David Gil and Dr. Maite Rejas for great assistance and guidance with Electron Microscopy, Henar Suarez for her help in bead-based flow cytometry and Ger Arkesteijn for his assistance with high resolution flow cytometry.

DECLARATION OF INTEREST STATEMENT

The authors declare no competing financial interest.

FUNDING SOURCES

This research was supported by grants from Fundación Ramón Areces and Ministerio de Economía y Competitividad (BFU2014-55478-R, REDIEX. SAF2015-71231-REDT, BIO2017-86500-R) cofounded by FEDER funds. E.L-A. was supported by the European Social Fund, GEIVEX Mobility and Autonomous University of Madrid STS fellowships, as well as by the European Union's Horizon 2020 research and innovation program under the Marie Skłodowska-Curie grant agreement No 722148.

REFERENCES

1. Yanez-Mo, M. e. a. (2015) Biological properties of extracellular vesicles and their physiological functions. *J Extracell Vesicles* **4**, 4:27066
2. Fais, S., O'Driscoll, L., Borras, F. E., Buzas, E., Camussi, G., Cappello, F., Carvalho, J., Cordeiro da Silva, A., Del Portillo, H., El Andaloussi, S., Ficko Trcek, T., Furlan, R., Hendrix, A., Gursel, I., Kralj-Iglic, V., Kaeffer, B., Kosanovic, M., Lekka, M. E., Lipps, G., Logozzi, M., Marcilla, A., Sammar, M., Llorente, A., Nazarenko, I., Oliveira, C., Pocsfalvi, G., Rajendran, L., Raposo, G., Rohde, E., Siljander, P., van Niel, G., Vasconcelos, M. H., Yanez-Mo, M., Yliperttula, M. L., Zarovni, N., Zavec, A. B., and Giebel, B. (2016) Evidence-Based Clinical Use of Nanoscale Extracellular Vesicles in Nanomedicine. *ACS Nano* **10**, 3886-3899
3. Consortium, E.-T., Van Deun, J., Mestdagh, P., Agostinis, P., Akay, O., Anand, S., Anckaert, J., Martinez, Z. A., Baetens, T., Beghein, E., Bertier, L., Berx, G., Boere, J., Boukouris, S., Bremer, M., Buschmann, D., Byrd, J. B., Casert, C., Cheng, L., Cmoch, A., Daveloose, D., De Smedt, E., Demirsoy, S., Depoorter, V., Dhondt, B., Driedonks, T. A., Dudek, A., Elsharawy, A., Floris, I., Foers, A. D., Gartner, K., Garg, A. D., Geeurickx, E., Gettemans, J., Ghazavi, F., Giebel, B., Kormelink, T. G., Hancock, G., Helsmoortel, H., Hill, A. F., Hyenne, V., Kalra, H., Kim, D., Kowal, J., Kraemer, S., Leidinger, P., Leonelli, C., Liang, Y., Lippens, L., Liu, S., Lo Cicero, A., Martin, S., Mathivanan, S., Mathiyalagan, P., Matusek, T., Milani, G., Monguio-Tortajada, M., Mus, L. M., Muth, D. C., Nemeth, A., Nolte-'t Hoen, E. N., O'Driscoll, L., Palmulli, R., Pfaffl, M. W., Primdal-Bengtson, B., Romano, E., Rousseau, Q., Sahoo, S., Sampaio, N., Samuel, M., Scicluna, B., Soen, B., Steels, A., Swinnen, J. V., Takatalo, M., Thaminy, S., Thery, C., Tulkens, J., Van Audenhove, I., van der Grein, S., Van Goethem, A., van Herwijnen, M. J., Van Niel, G., Van Roy, N., Van Vliet, A. R., Vandamme, N., Vanhauwaert, S., Vergauwen, G., Verweij, F., Wallaert, A., Wauben, M., Witwer, K. W., Zonneveld, M. I., De Wever, O., Vandesompele, J., and Hendrix, A. (2017) EV-TRACK: transparent reporting and centralizing knowledge in extracellular vesicle research. *Nat Methods* **14**, 228-232
4. Valkonen, S., van der Pol, E., Boing, A., Yuana, Y., Yliperttula, M., Nieuwland, R., Laitinen, S., and Siljander, P. R. (2017) Biological reference materials for extracellular vesicle studies. *Eur J Pharm Sci* **98**, 4-16
5. Garcia-Manrique, P., Matos, M., Gutierrez, G., Pazos, C., and Blanco-Lopez, M. C. (2018) Therapeutic biomaterials based on extracellular vesicles: classification of bio-engineering and mimetic preparation routes. *J Extracell Vesicles* **7**, 1422676
6. Marianecci, C., Di Marzio, L., Rinaldi, F., Celia, C., Paolino, D., Alhaique, F., Esposito, S., and Carafa, M. (2014) Niosomes from 80s to present: the state of the art. *Adv Colloid Interface Sci* **205**, 187-206
7. Chen, C., Zhu, S., Wang, S., Zhang, W., Cheng, Y., and Yan, X. (2017) Multiparameter Quantification of Liposomal Nanomedicines at the Single-Particle Level by High-Sensitivity Flow Cytometry. *ACS Appl Mater Interfaces* **9**, 13913-13919
8. van der Pol, E., Coumans, F. A., Sturk, A., Nieuwland, R., and van Leeuwen, T. G. (2014) Refractive index determination of nanoparticles in suspension using nanoparticle tracking analysis. *Nano Lett* **14**, 6195-6201
9. Bartelds, R., Nematollahi, M. H., Pols, T., Stuart, M. C. A., Pardakhty, A., Asadikaram, G., and Poolman, B. (2018) Niosomes, an alternative for liposomal delivery. *PLoS One* **13**, e0194179
10. Armstrong, J. P. K., and Stevens, M. M. (2018) Strategic design of extracellular vesicle drug delivery systems. *Adv Drug Deliv Rev*

11. Stipp, C. S., Kolesnikova, T. V., and Hemler, M. E. (2003) Functional domains in tetraspanin proteins. *Trends Biochem Sci* **28**, 106-112
12. Masciopinto, F., Campagnoli, S., Abrignani, S., Uematsu, Y., and Pileri, P. (2001) The small extracellular loop of CD81 is necessary for optimal surface expression of the large loop, a putative HCV receptor. *Virus Res* **80**, 1-10
13. Yanez-Mo, M., Tejedor, R., Rousselle, P., and Sanchez -Madrid, F. (2001) Tetraspanins in intercellular adhesion of polarized epithelial cells: spatial and functional relationship to integrins and cadherins. *J Cell Sci* **114**, 577-587
14. Mittelbrunn, M., Yanez-Mo, M., Sancho, D., Ursa, A., and Sanchez-Madrid, F. (2002) Cutting edge: dynamic redistribution of tetraspanin CD81 at the central zone of the immune synapse in both T lymphocytes and APC. *J Immunol* **169**, 6691-6695
15. Barreiro, O., Yanez-Mo, M., Sala-Valdes, M., Gutierrez-Lopez, M. D., Ovalle, S., Higginbottom, A., Monk, P. N., Cabanas, C., and Sanchez-Madrid, F. (2005) Endothelial tetraspanin microdomains regulate leukocyte firm adhesion during extravasation. *Blood* **105**, 2852-2861
16. Fairhead, M., and Howarth, M. (2015) Site-specific biotinylation of purified proteins using BirA. *Methods Mol Biol* **1266**, 171-184
17. Suarez, H., Gamez-Valero, A., Reyes, R., Lopez-Martin, S., Rodriguez, M. J., Carrascosa, J. L., Cabanas, C., Borras, F. E., and Yanez-Mo, M. (2017) A bead-assisted flow cytometry method for the semi-quantitative analysis of Extracellular Vesicles. *Sci Rep* **7**, 11271
18. Nolte-'t Hoen, E. N., van der Vlist, E. J., de Boer-Brouwer, M., Arkesteijn, G. J., Stoorvogel, W., and Wauben, M. H. (2013) Dynamics of dendritic cell-derived vesicles: high-resolution flow cytometric analysis of extracellular vesicle quantity and quality. *J Leukoc Biol* **93**, 395-402
19. Guo, F., and Jiang, W. (2014) Single particle cryo-electron microscopy and 3-D reconstruction of viruses. *Methods Mol Biol* **1117**, 401-443
20. van der Vlist, E. J., Nolte-'t Hoen, E. N., Stoorvogel, W., Arkesteijn, G. J., and Wauben, M. H. (2012) Fluorescent labeling of nano-sized vesicles released by cells and subsequent quantitative and qualitative analysis by high-resolution flow cytometry. *Nat Protoc* **7**, 1311-1326
21. Nolte-'t Hoen, E. N., van der Vlist, E. J., Aalberts, M., Mertens, H. C., Bosch, B. J., Bartelink, W., Mastrobattista, E., van Gaal, E. V., Stoorvogel, W., Arkesteijn, G. J., and Wauben, M. H. (2012) Quantitative and qualitative flow cytometric analysis of nanosized cell-derived membrane vesicles. *Nanomedicine* **8**, 712-720
22. Dubacheva, G. V., Araya-Callis, C., Geert Volbeda, A., Fairhead, M., Codee, J., Howarth, M., and Richter, R. P. (2017) Controlling Multivalent Binding through Surface Chemistry: Model Study on Streptavidin. *J Am Chem Soc* **139**, 4157-4167
23. Gonzalez, M., Bagatolli, L. A., Echabe, I., Arrondo, J. L., Argarana, C. E., Cantor, C. R., and Fidelio, G. D. (1997) Interaction of biotin with streptavidin. Thermostability and conformational changes upon binding. *J Biol Chem* **272**, 11288-11294
24. Wilchek, M., Bayer, E. A., and Livnah, O. (2006) Essentials of biorecognition: the (strept) avidin-biotin system as a model for protein-protein and protein-ligand interaction. *Immunol Lett* **103**, 27-32
25. Yuana, Y., Koning, R. I., Kuil, M. E., Rensen, P. C., Koster, A. J., Bertina, R. M., and Osanto, S. (2013) Cryo-electron microscopy of extracellular vesicles in fresh plasma. *J Extracell Vesicles* **2**
26. Zonneveld, M. I., Brisson, A. R., van Herwijnen, M. J., Tan, S., van de Lest, C. H., Redegeld, F. A., Garssen, J., Wauben, M. H., and Nolte-'t Hoen, E. N. (2014) Recovery of extracellular vesicles from human breast milk is influenced by sample collection and vesicle isolation procedures. *J Extracell Vesicles* **3**

27. Yi, H., Strauss, J. D., Ke, Z., Alonas, E., Dillard, R. S., Hampton, C. M., Lamb, K. M., Hammonds, J. E., Santangelo, P. J., Spearman, P. W., and Wright, E. R. (2015) Native immunogold labeling of cell surface proteins and viral glycoproteins for cryo-electron microscopy and cryo-electron tomography applications. *J Histochem Cytochem* **63**, 780-792
28. Stewart, P. L. (2017) Cryo-electron microscopy and cryo-electron tomography of nanoparticles. *Wiley Interdiscip Rev Nanomed Nanobiotechnol* **9**
29. Libregts, S., Arkesteijn, G. J. A., Nemeth, A., Nolte-'t Hoen, E. N. M., and Wauben, M. H. M. (2018) Flow cytometric analysis of extracellular vesicle subsets in plasma: impact of swarm by particles of non-interest. *J Thromb Haemost*
30. Konoshenko, M. Y., Lekchnov, E. A., Vlassov, A. V., and Laktionov, P. P. (2018) Isolation of Extracellular Vesicles: General Methodologies and Latest Trends. *Biomed Res Int* **2018**, 8545347
31. Groot Kormelink, T., Arkesteijn, G. J., Nauwelaers, F. A., van den Engh, G., Nolte-'t Hoen, E. N., and Wauben, M. H. (2016) Prerequisites for the analysis and sorting of extracellular vesicle subpopulations by high-resolution flow cytometry. *Cytometry A* **89**, 135-147
32. Nolan, J. P. (2015) Flow Cytometry of Extracellular Vesicles: Potential, Pitfalls, and Prospects. *Curr Protoc Cytom* **73**, 13 14 11-16
33. Kooijmans, S. A., Vader, P., van Dommelen, S. M., van Solinge, W. W., and Schiffelers, R. M. (2012) Exosome mimetics: a novel class of drug delivery systems. *Int J Nanomedicine* **7**, 1525-1541
34. Kim, O. Y., Lee, J., and Gho, Y. S. (2016) Extracellular vesicle mimetics: Novel alternatives to extracellular vesicle-based theranostics, drug delivery, and vaccines. *Semin Cell Dev Biol*
35. Mizrahy, S., Hazan-Halevy, I., Landesman-Milo, D., Ng, B. D., and Peer, D. (2017) Advanced Strategies in Immune Modulation of Cancer Using Lipid-Based Nanoparticles. *Front Immunol* **8**, 69
36. Smith, D. M., Simon, J. K., and Baker, J. R., Jr. (2013) Applications of nanotechnology for immunology. *Nat Rev Immunol* **13**, 592-605
37. Torchilin, V. P. (2005) Recent advances with liposomes as pharmaceutical carriers. *Nat Rev Drug Discov* **4**, 145-160
38. Lotvall, J., Hill, A. F., Hochberg, F., Buzas, E. I., Di Vizio, D., Gardiner, C., Gho, Y. S., Kurochkin, I. V., Mathivanan, S., Quesenberry, P., Sahoo, S., Tahara, H., Wauben, M. H., Witwer, K. W., and Thery, C. (2014) Minimal experimental requirements for definition of extracellular vesicles and their functions: a position statement from the International Society for Extracellular Vesicles. *J Extracell Vesicles* **3**, 26913

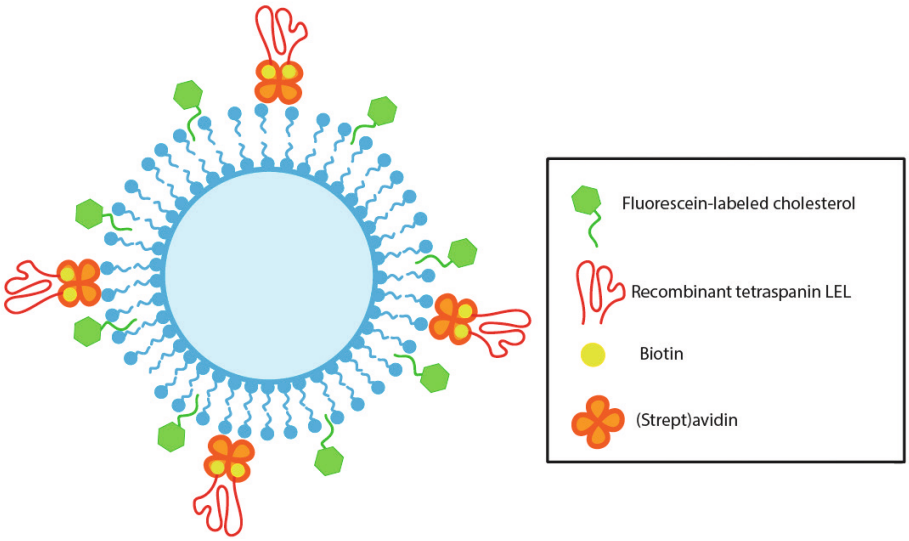

Graphical abstract. Schematic representation of the described EV-mimetic: fluorescent synthetic niosomes coated on the surface with (strept)avidin for decoration with the biotinylated recombinant antigenic regions of large extracellular loops (LEL) of tetraspanins. Fluorescein-labelled cholesterol corresponds to 1,2 dioleoyl-sn-glycerol phosphoethanolamine modified with carboxyfluorescein molecules that was included in the niosome formulation.

"If you feel safe in the area you're working in, you're not working in the right area. Always go a little further into the water than you feel you're capable of being in. Go a little bit out of your depth. And when you don't feel that your feet are quite touching the bottom, you're just about in the right place to do something exciting."

David Bowie

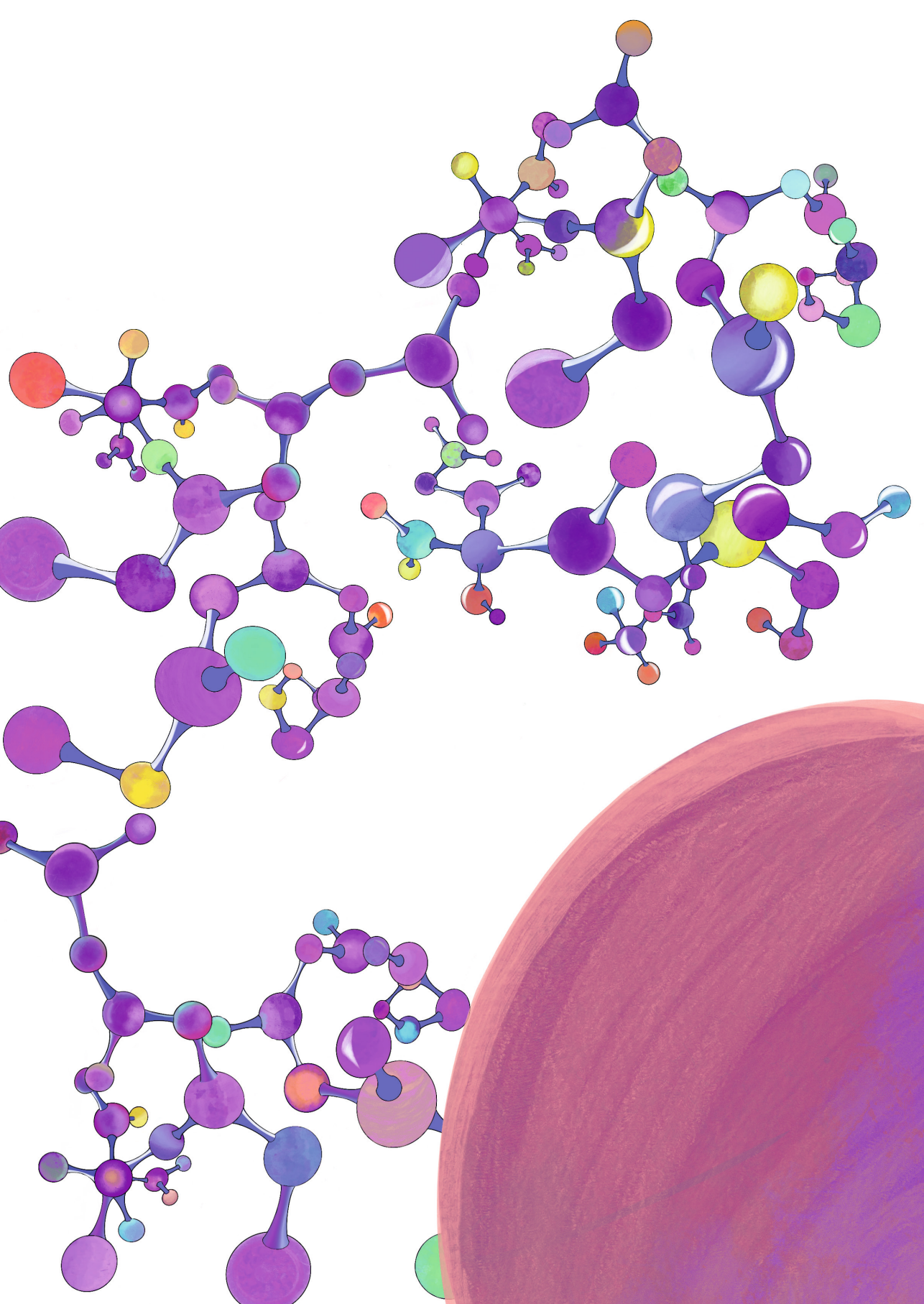

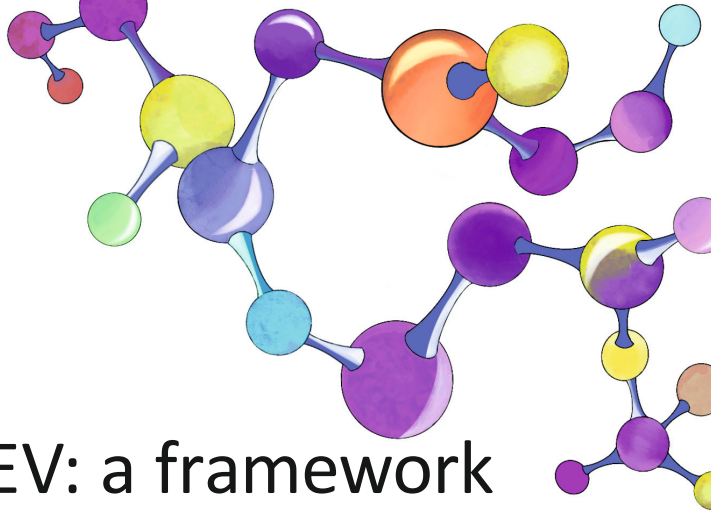

CHAPTER 3

MIFlowCyt-EV: a framework for standardized reporting of extracellular vesicle flow cytometry experiments

Joshua A. Welsh [a], Edwin Van Der Pol [b,c,d], Ger J.A. Arkesteijn [e], Michel Bremer [f], Alain Brisson [g], Frank Coumans [b,c,d], Françoise Dignat-George [h,i], Erika Duggan [j], Ionita Ghiran [k], Bernd Giebel [f], André Görgens [f,l,m], An Hendrix [n], Romaric Lacroix [h,i], Joanne Lannigan [o], Sten F.W.M. Libregts [e,p], **Estefanía Lozano-Andrés** [e], Aizea Morales-Kastresana [a], Stephane Robert [m], Leonie De Rond [b,c,d], Tobias Tertel [f], John Tigges [k,q], Olivier De Wever [n], Xiaomei Yan [r], Rienk Nieuwland [c,d], Marca H.M. Wauben [e], John P. Nolan [j] and Jennifer C. Jones [a]

a Translational Nanobiology Section, Laboratory of Pathology, Center for Cancer Research, National Cancer Institute, National Institutes of Health, Bethesda, MD, USA; b Biomedical Engineering and Physics, Amsterdam UMC, University of Amsterdam, Amsterdam, The Netherlands; c Laboratory Experimental Clinical Chemistry, Amsterdam UMC, University of Amsterdam, Amsterdam, The Netherlands; d Vesicle Observation Center, Amsterdam UMC, University of Amsterdam, Amsterdam, The Netherlands; e Department of Biochemistry and Cell Biology, Faculty of Veterinary Medicine, Utrecht University, Utrecht, The Netherlands; f Institute for Transfusion Medicine, University Hospital Essen, University of Duisburg-Essen, Essen, Germany; gUMR-5248-CBMN, CNRS-University of Bordeaux-IPB, Pessac, France; h Center of Cardiovascular Research and Nutrition (C2VN) UMR-INSERM INRA 1263, Aix-Marseille Université, INSERM, Marseille, France; i Hematology and Vascular Biology Department, CHU La Conception, Assistance Publique-Hôpitaux de Marseille, Marseille, France; j Scintillon Institute, San Diego, CA, USA; k Department of Medicine, Beth Israel Deaconess Medical Center, Harvard Medical School, Boston, MA, USA; l Clinical Research Center, Department for Laboratory Medicine, Karolinska Institutet, Stockholm, Sweden; m Evox Therapeutics Ltd, Oxford, UK; n Laboratory of Experimental Cancer Research, Department of Human Structure and Repair, Ghent University Hospital, Ghent, Belgium; o Flow Cytometry Core, School of Medicine, University of Virginia, Charlottesville, VA, USA; p NIHR Cambridge BRC Cell Phenotyping Hub, Department of Medicine, University of Cambridge, Cambridge, UK; q Flow Cytometry Core, Beth Israel Deaconess Medical Center, Boston, MA, USA; r MOE Key Laboratory of Spectrochemical Analysis & Instrumentation, Key Laboratory for Chemical Biology of Fujian Province, Department of Chemical Biology, College of Chemistry and Chemical Engineering, Xiamen University, Xiamen, People's Republic of China

Published:
Welsh et al., (2020). Journal of Extracellular Vesicles, VOL. 9, 1713526
https://doi.org/10.1080/20013078.2020.1713526

ABSTRACT

Extracellular vesicles (EVs) are small, heterogeneous, and difficult to measure. Flow cytometry (FC) is a key technology for the measurement of individual particles, but its application to the analysis of EVs and other submicron particles has presented many challenges and has produced a number of controversial results, in part due to limitations of instrument detection, lack of robust methods, and ambiguities in how data should be interpreted. These complications are exacerbated by the field's lack of a robust reporting framework, and many EV-FC manuscripts include incomplete descriptions of methods and results, contain artifacts stemming from an insufficient instrument sensitivity and inappropriate experimental design, and lack appropriate calibration and standardization. To address these issues, a working group (WG) of EV-FC researchers from ISEV, ISAC, and ISTH, worked together as an EV-FC WG, and developed a consensus framework for the minimum information that should be provided regarding EV-FC. This framework incorporates the existing MISEV (Minimum Information for Studies of EVs) guidelines and MIFlowCyt (Minimum Information about a FC experiment) standard in an EV-FC- specific reporting framework (MIFlowCyt-EV) that supports reporting of critical information related to sample staining, EV detection and measurement, and experimental design in manuscripts that report EV-FC data. MIFlowCyt-EV provides a structure for sharing EV-FC results, but it does not prescribe specific protocols, as there will continue to be rapid evolution of instruments and methods for the foreseeable future. MIFlowCyt-EV accommodates this evolution, while providing information needed to evaluate and compare different approaches. Because MIFlowCyt-EV will ensure consistency in the manner of reporting of EV-FC studies, over time we expect that adoption of MIFlowCyt-EV as a standard for reporting EV- FC studies will improve the ability to quantitatively compare results from different laboratories and to support the development of new instruments and assays for improved measurement of EVs.

Keywords: extracellular vesicles, flow cytometry, framework, reporting, standardization.

INTRODUCTION

Extracellular vesicles (EVs) have tremendous potential value as biomarkers and therapeutic targets [1, 2]. However, EVs are small, heterogeneous, and therefore difficult to measure. Sensitive and reproducible methods for single EV analysis are essential to understand the biogenesis, diversity, and fate of EVs, and to apply this understanding to improve human health. Flow cytometry (FC) is a powerful method that provides accurate and precise enumeration of single cells, and measurement of their molecular components. For these reasons there is an interest in applying FC to the measurement of individual EVs. However, most commercial flow cytometers, and the assays that employ them, (i) were designed for the analysis of cells that are orders of magnitude larger than EVs, (ii) are not readily adapted to the measurement of EVs, and (iii) generate data which can only be interpreted if all experimental details are reported. Limitations in instrument sensitivity, assay specificity, and a general failure to adequately report experimental details together have produced a scientific literature that is rife with artefacts.

General guidelines regarding methods and data reporting have been developed for both flow cytometry (Minimum Information about a Flow Cytometry experiment, MIFlowCyt) [3] and EV research (Minimum Information for the Study of EVs, MISEV) [4, 5]. In addition, the EV-TRACK initiative provides an open access platform for documenting essential information for EV publications [6]. However, these resources do not comprehensively address reporting component allowing full interpretation of FC data on EVs, which is critical for the validation and improvement of flow cytometry-based EV analysis. Here, a group of researchers active in the International Society of Extracellular Vesicles (ISEV), International Society for Advancement of Cytometry (ISAC), and/or International Society for Thrombosis and Haemostasis (ISTH) Vascular Biology Scientific Standardization Committee, have been working to develop a framework for reporting EV FC methods and results, named MIFlowCyt-EV. Consensus about what to report was reached by discussions spanning several years within the WG by teleconferences, and by speaking and presenting ideas to the wider community satellite meetings at ISEV, ISAC, and ISTH conferences.

MIFlowCyt-EV is intended to complement the MIFlowCyt and MISEV documents by providing a fundamental reporting structure, with seven categories, each with clearly defined specific components, that should be considered and reported for EV FC studies. MIFlowCyt-EV has been developed to account for the wide variety of protocols currently used. MIFlowCyt-EV will be refined and revised periodically, as EV-related technologies and applications develop, as is the case for the MIFlowCyt and MISEV guidelines. MIFlowCyt-EV is structured for researchers to simply document which of the seven categories and sub-components were considered, performed, and recorded in the studies. The WG feel that currently there is not a gold-standard EV flow cytom-

etry workflow, and the field will continue to struggle to identify robust methods until EV researchers adopt a standardized framework for reporting data in a consistent, benchmarked manner.

As well as a reporting framework, MIFlowCyt-EV can also serve as a guide for the development of educational resources for researchers desiring to measure EVs. We expect that this framework will support the development and validation of new technologies for EV analysis.

MIFlowCyt-EV structure and utilization

MIFlowCyt-EV utilizes the MISEV guidelines from ISEV for reporting preanalytical variables [4, 5], and the MIFlowCyt guidelines from ISAC for reporting FC experimental design and general variables related to FC [3]. The proposed framework for MIFlowCyt-EV integrates and extends these two established societal guidelines to promote more standardized reporting of single EV analyses using FC.

The MIFlowCyt-EV framework addresses seven areas: 1) preanalytical variables and experimental design, 2) sample preparation, 3) assay controls, 4) instrument calibration and data acquisition, 5) EV characterization, 6) FC data reporting, 7) FC data sharing. **Figure 1** shows an overview of the framework and its components, whereas **Table 1** provides a table for completion of the framework. This table template can be downloaded from www.evflowcytometry.org and found in **Supplementary Table 1**. The component for each category states: 'the rationale' for reporting and 'what to report'. **Table 2** provides a 'brief example' of the reporting component and are not intended as 'gold standards'. The hypothetical examples provided for each component are not exhaustive in detail and are not intended to promote the use of a single particular methodology, but instead to provide the manner in which each component should be reported.

Generally, if researchers have performed any of the components mentioned in this framework, it should be elaborated upon. However, it is not a requirement to complete all the framework components. Depending upon the design of an experiment, a motivation why a component was not necessary may be sufficient. It is at the reviewer's discretion to examine the completed reporting framework and decide if the level of detail and utilized controls were sufficiently conducted and reported.

1. Preanalytical variables and experimental design

Pre-analytical factors include: the method of sample collection, isolation, and storage before measuring. These preanalytical factors are critical determinants of experimental reproducibility. Isolation steps include procedures to enrich, fractionate, and/or concentrate EVs relative to other sample components. Relevant pre-analytical factors have been described extensively in the literature, leading to the development of the MISEV guidelines, the EV-TRACK platform, and other relevant guidelines from international

societies including: ISEV, ISAC, and ISTH [4-9]. We recommend that pre-analytical variables are reported according to the MISEV guidelines [4]. Furthermore, we recommend that the ISAC MIFlowCyt guidelines checklist is completed and reported for all EV-FC experiments, as well as to report experimental preanalytical variables related to basic flow cytometric equipment and reagents [3].

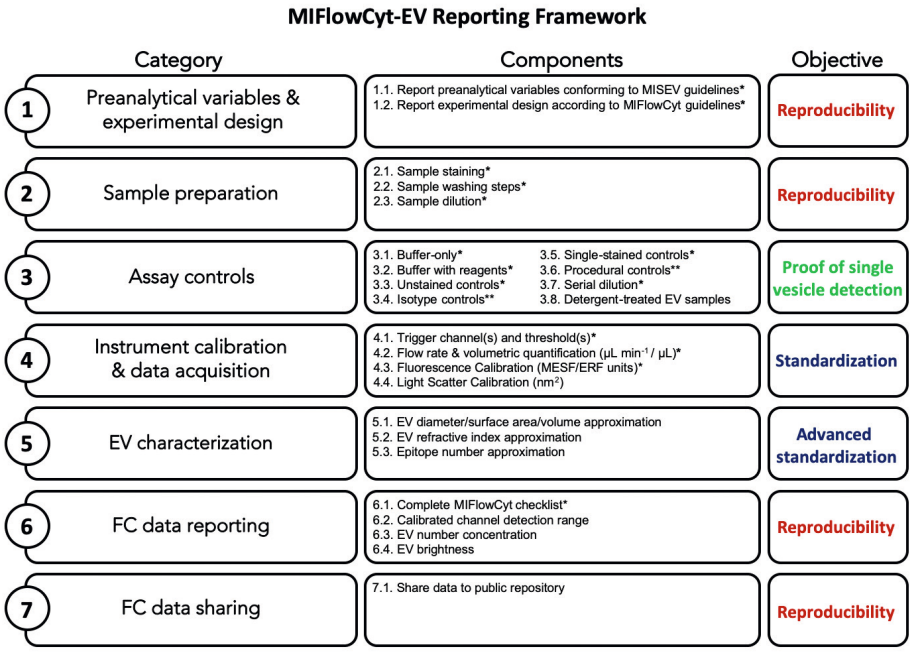

Figure 1. Overview of the MIFlowCyt EV Reporting Framework. The left column shows each category of the reporting framework and the middle column shows the components within each category, the right-hand column shows the broad objective of each row. *highlights the component that are broadly applicable to the majority of single-EV analysis experiments regardless of design or instrumentation. **highlights the components that are only applicable in cases where certain reagents or protocols are used.

1.1. Report preanalytical variables conforming to MISEV guidelines

Rationale: Preanalytical variables affect the purity and yield of EVs but vary depending on the sample sources. Preanalytical variables for clinical samples may include: needle gauge, collection tube type, sample handling, and EV isolation/enrichment. Furthermore, accounting for donor-associated variables, such as source, age, sex, or fasting status, may substantially alter biofluid EV characteristics and therefore the statistical associations of a study. For non-clinical samples, such as tissue culture-derived samples, pre-analytical variables may include: culture container, culture medium, incubation time, growth factors, and EV isolation procedures. ISEV periodically updates the MISEV guidelines to incorporate consensus on preanalytical variables for a wide range

of sample types and highlights position papers that detail best-practices for sample collection from different biological fluids [4, 5]. EV-FC experiments should be reported with information that states what guidelines or customized procedures were followed.

Report: Preanalytical variables relating to EV sample including source, collection, isolation, storage, and any others relevant and available in the performed study.

Framework Components:	Complete for each component:
1.1 Preanalytical variables conforming to MISEV guidelines*	
1.2 Experimental design according to MIFlowCyt guidelines*	
2.1 Sample staining details*	
2.2 Sample washing details*	
2.3 Sample dilution details*	
3.1 Buffer-only controls*	
3.2 Buffer with reagent controls*	
3.3 Unstained controls*	
3.4 Isotype controls**	
3.5 Single-stained controls*	
3.6 Procedural controls**	
3.7 Serial dilutions*	
3.8 Detergent-treated controls	
4.1 Trigger channel(s) and threshold(s)*	
4.2 Flow rate / volumetric quantification*	
4.3 Fluorescence calibration*	
4.4 Scatter calibration	
5.1 EV diameter/surface area/volume approximation	
5.2 EV refractive index approximation	
5.3 EV epitope number approximation	
6.1 Completion of MIFlowCyt checklist*	
6.2 Calibrated channel detection range	
6.3 EV number/concentration	
6.4 EV brightness	
7.1 Sharing of data to a public repository	

Table 1. MIFlowCyt-EV framework. *Highlights the components that are broadly applicable to the majority of single-EV analysis experiments regardless of design or instrumentation. **Highlights the components that are only applicable in cases where certain reagents or protocols are used.

1.2. Report experimental design according to MIFlowCyt guidelines

Rationale: Providing a clear purpose of the performed experiments and a concise and detailed description of the variables of a FC experiment(s) allows the reader to understand and interpret the subsequent data of the performed experiment(s).

Report: EV-FC manuscripts should provide a brief description of the experimental aim, keywords, and variables for the performed FC experiment(s) using MIFlowCyt checklist components: 1.1, 1.2, and 1.3, respectively [3]. Completion of the entire MIFlowCyt checklist at this point is also advised here, in order to address subsequent MIFlowCyt checklist components that are integral to the MIFlowCyt-EV framework components, such as **Components 2.1**, **4.1**, and **6.1**, below.

2. Sample preparation

The sample preparation components allow for the reporting of variables that pertain to the sample staining, washing, and dilution for flow cytometric analysis, and do not include preanalytical variables about the sample listed in **Category 1**.

2.1 Sample staining

Rationale: A number of variables affect the labelling efficacy of a sample, including: EV concentration, label concentration, incubation time, temperature, conjugation efficiency, label-type (and clone if monoclonal antibodies are used), and light exposure. A particularly critical reporting component of these is the final concentration of a label in appropriate units e.g. mole L^{-1} or µg mL^{-1}. There are cases where antibody concentration is not provided or where antibodies are self-conjugated. In these cases, antibody concentration should be approximated with a spectrophotometer and the methods reported appropriately. Self-conjugated antibodies should provide the conjugation kit catalogue number and lot number.

Report: State any steps relating to the staining of samples. Along with the method used for staining, provide relevant reagent descriptions as listed in MIFlowCyt guidelines (**Component 2.4** Fluorescence Reagent(s) Descriptions).

2.2 Sample washing

Rationale: Wash steps can affect FC sample measurements by decreasing the concentration of excess label, thereby increasing the signal-to-noise ratio. Depending on how these steps are performed, wash steps may also dilute or alter the characteristics of the sample being measured. Reporting details of any wash steps allows improved reproducibility of FC data.

Report: State any steps relating to the washing of samples.

Table 2. Example of a completed MIFlowCyt-EV framework. This example is of a hypothetical experiment. The WG does not currently believe there exists a 'gold-standard' methodology or endorse any particular purification methods, reagents, assays, or equipment. At the time of publication, no literature exists on the described hypothetical experiment. This hypothetical experiment was designed purely to require that every component of the framework be utilized and need a moderate level of detail. In many assays, every component of the framework may not need to be completed in detail if it is not relevant to the assay. In the case of a component not be relevant to an assay, a brief explanation as to why any specific component was not required should be reported. This completed example is purely a reference to the type of details that are relevant for each component and to the extent they should be discussed.

Component	Brief Example
1.1	Blood was collected from 100 individuals in 5 mL 0.109 M citrated plastic tubes (BD Vacutainer, Becton Dickinson) via antecubital vein puncture using a 21-gauge needle. The first 1 mL was discarded, prior to collection of 3.5 mL of blood. Tubes were transported vertically at room temperature. Within 1 hour of blood withdrawal, platelet-depleted plasma was prepared by centrifugation (Eppendorf 5810-R centrifuge, S-4-101 Rotor, Eppendorf) twice at 2500 ×*g* for 15 minutes at 20 °C. The lowest deceleration setting was used, setting '1'. The first centrifugation step was done with 3.5 mL whole blood in 5 mL tubes (BD Vacutainer, Becton Dickinson). Supernatant was collected 10 mm above the buffy coat. The second centrifugation step was done with 2.5 mL platelet-depleted plasma in 15 mL conical tubes (Falcon Conical, Corning). The absence of hemolysis is confirmed by the lack of a spectrophotometric absorbance peak of free hemoglobin at 414 nm using a BioDrop DUO spectrophotometer. 1 mL x2 aliquots of platelet-depleted plasma were transferred to 1.5 mL low-protein binding Eppendorf tubes (Thermo Fisher Scientific) and snap frozen in liquid nitrogen before being stored at −80 °C. Age, sex, fasting status, and smoking status were recorded for all individuals.
1.2	***1.1 Aim:*** To compare the concentration of CD41a+ platelet-derived EVs in platelet-depleted plasma between individuals with type-2 diabetes mellitus (T2DM) and healthy controls. We hypothesize that the concentration of platelet-derived EVs will be increased in individuals with T2DM as T2DM has been associated with increased platelet activation. ***1.2 Keywords:*** EV; extracellular vesicles, T2DM; type-2 diabetes mellitus. ***1.3 Experimental variables:*** Platelet-depleted plasma samples were measured from 50 individuals with T2DM and 50 healthy controls. There was no significant difference in age, sex, fasting-status, or smoking-status between individuals with and without T2DM. Scatter-based triggering was used for the detection of particles.

Table 2. Continued

Component	Brief Example
2.1	The presence of CD41a was determined using CD41a antibody staining. Please see **Table 2** for an overview of the reagents used. $5x10^9$ EVs (estimated by resistive pulse sensing (nCS1, Spectradyne) after size-exclusion chromatography (SEC) treatment) suspended in 495 µL of Dulbecco's phosphate-buffered saline (DPBS) were incubated with were incubated with 1x vFRed membrane stain (Cellarcus Biosciences), 5 mM $CaCl^2$ (Sigma Aldrich), 20 µM PPACK (Sigma Aldrich), and 5 µL of 25 µg mL^{-1} anti-human CD41a mouse-IgG1κ-PE (BioLegend) for one hour at 20 °C and protected from light. A matched isotype control; mouse-IgG1κ-PE (BioLegend), was incubated in the same conditions and concentration (0.25 µg mL^{-1}) as the anti-CD41a stained sample. The final concentration used for EV measurement using serial dilution 5 was (0.016 µg mL^{-1}) for anti-CD41a and its matched isotype.
2.2	Unbound antibody from CD41a-stained EV samples was removed using SEC. 500 µL of sample was added to a size exclusion column and performed according to manufacturer recommendations. Briefly, the column (qEV Original, Izon Science) was next eluted with 0.2 µm-filtered DPBS and 500 µL fractions were collected. Fractions 7-9 were subsequently pooled together for analysis. The column flow rate was ~0.8-1.2 µL min^{-1}, with 500 µL DPBS buffer manually maintained on top of the column.
2.3	30 µL of platelet-depleted plasma was added to 5 µL of reagents and 265 µL of DPBS, resulting in a 10-fold dilution. This 10-fold dilution was then serially diluted 6 times, with 150 µL of sample added to 150 µL of DBPS in a 96-well polypropylene plate (Corning). All wells were measured with the fifth serial dilution (320-fold dilution) in the series used for calculating EV concentration in the starting material.
3.1	A buffer-only control of 0.1 µm-filtered DPBS was recorded at the same flow cytometer acquisition settings as all other samples, including triggering threshold, voltages, and flow rate. The buffer-only control had a count of ~100 events s^{-1}.
3.2	A buffer with reagent control (0.25 µg mL-1 anti-human CD41a mouse-IgG1κ-PE (Clone: HIP8, Manufacturer: BioLegend, Cat No. 303706, Lot No. B250952) was recorded at the same flow cytometer acquisition settings as all other samples, including triggering threshold, voltages, and flow rate. This control was serially diluted 6 times, with 150 µL of buffer with reagent added to 150 µL of DBPS to allow comparisons between serially diluted stained samples. Buffer with reagent controls had an event rate of ~100 events s^{-1} and were therefore not changed from the buffer-only control.
3.3	Unstained controls were measured at the same dilution as matched stained and isotype controls. Flow cytometer acquisition settings were maintained for all samples, including triggering threshold, voltages, and flow rate. The event rate of unstained controls differed by <5% from isotype controls. No substantial changes in scatter or fluorescence signals were observed between unstained and matched isotype controls.

Table 2. Continued

Component	Brief Example
3.4	Isotype controls were used at the same concentration as matched stained controls and were recorded at the same dilution as matched stained and unstained controls and stained samples. Please see **Table 3** for further reagent information. Flow cytometer acquisition settings were maintained for all samples, including triggering threshold, voltages, and flow rate. No substantial changes in scatter or fluorescence signals were observed between unstained and matched isotype controls.
3.5	vFRed (Cellarcus Biosciences) and anti-human CD41a mouse-IgG1κ-PE (BioLegend) single-stained controls for a reference set of samples were analyzed to aid compensation of anti-human CD41a mouse-IgG1κ-PE into the vFRed channel when excited by the 488 nm laser.
3.6	Excess antibody was reduced by further purification of the stained EVs using SEC columns (qEV Original, Izon Science), with fractions 7-9 collected for analysis. To assess whether this step caused artefacts, 500 µL of each control sample (buffer alone, buffer with reagent, unstained, and isotype controls) was run through a SEC column with 500 µL fractions (7-9) collected for analysis. These SEC processed samples were compared to a sample of unprocessed buffer alone, buffer with reagent, unstained sample, isotype sample, and stained sample to demonstrate the removal of antibody with no artefacts being introduced from the procedure.
3.7	Samples were serially diluted 6 times, with 150 µL of sample added to 150 µL of DBPS, and measure using a 96-well polypropylene plate (Corning). The 4, 5, and 6^{th} dilutions showed a linear decrease between dilution factor and measured particle count over one minute. The median fluorescence and scatter intensity of all events for dilutions 4, 5, and 6 was maintained at 500 ± 18 PE molecules of equivalent soluble fluorophore (MESF; See **Component 4.3** for MESF calibration), and 3000 ± 31 side scatter arbitrary units, respectively. Dilutions 1-3 did not show a linear correlation between dilution factor and measured event count, nor were their fluorescence and scatter intensity maintained. The fifth serial dilution (320-fold dilution) in the series was therefore used to calculate EV concentration and report immunostaining data.
3.8	Stained samples, diluted 320-fold, were treated with 0.1% Triton X-100 for 5 minutes at 21°C to test the lability of vFRed and CD41a-PE stained events. These measurements were used to compare vFRed and CD41a-PE stained samples not treated with detergent. vFRed and CD41a-PE positive events decreased 87% ± 9% upon treatment with 0.1% Triton X-100 for 5 minutes.
4.1	Based on the buffer alone control (**Component 3.1**), detection was triggered on the 488 nm laser excited PE-Texas Red channel (630/30 bandpass filter) at a threshold of 500 arbitrary units, equivalent to ~50 PE-Texas Red MESF, determined using Spherotech Rainbow beads and the manufacturer's calibration values (see **Component 4.3** flor fluorescence calibration). The buffer alone control (**Component 3.1**) had an event rate of ~100 events s^{-1}.

Table 2. Continued

Component	Brief Example
4.2	Samples were enumerated using the integral instrument flow rate sensors, resulting in a flow rate of 10 µL min^{-1}. This was calibrated using weighed volumes of deionized water prior to analysis.
4.3	Arbitrary PE fluorescence scale units (channel number), excited by the 561 nm laser and collected using a 586/15 bandpass filter, were converted to MESF units using PE Quantibrite beads (Becton Dickinson, Cat. 100001, Lot. L1000001). Least-squares regression was performed between log_{10}-transformed values of PE-A intensities versus bead PE MESF units (provided by manufacturer) using the 3 dimmest bead populations. The resulting regression showed a high correlation with an R^2 value of 0.99, with a slope of 0.931 and intercept of 1.345.
4.4	Side scatter calibration was performed using Mie modelling software, taking into account the wavelength (405 nm) and polarization state (perpendicular to detection) of the laser, the light collection geometry (side scatter, numerical aperture 1.2), and the particle diameter and refractive index. Least square fitting was used to relate the median signal of each National Institute of Standards and Technology (NIST)-traceable polystyrene bead population to the theory, resulting in a linear scaling factor of 11.3 and an R^2 of 0.99. The limiting side scatter collection angle range of the instrument was determined to be 38-142°, based on the flow cell dimensions. Scatter calibration was shown by plotting modelled vs acquired polystyrene bead data.
5.1	EV diameter was approximated using the fluorescence intensity of a membrane intercalating dye; vFRed. The vFRed cytometer collection channel was calibrated using vFRed-stained liposomes of known population diameter (median 100 nm, range ~50-150 nm) and surface area distributions, determined using nanoparticle tracking analysis (NTA) and resistive pulse sensing (RPS). To calibrate flow cytometer fluorescence intensity in terms of equivalent surface area, a least-squares linear regression was performed between the liposome population surface area and vFRed fluorescence intensity distributions.
5.2	Particle refractive index was derived from the ratio of side and forward scatter signal (i.e. Flow-SR). NIST traceable polystyrene beads with known size and refractive index (Exometry, Netherlands) were used to create a mathematical model of the optical configuration of the flow cytometer using FCM_{PASS} software. Using this model, a Flow-SR versus diameter lookup table was calculated, which allows determination of the particle diameter from the measured Flow-SR. The determined diameter was subsequently used to derive the refractive index from a lookup table of side scatter versus diameter. Lookup tables were calculated for diameters ranging from 10 to 1000 nm, with step sizes of 1 nm, and refractive indices from 1.35 to 1.80 with step sizes of 0.001.

Table 2. Continued

Component	Brief Example
5.3	Anti-mouse antibody capture beads (ABC) (Quantum simply cellular, Bangs Laboratories, Cat No. 100001, Lot No. L1000001) were incubated with 5 µL of 25 µg mL^{-1} anti-CD41a mouse-IgG1κ-PE (Clone: HIP8, Manufacturer: BioLegend, Cat No. 303706, Lot No. B250952) for 15 minutes at 20 °C and protected from light. The PE channel units were converted to ABC units by performing regression between PE-A and ABC number using the 3 dimmest bead populations. Regression showed a high correlation with an R^2 value of 0.99.
6.1	The MIFlowCyt checklist v1.0.0 has been completed and attached in the Supplementary Information.
6.2	The median intensity of the unstained EV population was 200 PE MESF units. The maximum channel number (2^{18}), when scaled to MESF, was 592435 PE MESF units. Positive events on PE were assumed to be two standard deviations above the unstained EV population, 240 PE MESF units. The detection range of the PE channel used for PE-positive events was therefore 320 to 592435 PE MESF units.
6.3	The detected concentration of CD41a-PE positive EVs between calibrated detection range (240 and 592435 PE MESF units) was 5.62 x 108 particle mL-1. Flow cytometer acquisition settings were maintained for all samples, including triggering threshold, voltages, and flow rate.
6.4	EV brightness was compared using the median (25^{th}, 75^{th} percentile) PE MESF intensity, due to the non-parametric distribution of EV staining. Unstained platelet-derived EVs from healthy patients and T2DM patients had a median fluorescence intensity of 240 (290, 120) PE MESF. CD41a-positive platelet-derived EVs from healthy patients had a median fluorescence intensity of 535 (800, 205) PE MESF units. CD41a-positive platelet-derived EVs from T2DM patients had a median fluorescence intensity of 560 (890, 250) PE MESF units.
7.1	FC files and the analysis workspace have been uploaded FlowRepository and can also be obtained by contacting the corresponding author.

Table 3. Summary of reagents used for FC experiments

Characteristic(s) being measured	Analyte	Analyte Detector	Reporter	Isotype	Clone	Final Concentration	Manufacturer	Cat. Number	Lot Number
Lipid Membrane	Lipid membrane	vFRed	vFRed	NA	NA	Staining = 1x Serial Dilution 5 = 0.064x	Cellarcus Biosciences	CBS4	190415
Cell surface protein	Human CD41a	Anti-human CD41 antibody	PE	Mouse IgG1κ	HIP8	Staining = 0.25 µg mL-1, Serial Dilution 5 = 0.016 µg mL^{-1}	BioLegend	303706	B250952
Non-specific binding of antibody	NA	NA	PE	Mouse IgG1κ	MOPC-21	Staining = 0.25 µg mL-1, Serial Dilution 5 = 0.016 µg mL^{-1}	BioLegend	400112	B227349

2.3. Sample dilution

Rationale: The concentration of EVs in the starting material (body fluid, culture media) is a highly-reported statistic from EV-FC data but is affected by sample dilution. Sample dilution can occur from the addition of buffers, reagents, and wash steps. Accounting for all dilution steps that occurred from sample collection to analysis is therefore crucial.

Report: All methods and steps relating to sample dilution.

3. Assay controls

Due to the unique challenges of EV-FC several controls may be required that are typically not used when analyzing cells or other micron-sized particles. We recommend reporting whether the following controls have been included in an experiment: buffer alone, buffer with added reagents but without EVs, procedural controls, detergent-treatment of samples, and demonstration of single particle detection.

3.1. Buffer-only

Rationale: Flow cytometer background noise depends on several factors across the instrument's optics, electronics, and fluidics. The acquisition of a buffer-only control provides a measure of the instrument's background event rate at the same settings used to analyze EV samples and further controls[10]. Flow cytometers tend to use water or buffered saline solution as sheath buffer. Differences between sample solution and sheath buffer can contribute to background in flow cytometric analysis [11]. The effects of sample solution on background signals are well known in cellular FC, e.g. analysis of cells in media solution containing phenol red, can contribute to elevated fluorescence and may interfere with the analysis of "staining" with a fluorophore that has spectral overlap. When analyzing small particles at the limits of a flow cytometer's sensitivity, it is important to provide a reference of the recorded event rate from a sample which contains only the buffer used for diluting EV-containing samples.

Report: State whether a buffer-only control was analyzed at the same settings and during the same experiment as the samples of interest. If utilized it is recommended that all samples be recorded for a consistent set period of time e.g. 5 minutes, rather than stopping analysis at a set recorded event count e.g. 100,000 events. This allows comparisons of total particle counts between controls and samples.

3.2. Buffer with reagents

Rationale: To demonstrate if the background signal is altered e.g. buffer with reagent control shows events that appear positive for fluorescence and light scatter in the absence of EV-containing samples. This control is a direct comparison to the buffer-only control (**Component 3.1**). The appearance or change of a population allows the identification of reagent-related effects that could affect the analysis of EV-stained samples [12]. When unbound labels or aggregates of labels are not removed, some instruments

are able to detect the signal of these molecules which may be artifactually interpreted as EVs [10, 13-15].

Report: State whether a buffer with reagent control was analyzed at the same settings, same concentrations, and during the same experiment as the samples of interest. If used state what the results were.

3.3. Unstained controls

Rationale: Unstained controls provide an estimate of the background events and/or signal that may be expected with isotype and/or stained samples. These controls are a useful tool to compare between other samples and controls for the event rate, signal intensity, and gating strategies.

Report: State whether unstained control samples were analyzed at the same settings and during the same experiment as stained samples. If used, state what the results were, preferably in standard units.

3.4. Isotype controls

Rationale: The effect of isotype controls compared to unstained controls and stained samples, can provide a useful method of identifying confounding effects related to antibody specificity. Along with the buffer with reagent control and procedural controls, isotype controls may also helpful to identify false-positive expression of markers due to the presence of high-amounts of unbound antibodies [16].

Report: The use of isotype controls is applicable to immunofluorescence labelling only. State whether isotype controls were analyzed at the same settings and during the same experiment as stained samples. If utilized, state which antibody they are matched to, the concentration used, and what the results were (**Component 4.2, 4.3, 4.4**). Due to conjugation differences between manufacturers if should be stated if the isotype controls are from the same manufacturer as the matched antibodies.

3.5. Single-stained controls

Rationale: FC experiments often use multiple fluorescent reagents. Therefore, it is important to be able to assess whether a fluorescent reagent's spectrum is affecting the measurements in the detection parameter of another fluorescent reagent. Single stained controls may also be useful for compensation, validating compensation by other means such as compensation beads, or identifying potential confounding factors from staining e.g. fluorescence quenching.

Report: State whether single-stained controls were included. If used state whether the single-stained controls were recorded using the same settings, dilutions, and during

the same experiment as stained samples and state what the results were, preferably in standard units (**Component 4.2, 4.3, 4.4**).

3.6. Procedural controls

Rationale: Some staining methods require further purification/processing after labelling of EVs to remove excess dye [10, 14, 15, 17]. In these cases, including procedural controls can show that no artefacts were introduced into the sample during post-staining processing. Procedural controls would include the same buffer-only and buffer with reagent(s) controls (**Component 3.1** and **Component 3.2) but** prepared according to the procedure used to further purify/process the stained samples. These controls can then be compared to controls from **Component 3.1** and **Component 3.2** to show that the further purification/processing steps did not produce artefacts. Examples of post-staining purification/processing method that may require procedural controls include ultracentrifugation, density gradient flotation, (ultra)filtration, and size-exclusion chromatography (SEC).

Report: State whether procedural controls were included. If used, state the procedure and if the procedural controls were acquired at the same settings and during the same experiment as stained samples.

3.7. Serial dilution

Rationale: Serial sample dilution can assist with the evaluation of whether EVs are being detected as single particles. This is to avoid coincidence detection, also known as 'swarm detection', whereby multiple particles are present in the illuminated region of the core stream and their combined light scatter and fluorescence signals are merged into a single event[18]. Serial dilutions can also determine whether confounding factors such as background particles and unbound dyes/antibodies are affecting scatter or fluorescence signals. Serially diluting samples whilst maintaining a consistent fluorescence and/or scatter signal intensity, and maintaining a linear particle count consistent with the dilution factor, have been used to in literature to statistically demonstrate the detection of single-particles of interest [10, 16, 19-22]. Further gating strategies can also be applied to avoid coincidence detection.

Report: State whether serial dilutions were performed on samples and note the dilution range and manner of testing. The fluorescence and/or scatter signal intensity would ideally be reported in standard units (see **Component 4.3, 4.4**) but arbitrary units can also be used. This data is best reported by plotting the recorded number events/concentration over a set period of time at different sample dilution. The median fluorescence intensity at each of the dilutions should also ideally be plotted on the same or a separate plot. An example is shown in **Figure 3A**.

3.8. Detergent-treated EV samples

Rationale: Detergent controls aid in determining whether detected events are membrane-enclosed vesicles or other protein complexes. Complexes can be present when measuring heterogeneous samples such as plasma and serum, or when using reagents are used that may cause precipitation, such as calcium phosphate. Detergent-treatment will lyse membrane-enclosed vesicles, reducing their number and signals. Detergent resistant particles, such as protein complexes or other particulates, will persist following detergent lysis, thereby allowing differentiation from EVs [20, 23-25].

Report: State whether samples were detergent treated to assess lability. If utilized, state what detergent was used, the end concentration of the detergent, and what the results were of the lysis.

4. Instrument calibration and data acquisition

Flow cytometers have numerous operating parameters that will affect the measured events. Completing the MiFlowCyt checklist in **Component 1.2** of this reporting framework covers the reporting of many of these parameters. However, some flow cytometer parameters are conventionally set and reported in arbitrary units. To support the comparison and validation of data between experiments, instruments, laboratories, and institutions, this section provides the components and rationale for reporting the settings and readouts of flow cytometers in standard units. Here, calibration refers to the conversion of arbitrary units into standard units. This relies upon interpolation and extrapolation of signals from reference particles, as summarized and referenced below. This is distinctly different from instrument configuration whereby beads may be analyzed to find optimal detection settings.

4.1. Trigger channel(s) and threshold(s)

Rationale: Instrument trigger and threshold parameters are critical in defining the instrument is and is not able to detect, and therefore the data collected for analysis. For EV-FC experiments to be reproduced, similar trigger and threshold settings are required, and for different investigators to reproduce these settings on different instruments, it is necessary for the settings to be able to be approximated based on standardized metrics. The reporting of trigger(s) and/or threshold(s) is an integral element of the MIFlowCyt reporting guidelines for all FC experiments.

Report: The trigger channel(s) and threshold(s) used for event detection. Preferably, the fluorescence calibration (**Component 4.3**) and/or scatter calibration (**Component 4.4**) should be used in order to report the trigger channel(s) and threshold(s) in standardized units.

4.2. Flow rate / volumetric quantification

Rationale: Calculation of the EV concentration requires a known flow rate. However, because the adjusted flow rate may deviate from the actual flow rate, it is good practice to measure the flow rate periodically. Methods for flow rate determination depend on the flow cytometer. There are various methods for monitoring flow rate, including counting beads, weighing samples before and after acquisition, and integral instrument flow rate sensors [26, 27].

Report: State if the flow rate was quantified/validated and if so, report the result and how they were obtained.

4.3. Fluorescence calibration

Rationale: Flow cytometers differ in their fluorescence sensitivity and dynamic range. A number of factors can lead to changes to an instruments sensitivity and dynamic range over time and therefore results in differences between experiments. Due to differences between instrument sensitivities, EVs may be identified as positive on one instrument, but appear negative on another instrument. In order to accurately compare data between flow cytometers, whose axes are in arbitrary units, a calibration must be performed to convert data from arbitrary to standard measurement units. Calibrating fluorescence scales from arbitrary units into standardized units for reporting provides improved comparisons of results between different experimental protocols and instruments with different sensitivities and differing experimental protocols [10, 16, 25, 28]. Fluorescence calibration is relatively simple to perform with protocols and reagents available from multiple manufacturers, and most commercially available cytometry software capable of performing it. Put simply, the known fluorescent values of each bead population are plotted against their arbitrary unit intensity and a regression line is drawn through these points. The slope and intercept of the regression line are then used to convert the arbitrary values to a calibrated scale. A number of common fluorophores are available with molecules of equivalent soluble fluorophore (MESF) beads. In the absence of MESF bead availability for a specific fluorophore, it is possible to use beads with a known binding capacity for IgG (antibody bound per cell (ABC) beads) which capture the conjugated antibody being used standardized in the assay. In cases where it is not possible to use MESF or ABC beads (such as membrane dyes), equivalent reference fluorophore (ERF) beads can be used. These beads have a broad emission spectrum and can standardize work on cytometers using the same filter sets. However, ERF beads are less accurate than MESF or ABC beads but are a useful method to approximate fluorescent measurements in a standard manner.

Report: State whether fluorescence calibration was implemented, and if so, report the materials and methods used, catalogue numbers, lot numbers, and supplied reference units for the standards. Fluorescence parameters may be reported in standardized units of MESF, ERF, or ABC beads. The type of regression used, and the resulting scatter plot

of arbitrary data vs standard data for the reference particles should be supplied. An example plot is shown in **Figure 3B.**

4.4. Light scatter calibration

Rationale: Light scatter signals are complex to standardize across different FC platforms. This is because the amount of light scatter detected from any given particle is dependent on a number of variables, including: its diameter, its composition and refractive index, the refractive index of the suspension medium, and the range of angles and geometry of light collected by a FC platform [18]. Due to these differences, the use of polystyrene beads alone does not result in a calibrated scatter detector, nor can it be used to compare instrument resolution and sensitivity for particles other than polystyrene beads. Thus, a gating strategy based on polystyrene beads alone is not a sound standardization methodology [18, 29]. The calibration of any scattering channel (FSC, SSC, MALS, etc.) from arbitrary units to standard units requires the use of Mie modeling software [18, 22, 30-32]. Light scatter calibration provides information that is essential for any cross-platform interpretation and will allow reproducibility of EV measurements performed on instruments with different optical configurations and settings. The use of modelling also provides a method of displaying instrument light scatter sensitivity independently or refractive index (**Figure 3C**) [18, 22, 31, 32].

Report: State whether and how light scatter calibration was implemented. Light scatter parameters may be reported in standardized units of nm^2, along with information required to reproduce the model.

5. EV characterization

A number of EV characteristics can potentially be inferred from FC data, including diameter, refractive index, and number of epitopes. Understanding the derivation of EV characteristics requires expertise as well as specific controls. Currently, the majority of the EV-FC-WG, as referees, would not expect these characterizations to be performed in all or most manuscripts (**Figure 2**). If performed, however, these advanced derivations should be reported as follows.

5.1. EV diameter/surface area/volume approximation

Rationale: The determination of EV diameter provides a method of normalizing data between experiments and having a quantification of instrument sensitivity. This has been demonstrated using Mie modeling of one scatter detector, by calibrating the ratio between side and forward scatter, and by surface area approximation using fluorescence [24, 25, 30, 31, 33].

Report: State whether and how EV diameter, surface area, and/or volume has been calculated using FC measurements.

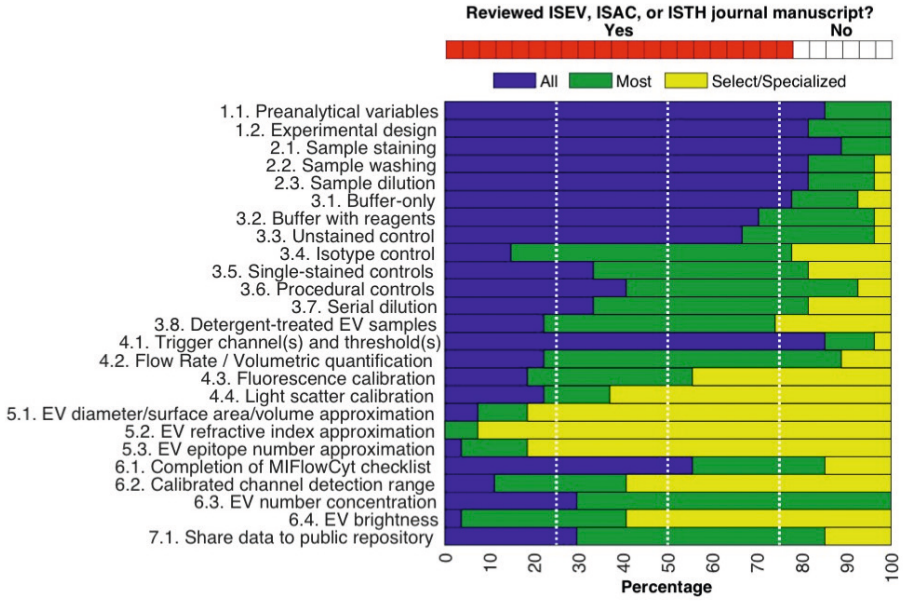

Figure 2. Summary of a poll about what extracellular vesicles (EV) flow cytometry (FCM) working group (WG) members expect to be reported in scientific manuscripts on EV-FC. The top chart shows the number of working group members who have experience reviewing manuscripts from the ISEV, ISAC, ISTH journals (red), and those that have not (white). The bottom bar graph summarizes the personal expectations of all co-authors regarding components to be reported in EV-FC manuscript published in ISEV, ISAC, and ISTH journals. The expectations fall into categories of all (blue), most (green), or select/specialized (yellow) manuscripts.

5.2. EV refractive index approxiswmation

Rationale: The determination of refractive index may indicate differences in EV composition (protein vs. lipid levels, cargo) or allow a method for defining gates for EV analysis or exclusion of events from analysis. Refractive index approximation using data from FC instruments has been demonstrated for EVs larger than 200 nm using the flow cytometry scatter-ratio (Flow-SR) methodology (**Figure 3D**) [33] and multi-angle scattering detection [34].

Report: State whether the EV refractive index has been approximated and how this was done.

5.3. EV epitope number approximation

Rationale: EV epitope number may provide an insightful method of normalizing data between experiments. This differs from EV brightness in MESF/ERF/ABC units as it must account for further variables such as antibody valency, avidity, clone, and conjugation [35, 36].

Report: State whether EV epitope number has been approximated, and if so, how it was approximated.

6. FC data reporting

Most EV-FC experiments are performed to determine what markers can be detected on individual EVs and what the concentration of those EVs is in a sample. In order to ensure that these measurements can be reproduced across laboratories that are using different instruments with different configurations and settings, it is important that the data from these experiments are presented in a way that is standardized. These standardized measurements will, in turn, help the research community compare available cytometers and protocols for EV analysis.

6.1. Complete MIFlowCyt checklist

Rationale: The MIFlowCyt checklist was developed in order to provide a standardized method of reporting experimental and flow cytometer parameter pertinent to the experiment interpretation and reproducibility. These include the reporting of instrument settings such as laser power, detector settings, and filter sets. It should be noted that many instrument settings are automatically saved to the ".fcs" -files that are generated by flow cytometers. FC software analysis packages also have built-in functions to record MIFlowCyt checklist parameters to the experiment workspace, which in turn can also be uploaded to public repositories such as FlowRepository. When uploaded to public repositories such as FlowRepository which read each ".fcs'-file, instrument settings are also imported and are therefore easily accessible [3, 37].

Report: Complete MIFlowCyt checklist components 1 to 4 using the MIFlowCyt guidelines.

6.2. Calibrated channel detection range

Rationale: Flow cytometers have a limited dynamic range and are therefore only capable of detecting signals between a set range. Stating the lower and upper limited of the detection channel range is a method of normalizing data between instruments with different sensitivity limits.

Report: If fluorescence or scatter calibration has been carried out, authors should state whether the upper and lower limits of a calibrated detection channel were calculated in standardized units. This can be done by converting the arbitrary unit scale to a calibrated scaled, as discussed in **Component 4.3 and 4.4**, and providing the highest unit on this scale and the lowest detectable unit above the unstained population. The lowest unit at which a population is deemed 'positive' can be determined a variety of ways, including reporting the 99th percentile measurement unit of the unstained population for fluorescence. The chosen method for determining at what unit an event was deemed positive should be clearly outlined.

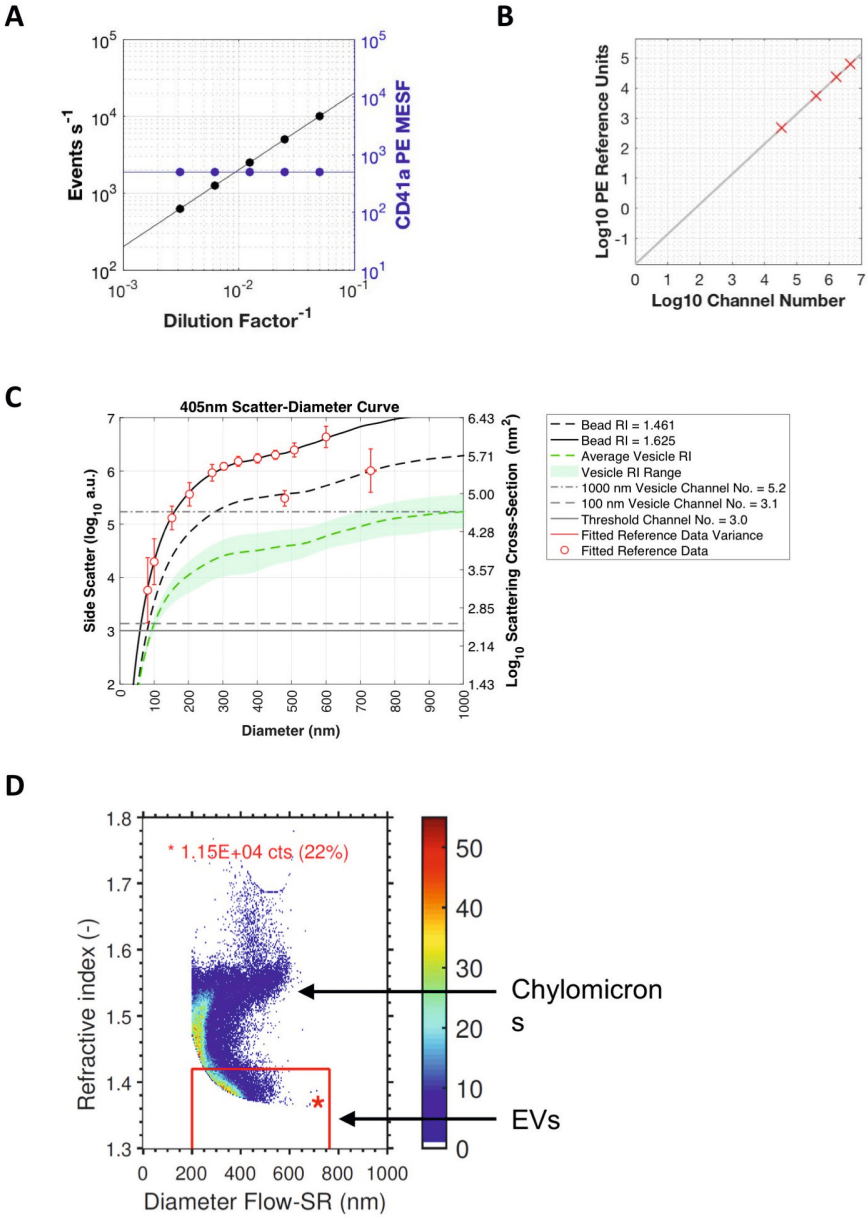

Figure 3. A. shows an example plot of reporting serial dilutions data, with event count per second on the left y-axis, median PE MESF intensity of the recorded data on the right y-axis and the dilution factor on the x-axis. B. shows an example plot of reporting fluorescence calibration using regression. The fluorescent intensity in arbitrary units (channel number) is on the x-axis with the related fluorescence population reference units on the y-axis. C. provides an example plot of light scatter calibration at 405 nm using FCM_{PASS} software default values. D. provides an example plot of refractive index and diameter determination using Flow-SR. methodology.

6.3. EV number concentration

Rationale: Due to flow cytometers having a varying sensitivity and a limited detection range (**Component 6.2**), only a portion of the full EV population may be detected. Reporting concentration as a number of detected EVs between a calibrated detection range enables standardized reporting and makes data reproducibility and validation possible. This detection range can take the form of MESF units, scattering units (nm^2), diameter, or others [38]. Due to cytometers being unable to differentiate between very dim and negative populations percentages should not be used to quantify EVs using immunophenotyping.

Report: State whether EV number/concentration has been reported. If calculated, it is preferable to report EV number/concentration in a standardized manner, stating the number/concentration between a set detection range.

6.4. EV brightness

Rationale: Using calibrated units to report the fluorescence and/or scatter signals as statistical summaries, histograms, or scatter plots, provides a standardized reporting method that makes data reproducibility and validation possible.

Report: When applicable, state the method by which the brightness of EVs is reported in standardized units of scatter and/or fluorescence.

7. FC data sharing

Scientific publications have limited space for extensive figures and both journals and scientists tend not to publish many control data points. It is however important as a reader or reviewer to be able to inspect the quality of data acquisition and particularly the experimental controls (described in **Category 3**), when interpreting a piece of published work.

7.1. Share data to public repository

Rationale: Public access to published data allows other researchers to inspect control and acquired sample data. Public access to data has been found to improve the reporting accuracy in manuscripts and provides important transparency for referees and readers of published work. For these reasons many funding agencies require public release of data. All human subject's data with Personally Identifying Information (PII) must be deidentified prior to collection or data deposition. FlowRepository was developed in tandem with the MIFlowCyt guidelines as a public data repository to support open access of data from published and unpublished work, and aids the completion of the MIFlowCyt components (**Component 1.2, Component 6.1**) by archiving data from the FC ".fcs"-files [37]. Data repositories tailored to EV-FC data are yet to be developed, but standard format (FC) data may be deposited at a number of data repositories (FlowRepository, Immport, Mendeley, Zenodo, figshare, etc.).

Report: Provide a link to the experimental data in a public data repository.

Broadly applicable experimental components of MIFlowCyt-EV

While this work aims to outline a standard reporting framework rather than set guidelines, it is clear that some components of the MIFlowCyt-EV framework are important to utilized and reported in the majority of single-EV analysis experiments regardless of design or instrumentation. These include components 1.1, 1.2, 2.1, 2.2, 2.3, 3.1, 3.2, 3.3, 3.5, 3.7, 4.1, 4.2, 4.3 and 6.1, as highlighted in **Table 1** and **Figure 1**. The use of components 3.4 and 3.6 should also be seen as a necessity should antibody staining, or post-stain wash methods be utilized, respectively. While the other components are still applicable, the other framework components have different degrees of importance, depending on the experimental objectives and design, and on the scope of claims that are based on the reported EV FC results. For example, **Component 5.1** is not relevant if work does not describe the detection limit of an instrument using diameter related claims. However, if a piece of work does make conclusions about the limit of an instrument detection using size related claims, **Component 5.1** should be addressed.

DISCUSSION

In the course of attempting to execute two sequential ISEV-ISAC-ISTH EV FCM WG Standardization Studies, with standards and samples distributed to 12-18 WG laboratories worldwide, we found that, even among EV FC groups that are at the forefront of the EV FC research field, we were not able to define a consensus guidelines for the best methods, instruments, controls, and analytical tools to use for a simple set of reference samples. However, the WG did arrive at a consensus regarding what information would assist with the interpretation and reproducibility of results across different platforms, sample types, and methods. This consensus is reflected in the MIFlowCyt-EV Framework for reporting EV FC studies.

The MIFlowCyt-EV framework stems from several years of collaborative work by an international group of researchers working together in the ISEV-ISAC-ISTH EV-FC WG. While an implied goal of these efforts is the comparison of methods and technologies for EV measurement, it quickly became clear that more complete and uniform reporting of assay methods and results would be required for this to be possible, since most members employ a diverse range of instruments and assay designs to measure a common set of representative EV samples. However, the ISEV-ISAC-ISTH EV-FC-WG also realized the importance of developing such a framework by consensus. Presentations, discussions and workshops taking place at the ISEV, ISAC, and ISTH annual conferences have been fundamental to its development.

A poll of the active participants of the EV-FC-WG provided insight into the level of current consensus on the necessity of reporting/carrying out each of the framework

components regardless of the EV-FC experiment being reported. This poll was not a reflection of the framework itself, as it was fully agreed upon by all members of the WG. The poll was instead a method to stratify the current experimental expectations of the field which was not addressed in this work. The group voted unanimously that preanalytical variables and experimental design (**Category 1**) should be reported in all or most manuscripts. More than 95% of the group voted that sample preparation steps (**Category 2**) should be reported in all or most manuscripts. The reporting of assay controls (**Category 3**) was voted to be expected in all or most EV-FC manuscripts by >80% of the WG members, with the exceptions of isotype (**Component 3.4**) and detergent controls (**Component 3.8**), which were 77% and 74%, respectively. The poll showed varied expectations for reporting of instrument data acquisition and calibration components (**Category 4**). The reporting of trigger channel(s) and threshold(s), and flow rate / volumetric quantification was expected to be reported in all or most EV-FC manuscripts by ≥88%, while fluorescence calibration and scatter calibration were voted for in all or most EV-FC manuscripts by 55% and 37%, respectively. The reporting of EV characterization (**Category 5**) in terms of diameter, refractive index, and epitope number using FC was the least expected information to be required in all or most EV-FC manuscripts, voted for by ≤20%. The poll showed that the expectation for reporting of FC data (**Category 6**) components in all or most EV-FC manuscripts was varied, with EV concentration reporting unanimously expected, the completion of the MIFlowCyt checklist (85%), and the calibration of detection channel range along with reporting EV brightness expected in all or most manuscripts by 41% of the participants. Finally, the sharing of FC data (**Category 7**) was expected to be reported by 88% of the WG.

In summary, the majority (>50%) of WG authors would expect details pertaining to 19 of 25 framework components to be conducted/reported in manuscripts using single EV-FC, with >75% consensus on 17 of 25 of the framework components. The MIFlowCyt-EV components that the majority of WG authors would currently only expect to be conducted and reported in select/specialized manuscript, are those that utilize relatively advanced protocols and understanding, such as light scatter calibration (**Component 4.4**), detection channel calibration (**Component 6.2**), EV characterization (**Component 5.1, 5.2, 5.3**), and reporting of EV brightness (**Component 6.4**). While these topics are critical for future standardization, they are areas that involve the development of new techniques, and where more tools, teaching, and validation studies may be required before becoming widely utilized. The WG authors in this manuscript have outlined a set of components that should be broadly considered for all single-FC experiments, regardless or instrument or assay, and feel the utilization of these components will aid in the development of more standardized small particle literature.

MIFlowCyt-EV has been developed specifically for the reporting of single EV-FC experiments and are generally applicable to other small particles e.g. viruses. A future framework aiming at alternative bulk-EV analysis methods using FC, such as capture-bead

assays, may also be useful. Due to the EV-field being in its infancy, the MIFlowCyt-EV is not yet exhaustive and will likely be adapted and updated in time as the field progresses. The utilization of this reporting framework will be key in the development of: (i) standard operating procedures, (ii) reference materials, (iii) and validation studies. The development of each of these is required to advance the field and further improve standardization efforts and will supported by this WG. More information on the ISEV-ISAC-ISTH EV flow cytometry WG updates and resources can be found at: www.evflowcytometry.org.

FUNDING ACKNOWLEDGEMENTS

- JAW is an International Society for Advancement of Cytometry (ISAC) Marylou Ingram Scholar 2019-2023.
- RN, FC, EvdP, LdR acknowledge funding from the Netherlands Organisation for Scientific Research - Domain Applied and Engineering Sciences (NWO-TTW), research programs VENI 13681 (FC) and VENI 15924 (EvdP) and STW perspectief CANCER-ID 14195 (LdR).
- IG acknowledges U01-126497; U01-OD-019750; R01 CA218500; R01 HL1266497
- AG is an International Society for Advancement of Cytometry (ISAC) Marylou Ingram Scholar 2019-2023.
- AH and ODW are supported by Fund for Scientific Research (FWO), Foundation against Cancer (STK), Stand up to Cancer (KOTK) and Special Research Fund Ghent University (BOF).
- SFWML was supported by the Dutch Technology Foundation STW (Perspectief Program Cancer ID, project 14191), which is part of the Netherlands Organization for Scientific Research (NWO), and which is partly funded by the Ministry of Economic Affairs.
- ELA is supported by the European Union's Horizon 2020 Research and Innovation Programme under the Marie Skłodowska-Curie grant agreement No. 722148. (TRAIN-EV)
- JN acknowledges NIH R01 EB003824, UH3 TR000931; UH3 TR000891; UH3 TR000903.
- JCJ, JAW, and AMK were supported by the Intramural Research Program of the National Institutes of Health (NIH), National Cancer Institute, and Center for Cancer Research

DECLARATION OF INTEREST STATEMENT

- MB, FDG, IG, BG, AH, RL, JL, SR, TT, JT, OdW declare no conflict of interest.
- The Wauben research group (MHMW, GJAA, SFWML, ELA), Utrecht University, Faculty of Veterinary Medicine, Department of Biochemistry and Cell Biology had a collaborative research agreement with BD Biosciences Europe, Erembodegem, Belgium, to optimize analysis of EVs with the BD Influx.
- AB is founder and CEO of Exo-Analysis
- AG is an inventor on patents and patent applications related to EV analysis, and is consultant for and has equity interest in Evox Therapeutics Ltd., Oxford, United Kingdom
- FC and EvdP are co-founder and stakeholders of Exometry B.V.
- AMC (RN, EvP, FC, LdR) and BD Biosciences Europe, Erembodegem, Belgium have a collaboration in research program STW perspectief CANCER-ID.
- JPN and ED are inventors on patents and patent applications related to flow cytometry and have a financial interest in Cellarcus Biosciences, which offers vesicle analysis products and services.
- NCI holds a collaborative research and development agreement (CRADA) with Beckman Coulter.
- NCI investigators, JCJ, AMK, and JAW, are inventors on patents and patent applications related to EV analysis.
- XY declares competing financial interests as a co-founder of NanoFCM Inc.

REFERENCES

1. Yanez-Mo, M., et al., *Biological properties of extracellular vesicles and their physiological functions.* J Extracell Vesicles, 2015. **4**: p. 27066.
2. Fais, S., et al., *Evidence-Based Clinical Use of Nanoscale Extracellular Vesicles in Nanomedicine.* ACS Nano, 2016. **10**(4): p. 3886-99.
3. Lee, J.A., et al., *MIFlowCyt: the minimum information about a Flow Cytometry Experiment.* Cytometry A, 2008. **73**(10): p. 926-30.
4. Thery, C., et al., *Minimal information for studies of extracellular vesicles 2018 (MISEV2018): a position statement of the International Society for Extracellular Vesicles and update of the MISEV2014 guidelines.* J Extracell Vesicles, 2018. **7**(1): p. 1535750.
5. Witwer, K.W., et al., *Standardization of sample collection, isolation and analysis methods in extracellular vesicle research.* Journal of Extracellular Vesicles, 2013. **2**(1): p. 20360.
6. Consortium, E.-T., et al., *EV-TRACK: transparent reporting and centralizing knowledge in extracellular vesicle research.* Nat Methods, 2017. **14**(3): p. 228-232.
7. Lacroix, R., et al., *Standardization of pre-analytical variables in plasma microparticle determination: results of the International Society on Thrombosis and Haemostasis SSC Collaborative workshop.* Journal of Thrombosis and Haemostasis, 2013. **11**(6): p. 1190-1193.
8. Coumans, F.A.W., et al., *Methodological Guidelines to Study Extracellular Vesicles.* Circ Res, 2017. **120**(10): p. 1632-1648.
9. Ridger, V.C., et al., *Microvesicles in vascular homeostasis and diseases. Position Paper of the European Society of Cardiology (ESC) Working Group on Atherosclerosis and Vascular Biology.* Thromb Haemost, 2017. **117**(7): p. 1296-1316.
10. Morales-Kastresana, A., et al., *High-fidelity detection and sorting of nanoscale vesicles in viral disease and cancer.* Journal of Extracellular Vesicles, 2019. **8**(1).
11. Nolan, J.P. and S.A. Stoner, *A trigger channel threshold artifact in nanoparticle analysis.* Cytometry A, 2013. **83**(3): p. 301-5.
12. Inglis, H.C., et al., *Techniques to improve detection and analysis of extracellular vesicles using flow cytometry.* Cytometry A, 2015. **87**(11): p. 1052-63.
13. de Rond, L., et al., *Comparison of Generic Fluorescent Markers for Detection of Extracellular Vesicles by Flow Cytometry.* Clin Chem, 2018. **64**(4): p. 680-689.
14. Morales-Kastresana, A., et al., *Labeling Extracellular Vesicles for Nanoscale Flow Cytometry.* Sci Rep, 2017. **7**(1): p. 1878.
15. van der Vlist, E.J., et al., *Fluorescent labeling of nano-sized vesicles released by cells and subsequent quantitative and qualitative analysis by high-resolution flow cytometry.* Nat Protoc, 2012. **7**(7): p. 1311-26.
16. Gorgens, A., et al., *Optimisation of imaging flow cytometry for the analysis of single extracellular vesicles by using fluorescence-tagged vesicles as biological reference material.* Journal of Extracellular Vesicles, 2019. **8**(1).
17. Nolte-'t Hoen, E.N., et al., *Quantitative and qualitative flow cytometric analysis of nanosized cell-derived membrane vesicles.* Nanomedicine, 2012. **8**(5): p. 712-20.
18. van der Pol, E., et al., *Single vs. swarm detection of microparticles and exosomes by flow cytometry.* J Thromb Haemost, 2012. **10**(5): p. 919-30.
19. Libregts, S., et al., *Flow cytometric analysis of extracellular vesicle subsets in plasma: impact of swarm by particles of non-interest.* J Thromb Haemost, 2018. **16**(7): p. 1423-1436.

20. Nolan, J.P. and E. Duggan, *Analysis of Individual Extracellular Vesicles by Flow Cytometry.* Methods Mol Biol, 2018. **1678**: p. 79-92.
21. Groot Kormelink, T., et al., *Prerequisites for the analysis and sorting of extracellular vesicle subpopulations by high-resolution flow cytometry.* Cytometry A, 2016. **89**(2): p. 135-47.
22. Welsh, J.A., et al., *Prospective Use of High-Refractive Index Materials for Single Molecule Detection in Flow Cytometry.* Sensors (Basel, Switzerland), 2018. **18**(8).
23. Osteikoetxea, X., et al., *Differential detergent sensitivity of extracellular vesicle subpopulations.* Org Biomol Chem, 2015. **13**(38): p. 9775-82.
24. Tian, Y., et al., *Protein Profiling and Sizing of Extracellular Vesicles from Colorectal Cancer Patients via Flow Cytometry.* ACS Nano, 2018. **12**(1): p. 671-680.
25. Stoner, S.A., et al., *High sensitivity flow cytometry of membrane vesicles.* Cytometry A, 2016. **89**(2): p. 196-206.
26. Shapiro, H.M., *Practical flow cytometry*. 4th ed. 2003, New York: Wiley-Liss. l, 681 p.
27. Nolan, J.P., *Flow Cytometry of Extracellular Vesicles: Potential, Pitfalls, and Prospects.* Curr Protoc Cytom, 2015. **73**: p. 13 14 1-16.
28. Wang, L. and R.A. Hoffman, *Standardization, Calibration, and Control in Flow Cytometry.* Curr Protoc Cytom, 2017. **79**: p. 1 3 1-1 3 27.
29. Chandler, W.L., W. Yeung, and J.F. Tait, *A new microparticle size calibration standard for use in measuring smaller microparticles using a new flow cytometer.* J Thromb Haemost, 2011. **9**(6): p. 1216-24.
30. Welsh, J.A., et al., *FCMPASS Software Aids Extracellular Vesicle Light Scatter Standardization.* Cytometry Part A. **0**(0).
31. de Rond, L., et al., *Deriving Extracellular Vesicle Size From Scatter Intensities Measured by Flow Cytometry.* Curr Protoc Cytom, 2018. **86**(1): p. e43.
32. Zhang, W., et al., *Light-Scattering Sizing of Single Submicron Particles by High-Sensitivity Flow Cytometry.* Anal Chem, 2018. **90**(21): p. 12768-12775.
33. van der Pol, E., et al., *Absolute sizing and label-free identification of extracellular vesicles by flow cytometry.* Nanomedicine, 2018. **14**(3): p. 801-810.
34. Konokhova, A.I., et al., *Super-resolved calibration-free flow cytometric characterization of platelets and cell-derived microparticles in platelet-rich plasma.* Cytometry A, 2016. **89**(2): p. 159-68.
35. Davis, K.A., et al., *Determination of CD4 antigen density on cells: role of antibody valency, avidity, clones, and conjugation.* Cytometry, 1998. **33**(2): p. 197-205.
36. Arraud, N., et al., *Fluorescence triggering: A general strategy for enumerating and phenotyping extracellular vesicles by flow cytometry.* Cytometry A, 2016. **89**(2): p. 184-95.
37. Spidlen, J., et al., *FlowRepository: a resource of annotated flow cytometry datasets associated with peer-reviewed publications.* Cytometry A, 2012. **81**(9): p. 727-31.
38. van der Pol, E., et al., *Optical and non-optical methods for detection and characterization of microparticles and exosomes.* J Thromb Haemost, 2010. **8**(12): p. 2596-607.

“Great things are done by a series of small things brought together.”

Vincent van Gogh

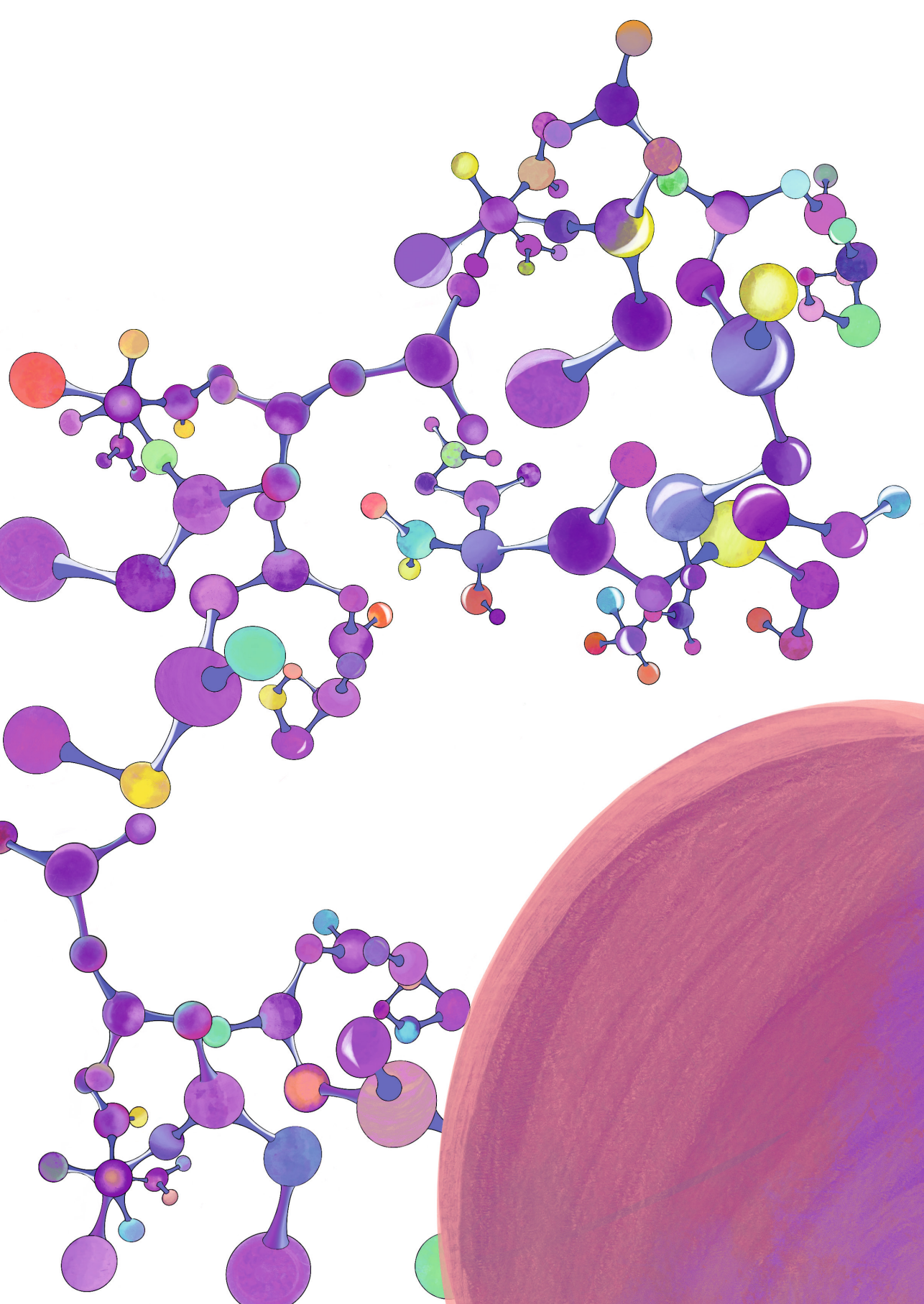

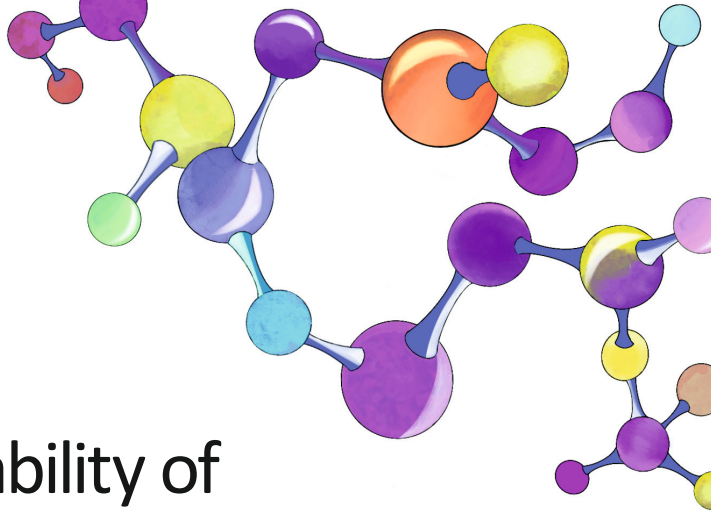

CHAPTER 4

Intrinsic variability of fluorescence calibrators impacts the assignment of MESF or ERF values to nanoparticles and extracellular vesicles by flow cytometry

Estefanía Lozano-Andrés [1,#], Tina Van Den Broeck [2,#], Lili Wang [3], Majid Mehrpouyan [4], Ye Tian [5], Xiaomei Yan [5], Marca H.M. Wauben [*1,#], Ger. J.A. Arkesteijn [*1]

1 Department of Biomolecular Health Sciences, Faculty of Veterinary Medicine, Utrecht University, Utrecht, The Netherlands
2 BD Biosciences, Erembodegem, Belgium
3 Biosystems and Biomaterials Division, National Institutes of Standards and Technology (NIST), Gaithersburg, MD 20899
4 BD Biosciences, San Jose, CA 95131
5 Department of Chemical Biology, MOE Key Laboratory of Spectrochemical Analysis & Instrumentation, Key Laboratory for Chemical Biology of Fujian Province, College of Chemistry and Chemical Engineering, Xiamen University, Xiamen 361005, People's Republic of China
TRAIN-EV Marie Skłodowska-Curie Action-Innovative Training Network, train-ev.eu
*Both authors contributed equally

To be submitted:
Lozano-Andrés E. et al., (2022). BioRxiv
https://doi.org/10.1101/2021.03.01.433358

ABSTRACT

Flow cytometry is commonly used to characterize nanoparticles (NPs) and extracellular vesicles (EVs) but results are often expressed in arbitrary units to indicate fluorescence intensity. This hampers interlaboratory and inter-platform comparisons. We investigated the use of molecules of equivalent soluble fluorophores (MESF)-beads for assignment of fluorescence values to NPs and EVs by comparing two FITC-MESF bead sets as calibrators on different flow cytometry platforms (BD Influx™, CytoFLEX LX™ and SORP BD FACSCelesta™). Next, fluorescence signals of NPs and EVs were calibrated using different sets of FITC and PE-MESF beads. Fluorescence calibration using beads designed for cellular flow cytometry allowed inter-platform comparison. However, the intrinsic uncertainty in the fluorescence assignment to these MESF beads impacts the reliable assignment of MESF values to NPs and EVs based on extrapolation into the dim fluorescence range. Our findings demonstrate that the use of the same set of calibration materials (vendor and lot number) and the same number of calibration points, greatly improves robust interlaboratory and inter-platform comparison of fluorescent submicron sized particles.

Keywords: fluorescence, calibration, standardization, MESF, extracellular vesicles, nanoparticles, flow cytometry

INTRODUCTION

A well-known fluorescence calibration method in flow cytometry (FC) is the use of fluorescent beads to which a measurement value is assigned using standardized units established by the National Institute of Standards and Technology (NIST), such as molecules of equivalent soluble fluorophores (MESF) or equivalent number of reference fluorophore (ERF). This calibration method was developed for cellular FC and allows for quantifiable fluorescence measurements and platform comparison. The fluorescence intensity on the calibrator beads matches the expected intensity on the labeled cells. Therefore, the calibrated cellular fluorescence variation closely compares to the intrinsic variation on the calibrator and allows for data interpolation [1-4]. In 2012, a NIST/ISAC standardization study reported differences in the assigned units to calibrators from different manufactures, indicating the importance of the examination of the accuracy and precision of available calibrators [5]. Nevertheless, the assignment of a specific MESF or ERF value to calibration beads is inextricably bound to a variation around this value. This variation translates in an uncertainty level between the measured and the assigned values that remains acceptable as long as the sample values are within the range of the calibrator.

During the last decade, small particle FC has become a powerful tool for high-throughput analysis of nanoparticles (NPs) and cell-derived extracellular vesicles (EVs) [6, 7]. However, EV measurements are challenging, mainly because the vast majority of EVs is small in size (<200nm) and their light scattering and fluorescent signals are typically close to, at, or below the instrument's detection limit [8]. Furthermore, the majority of data is reported in arbitrary units of fluorescence, which is cumbersome for the analysis of dim and small particles, whereby particles cannot be fully discriminated from negative counterparts and background signals. The MIFlowCyt-EV framework recommends the use of MESF beads for calibration and standardized reporting of EV flow cytometric experiments, especially when a fluorescent threshold is applied [8]. However, since available calibrators are developed for cells and as such are much brighter in fluorescence than EVs it is unknown to which extend these calibrators will provide precision and/or accuracy for the assignment of fluorescent values to NPs and EVs. We investigated how the given units of the calibrator impact the regression line for assignment of MESF and/or ERF units to NPs and EVs. Therefore, we evaluated custom-made calibrator beads sets from the same manufacturer on three different flow cytometers and provide insights on how different bead sets affect the calibration of fluorescence signals from NPs and EVs.

MATERIAL AND METHODS

Calibration beads

For calibration of the fluorescence axis in the fluorescein isothiocyanate (FITC) channel we used two different sets of FITC MESF beads (custom-made, 6 µm lot MM2307 #131-10; #131-8; #130-6; #130-5; #130-3 and 2 µm lot MM2307#156; #159.1; #159.2; #122.3, BD Biosciences, San Jose, CA). For calibration of the fluorescence axis in the PE channel, we used two different sets of PE MESF beads (6 µm, commercial QuantiBrite, Catalog No. 340495 lot 62981 and 2 µm, custom made, lot MM2327#153.1; #153.2; #153.4; #153.5; #153.6, BD Biosciences, San Jose, CA).

The 6 µm FITC MESF beads were prepared by reacting various concentration of FITC with PMMA Beads (Bangs Labs) in borate buffer at pH 9.2. The 2 µm FITC beads were prepared by reacting various concentrations of FITC-BSA (with a FITC/BSA molar ratio of 2) with 2 µm carboxylic beads (Bangs Labs) using EDC/NHS chemistry. The 2 µm PE beads were made as described above except various concentrations of PE were used with 2 µm carboxylic beads in EDC/NHS chemistry. These beads were analyzed on a BD LSRFortessa™ (BD Biosciences) and their MESF values were assigned by cross-calibration using commercially available MESF beads (Flow Cytometry Standards Corp.). The FITC ERF values were assigned to both 2 µm and 6 µm beads using a specific lot of FITC-FC Bead (BD Biosciences) as a calibrator with known ERF value, which has been assigned by NIST. This provided us with two distinct calibrator bead sets that were produced through the same manufacturing process and assigned using the same instruments and the same internal NIST traceable calibrator to exclude internal processing variations.

In addition, we measured commercially available Quantum™ FITC-5 MESF (7 µm, Catalog No. 555, lot 14609, Bangs Laboratories) and AccuCheck ERF Reference Particles Kit (3 µm, Catalog No. A55950, lot #081220207, #081220203, #081220208, Thermo Fisher) which were prepared according to the manufacturer's instructions.

All calibration bead sets were measured with gain or voltage settings as would be used for the analysis of small particles (i.e. EVs). In addition, not all beads could be measured on every instrument. For fair cross-platform comparison of the slopes of the regression lines, only the bead populations that could be measured on all instruments were included for linear regression analysis.

Flow cytometer platforms

In this study three flow cytometers were used. A jet in air-based BD Influx (BD Biosciences, San Jose, CA), a BC CytoFLEX LX (Beckman Coulter, Brea, CA) with a cuvette-based system and a cuvette-based SORP BD FACSCelesta™ (BD Biosciences, San Jose, CA) equipped with a prototype small particle side scatter module.

The BD Influx flow cytometer was modified and optimized for detection of submicron-sized particles [10]. In brief, FITC was excited with a 488 nm laser (Sapphire, Coherent 200 mW) and fluorescence was collected through a 530/40 bandpass filter. PE was excited with a 562 nm laser (Jive, Cobolt 150 mW) and fluorescence was collected through a 585/42 bandpass filter. Optical configuration of the forward scatter detector was adapted by mounting a smaller pinhole and an enlarged obscuration bar in order to reduce optical background. This reduced wide-angle FSC (rwFSC) allowed detection of sub-micron particles above the background based on forward scatter [10, 16]. Upon acquisition, all scatter and fluorescence parameters were set to a logarithmic scale. To minimize day to day variations, the BD Influx was standardized at the beginning of each experiment by running 100 and 200 nm yellow-green (505/515) FluoSphere beads (Invitrogen, F8803 and F8848). The instrument was aligned until predefined MFI and scatter intensities where reached with the smallest possible coefficient of variation (CV) for rwFSC, SSC and fluorescence. After optimal alignment, PMT settings required no or minimal day to day adjustment and ensured that each measurement was comparable. MESF beads and NPs were measured with a FSC threshold set at 1.0 while for biological EVs a fluorescence threshold was set at 0.67 by allowing an event rate of 10-20 events/second while running a clean PBS control sample.

When performing quantitative and qualitative analysis of synthetic NPs and biological EVs, preparations were diluted in PBS as indicated. Upon loading on the Influx, the sample was boosted into the flow cytometer until events appeared, after which the system was allowed to stabilize for 30 seconds. Measurements were performed either by a fixed 30 second time or by setting a gate around the spike-in beads and allowing to record a defined number of events in the gate (80 000 events) using BD FACS Sortware 1.01.654 (BD Biosciences).

The CytoFLEX LX was used without any tailor-made modifications in the configuration. Before measurements, the manufacturer recommended startup and QC procedure were run first. All scatter and fluorescence parameters were set to a logarithmic scale. FITC was measured with a 50 mW 488 nm laser and fluorescence was measured through a 525/40 band pass filter at gain 1.0. FITC MESF beads were recorded with an FSC threshold at 1000. Measurements were performed using CytExpert 2.1 (Beckman Coulter).

The SORP BD FACSCelesta™ was equipped with a prototype small particle SSC module for improved scatter detection. Before measurement, the recommended CS&T performance check was run to monitor performance on a daily basis and to optimize laser delay. All scatter and fluorescence parameters were set to a logarithmic scale. 100 nm yellow-green (505/515) FluoSphere beads (Invitrogen, F8803) were acquired and used to set optimal fluorescence (FITC detector) PMT-V values. FITC was measured with a 100 mW 488 nm laser through a 530/30 band pass filter. FITC-MESF beads were recorded

with an SSC threshold at 200. Measurements were performed using BD FACSDiva™ Software v8.0.3 (BD Biosciences).

Further descriptions of each instrument and methods are provided in Data S1 (MIFlowCyt checklist) and Data S2 (MiFlowCyt-EV framework).

Preparation of FITC-doped silica nanoparticles

Synthetic silica nanoparticles (SiNPs) of 550 nm diameter with six different FITC fluorescence intensities were produced by using a modified method of literature reports [17-19]. Briefly, the amine reactive FITC molecules were covalently linked to the silane coupling agent, (3-aminopropyl)-triethoxylsilane (APTES) in anhydrous ethanol. Monodisperse silica seeds of ~90 nm prepared by using amino acid as the base catalyst [17, 18] were suspended in a solvent mixture containing ethanol, water and ammonia. Then tetraethyl orthosilicate (TEOS) and different volumes of APTES−FITC solutions were added for growing FITC-doped SiNPs by a modified Stöber method [19, 20]. Upon washing three times with anhydrous ethanol, the FITC-doped SiNPs were reacted with TEOS in the solvent mixture to allow growth of a silica layer. The synthesized SiNPs were washed three times with anhydrous ethanol and stocked in anhydrous ethanol. The diameters of SiNPs were measured by transmission electron microscopy.

Isolation and fluorescent staining of extracellular vesicles for flow cytometric analysis

EV-containing samples were obtained from 4T1 mouse mammary carcinoma cell culture supernatants (ATCC, Manassas, VA) as previously described [16, 21, 22]. EVs were stained with 5-(and-6)-Carboxyfluorescein diacetate succinimidyl ester (CFDA-SE, hereinafter referred as CFSE) (Thermo Fisher, Catalog No. C1157) and separated as described previously [10]. Briefly, 2 µl of the isolated 4T1 EVs (corresponding to a concentration of 1.44 E12 particles/mL as determined by nanoparticle tracking analysis) were mixed with 18 µl PBS/0.1% aggregate-depleted (ad)BSA. For antibody labeling, samples were first resuspended in 15.5 µL PBS/0.1% adBSA and incubated with 0.5 µg of rat anti-mouse CD9-PE (Clone: KMC8, IgG2a, κ, lot 7268877, BD Biosciences) or matched isotype antibodies (Rat IgG2a, κ, PE-conjugated, lot 8096525, BD Biosciences) for 1h at RT while protected from light. EVs were then stained with 40 µM CFSE in a final volume of 40 µl. The sealed tube was incubated for 2h at 37°C while protected from light. Next, staining was stopped by adding 260 µl PBS/0.1% adBSA. After fluorescent staining, EVs were separated from protein aggregates and free reagents by bottom-up density gradient centrifugation in sucrose for 17.30 h at 192,000 g and 4°C using a SW40 rotor (k-factor 144.5; Beckman Coulter, Fullerton, California, USA). Twelve fractions of 1 mL were then collected from the top of the gradient and respective densities were determined by refractometry using an Atago Illuminator (Japan). For analysis by flow cytometry, EV samples corresponding to a 1.14 g/mL density were diluted 1:20 in PBS prior measurement. MIFlowCyt-EV framework [8] were followed whenever applicable (Data S2).

Concentration determination by using spike-in beads

EV concentration was normalized using a spiked-in external standard containing 200 nm orange (540/560) fluorescent beads (Invitrogen, F8809). The concentration of the beads was determined by Flow NanoAnalyzer N30 (NanoFCM, Xiamen, China) and stocked at 5.7E10 particles/mL. Beads were diluted 1:10^4 in PBS and added to the EV samples, mixed and measured on the flow cytometer. Bead count was used to calculate the EV concentration for BD Influx measurements.

Data analysis

For fluorescence calibration each bead peak population was gated using FlowJo Version 10.5.0 and MFI were obtained for further least square linear regression analysis. Data was handled in Microsoft Excel and figures were prepared using GraphPad Prism version 8.0 (GraphPad Software Inc). The software FCMPASS Version v2.17 was used to generate files with calibrated axis units in the histograms and dot plots shown [23] (Software is available on http://go.cancer.gov/a/y4ZeFtA).

Data availability

All EV data of our experiments have been submitted to the EV-TRACK knowledgebase (EV-TRACK ID: EV210047) [24]. All flow cytometric data files have been deposited at the Flow Repository (FR-FCM-Z3FJ).

RESULTS

Assessment of precision and accuracy of different MESF bead sets for fluorescence calibration across platforms

To assess the precision and accuracy of MESF bead sets for fluorescence calibration across platforms, two FITC MESF bead sets of 6 µm and 2 µm, containing respectively five or four fluorescent bead populations, were selected for measurements on three different instruments, namely a BD Influx, a BC CytoFLEX and a SORP BD FACSCelesta™. Since calibrator bead sets can differ in the number of fluorescent bead populations (typically ranging from 3 to 5) and the number of calibrator points can impact the slope of the regression line (Figure S1a-b), we included for fluorescence calibration across platforms equal numbers of fluorescent bead populations (n=4) of the two FITC MESF bead sets that were consistently measured on all three platforms (Figure 1).

Singlet gated populations are displayed as overlays in histograms showing the FITC fluorescence (Figure 1a) and indicated from dim to bright as p1, p2, p3 and p4 (Figure 1b). The 6 µm FITC MESF beads contained overall brighter fluorescent intensities, whose assigned values range from 25,910 to 715,225 FITC MESF, while the 2 µm FITC MESF beads covered a dimmer part of the fluorescence intensity range with assigned values ranging from 3,634 to 103,706 FITC MESF. Clearly, MFI arbitrary units cannot be directly compared between instruments (Figure 1b), but after fluorescence calibration

comparable FITC MESF units could be assigned (Figure 1c-d). Nevertheless, the two calibration bead sets displayed a different slope with a consistent tendency across the three platforms, suggesting a variation introduced by an inherent attribute of the beads themselves. This lead us to further examine the robustness of the calibration. To gain insight into the precision and accuracy of MESF assignments we selected specific bead populations from one set, referred to as 'unknown' in Figure 1d, to recalculate their FITC MESF units using the regression line from the other bead set. The selected 'unknown' samples used were: (i) p1 and p4 of the 2 µm bead set for which the FITC MESF values were calculated using the regression line of the 6 µm bead set and (ii) p1 and p2 of the 6 µm bead set for which the FITC MESF values were calculated using the regression line of the 2 µm bead set (Figure 1c). Using this approach, the calculated MESF values of p4 from the 2 µm beads and p2 from the 6 µm beads showed less than 20% variation (10% above or 10% below actual values) of the actual value, while data were precise when compared between platforms (Figure 1d). Also the MESF values of the dimmest p1 2 µm and 6 µm beads, calculated using respectively the regression lines of the 6 µm and 2 µm bead sets, were comparable between platforms. However, the calculated values revealed more than a 20% variation from the given value, leading to either an under-estimation or an overestimation of the FITC MESF units (Figure 1d). These results show that slight differences in the slope of the calibration lines of the different MESF bead sets become more prominent when extrapolation needs to be extended into the dim area beyond the fluorescence intensities of the calibration beads themselves. Since the same slope differences occurred on all three platforms (Figure 1c), this observation is not related to the type of instrument used (e.g.; digital or analog, photomultiplier (PMT) or avalanche photodiode (APD), jet-in-air or cuvette based). Furthermore, this recurring pattern on all platforms makes it unlikely that differences in slopes were caused by instrument non-linearity. Further evidence to rule out non-linearity issues is provided by linear plotting of the values, showing no non-linearity issues (Figure S2a-c), and demonstrating instrument linearity on the BD Influx following the approach described by Bagwell et al [9] (Figure S3). Furthermore, we ruled out that slope differences were a result of variations between separate measurements (Figure S4), and confirmed by testing both custom-made and commercial FITC MESF beads (Figure S1) and FITC MESF beads and PE MESF beads (Figure S2 d-f) that slope variability is inherent to the use of calibrator beads.

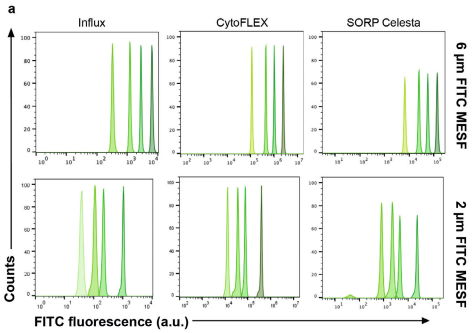

b

Brightness	6 µm beads	MFI Influx	MFI CytoFLEX	MFI SORP Celesta	FITC MESF
	p1	317	107336	6321	25910
	p2	1173	421852	23322	118192
	p3	2684	962928	53219	275288
	p4	6111	2324148	127668	715225

Brightness	2 µm beads	MFI Influx	MFI CytoFLEX	MFI SORP Celesta	FITC MESF
	p1	37	12357	780	3634
	p2	106	34544	2169	10520
	p3	210	73054	4380	22841
	p4	991	367458	22370	103706

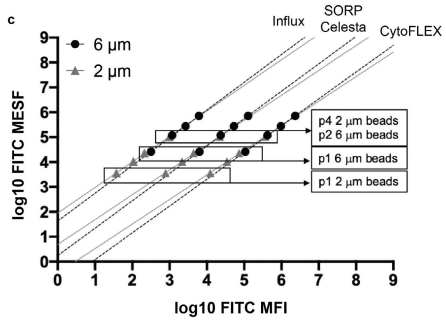

	6 µm FITC MESF beads	2 µm FITC MESF beads
Influx	Y = 1.1146*X + 1.6325 R^2 = 0.9995	Y = 1.0261*X + 1.951 R^2 = 0.9993
CytoFLEX	Y = 1.0762*X – 0.9947 R^2 = 0.9998	Y = 0.9869*X – 0.4632 R^2 = 0.9992
SORP Celesta	Y = 1.1004*X – 0.2432 R^2 = 0.9993	Y = 0.9989*X + 0.6884 R^2 = 0.9985

d

		Assigned FITC MESF	Calculated FITC MESF values		
Used as calibrator	**Used as unknown**	**Given values**	**Influx**	**CytoFLEX**	**SORP Celesta**
6 µm FITC beads	p4:::2 µm FITC beads	103706	93745	98759	107046
2 µm FITC beads	p2:::6 µm FITC beads	118192	125680	122538	112554
6 µm FITC beads	p1:::2 µm FITC beads	3634	2432	2565	2665
2 µm FITC beads	p1:::6 µm FITC beads	25910	32904	31743	30550

Figure 1. Evaluation of two different FITC MESF bead sets for the calibration of fluorescent intensities across three flow cytometer platforms. (a) Histogram overlays (axis in arbitrary units) of FITC fluorescent intensity peaks derived from the 6 µm (upper row) or the 2 µm (lower row) FITC MESF beads **(b)** Table showing the median fluorescence intensity (MFI) statistic derived from each of the fluorescent intensity peaks from dimmer to brighter being expressed in arbitrary units as well as the assigned MESF values (right column). **(c)** Least square linear regression analysis of 6 µm (black circles) and 2 µm (grey triangles) FITC MESF beads. Provided FITC MESF and measured FITC MFI values were transformed to log and plotted in a log-log fashion for the three platforms. **(d)** Table indicating the expected and calculated FITC MESF values for each sample used in the analysis.

MESF assignments of FITC fluorescence intensities to synthetic silica nanoparticles depend on the MESF-bead calibrator set

We next investigated how calibration with the two FITC MESF bead sets of 6 µm and 2 µm impacts fluorescent assignment to dim fluorescent nanoparticles. For this purpose 550 nm silica NPs containing 6 populations with FITC fluorescence intensities below or within the range of the calibration beads were measured on the BD Influx. Singlets were gated (Figure S5) and an histogram overlay was generated showing 6 different FITC fluorescence intensities (Figure 2a, left). Histograms showing the calibrated FITC MESF units of these silica NPs based on fluorescence calibration with either the 6 µm or 2 µm FITC MESF calibrator bead set are displayed in Figure 2a (respectively middle or right). The obtained MFI and CV values for each silica NP population, as well as the calculated FITC MESF values based on the two calibrator sets are shown in Figure 2b. The calculated FITC MESF values for the silica NPs appeared consistently lower when the regression line of the 6 µm calibration bead sets was used (Figure 2b). This phenomenon is not limited to the use of FITC MESF beads and can solely be explained by the difference in the slope of the regression line of the two calibrator bead sets, as was confirmed by calculating the fluorescent intensity in terms of PE ERF for 200 nm broad spectrum fluorescent polystyrene NPs based on the 6 µm and 2 µm PE MESF calibrator bead sets (Figure S6a). Importantly, multi-intensity peak analysis of the silica NPs revealed that the difference in FITC MESF values of these NPs obtained by the two calibrator bead sets increased in the dimmer range of the fluorescence, with 27.3% variation for the brightest fluorescent peak (p6) to 76.5% variation for the dimmest population of these NPs (Figure 2b). Also the PE ERF values calculated for the relatively dim 200 nm broad spectrum fluorescent polystyrene NPs based on the 6 µm or 2 µm PE MESF calibrator bead sets showed a variation of 41.3% (Figure S6a). These results can be explained by the fact that the differences in calculated values increase by extrapolation into the dim area as a consequence of the differences in the slopes of the regression lines between the calibrator bead sets.

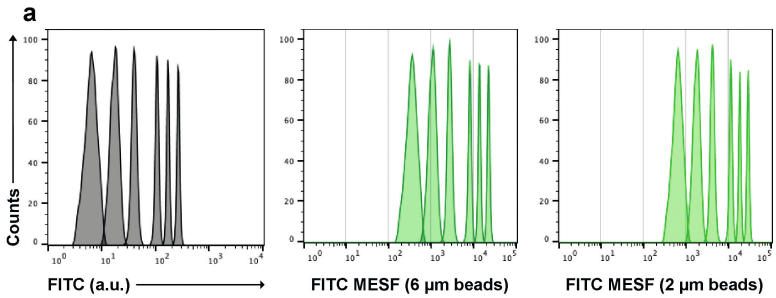

b

			Calculated FITC MESF values Used as calibrator		
Unknown	MFI	CV	6 µm FITC beads	2 µm FITC beads	% variation
p1	6.35	25.53	337	595	76.5
p2	17.20	17.83	1022	1654	61.8
p3	39.60	10.89	2590	3894	50.3
p4	104.90	6.86	7671	10581	37.9
p5	167.00	5.12	12881	17050	32.4
p6	258.90	5.10	20995	26734	27.3

Figure 2. MESF bead-based calibration of fluorescence signals from synthetic silica NPs. (a) Histogram overlay showing FITC fluorescence in arbitrary units (a.u.) (left), FITC MESF calibrated axis based on the 6 µm (middle) and 2 µm FITC MESF beads (right) from the six differently FITC-labeled 550 nm NP gated populations. **(b)** Table showing the MFI and CV as well as the calculated FITC MESF values for each of the unknown populations with the percentage of variation between the two calculated reference values.

MESF calibration using different bead sets leads to variable ERF and MESF values assigned to fluorescently CFSE stained and CD9 labeled extracellular vesicles

We next demonstrate the impact of the assignment of FITC ERF units and PE MESF units to a biological EV sample measured on BD Influx by using the four different MESF calibrator sets, i.e. 6 and 2 µm FITC MESF and the 6 and 2 µm PE MESF beads. Since the light scatter of these EVs was too low to resolve the EV population from the background signals, fluorescence thresholding was applied [10] based on the CFSE luminal dye staining. Furthermore, the expression of CD9, a tetraspanin enriched on the surface of the 4T1-derived EVs, was analyzed by using a CD9-PE antibody (Figure 3a). Unstained EVs and CFSE stained EVs with a matching isotype-PE control were measured side-by-side (Figure 3a) and fluorescent polystyrene spike-in beads (200 nm) were added to EV samples to determine the EV-concentration and define the EV-gating (Figure S7a). In Figure 3c-d, the histogram overlays show how the fluorescence intensities of the calibrators relate to the fluorescent signals generated by CFSE stained and CD9-PE labeled EVs. Our calibration results revealed a 76.6% variation in the calculated CFSE ERF units on CFSE stained EV and a 156.9% variation in the calculated PE MESF units on CD9-PE labeled EVs when the different MESF calibrator sets were used (Figure 3a-b).

Moreover, the fluorescent threshold value of 0.67 used on the BD Influx corresponds to an equivalent of 150 FITC MESF based on the 6 µm beads or 300 FITC MESF based on the 2 µm beads (Figure 3a), which also shows the variation between two bead sets when reporting the level of detection in standardized units.

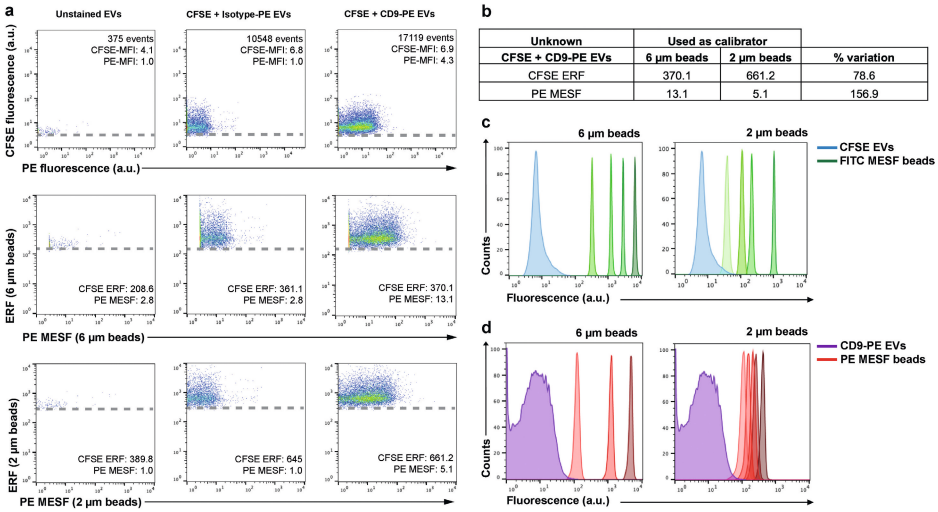

Figure 3. MESF bead-based calibration of fluorescent signals from biological EV samples. (a) Analysis of EV samples by using a fluorescence threshold. Unstained EVs control (left), CFSE and isotype-PE stained EVs (middle) and CFSE and CD9-PE stained EVs (right) dot plots showing CFSE fluorescence Vs PE fluorescence in arbitrary units (a.u.) (upper row) or CFSE ERF Vs PE MESF calibrated axis based on either the 6 µm (middle row) or 2 µm calibration beads (lower row). The dashed line in each dot plot indicates the fluorescence threshold value used. Number of events within the EV gate and MFI values for either CFSE or PE fluorescence (a.u.) are indicated in the top row. CFSE ERF and PE MESF values are indicated based on the 6 µm (middle row) or 2 µm beads (lower row). **(b)** Table showing the ERF or MESF values obtained after calibration for the CFSE and CD9-PE stained EVs and the percentage of variation between the use of the 6 µm or 2 µm bead sets. **(c)** Histogram overlays displaying fluorescence in arbitrary units from CFSE stained EVs (blue) next to the 6 µm or 2 µm FITC-MESF bead set (green). **(d)** Histogram overlays displaying fluorescence in arbitrary units from CD9-PE labeled EVs (purple) next to the 6 µm or 2 µm PE-MESF bead set (red).

DISCUSSION

The field of small particle flow cytometry is rapidly evolving, where the definition of what and how much can be detected is crucial. Besides the inter-comparability of data, the use of MESF/ERF values generates awareness about the range of fluorescence intensities that can be expected for small particles, such as EVs, and allows to indicate

instrument detection sensitivity and to report fluorescence thresholding in calibrated units [8, 11].

In line with previous findings, we here showed that linear regression curves derived from calibration beads developed for calibration of fluorescence on cells, can be used to calculate MESF/ERF values for dim NPs and EVs, allowing data inter-comparability with acceptable precision when the same calibrator is used [11]. Since earlier reports pointed out towards variabilities in MESF/ERF assignments between manufacturer's [5], we used different calibrator bead sets from the same manufacturer, assigned by using the same method and internal NIST traceable calibrator and prepared by following the same manufacturing process. Nevertheless, we found that the robustness of a calculated MESF/ERF value varies upon the use of different calibrator bead sets.

We here demonstrate that the calibration of dim NPs and EVs is substantially affected by the intrinsic variation within the assignment of MESF/ERF values to the calibrator beads [12]. Since the fluorescent intensities of EVs, based on generic staining and/or on antibody labeling, are far dimmer than the available calibrators calculation of their MESF/ERF values relies on extrapolation of the regression line of the calibrator beads into the dim area. Our data demonstrate that regression lines of different calibrator sets result in different calculated MESF/ERF values for NPs and EVs that have fluorescent intensities at the lower end or below the intensities of the calibrator beads themselves. Due to the increased separation of regression lines with slightly different slopes at the lower end, increasing uncertainties exist in the MESF/ERF assignment for dim NPs and EVs, which compromise the accuracy of the MESF/ERF assignment. Importantly, most available calibrator bead sets do not provide uncertainty values around the given MESF/ERF units, which would help to create awareness about the possibilities and limitations related to MESF/ERF unit reporting. Based on our findings, the use of the same calibrator bead set and the same number of data points of the calibrators used for linear regression would increase robustness of the calculation of MESF/ERF values for inter-laboratory and inter-platform comparison, and detailed description of calibration materials and calculation of MESF/ERF values would increase reproducibility.

Clearly, a calibrator with MESF/ERF values closer to the range of fluorescence intensities of the sample of interest and with a low uncertainty of assignment is preferable. Importantly, novel state-of-the-art flow cytometers that are designed to measure small particles rely obligately on sub-micron sized beads to perform MESF/ERF calibration. These state-of-the-art platforms cannot measure the 'standard' 6 µm MESF beads [13]. Therefore, there is an urgent need for calibration beads that are validated for small particle flow cytometry.

In summary, our results confirm that fluorescence calibration enables data comparison and provides information on the detection sensitivity of the instrument in standardized

units [14, 15], but also urge for awareness of the limitations when fluorescence calibration is being employed for EVs and NPs, especially in terms of accuracy. Lastly, for robust assignments of fluorescence values to NPs and EVs, there is a need for multi-institutional collaborations (between research labs, companies and metrology institutions, such as NIST) to produce and validate calibration materials that have low and well-characterized uncertainty of assigned fluorescent values, ideally allowing for data interpolation and with a size range that is compatible for all flow cytometer platforms.

FUNDING STATEMENT

This research is supported by the European Union's Horizon 2020 research and innovation programme under the Marie Skłodowska-Curie grant agreement No 722148 and by the National Natural Science Foundation of China (21934004 and 21627811). E. L. A. is supported by the European Union's Horizon 2020 research and innovation programme under the Marie Skłodowska-Curie grant agreement No 722148.

AUTHOR CONTRIBUTIONS

E.L.A. designed and performed experiments, analyzed data and wrote the manuscript. T.B. performed experiments and gave conceptual advice. L.W. gave technical and conceptual advice. M.M., Y.T. and X.Y. prepared materials and gave technical advice. G.J.A.A. and M.H.M.W. supervised the research, designed (performed) experiments and wrote the manuscript. G.J.A.A. and M.H.M.W. contributed equally as senior author. All authors critically reviewed and edited the manuscript.

ACKNOWLEDGMENTS

The authors would like to thank Prof. An Hendrix (Laboratory of Experimental Cancer Research, Ghent University, Belgium) for the possibility to prepare and analyze M4T1 derived EV in her lab, Dr. Joshua A. Welsh (National Cancer Institute, Bethesda, MD) for helpful discussion and Ludo Monheim (BD Biosciences, Erembodegem, Belgium) for helpful technical support. FITC-MESF and 2 µm PE-MESF beads were kindly provided by BD Biosciences (prepared by Dr. Majid Mehrpouyan) as part of the European Union's Horizon 2020 research and innovation programme under the Marie Skłodowska-Curie grant agreement No 722148.

DECLARATION OF INTEREST DISCLOSURE

Tina Van Den Broeck and Majid Mehrpouyan are both employees of BD Biosciences, a business unit of Becton, Dickinson and Company. During the course of this study, the Wauben research group, Utrecht University, Faculty of Veterinary Medicine, Department of Biomolecular Health Sciences and BD Biosciences collaborated as a co-joined

partner in the European Union's Horizon 2020 research and innovation programme under the Marie Skłodowska-Curie grant agreement No 722148. Xiaomei Yan declares competing financial interests as a cofounder of NanoFCM Inc., a company committed to commercializing the nano-flow cytometry (nFCM) technology.

SUPPORTING INFORMATION

Additional supporting information can be found online in the corresponding section at the end of the article.

Data S1. Author Checklist: MIFlowCyt-Compliant Items.

Data S2. MIFlowCyt-EV framework.

Figure S1. Comparison of the inclusion of different data points into linear regression analysis by using custom-made and commercial FITC MESF bead sets.

Figure S2. Analysis of different MESF bead sets measured on the BD Influx.

Figure S3. Analysis of instrument linearity on the BD Influx.

Figure S4. Evaluation of measurement variability of 2 µm FITC MESF beads measured on the BD Influx.

Figure S5. Gating strategy for synthetic silica NPs.

Figure S6. 200 nm fluorescent polystyrene NPs.

Figure S7. Gating strategy for external spiked-in beads and biological EV samples.

ORCID

Estefanía Lozano-Andrés https://orcid.org/0000-0002-7305-0776
Lili Wang https://orcid.org/0000-0003-2456-898X
Xiaomei Yan http://orcid.org/0000-0002-7482-6863
Marca H.M. Wauben https://orcid.org/0000-0003-0360-0311
Ger. J.A. Arkesteijn https://orcid.org/0000-0001-7739-582X

REFERENCES

1. Hoffman, R.A., *Standardization, calibration, and control in flow cytometry.* Curr Protoc Cytom, 2005. **Chapter 1**: p. Unit 1 3.
2. Wang, L. and R.A. Hoffman, *Standardization, Calibration, and Control in Flow Cytometry.* Curr Protoc Cytom, 2017. **79**: p. 1 3 1-1 3 27.
3. Gaigalas, A.K., et al., *Quantitating Fluorescence Intensity From Fluorophore: Assignment of MESF Values.* J Res Natl Inst Stand Technol, 2005. **110**(2): p. 101-14.
4. Wang, L., et al., *Quantitating Fluorescence Intensity From Fluorophores: Practical Use of MESF Values.* J Res Natl Inst Stand Technol, 2002. **107**(4): p. 339-53.
5. Hoffman, R.A., et al., *NIST/ISAC standardization study: variability in assignment of intensity values to fluorescence standard beads and in cross calibration of standard beads to hard dyed beads.* Cytometry A, 2012. **81**(9): p. 785-96.
6. Nolan, J.P., *Flow Cytometry of Extracellular Vesicles: Potential, Pitfalls, and Prospects.* Curr Protoc Cytom, 2015. **73**: p. 13 14 1-16.
7. Lian, H., et al., *Flow Cytometric Analysis of Nanoscale Biological Particles and Organelles.* Annu Rev Anal Chem (Palo Alto Calif), 2019. **12**(1): p. 389-409.
8. Welsh, J.A., et al., *MIFlowCyt-EV: a framework for standardized reporting of extracellular vesicle flow cytometry experiments.* J Extracell Vesicles, 2020. **9**(1): p. 1713526.
9. Bagwell, C.B., et al., *A simple and rapid method for determining the linearity of a flow cytometer amplification system.* Cytometry, 1989. **10**(6): p. 689-94.
10. van der Vlist, E.J., et al., *Fluorescent labeling of nano-sized vesicles released by cells and subsequent quantitative and qualitative analysis by high-resolution flow cytometry.* Nat Protoc, 2012. **7**(7): p. 1311-26.
11. Welsh, J.A. and J.C. Jones, *Small Particle Fluorescence and Light Scatter Calibration Using FCMPASS Software.* Curr Protoc Cytom, 2020. **94**(1): p. e79.
12. Draper, N.R. and H. Smith, *Applied regression analysis*. 1981, New York: Wiley.
13. Tian, Y., et al., *Protein Profiling and Sizing of Extracellular Vesicles from Colorectal Cancer Patients via Flow Cytometry.* ACS Nano, 2018. **12**(1): p. 671-680.
14. Welsh, J.A., J.C. Jones, and V.A. Tang, *Fluorescence and Light Scatter Calibration Allow Comparisons of Small Particle Data in Standard Units across Different Flow Cytometry Platforms and Detector Settings.* Cytometry A, 2020. **97**(6): p. 592-601.
15. Nolan, J.P. and S.A. Stoner, *A trigger channel threshold artifact in nanoparticle analysis.* Cytometry A, 2013. **83**(3): p. 301-5.
16. Arkesteijn, G.J.A., et al., *Improved Flow Cytometric Light Scatter Detection of Submicron-Sized Particles by Reduction of Optical Background Signals.* Cytometry A, 2020. **97**(6): p. 610-619.
17. Yokoi, T., et al., *Periodic arrangement of silica nanospheres assisted by amino acids.* J Am Chem Soc, 2006. **128**(42): p. 13664-5.
18. Yokoi, T., et al., *Mechanism of Formation of Uniform-Sized Silica Nanospheres Catalyzed by Basic Amino Acids.* Chemistry of Materials, 2009. **21**(15): p. 3719-3729.
19. Stöber, W., A. Fink, and E. Bohn, *Controlled growth of monodisperse silica spheres in the micron size range.* Journal of Colloid and Interface Science, 1968. **26**(1): p. 62-69.
20. Giesche, H., *Synthesis of monodispersed silica powders II. Controlled growth reaction and continuous production process.* Journal of the European Ceramic Society, 1994. **14**(3): p. 205-214.

21. Vergauwen, G., et al., *Confounding factors of ultrafiltration and protein analysis in extracellular vesicle research.* Sci Rep, 2017. **7**(1): p. 2704.
22. Geeurickx, E., et al., *The generation and use of recombinant extracellular vesicles as biological reference material.* Nat Commun, 2019. **10**(1): p. 3288.
23. Welsh, J.A., et al., *FCMPASS Software Aids Extracellular Vesicle Light Scatter Standardization.* Cytometry A, 2019.
24. Consortium, E.-T., et al., *EV-TRACK: transparent reporting and centralizing knowledge in extracellular vesicle research.* Nat Methods, 2017. **14**(3): p. 228-232.

SUPPLEMENTARY INFORMATION

Data S1. Author Checklist: MIFlowCyt-Compliant Items.

Requirement	Please Include Requested Information
1.1. Purpose	Evaluate the advised use of MESF bead-based calibration for the assignment of absolute fluorescent values to nanoparticles and extracellular vesicles.
1.2. Keywords	flow cytometry, fluorescence, calibration, standardization, MESF, extracellular vesicles, nanoparticles
1.3. Experiment variables	MESF bead, flow cytometer
1.4. Organization name and address	Department of Biomolecular Health Sciences, Faculty of Veterinary Medicine, Yalelaan 2 (Nieuw Gildestein Room 203), University of Utrecht PO Box 80176, 3508 TD Utrecht, The Netherlands
1.5. Primary contact name and email address	Estefanía Lozano-Andrés e.lozanoandres@uu.nl Marca H. M. Wauben m.h.m.wauben@uu.nl
1.6. Date or time period of experiment	January 2019 until October 2021
1.7. Conclusions	By testing various MESF bead sets we found differences in the slopes of the regression lines consistent between different calibrator bead sets and not dependent on the flow cytometer platform used. These differences are caused by uncertainties in the assignment of MESF to the calibrators and are exaggerated during extrapolation through linear regression into the dimmer fluorescent area.
1.8. Quality control measures	100 nm polystyrene beads, 200 nm polystyrene beads, QC samples as provided by manufacturers.
2.1.1.1. Sample description	Fluorescent 100 nm polystyrene beads, Fluorescent 200 nm polystyrene beads, two different sets of FITC MESF beads (6 µm and 2 µm), two different sets of PE MESF beads (6 µm and 2 µm), 550 nm Silica Nanoparticles FITC-labeled, 200 nm fluorescent polystyrene beads for concentration determination, extracellular vesicles (EVs) isolated from 4T1 cell culture supernatant.
2.1.1.2. Biological sample source description	Murine mammary carcinoma cell line 4T1 (ATCC, Manassas, VA).

S1 Continued

Requirement	Please Include Requested Information
2.1.1.3. Biological sample source organism description	Mouse
2.1.2.2. Environmental sample location	NA
2.3. Sample treatment description	EV samples were succumbed to differential ultracentrifugation, ultrafiltration and density gradient floatation.
2.4. Fluorescence reagent(s) description	EV sample were stained with with 5-(and-6)-Carboxyfluorescein Diacetate Succinimidyl Ester (CFDA-SE, hereinafter referred as CFSE) (ThermoFisher, catalog number C1157) and labeled with 0.5 µg of Rat anti-mouse CD9-PE (Clone: KMC8, IgG2a, κ, Lot. no. 7268877, BD Biosciences) or matched Isotype antibodies (Rat IgG2a, κ, PE-conjugated, Lot. no. 8096525, BD Biosciences).
3.1. Instrument manufacturer	BD Biosciences, Beckman Coulter.
3.2. Instrument model	BD Influx™, BC CytoFLEX LX™ and SORP BD FACSCelesta™
3.3. Instrument configuration and settings	The BD Influx™ was optimized for detection of sub-micron sized particles as described previously in Van der Vlist *et al.* – Nature Protocols 2012. Based in that configuration various combinations of pinholes and obscuration bars were tested as described in the manuscript. Prior to each measurement, 100 nm yellow-green (505/515) FluoSphere beads (Invitrogen, F8803) were used to set optimal values. FITC was measured with a 200 mW 488nm laser (Sapphire, Coherent) placed in front of the first pinhole and through a PMT 530/40 band pass filter. PE was measured with a 150 mW 561nm laser (Jive, Cobolt) placed in front of the third pinhole and through a PMT 585/42 band pass filter. FITC MESF and PE MESF beads were recorded with an FSC threshold at 1.00. Synthetic Nanoparticles and Biological EV samples were recorded with a FL threshold at 0.67.

S1 Continued

Requirement	Please Include Requested Information
	CytoFLEX LX™ was used without any tailor-made modifications. Standard startup and QC procedure were run prior measurements as recommended by the manufacturer. All scatter and fluorescence parameters were set to a logarithmic scale. FITC was measured with a 50 mW 488 nm laser and fluorescence was measured through an APD 525/40 band pass filter. Samples were recorded with a FSC threshold at 1000. The SORP BD FACSCelesta™ was equipped with a small particle SSC module for improved scatter detection. Before measurement, the standard setup and QC procedures were performed. All scatter and fluorescence parameters were set to a logarithmic scale. 100 nm yellow-green (505/515) FluoSphere beads (Invitrogen, F8803) were acquired and used to set optimal small particle-SSC and fluorescence (FITC detector) PMT-V values. FITC was measured with a 100 mW 488 nm laser through a PMT 530/30 band pass filter. FITC-MESF beads were recorded with an SSC threshold at 200.
4.1. List-mode data files	The flow repository ID for peer-review process: FR-FCM-Z3FJ
4.2. Compensation description	No compensation was applied.
4.3. Data transformation	No data transformation was applied.
4.4.1. Gate description	Gates were defined by using FlowJo Version 10.5.0. Briefly, for MESF bead gating on the BD Influx™ singlets were gated based on the parameters trigger pulse width Vs SSC, then a histogram displaying fluorescence was plotted to gate the individual peak populations, SiNPs and EVs gating strategy can be found in the Supporting Information of this manuscript (Figure S3 and S5, respectively). For MESF bead gating on the CytoFLEX LX™ singlets were gated based on SSC Vs FSC, then a histogram displaying fluorescence was plotted to gate the individual peak populations. For MESF bead gating on the SORP BD FACSCelesta™ singlets were gated based on SSC Vs FSC, then a histogram displaying fluorescence was plotted to gate the individual peak populations.
4.4.2. Gate statistics	Plots show the MFI (Median Fluorescence Intensity) for each population on the described parameter. See figures of the manuscript and results section for further details.
4.4.3. Gate boundaries	Gates boundaries were set according to each population. See additional Supporting Information.

Data S2. MIFlowCyt-EV framework.

1.1 Preanalytical variables conforming to MISEV guidelines	Yes, all relevant data has been submitted to EV-TRACK for transparent reporting and centralizing knowledge in extracellular vesicle research (EV-TRACK ID: EV210047).
1.2 Experimental design according to MIFlowCyt guidelines	Yes, MIFlowCyt checklist can be found as part of the supporting information of this manuscript (Data S1).
2.1 Sample staining details	Yes, described in Materials and Methods.
2.2 Sample washing details	Yes, described in Materials and Methods.
2.3 Sample dilution details	Yes, described in Materials and Methods.
3.1 Buffer-only controls	Yes, relevant buffer controls were measured.
3.2 Buffer with reagent controls	Yes, see Figure S5.
3.3 Unstained controls	Yes, see Figure 3.
3.4 Isotype controls	Yes, see Figure 3.
3.5 Single-stained controls	N/A
3.6 Procedural controls	Yes, see Figure S5b.
3.7 Serial dilutions	Yes, serial dilutions were performed in previous characterization experiments to determine the ideal dilution used in this study.
3.8 Detergent-treated controls	Yes, sensitivity to triton X-100 for this EV sample was previously determined.
4.1 Trigger channel(s) and threshold(s)	Yes, all relevant details can be found in Materials and Methods.
4.2 Flow rate / volumetric quantification	Yes, low flow rate was kept constant and is described in Materials and Methods.
4.3 Fluorescence calibration	Yes
4.4 Scatter calibration	N/A
5.1 EV diameter/surface area/ volume approximation	N/A
5.2 EV refractive index approximation	N/A
5.3 EV epitope number approximation	N/A
6.1 Completion of MIFlowCyt checklist	Yes, see Data S1
6.2 Calibrated channel detection range	BD Influx
6.3 EV number/concentration	Yes, see Supporting Information Figure S5.
6.4 EV brightness	Yes, reported in ERF or MESF, see Figure 3.
7.1 Sharing of data to a public repository	Yes, all experimental details can be found in EV-TRACK. Data files have been submitted to http://flowrepository.org under FR-FCM-Z3FJ and are available upon request

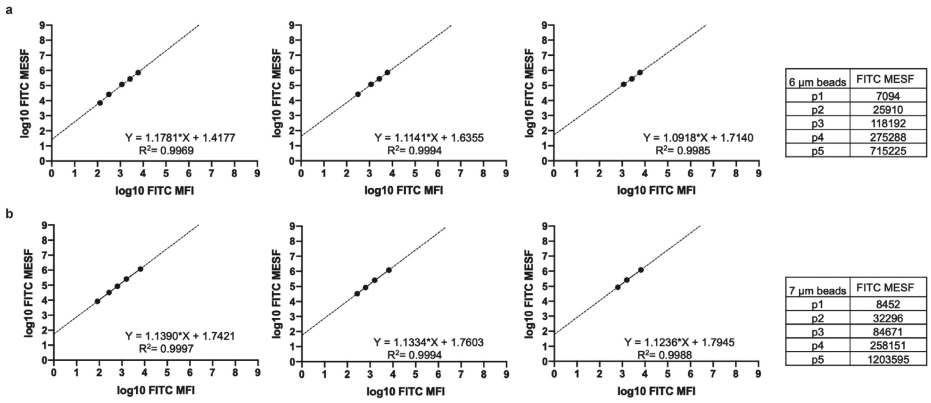

6 µm beads	FITC MESF
p1	7094
p2	25910
p3	118192
p4	275288
p5	715225

7 µm beads	FITC MESF
p1	8452
p2	32296
p3	84671
p4	258151
p5	1203595

Figure S1. Comparison of the inclusion of different data points into linear regression analysis by using custom-made and commercial FITC MESF bead sets. (a) Least square linear regression analysis of custom-made 6 µm FITC MESF beads and **(b)** 7 µm Quantum™ FITC-5 MESF beads measured on the BD Influx. Provided FITC MESF for both sets (indicated in the figure) and measured FITC MFI values were transformed to log and plotted in a log-log fashion. Graphs including either five, four or three fluorescent populations (from left to right).

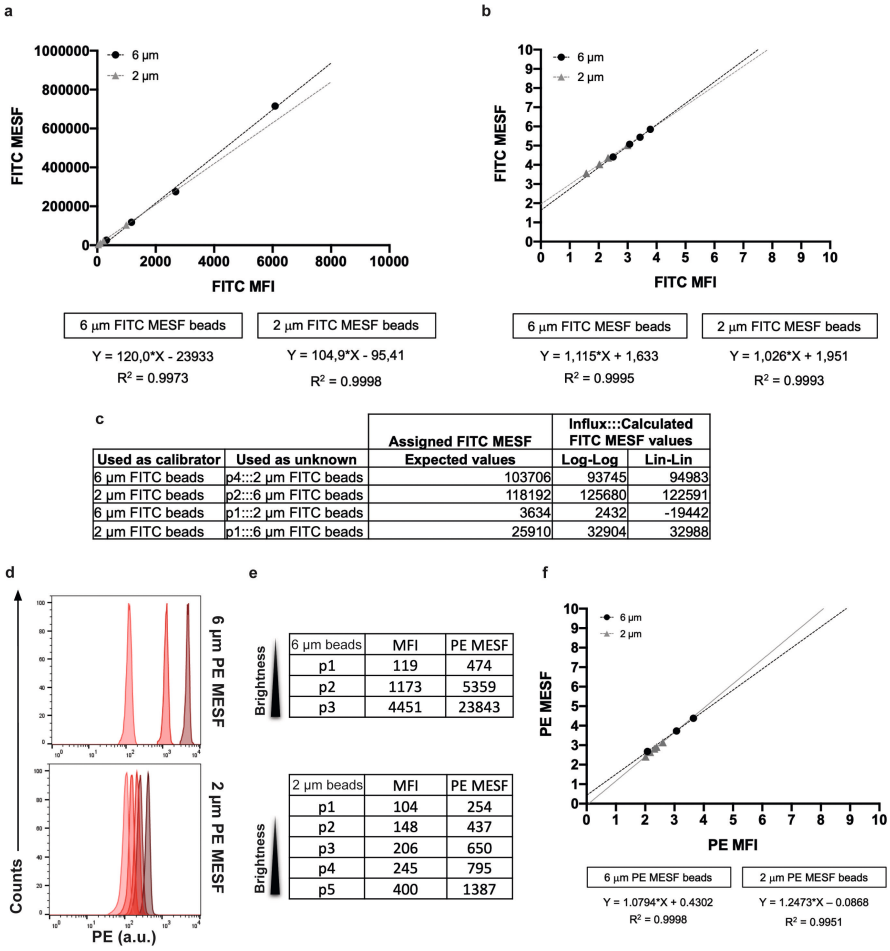

		Assigned FITC MESF	Influx:::Calculated FITC MESF values	
Used as calibrator	**Used as unknown**	**Expected values**	**Log-Log**	**Lin-Lin**
6 µm FITC beads	p4:::2 µm FITC beads	103706	93745	94983
2 µm FITC beads	p2:::6 µm FITC beads	118192	125680	122591
6 µm FITC beads	p1:::2 µm FITC beads	3634	2432	-19442
2 µm FITC beads	p1:::6 µm FITC beads	25910	32904	32988

6 µm beads	MFI	PE MESF
p1	119	474
p2	1173	5359
p3	4451	23843

2 µm beads	MFI	PE MESF
p1	104	254
p2	148	437
p3	206	650
p4	245	795
p5	400	1387

Figure S2. Analysis of different MESF bead sets measured on the BD Influx. (a) Least square linear regression analysis of 6 µm (black circles) and 2 µm (grey triangles) FITC MESF beads by using linear plotting or **(b)** log-transformed plotting. **(c)** Table indicating the assigned FITC MESF values for each population and the calculated FITC MESF values for each sample. **(d)** Histogram overlays of PE fluorescent intensity peaks derived from the 6 µm or the 2 µm PE MESF beads (arbitrary units). **(e)** Table showing the median intensity fluorescence (MFI) statistic derived from each of the fluorescent intensity peaks from dimmer to brighter expressed in arbitrary units. **(f)** Least square linear regression analysis of 6 µm (black circles) and 2 µm (grey triangles) PE MESF beads. Provided PE MESF and measured PE MFI values were transformed to log and plotted in a log-log fashion.

a

	488 nm laser		
	Geo Mean (FITC)		
PMT1 voltage (530/30)	p2	p6	p2-p6
41.85	5719	104	5615
38.85	3287	57.2	3229.8
35.85	1923	31.6	1891.4
32.85	963	15.7	947.3

b

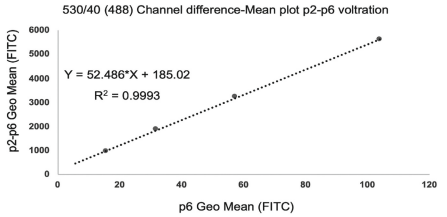

c

	561 nm laser		
	Geo Mean (PE)		
PMT11 voltage (585/40)	p5	p6	p5-p6
71.1	300	106	194
68.1	222	71.1	150.9
65.1	158	48.8	109.2
62.1	108	31.1	76.9

d

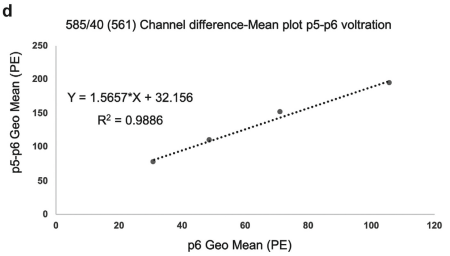

Figure S3. Analysis of instrument linearity on the BD Influx. (a) Table indicating the PMT1 voltage and the FITC MFI values for either population p2 or p6 from the beads. **(b)** Linear regression analysis showing the MFI difference between population p2 and p6 relative to the MFI from population p6 and the respective equation. **(c)** Table indicating the PMT11 voltage and the PE MFI values for either population p5 or p6 from the beads. **(d)** Linear regression analysis showing the MFI difference between population p5 and p6 relative to the MFI from population p6 and the respective equation.

a

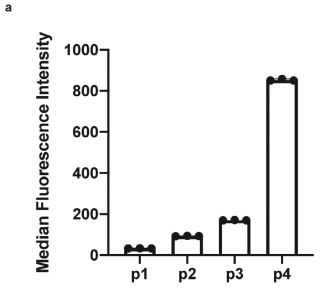

b

	MFI measured values		
Sample	n = 1	n = 2	n = 3
p1:::2 µm FITC beads	32.93	33.38	32.78
p2:::2 µm FITC beads	92.43	93.48	92.64
p3:::2 µm FITC beads	169.63	171.54	169.63
p4:::2 µm FITC beads	850.53	858.21	850.53

c

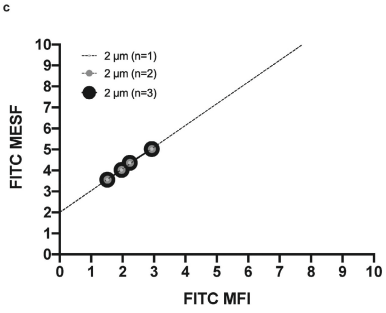

2 µm FITC MESF beads (n=1)	2 µm FITC MESF beads (n=2)	2 µm FITC MESF beads (n=3)
Y = 1.035*X + 2.003	Y = 1.0364*X + 1.9949	Y = 1.0339*X + 2.0055
R² = 0.9972	R² = 0.9972	R² = 0.9972

Figure S4. Evaluation of measurement variability of 2 µm FITC MESF beads measured on the BD Influx. (a) Bar graph displaying the MFI values for the four fluorescent bead populations present in the 2 µm FITC MESF bead set from three independent measurements. **(b)** Table indicating the FITC MFI values for each population from three independent measurements. **(c)** Least square linear regression analysis showing three independent measurements of the 2 µm FITC MESF beads by using log-transformed plotting and their respective equations.

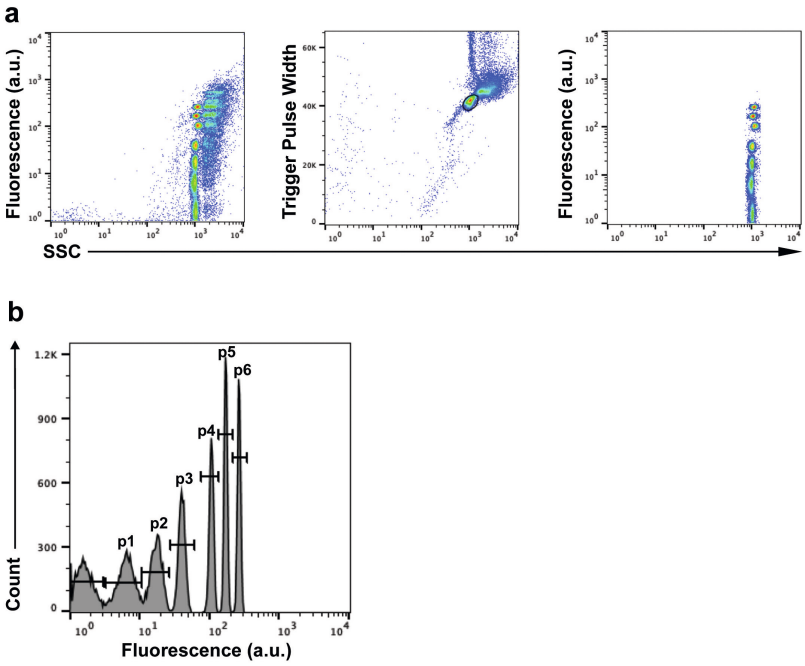

Figure S5. Gating strategy for synthetic silica NPs. (a) Dot plots showing fluorescence in arbitrary units vs SSC from 550 nm silica NPs. Ungated events are displayed in a fluorescence vs SSC dot plot (left panel). A gate was placed around the singlet population based on trigger pulse width vs SSC (mid panel). Singlets displaying six FITC intensities and a blank NP population are shown in the Fluorescence Vs SSC (right panel). **(b)** Histogram showing the gated 6 fluorescence intensities (p1-p6) and the blank NP population.

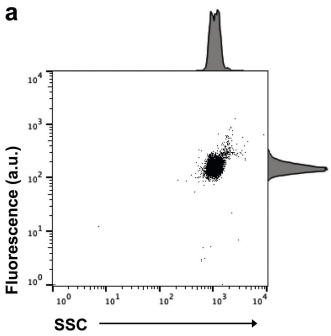

b

		Calculated ERF values Used as calibrator		
Unknown	**MFI**	**6 µm PE beads**	**2 µm PE beads**	**% variation**
200 nm NPs	154	619	438	41.3

Figure S6. 200 nm fluorescent polystyrene NPs. (a) Dot plots showing fluorescence in arbitrary units (a.u.) in the PE channel vs SSC from a sample containing 200 nm broad spectrum fluorescent polystyrene synthetic NPs. **(b)** Table indicating the ERF values for the 200 nm fluorescent NPs calculated either using 6 or 2 µm PE MESF beads.

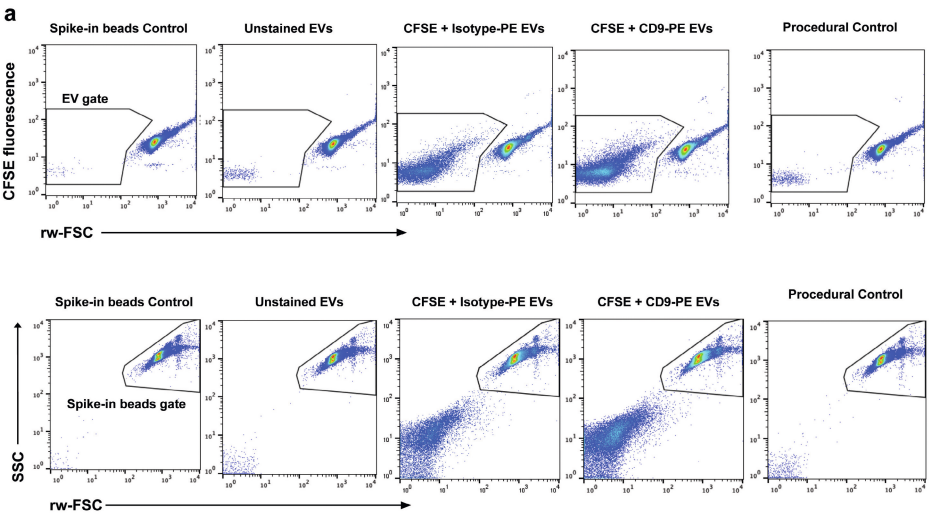

Figure S7. Gating strategy for external spiked-in beads and biological EV samples. (a) Dot plots showing fluorescence in arbitrary units (a.u.) vs rw-FSC or SSC vs rw-FSC from a spike-in beads control, an unstained EVs control, an isotype EVs control, a CFSE-stained and CD9-PE labeled EV sample and a procedural control. The concentration of the CFSE stained and CD9-PE labeled EV sample was calculated using the spike-in beads (previously described in Material and Methods) and estimated to be $2.34 \acute{} 10^{7}$ particles/mL.

“If you run into a wall, don’t turn around and give up.
Figure out how to climb it, go through it or work around it.”

Michael Jordan

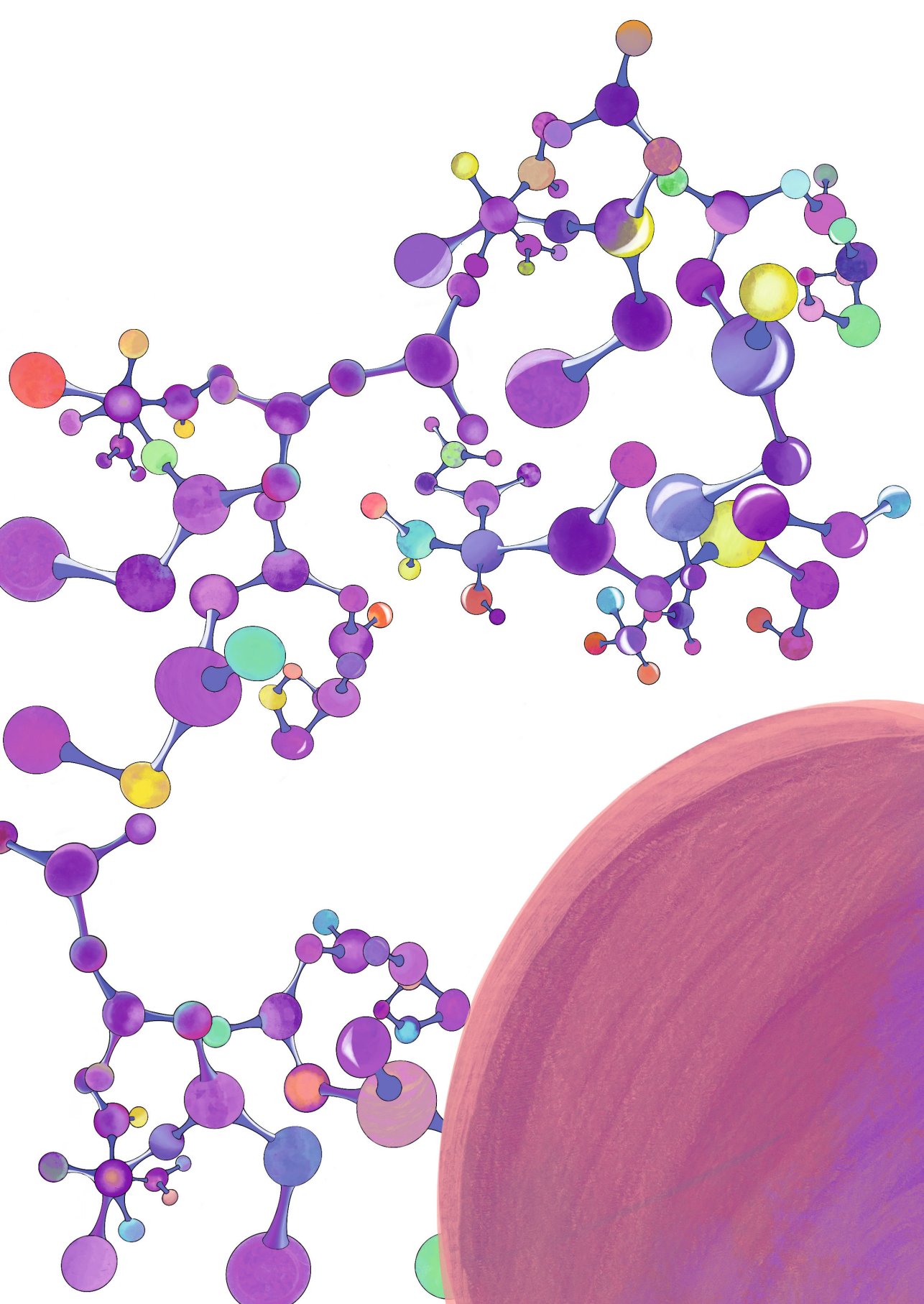

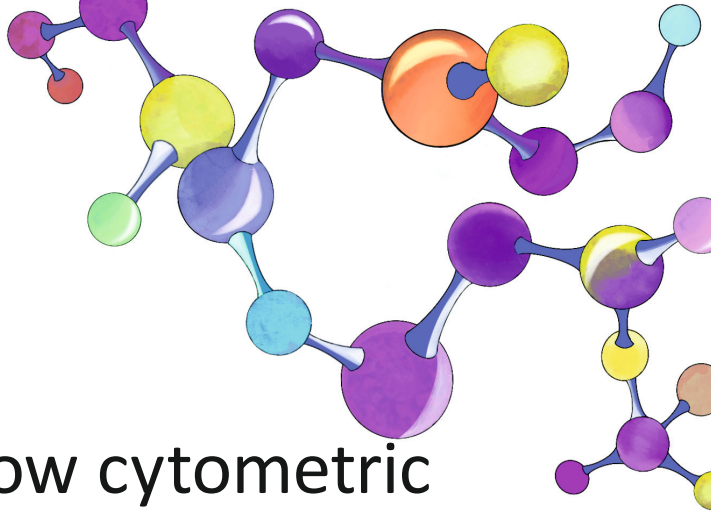

CHAPTER 5

Improved flow cytometric light scatter detection of submicron-sized particles by reduction of optical background signals

Ger J. A. Arkesteijn,1,2* **Estefanía Lozano-Andrés**,1 Sten F. W. M. Libregts,1 Marca H. M. Wauben1
1 Department of Biochemistry and Cell Biology, Faculty of Veterinary Medicine, Utrecht University, Utrecht, The Netherlands
2 Department of Immunology and Infectious Diseases, Faculty of Veterinary Medicine, Utrecht University, Utrecht, The Netherlands

Published:
Arkesteijn G. et al., (2020). Cytometry Part A, Volume 97, Issue 6
https://doi.org/10.1002/cyto.a.24036

ABSTRACT

Flow cytometry allows multi-parameter analysis on a single cell basis and is currently the method of choice to rapidly assess heterogeneity of cell populations in suspension. With the research field of extracellular vesicles (EV) rapidly expanding, there is an increased demand to address heterogeneity of EV populations in biological samples. Although flow cytometry would be the ideal technique to do so, the available instruments are in general not equipped to optimally detect the dim light scatter signals generated by submicron-sized particles like EV. Whereas sideward scattered light (SSC) and fluorescence are currently used as a threshold signal to identify EV within samples, the forward scatter light (FSC) parameter is often neglected due to the lack of resolution to distinguish EV-related signals from noise. However, after optimization of FSC detection by adjusting the size of the obscuration bar, we recently showed that certain EV-subsets could only be identified based on FSC. This observation made us to further study the possibilities to enhance FSC-detection of submicron-sized particles. By testing differently sized obscuration bars and differently sized pinholes in the focal plane behind the FSC detection lens, we generated a matrix that allowed us to determine which combination resulted in the lowest optical background in terms of numbers of events regarding FSC detection of submicron-sized particles. We found that a combination of an 8 mm obscuration bar and a 200 µm pinhole reduced optical background in a reproducible manner to such extent that it allowed a robust separation of 100 nm polystyrene beads from background signals within the FSC channel, and even allowed thresholding on FSC without the interference of massive background signals when both beads and EV were measured. These technical adaptations thus significantly improved FSC detection of submicron-sized particles and provide an important lead for the further development and design of flow cytometers that aid in detection of submicron-sized particles.

Key terms: extracellular vesicle; exosome; microvesicle; optical background; light scatter; flow cytometry

INTRODUCTION

Flow cytometry has become an indispensable tool in biological research. Besides multi-parameter analysis of cells in biological samples, flow cytometry is widely used to sort and purify sub-sets of cells from a heterogeneous population at high speed based on single cell characteristics. For decades, the design of flow cytometers fulfilled the demands to process cells or cell-sized particles. In recent years however, there is an increasing demand to process and analyze submicron-sized particles, not least driven by the rapidly expanding research field of extracellular vesicles (EV). It has become evident that EV play crucial roles in many biological processes and bear great potential for biomarker analysis (1). For characterization of EV, flow cytometry is one of the methods of choice due to the fact that samples can be measured quantitatively and qualitatively with high speed on a single particle basis. However, considerations have to be taken into account and requirements have to be met before this can be achieved (2). One is the choice of the threshold signal. Historically, the threshold signal used to measure cells is one of the light scatter parameter. All cells and particles scatter light upon interrogation with a laser and thereby produce signals of sufficient strength for detection by even the simplest photodiodes. Therefore, all cells will be 'seen' by the flow cytometer and detected as events. Differentiation between cell types, their subset and other particles, can then take place based on the other parameters taken along in the measurement.

Considering the fact that the strength of the light scatter signals is highly dependent on size and refractive index of the particles that are being analyzed, the shortcomings of current flow cytometers regarding light scatter detection quickly become evident for submicron-sized particles like EV, of which the vast majority is smaller than 500 nm (3-6). When measurements rely on light scatter detection, SSC is the preferred parameter of choice since position of the collection lens perpendicular to the laser direction results in significantly lower laser light background. For the measurement of sub-micron sized particles the light scatter signals have to be markedly amplified. Increasing the intensity of the laser at the interrogation point is one step in improving strength of dim signals. This could be accomplished by either increasing laser power, applying optical components to decrease the beam waist at the interrogation point, or a combination of both. Increasing laser power will go hand in hand with increased background signals, thereby negatively impacting the detection of light scatter signals of interest. On top of that, increasing illumination intensities cannot be limitlessly applied in cases where fluorescence comes into play (7). Alternatively, the PMT voltage or gains can be increased to enhance detection, but as such, the optical and electronic background will be prominently amplified as well, thereby hampering the proper read-out of sample specific light scatter signals. To tackle the problem of detection of dim light scatter signals, other threshold parameters with stronger and more specific signals can be deployed. A prerequisite for this is that the signal of the threshold parameter has to be unique and equally strong for all particles that need to be investigated. In the past

several approaches have been undertaken to improve the detection of submicron-sized particles, such as prolonging dwell time, application of high resolution optics and differing scatter collection angles (8, 9), resulting in commercially available flow cytometers dedicated for small particle detection. Due to the configuration of most commercially available flow cytometers, SSC generally allows for a better signal to noise ratio and provides a better alternative than FSC to discriminate dim signals above background (10). We have however realized the importance of FSC signals when analyzing EV populations derived from virus-infected cells, in which virus and non-virus containing EVs could solely be discriminated based on different FSC signals (11). This finding illustrates that FSC signals contain valuable information for EV-subset analysis. Alternatively, fluorescence could provide selective threshold signals (12). In recent years, we therefore have developed a method to generically stain EV in suspension with a fluorescent dye and use emitted fluorescent light as a threshold signal (13). Along with that, we applied specific hardware adaptations to improve the resolution of the FSC parameter (14). This enabled us to quantitatively and qualitatively analyze EV and to sort sub-populations of EV to high purity (11, 15). Measurements that are performed in this way, provide information on all EV that emit fluorescent signals above a set threshold level and implicate that all unstained particles remain undetectable. Although this effectively cleans up the measurement by eliminating all particles without enough fluorescence, we have recently shown that particles that remain undetectable when a fluorescence-threshold is performed can have a significant impact on light scatter parameters when they occur in high concentrations (16). Here, we aimed at reduction of optical background signals on FSC detection to be able to obtain more reliable information about the weak FSC signals generated by sub-micron sized particles. Optical background as such is the contribution of all photons reaching the FSC detector that are not related to the direct scattering from the particles in the core of the fluid stream. It could either be derived from ambient light, scatter light from particles in the surrounding sheath fluid, or stray light from the laser. Since laser light freely passes the band pass filter in front of the detector, it is a major component of the optical background in the FSC detector.

This made us pursue to find the most sensitive configuration for FSC detection. Key in improving the detection of dim FSC signals is to reduce signals caused by stray light, while keeping specific light scatter unaffected (17). Since the FSC-detector is in a straight line with the optical path of the laser from which FSC-signals are derived, direct laser light needs to be blocked to prevent it from reaching the detector. An obscuration bar is therefore placed in front of the FSC detection lens to block out direct laser light, while light scatter from passing particles, which scatter light in all angles, pass above and below the obscuration bar and get focused by the collection lens onto the FSC detector. Although in this way most direct laser light is blocked, there will be a fraction of stray light within the flow chamber, unrelated to any particle passage, that additionally scatters in multiple directions. As the FSC detector is equipped with an optical filter that matches the wavelength of the detecting laser, this additional stray light can reach

the FSC detector without restriction. Stray light therefore imposes the adjustment of the threshold on the light scatter parameter to a higher level, thereby restricting the measurement to particles with a higher light scattering power.

We have previously demonstrated that we could improve FSC-detection of submicron-sized particles by increasing the laser power in combination with a wider obscuration bar in front of the FSC collections lens (14). Here we present a method to further improve the resolution of the FSC parameter by significantly reducing background light scatter signals during the detection of submicron-sized particles. To configure the flow cytometer, we started off with the small particle detector (SPD) commercially available by BD. The original design held an optical glass plate that had to be placed at Brewster angle. The rationale of the original design of this detector is that polarization direction is altered by small particles depending on size and composition. Both parallel and perpendicular polarization directions can be separated by the Brewster plates and be read as different forward scatter parameters in this SPD. In the past we have extensively studied this but we did not find any discriminatory effect between EV in biological samples. We therefor decided to move away from this principle and actually only use the housing of the detector to build our own SPD. The main effective principle we applied is confocal detection and figure 1 shows a schematic representation of how the confocal system works in our configuration. For every particle out of the focal spot, the scattering light will be reduced because it is not perfectly focused on the pinhole. Although this figure shows this principle for particles in the sheath, it is applicable for light coming in from any direction that is different than light coming from the focal spot. The aim in this manuscript is to tackle optical background caused by ambient light and laser stray light coming in from any aberrant angle. It has to be considered that such a simplified confocal construction works mainly for non-imaging optical techniques such as flow cytometry. With this in mind we then investigated whether there is an optimal combination for pinhole and blocker bar sizes that aid in reducing the background noise and enhance the signal-to-noise ratio of the FSC-parameter in a reproducible and stable manner.

MATERIALS AND METHODS

Flow Cytometer Setup

We used a BD Influx Jet in Air sorter that was modified as fully described in van der Vlist et al. (14). FSC was collected with a Plan Apo 20x (NA 0.42) lens (Mitutoyo, Japan). The lens was at near focal distance of the sample core (depending on the adjustment per configuration approximately 19 mm). In front of the objective lens a height adjustable obscuration bar was mounted at a distance of 7 mm to the collection objective. Directly behind the collection objective, a converging 50 mm lens was mounted to focus the light on a pinhole. This pinhole was at 18 mm distance from the glass surface of the PMT. On the basis of this configuration we further experimented with mounting a variety of

obscuration bars and pinholes. The sizes of the obscuration bars tested were: 2.5, 3, 5, 8 and 10 mm, whereas the diameter of the tested pinholes were: 30, 50, 100, 200, 400 and 700 µm. All obscuration bars were custom made by Becton Dickinson. All pinhole formats were purchased from Thor labs (Newton, NJ), except for the 700 µm pinhole, which was custom made by Becton Dickinson. To observe the relative improvement of FSC detection upon application of the various obscuration bars and pinholes we used 100 nm yellow-green fluorescent (505/515) Carboxylate-Modified Microspheres (FluoSpheres™, ThermoFisher Scientific / Invitrogen, Eugene, F8803, Lot. 1832955) to align the lasers and fluid stream and to normalize each measurement. Trigger signals are taken from the first laser (488 nm). In the analog system of the BD Influx this is also the parameter where the threshold is set on. The term "threshold(ed)" is used throughout the manuscript. For the BD Influx, part of the pulse processing and related baseline calculations are not sufficiently described, and uncertainty remains about the output value of pulse area. The BD Influx displayed the closest match with other instruments when calibration beads were measured in pulse height mode. Based on this empirical finding, pulse height was used for all measurements in this study. Preamps of the ADC's with a 1.2 µs time constant were used for all of the non-trigger parameters (instead of 0.12 µs, which was used for triggering only).

For normalization of signals, we marked the position of 100 nm Fluospheres in a saved workspace containing dot plots with narrow gates and upon swapping obscuration bars or pinholes the system was carefully re-aligned to reach the highest possible signals (as expressed by the mean fluorescent intensities (MFI)). Thereafter PMT voltages were adjusted such that the 100 nm bead cluster displayed identical MFI and mean light scatter values for each subsequent measurement.

Importantly, to prevent contaminating events to be released from the sample input tube and to clearly visualize the absolute background noise of the flow cytometer and eventual particles residing within the sheath, background measurements were recorded in backflush mode (no sample passing the laser). Next, 100 nm Fluospheres were measured and thresholded on either FSC or fluorescence, using the threshold levels indicated in the results section at an event rate of 2000/s. Each sample was run with the same sample (4.29 psi) and sheath (5.0 psi) pressure. Under these conditions the sample core diameter is 6 µm. Calculation of the core diameter was based on the expel of fluid from the nozzle tip (4.56 ml/min) and the sample fluid consumption during a given time period (0.01 ml/min). To calculate the core diameter of the sample, the total sheath volume per time unit was divided by the volume of the sample during the same time. The following formula was then used (18) to calculate the core diameter:

$$d_c = \sqrt{d_s^2 \times Q}$$

where d_c = core diameter, d_s^2 = stream diameter; Q = sample volume/total volume.

The pulse length as observed on the digital storage oscilloscope relates to the time the particle dwells in the laser spot. For particles in the sub-micron range this is 2.5 µs in the described configuration. With the volumetric measurements above we calculated the height of the laser spot to be 13.7 µm and the speed of the particle 5.5 m/s.

Before acquisition, each sample was boosted until events appeared, the stream was then allowed to stabilize for 30 seconds, after which data were recorded for 30 seconds using BD Sortware version 1.2.0.142. Data analysis was performed with FlowJo Version 10.5.0 and dot plots presented in this manuscript display ungated data from all events acquired during a 30 second measurement.

Isolation of cell culture supernatant-derived EV

EV-containing samples were obtained from 4T1 mouse mammary carcinoma cell culture supernatants (ATCC, Manassas, VA) as previously described (19, 20), Briefly, cells were maintained in Dulbecco's minimal essential medium (DMEM) supplemented with 10% fetal calf serum, 100 U/ml penicillin and 100 µg/ml streptomycin (Invitrogen, Carlsbad, CA). To prepare conditioned medium (CM), 4T1 cells were washed once with DMEM, followed by three washing steps with DMEM supplemented with 0.5% EV-depleted fetal bovine serum (EDS). EDS was obtained after 18 hours of ultracentrifugation at 100,000 g and 4 °C using a SW55 Ti rotor (Beckman Coulter, Fullerton, California, USA) and filtered through a 0.22 µm filter (Whatman, Dassel, Germany). Flasks were incubated at 37 °C and 5% CO2 with 15 ml DMEM containing 0.5% EDS. After 24 h, CM was collected and centrifuged for 10 min at 200 g and 4 °C. Prior to the collection of the CM, cell counting was performed with trypan blue staining to assess cell viability (>90%) by using an automated cell counter (CountessTM, Thermo Fisher Scientific). The supernatant was passed through a 0.45 µm cellulose acetate filter (Corning, New York, USA) and CM was concentrated at 4 °C approximately 300 times using a 10 kDa Centricon Plus-70 centrifugal unit (Merck Millipore, Billerica, Massachusetts, USA). After filtering through a 0.22 µm filter (Whatman, Dassel, Germany), 1 ml of the concentrated conditioned medium (CCM) was used for EV isolation by a combination of Optiprep Density Gradient Ultracentrifugation (ODG) and Size Exclusion Chromatography (SEC), as previously described (19, 20). Briefly, a discontinuous gradient was made by layering 4 ml of 40%, 4 ml of 20%, 4 ml of 10% and 3.5 ml of 5% iodixanol (Axis-Shield, Oslo, Norway) in a 16.8 ml open top polyallomer tube (Beckman Coulter, Fullerton, California, USA). One milliliter of CCM was placed on top of the gradient, followed by 18.11 h ultracentrifugation at 100,000 g and 4 °C using a SW32.1 Ti rotor (Beckman Coulter, Fullerton, California, USA). Fractions of 1 ml were collected and EV-rich fractions, being 9 and 10, were pooled together. For size-exclusion chromatography (SEC), Sepharose CL-2B (GE Healthcare, Uppsala, Sweden) was washed three times with PBS containing 0.32% trisodiumcitrate dihydrate (ChemCruz, Dallas, Texas, USA). For preparation of one column, a nylon net with 20µm pore size (NY2002500, Merck Millipore, Billerica, Massachusetts, USA) was placed on the bottom of a 10 ml syringe (BD Biosciences, San

Jose, California, USA), followed by stacking of 10 ml Sepharose CL-2B. On top of the SEC column, 2 ml of sample was loaded and fractions of 1 ml eluate were collected. The EV-enriched eluates, being 4-7, were pooled and concentrated approximately 40 times using a centrifugal filter Amicon Ultra-2 10k (Merck Millipore, Billerica, Massachusetts, USA). EV-pooled eluates were centrifuged at 3,202 g using a A-4-62 swinging bucket rotor at 4 °C for 10–20 min. Concentrated samples were recovered following the manufactures instructions by centrifugation at 1,000 g and 4 °C for 5 min. Eluates were collected from the flow-through reservoir and resuspended in PBS to a final volume of 100 µl. Samples were next aliquoted in Eppendorf tubes (20 µl) and stored at -80 °C until used. The EV obtained from this batch stock were used in the experiments shown. The EV characterization by Nanoparticle Tracking Analysis (NTA) is shown in Supplementary Figure 1 and described in the supplementary Material & Methods.

Fluorescent staining of EV

EV were stained with PKH67 and separated from contaminants as fully described previously (14). In brief, 10 µl of the isolated reference 4T1 EV (corresponding to a concentration of 1.44 E12 particles/mL as determined by NTA) were stained with PKH67 (Sigma-Aldrich, St Louis, MO, USA), and separated from protein aggregates and free dye by bottom-up density gradient centrifugation in sucrose for 17.30 h at 192,000 g and 4°C using a SW40 rotor (k-factor 144.5; Beckman Coulter, Fullerton, California, USA). Twelve fractions of 1 ml were then collected from the top of the gradient and respective densities were determined by refractometry using an Atago Illuminator (Japan). No further SEC was required on these pure EV fractions. For subsequent analysis by flow cytometry, M4T1 EV-PKH67 samples corresponding to a 1.14 g/ml density were diluted 1:20 in PBS (Figure 3) and further serially diluted to 1:40 and 1:80 in PBS (Supplementary Figure 1C-D). MIFlowCyt-EV guidelines (21) were followed whenever applicable (supplementary material).

Fluorescence calibration

For calibration of the fluorescence axis we used FITC MESF beads (custom made, lot MM2307 #131-10; #131-8; #130-6; #130-5; 130-3, BD Biosciences, San Jose, CA). FITC MESF beads were provided with assigned numbers of molecules of equivalent soluble fluorochrome (MESF) for each peak intensity. Briefly, each bead peak population was gated using FlowJo Version 10.5.0 and median fluorescence intensities (MFI) were obtained (Supplementary Figure 2A-C). Next, the software FCM_{PASS} Version v2.17 was used to perform a least square linear regression analysis and to generate the histogram showing FITC MESF calibrated axis units (Figure 3F) (22) (Software is available on http:go.cancer.gov/a/y4ZeFtA).

Data availability

All EV data of our experiments have been submitted to the EV-TRACK knowledgebase (EV-TRACK ID: EV190050) (23). All flow cytometric data files have been deposited at the Flow Repository (FR-FCM-Z272).

RESULTS

We here tested a combination of differently sized obscuration bars and differently sized pinholes in the optical light path of the FSC detector. With the appropriate pinhole fitted and after careful focusing, the light reaching the detector can be confined to the core of the fluid stream, eliminating the majority of light coming from other directions (Figure 1).

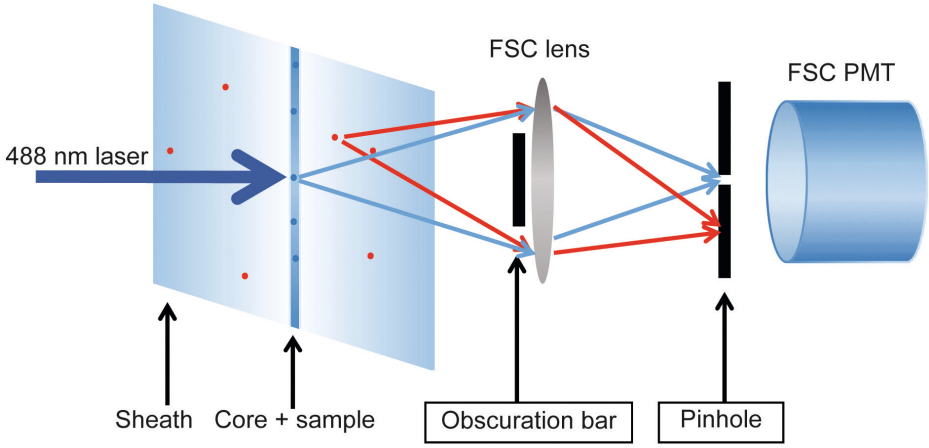

Figure 1. Schematic representation of the optical configuration in front of the FSC detector. With a small pinhole in place, scatter light derived from a confined small area around the core stream only can reach the FSC detector (blue arrows), while light coming in with other angles (either stray light or scatter from occasional particles in the sheath fluid) are blocked (red arrows). The figure does not reflect actual relative sizes and dimensions.

We deployed a matrix in which all possible combinations of 5 differently sized obscuration bars and 6 different pinholes were tested in front of the FSC-detector. For each combination, the PMT voltages were adjusted to allow the 100 nm Fluospheres cluster to reach the exact same mean light scatter and fluorescence values for all measurements. This was done to allow a fair comparison between the specific signals and the background noise in each specific situation. Subsequently, a file without a sample running was recorded to determine the amount of background events for each condition. The electronics of the BD Influx can process up to 200.000 events/s. The closer this rate is reached, the more unreliable the total number of events per measurement will be. All measurements in the range of 200.000 events/s were defined as “too many to count” (TMTC) as indicated by the color gradient in table 1. Each measurement was recorded

twice; once with a fluorescence (FL) threshold at a value of 0.62 and once with a FSC threshold at a value of 0.72. The latter threshold was set slightly higher to avoid the situation of having TMTC in a large number of (sub-optimal) combinations. The number of ungated events collected during 30 seconds without a sample running was next displayed in a heat map matrix (Figure 2). Data in red indicate TMTC, whereas all data in orange, yellow and green fall within the reliable detection range. As expected, the measurements performed with a threshold based on fluorescence display a relatively constant level of background noise for all applied combinations of obscuration bars and pinholes (Figure 2A). As the changes in configuration only took place on the FSC detector, these data show that the number of fluorescent background events remain unaffected by modification of the FSC optical axis. When a FSC threshold was applied the total number of detected background events was however severely affected by the different combinations of obscuration bars and pinholes fitted in the optical axis of the FSC detector (Figure 2B). The number of background events reduce at increasing sizes of obscuration bars and decreasing pinhole sizes, but counter intuitively at pinhole sizes of 100 µm and smaller the number of background events increases again. It has to be considered that the measurements were normalized. Under each condition in which the pinhole size was decreased or the obscuration bar size was increased, the voltage of the FSC detector had to be increased to reach the given mean scatter and fluorescence values. This indicates that specific signal is reduced as well but to a lesser extent than background light and scatter light from out-of-focus particles. This selective reduction of background light works down to a pinhole size of 200 µm. Below the 200 µm pinhole, the sizes of the smaller pinholes do not allow full passage of the scatter derived from the focused particle and the apparent background becomes visible in these normalized measurements because of increasing voltage settings. Highest voltage applied in this series was 582.6. These effects on the of the number of background events can be explained by the fact that background light is a not-to-be neglected component of the total noise in the signal and is effectively reduced by decreasing pinhole and/or increasing obscuration bar sizes until the combination of a 200 µm pinhole with an 8 mm blocker bar on this BD Influx.

Next, the combinations that resulted in the lowest numbers of background in Figure 2B (FSC threshold) were selected (50 µm, 100 µm, 200 µm pinholes in combination with either a 5 mm, 8 mm or 10 mm obscuration bar) and were recorded again, but now with a reduced FSC threshold value of 0.27 (Figure 2C). These data show that the combination of an 8 mm blocker bar and a 200 µm pinhole clearly stands out from the other 29 tested combinations regarding the number of background events that are being detected during FSC thresholding.

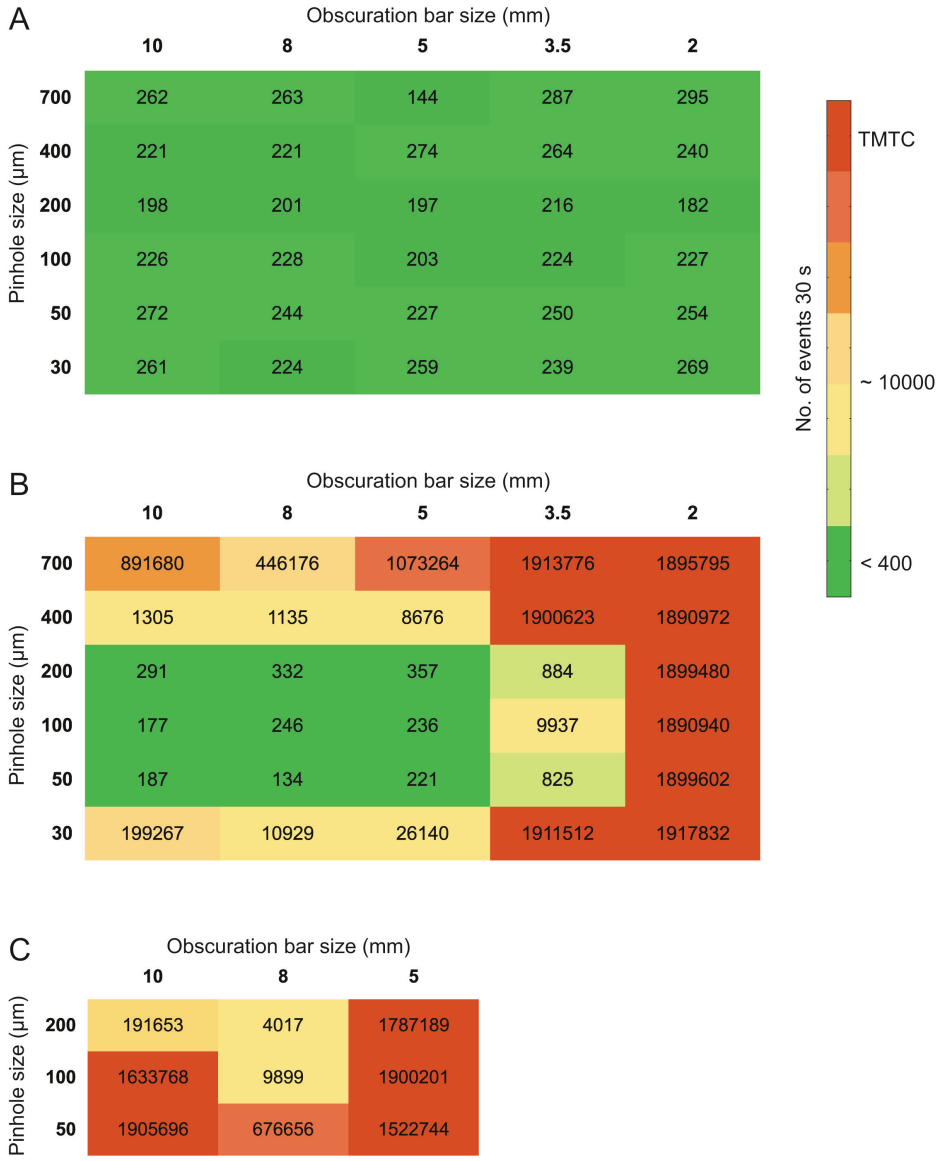

Figure 2. Matrix showing the number of events from a 30 s background measurement. The numbers in each cell represents the number of events under conditions as defined by the size of the obscuration bar (horizontal) and the size of the pinhole (vertical). Panel A shows the results when fluorescence threshold is applied (threshold 0.62). Panel B shows the results for the same configurations as in Panel A but in FSC threshold mode (threshold 0.72). To further enhance configurations with the lowest numbers of events in the FSC threshold mode (50-, 100-, 200-nm pinholes in combination with either a 5-, 8-, or 10-mm obscuration bar), these combinations were recorded again, with a reduced threshold (0.27) as displayed in Panel C.

Since fluorescence threshold in our hands displays the highest signal-to-noise ratio and generates the most reliable results when measuring submicron-sized particles, we next compared the standard configuration (5 mm obscuration bar, 700 µm pinhole), as described in van der Vlist et al. (14) with the optimized configuration (8 mm obscuration bar, 200 µm pinhole) using a FL threshold on 100 nm Fluospheres and without a sample running (Figure 3A-D). When compared to the standard configuration, density dot plots clearly display a reduced number of background noise events within the FSC channel of both the 100 nm Fluospheres (Fig 3A-B) and the measurement without sample running (Fig 3C-D) when the 8 mm obscuration bar and 200 µm pinhole were fitted.

With the optical background within the FSC channel now effectively being reduced by the bigger obscuration bar and smaller pinhole, we next tested whether the enhanced signal-to-noise ratio also allowed for enhanced detection of 100 nm Fluospheres and reduction of noise using FSC- thresholding (Fig 3E-J). While there is a high amount of background noise present within the density dot plots of the backflush and 100 nm Fluospheres, when the standard configuration of obscuration bar and pinhole is applied (Fig 3E, H), the optical background is significantly reduced upon fitting the 8 mm obscuration bar and 200 µm pinhole for both beads and backflush (Fig 3F, I, respectively). However, since part of the 100 nm fluorescent bead cluster was below the applied threshold of 0.72 when the optimized configuration was fitted (Figure 3F) a lower threshold (0.27) was applied to resolve the entire bead population (Figure 3G, J). Although this resulted in more background noise (Figure 3J), our data show that when a 8 mm obscuration bar and 200 µm pinhole were deployed, the 100 nm polystyrene beads could be clearly resolved from background noise upon FSC thresholding (Figure 3G) with an acceptable level of background. Taken together, these data thus show that when the optical background is reduced by applying an optimally sized obscuration bar and pinhole in front of the FSC detector, the signal-to-noise-ratio of the FSC-parameter can be significantly improved for submicron-sized particles.

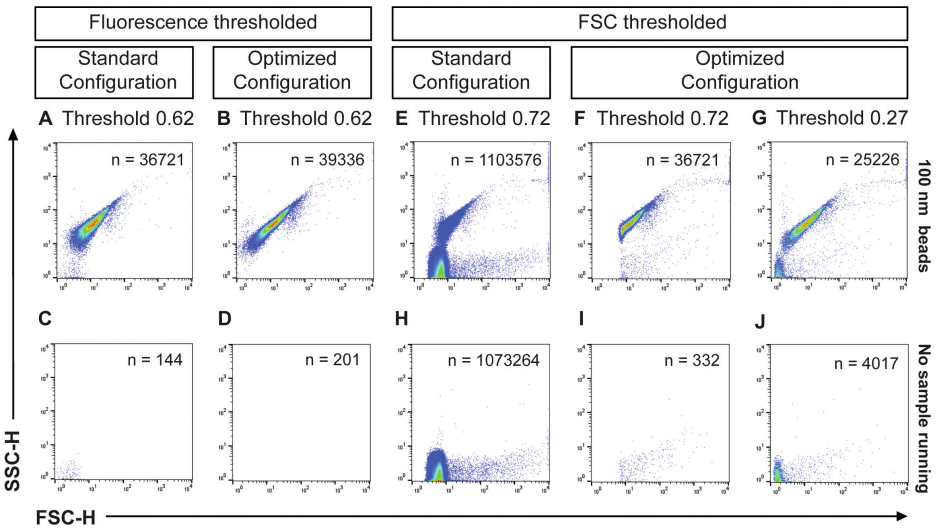

Figure 3. Measurements of 100 nm polystyrene beads in fluorescence (A, B) or FSC (E–G) threshold mode with the respective measurements without sample running (C, D) and (H–J) as background definition. Density plots show a comparison between the standard configuration (5-mm obscuration bar, 700-µm pinhole) and the optimized configuration (8-mm obscuration bar, 200-µm pinhole).

We have realized the importance of FSC by analysis of virus-containing EV populations that could solely be discriminated from non-virus containing EV based on the contribution of FSC (11). Since EV have a comparable size, but a distinctly lower refractive index (RI ≈1.4) than polystyrene beads (RI ≈1.6), we finally tested the significance of improved background reduction on a biological sample containing EV. Hence, we isolated and characterized an EV sample derived from mouse mammary carcinoma 4T1 cell culture supernatants (M4T1 EV, supplementary Figure 1 and Supplementary Materials and Methods) and fluorescently stained the EV with the lipophilic generic membrane dye PKH67. Next we compared the standard configuration and optimized obscuration bar-pinhole configuration by measuring these PKH67-stained M4T1 derived EV using a FL or FSC thresholding (Figure 4). When the standard configuration (Figure 4A) is compared to the optimized configuration (Figure 4B) during fluorescence thresholding a clear improvement is observed, as noise events overlapping the EV move towards the FSC baseline, thereby allowing a noise-free display of the EV cluster (Figure 4B). The combination of an 8 mm obscuration bar and 200 µm pinhole thereby allowed a better separation between fluorescently stained EV and noise that appeared above the fluorescence threshold. Using FSC thresholding in the standard configuration (Figure 4C) the threshold had to be set at 0.72 to avoid an unacceptable high number of background counts. Because of this threshold level, a large part of the EV remain below the FSC threshold level and the EV cluster in the density plot appears to be clipped. This becomes even more evident when using this threshold setting in the optimized configuration (Figure 4D). However, for this highly purified EV sample the optimized configuration allowed to resolve the vast majority of EV after FSC threshold was reduced to a value of 0.27 (Figure 4E). Panel 4F shows the histogram of the EV plotted with a FITC calibrated axis to give an indication of the median PKH67 fluorescence intensity of the EV population in standard units of molecules of equivalent soluble fluorochrome (MESF). The majority of the EV population has a fluorescence intensity equivalent to approximately 300 FITC MESF when measured on this instrument. The fluorescence threshold value of 0.62 on this BD Influx corresponds to an equivalent of 100 FITC MESF, which corresponds with the lower end of the population in the histogram. The bar graph (Figure 4G) shows the number of events measured for the same sample with the optimized configuration in a quantitative manner. The background number of events derived from clean PBS measurements in identical configurations were subtracted to allow a fair comparison. While measurements performed in the optimized configuration with high FSC threshold (0.72) show lower numbers of events as compared to FL thresholding, the measurements performed with low FSC threshold (0.27) clearly show the improvement in the detection of EV, thereby allowing for the visualization of comparable numbers of EV to those observed in the FL thresholded measurements.

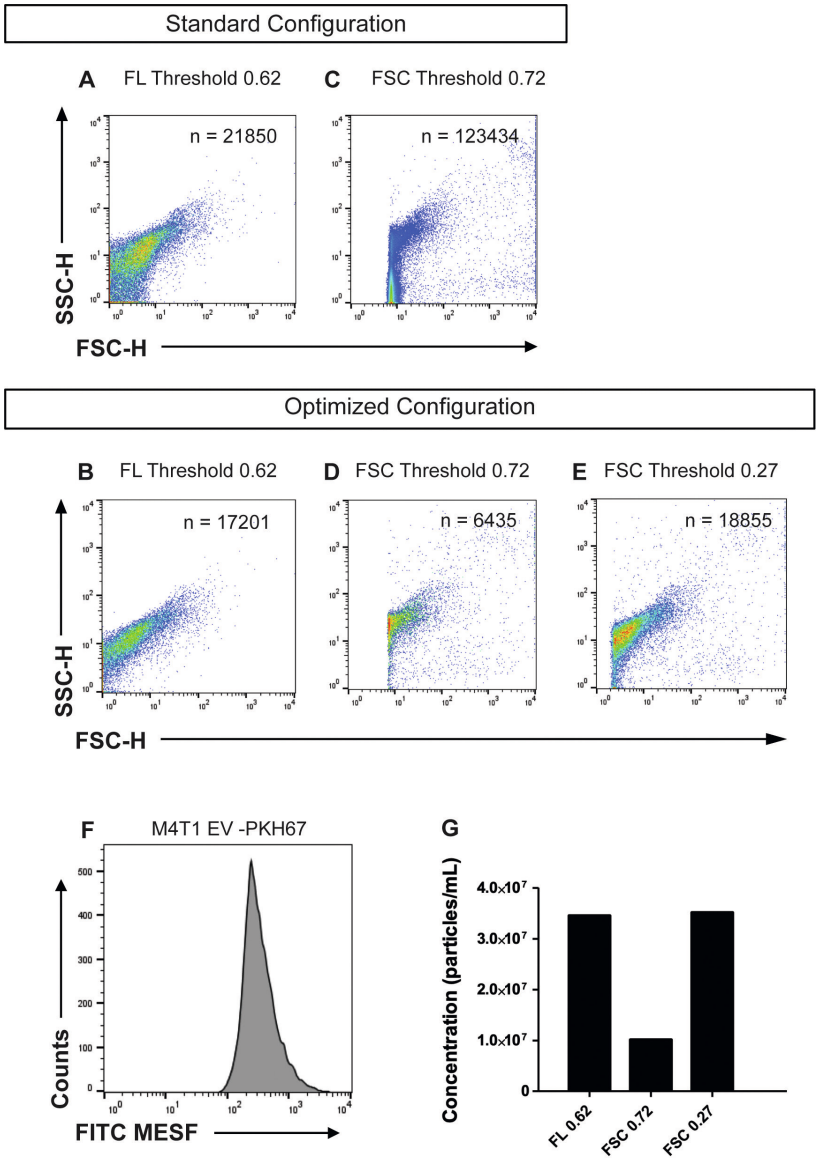

Figure 4. Density plots showing measurements of PKH67-stained M4T1 derived EV in a comparison between the standard configuration of the FSC detector optics (5-mm obscuration bar, 700-µm pinhole, A, C) and the optimized configuration (8-mm obscuration bar, 200-µm pinhole, B, D, E). Panels A and B are in fluorescence thresholding mode. Panels C–E are in FSC thresholding mode. F Histogram displaying FITC-MESF calibrated axis for PKH67 stained M4T1 EV, same as shown in Panel B. (G) Bar graph displaying concentration measured with the optimized configuration in fluorescence thresholding mode (threshold value of 0.62) and FSC thresholding mode (threshold values of 0.72 and 0.27) as indicated. Concentration was corrected for dilution, flow rate, time measurement and the number of events detected in PBS background controls (which total numbers of events were 185, 1,456, and 1,522 respectively).

DISCUSSION

The signal-to-noise ratio on a flow cytometer greatly determines its resolution and sensitivity and this becomes specifically evident when measuring the dim signals transmitted by submicron-sized particles. One prominent source of background noise is optical background caused by laser stray light, and particularly light scatter parameters are vulnerable to the optical background caused by stray light of the thresholding laser. The overarching aim of this study was to improve the information obtained from the FSC detector during the analysis of submicron-sized particles. To do so, we have tested a series of differently sized obscuration bars and pinholes on the forward scatter light detection unit of a BD Influx flow cytometer that was previously optimized for the detection of submicron-sized particles (14). The main effective principle in our configuration is confocal detection. For every particle out of the focal spot, the scattering light will be reduced because it is not perfectly focused on the pinhole. This reduction also applies for optical background caused by ambient light and laser stray light that is coming in from any aberrant direction. The purpose was to find an optimal combination of obscuration bar and pinhole to allow a better separation between signal and background when measuring small and dim particles, such as EV. With the various combinations of obscuration bars and pinholes we have tested, absolute values of the signals of interest were going down with an increase in obscuration bar size or a decrease in pinhole size. Background signals reduce concurrently, but when an optimized configuration using a combination of an 8 mm obscuration bar and 200 µm pinhole was fitted, the specific signal improved relative to the background (Figure 2). With a FL threshold set at 0.62, reduction on background was such that we could separate 100 nm polystyrene beads from noise in the FSC channel, something that was not possible when the standard configuration (5 mm obscuration bar and 700 µm pinhole) was used (Figure 3 A-D). Moreover, when the optimized configuration was applied even FSC thresholded measurements of 100 nm polystyrene beads could be performed while maintaining acceptable background levels (Figure 2 G,J). Importantly, with the optimized configuration we were not only able to diminish noise during fluorescent thresholded analysis of purified fluorescently stained EV (Fig 4B), but we even managed to improve detection of these EV (mean size: 139.8 nm as determined by NTA and shown in supplementary Fig 1A) by performing FSC- thresholded measurements (Fig 4E). Although we have shown that there is an optimal obscuration bar/pinhole combination, the semi-quantitative analysis presented in this study does not address the details of collection efficiency and the description in terms of the Fourier optical system. Future work is required to confirm the configuration effects in detail with regards to these points.

Despite the fact that these improvements allow for the detection of purified EV on the basis of forward scatter light, biological samples are likely to contain massive amounts of non-EV-related material (i.e. insoluble protein complexes, lipoprotein particles and salt crystals) that scatters light and that can interfere with the detection of EV of interest

(24) (25). Hence, to allow acquisition of EV in complex biological samples using these optimized settings, thorough EV purification still remains mandatory for a clear-cut distinction between EV, optical noise and events of non-interest by forward light scatter thresholding. Performing a generic fluorescent staining strategy can aid to exclude non-EV related signals from the sample and can help to resolve smaller sized EV from background noise. In this study we have used PKH67 stained EV that were characterized to have an approximate median fluorescence intensity of an equivalent of 300 FITC MESF (Figure 4F). There are however two points that need to be considered here. Firstly, plotting non-FITC labeled EV on a FITC calibrated axis is dependent on the type and quality of the band pass filter used, as samples might turn out to have different values when measured on other instruments. Inter-comparison of instruments therefor requires that spectrally unmatched fluorophore related correction factors should be defined and applied (26). Secondly, MESF values in the very dim area are obtained by extrapolation of the regression line in the log-log converted calibration plot. This relies heavily on the linearity of the measurements and the subsequent fit of the regression line. Small deviations within the fluorochrome range of the calibration beads will have substantial effects in the area where EV related fluorescence can be expected. The average of 300 FITC MESF for PKH67 labeled EV in figure 4F therefor has to be considered as the best possible approximation in standardized units, using currently available bright FITC-calibration beads, that applies to the specific filter settings on the used BD Influx.

With orientation of the collection angle and the scattering effects of sub-micron particles in mind, SSC remains the better scatter parameter to resolve submicron-sized particles like EV on the majority of conventional flow cytometers (27) (28). It however cannot be ignored that the FSC detection unit on conventional flow cytometers is often designed with cost-efficiency in mind, not resolution. For the analysis of submicron-sized particles, the current design of most FSC detection units is thus insufficient and data considering FSC are largely ignored and uninterpretable. In the current study we show that the signal-to-noise ratio on the FSC detector can be significantly improved using simple technical modifications on a BD Influx jet-in-air flow sorter. We would like to stress that our study is meant to create awareness that optical background is a serious component influencing the detection limits of flow cytometers. As our findings allow improved FSC detection of submicron-sized particles, these considerations might be put into effect in dedicated small particle instruments that are brought on the market in the future.

ACKNOWLEDGEMENTS

The authors would like to thank Prof. An Hendrix (Laboratory of Experimental Cancer Research, Ghent University, Belgium) for the possibility to prepare and analyze M4T1 derived EV in her lab and Dr. Joshua A. Welsh (National Cancer Institute, Bethesda, Maryland) for helpful discussion. FITC-MESF beads were kindly provided as a gift by BD Biosciences (custom beads, prepared by Dr. Majid Mehrpouyan).

FUNDING SOURCES

ELA is supported by the European Union's Horizon 2020 research and innovation programme under the Marie Skłodowska-Curie grant agreement No 722148. SFWML was supported by the Dutch Technology Foundation STW (Perspectief Program Cancer ID, project 14191), which is part of the Netherlands Organization for Scientific Research (NWO), and which is partly funded by the Ministry of Economic Affairs.

DISCLOSURE OF CONFLICT OF INTERESTS

During this study, the Wauben research group, Utrecht University, Faculty of Veterinary Medicine, Department of Biochemistry and Cell Biology, had a collaborative research agreement with BD Biosciences Europe, Erembodegem, Belgium.

REFERENCES

1. van Niel G, D'Angelo G, Raposo G. Shedding light on the cell biology of extracellular vesicles. Nature reviewsMolecular cell biology. 2018;19(4):213-28.
2. Nolan JP. Flow Cytometry of Extracellular Vesicles: Potential, Pitfalls, and Prospects. Current protocols in cytometry. 2015;73:13.4.1-6.
3. Lacroix R, Robert S, Poncelet P, Kasthuri RS, Key NS, Dignat-George F, et al. Standardization of platelet-derived microparticle enumeration by flow cytometry with calibrated beads: results of the International Society on Thrombosis and Haemostasis SSC Collaborative workshop. Journal of thrombosis and haemostasis : JTH. 2010;8(11):2571-4.
4. Chandler WL, Yeung W, Tait JF. A new microparticle size calibration standard for use in measuring smaller microparticles using a new flow cytometer. Journal of thrombosis and haemostasis : JTH. 2011;9(6):1216-24.
5. Robert S, Poncelet P, Lacroix R, Raoult D, Dignat-George F. More on: calibration for the measurement of microparticles: value of calibrated polystyrene beads for flow cytometry-based sizing of biological microparticles. Journal of thrombosis and haemostasis : JTH. 2011;9(8):1676-8; author reply 81-2.
6. Mullier F, Bailly N, Chatelain C, Dogne JM, Chatelain B. More on: calibration for the measurement of microparticles: needs, interests, and limitations of calibrated polystyrene beads for flow cytometry-based quantification of biological microparticles. Journal of thrombosis and haemostasis : JTH. 2011;9(8):1679-81; author reply 81-2.
7. Zhu S, Ma L, Wang S, Chen C, Zhang W, Yang L, et al. Light-scattering detection below the level of single fluorescent molecules for high-resolution characterization of functional nanoparticles. ACS Nano. 2014;8(10):10998-1006.
8. Steen HB. Flow cytometer for measurement of the light scattering of viral and other submicroscopic particles. CytometryPart A : the journal of the International Society for Analytical Cytology. 2004;57(2):94-9.
9. Yang L, Zhu S, Hang W, Wu L, Yan X. Development of an ultrasensitive dual-channel flow cytometer for the individual analysis of nanosized particles and biomolecules. Analytical Chemistry. 2009;81(7):2555-63.
10. Zucker RM, Ortenzio JN, Boyes WK. Characterization, detection, and counting of metal nanoparticles using flow cytometry. CytometryPart A : the journal of the International Society for Analytical Cytology. 2016;89(2):169-83.
11. van der Grein SG, Defourny KAY, Rabouw HH, Galiveti CR, Langereis MA, Wauben MHM, et al. Picornavirus infection induces temporal release of multiple extracellular vesicle subsets that differ in molecular composition and infectious potential. PLoS pathogens. 2019;15(2):e1007594.
12. Arraud N, Gounou C, Turpin D, Brisson AR. Fluorescence triggering: A general strategy for enumerating and phenotyping extracellular vesicles by flow cytometry. CytometryPart A : the journal of the International Society for Analytical Cytology. 2016;89(2):184-95.
13. Nolte-'t Hoen EN, van der Vlist EJ, Aalberts M, Mertens HC, Bosch BJ, Bartelink W, et al. Quantitative and qualitative flow cytometric analysis of nanosized cell-derived membrane vesicles. Nanomedicine : nanotechnology, biology, and medicine. 2012;8(5):712-20.
14. van der Vlist EJ, Nolte-'t Hoen EN, Stoorvogel W, Arkesteijn GJ, Wauben MH. Fluorescent labeling of nano-sized vesicles released by cells and subsequent quantitative and qualitative analysis by high-resolution flow cytometry. Nature protocols. 2012;7(7):1311-26.

15. Groot Kormelink T, Arkesteijn GJ, Nauwelaers FA, van den Engh G, Nolte-'t Hoen EN, Wauben MH. Prerequisites for the analysis and sorting of extracellular vesicle subpopulations by high-resolution flow cytometry. CytometryPart A : the journal of the International Society for Analytical Cytology. 2016;89(2):135-47.
16. Libregts SFWM, Arkesteijn GJA, Nemeth A, Nolte-'t Hoen ENM, Wauben MHM. Flow cytometric analysis of extracellular vesicle subsets in plasma: impact of swarm by particles of non-interest. Journal of thrombosis and haemostasis : JTH. 2018;16(7):1423-36.
17. Wood JC, Hoffman RA. Evaluating fluorescence sensitivity on flow cytometers: an overview. Cytometry. 1998;33(2):256-9.
18. Blume P. A spectrophotometric method for determining the stream sample core diameter of a flow cytometer. Cytometry. 1989;10(3):351-3.
19. Geeurickx E, Tulkens J, Dhondt B, Van Deun J, Lippens L, Vergauwen G, et al. The generation and use of recombinant extracellular vesicles as biological reference material. Nature communications. 2019;10(1):3288-019-11182-0.
20. Vergauwen G, Dhondt B, Van Deun J, De Smedt E, Berx G, Timmerman E, et al. Confounding factors of ultrafiltration and protein analysis in extracellular vesicle research. Scientific reports. 2017;7(1):2704-017-02599-y.
21. Welsh JA, Van Der Pol E, Arkesteijn GJA, Bremer M, Brisson A, Coumans F, et al. MIFlowCyt-EV: a framework for standardized reporting of extracellular vesicle flow cytometry experiments. J Extracell Vesicles. 2020;9(1):1713526.
22. Welsh JA, Horak P, Wilkinson JS, Ford VJ, Jones JC, Smith D, et al. FCMPASS Software Aids Extracellular Vesicle Light Scatter Standardization. Cytometry A. 2019.
23. Consortium E-T, Van Deun J, Mestdagh P, Agostinis P, Akay O, Anand S, et al. EV-TRACK: transparent reporting and centralizing knowledge in extracellular vesicle research. Nature methods. 2017;14(3):228-32.
24. Yuana Y, Levels J, Grootemaat A, Sturk A, Nieuwland R. Co-isolation of extracellular vesicles and high-density lipoproteins using density gradient ultracentrifugation. Journal of extracellular vesicles. 2014;3:10.3402/jev.v3.23262. eCollection 2014.
25. Sodar BW, Kittel A, Paloczi K, Vukman KV, Osteikoetxea X, Szabo-Taylor K, et al. Low-density lipoprotein mimics blood plasma-derived exosomes and microvesicles during isolation and detection. Scientific reports. 2016;6:24316.
26. Hoffman RA, Wang L, Bigos M, Nolan JP. NIST/ISAC standardization study: variability in assignment of intensity values to fluorescence standard beads and in cross calibration of standard beads to hard dyed beads. Cytometry A. 2012;81(9):785-96.
27. de Rond L, van der Pol E, Hau CM, Varga Z, Sturk A, van Leeuwen TG, et al. Comparison of Generic Fluorescent Markers for Detection of Extracellular Vesicles by Flow Cytometry. Clinical chemistry. 2018;64(4):680-9.
28. McVey MJ, Spring CM, Kuebler WM. Improved resolution in extracellular vesicle populations using 405 instead of 488 nm side scatter. Journal of extracellular vesicles. 2018;7(1):1454776.

SUPPLEMENTARY INFORMATION

SUPPLEMENTARY MATERIAL & METHODS

Nanoparticle tracking analysis (NTA)

Size distribution and concentration of isolated EVs were determined by measuring the Brownian motion of particles using a NanoSight LM10-HS system microscope (NanoSight Ltd, Amesbury, UK) that was equipped with a 405 nm laser and sCMOS camera. An automatic pumping system was used to inject the sample with an infusion speed of 20. For each sample, 3 videos of 30 seconds were recorded and analyzed with a detection threshold of 3 and camera level of 13. Measurements were performed and monitored at ambient temperature, which did not exceed 25°C. Recorded videos were then analyzed with NTA Software version 3.1. For optimal measurements, samples were diluted in PBS until particle concentration was within the dynamic range of NTA Software (between 3E8 and 5E9 particles/ml).

Fluorescence calibration

FITC MESF calibration beads were used according to the manufacturer's instructions. FITC MESF beads were measured with the identical voltage on the PMT used for the detection of fluorescent signals (488-530/40) as the EV measurements shown in Figure 3 with the optimized configuration.

SUPPLEMENTARY DATA

MIFlowCyt EV-Item-Checklist

1.1 Preanalytical variables conforming to MISEV guidelines	Yes, all relevant data has been submitted to EV-TRACK for transparent reporting and centralizing knowledge in extracellular vesicle research (EV-TRACK ID: EV190050).
1.2 Experimental design according to MIFlowCyt guidelines	Yes, MIFlowCyt checklist can be found as part of the supporting information of this manuscript.
2.1 Sample staining details	Yes, described in Materials and Methods.
2.2 Sample washing details	Yes, described in Materials and Methods.
2.3 Sample dilution details	Yes, described in Materials and Methods.
3.1 Buffer-only controls	Yes, relevant buffer controls were measure and are shown.
3.2 Buffer with reagent controls	N/A
3.3 Unstained controls	N/A
3.4 Isotype controls	N/A
3.5 Single-stained controls	N/A
3.6 Procedural controls	Yes, procedural controls were performed
3.7 Serial dilutions	Yes, serial dilutions were performed to ensure single particle detection and are shown in Supplementary Figure 1.
3.8 Detergent-treated controls	Yes, samples were treated with triton X-100 as described and shown in Supplementary Figure 1.
4.1 Trigger channel(s) and threshold(s)	Yes, all relevant details can be found in Materials and Methods.
4.2 Flow rate / volumetric quantification	Yes, low flow rate was kept constant and is described in Materials and Methods.
4.3 Fluorescence calibration	Yes
4.4 Scatter calibration	No
5.1 EV diameter/surface area/ volume approximation	No
5.2 EV refractive index approximation	No
5.3 EV epitope number approximation	N/A
6.1 Completion of MIFlowCyt checklist	Yes, Corresponding data files can be found at FR-FCM-Z272 in the flow repository database
6.2 Calibrated channel detection range	200 (estimated extrapolation) until 800,000 FITC MESH
6.3 EV number/concentration	N/A

MIFlowCyt EV-Item-Checklist Continued

6.4 EV brightness	N/A
7.1 Sharing of data to a public repository	Yes, all experimental details about the biological sample preparation can be found in EV-TRACK. All data files have been submitted to http://flowrepository.org FR-FCM-Z272

MIFlowCyt-Item-Checklist

Author Checklist: MIFlowCyt-Compliant Items

Requirement	Please Include Requested Information
1.1. Purpose	Enhance flow cytometric forward scatter light detection of submicron-sized particles
1.2. Keywords	extracellular vesicles; optical background; light scatter; flow cytometry
1.3. Experiment variables	Threshold triggering strategy, pinhole size, obscuration bar size,
1.4. Organization name and address	Department of Biochemistry & Cell Biology, Faculty of Veterinary Medicine, Yalelaan 2 (Nieuw Gildestein Room 203) University of Utrecht PO Box 80176, 3508 TD Utrecht, The Netherlands
1.5. Primary contact name and email address	Ger Arkesteijn, g.j.a.arkesteijn@uu.nl
1.6. Date or time period of experiment	01-01-2019 until 31-03-2019
1.7. Conclusions	By testing various sizes of obscuration bars and pinholes in front of the forward scatter light detector background noise could be reduced and detection of submicron-sized particles could significantly enhanced
1.8. Quality control measures	100 nm polystyrene beads
2.1.1.1. (2.1.2.1., 2.1.3.1.) Sample description	Fluorescent 100 nm polystyrene beads, extracellular vesicles (EV) isolated from 4T1 cell culture supernatant
2.1.1.2. Biological sample source description	Murine mammary carcinoma cell line 4T1 (ATCC, Manassas, VA)

Author Checklist: MIFlowCyt-Compliant Items Continued

Requirement	Please Include Requested Information
2.1.1.3. Biological sample source organism description	Mouse
2.1.2.2. Environmental sample location	NA
2.3. Sample treatment description	EV samples were succumbed to differential ultracentrifugation, ultrafiltration and density gradient floatation . EV samples were treated with triton X-100 (SERVA Electrophoresis GmbH, Heidelberg, Germany) at a final concentration of 0.1% for 30 seconds prior to re-analysis.
2.4. Fluorescence reagent(s) description	EV sample were stained PKH67 (Sigma-Aldrich)
3.1. Instrument manufacturer	Becton Dickinson.
3.2. Instrument model	BD Influx™,
3.3. Instrument configuration and settings	The BD Influx was optimized for detection of sub-micron sized particles as described previously in Van der Vlist *et al.* – Nature Protocols 2012. Based in that configuration various combinations of pinholes and obscuration bars were tested as described in the manuscript. Prior to each measurement, the machine was standardized with 100 nm polystyrene beads for each different configuration in order to reach a fair comparison between all measurements
4.1. List-mode data files	1) The link for peer-review process: http://flowrepository.org/id /RvFr3STw6dAlSOXJt91gSp1nmRFji6NbRhnW1XoaHVm7eYrfiYEe 9eIqB7Df8DrH
4.2. Compensation description	No compensation was applied.
4.3. Data transformation details	No data transformation was applied.
4.4.1. Gate description	No gates were defined throughout the manuscript.
4.4.2. Gate statistics	Plots show the total number of events recorded in a 30 seconds measurements without any background correction.
4.4.3. Gate boundaries	No gates were defined throughout the manuscript.

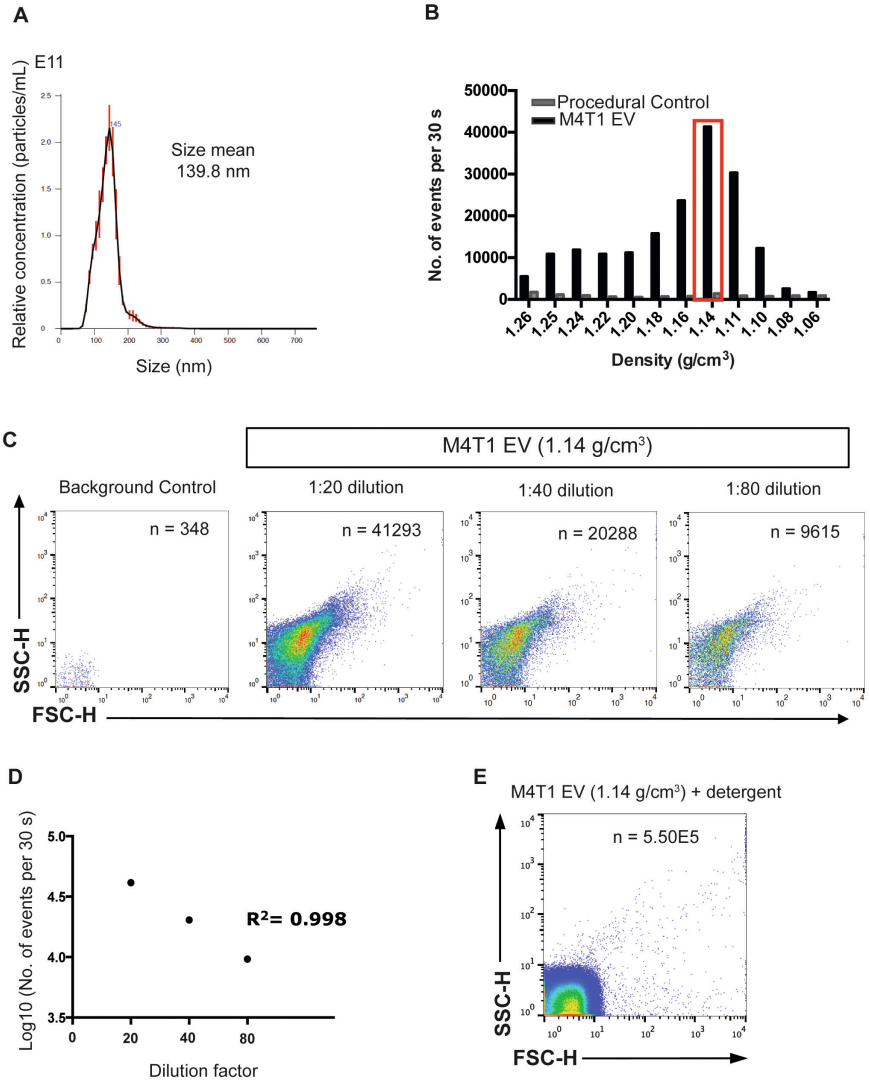

Figure S1. Characterization of M4T1 derived EV. (A) NTA-based size determination and quantification. Size distribution and concentration of the isolated EV were measured, a representative graph is shown. (B) Bar graph displaying the fractionation profile of PKH67-stained EV after sucrose gradient floatation. Fractions were diluted 1:20 in PBS prior to measurement. The total number of events in each fraction was determined by measuring samples during a fixed time of 30 s by flow cytometry. Peak fraction corresponded to a density of 1.14 g/cm3. Procedural control, PKH67 dye without EV, is shown next to the M4T1 EV. (C) Background control and serial dilutions of EV measured at standard configuration. Background was determined by measuring PBS only. Density plots of the serially diluted EV are shown and total number of events is indicated. (D) Bar graph displaying the expected straight line of serially diluted samples, indicating single EV detection at the measured concentration. (E) Effect of detergent lysis. Measurement at standard configuration of the same sample as in panel C after lysis with 0.1 % triton X-100.

A

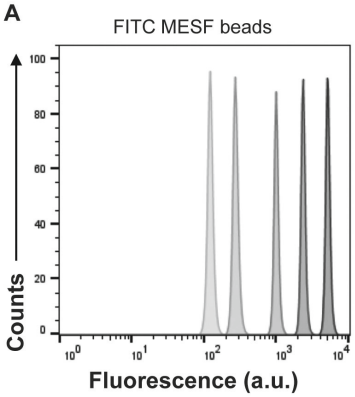

B

Peak	MFI	LogMFI	FITC MESF	LogFITC MESF
P1	120	2,0791	7094	3,8508
P2	267	2,4265	25910	4,4134
P3	967	2,9854	118192	5,0725
P4	2272	3,3564	275288	5,4397
P5	4947	3,6943	715225	5,8544

C

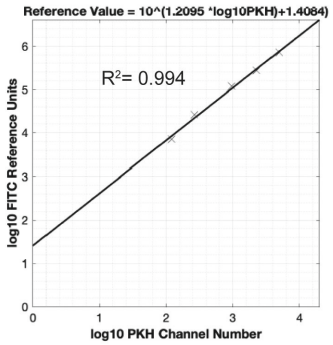

Figure S2. (A) Histogram overlay of FITC-MESF beads. Axis is in arbitrary fluorescence units. (B) Characterization of the FITC-MESF beads. Shown are the peak numbers, the corresponding MFI as measured on the BD Influx, the log10 conversion thereof, the number of FITC-MESF per bead and the log10 conversion thereof. (C) Relation between log10 fluorescence channel numbers and log10 FITC-MESF values

“I’m just a curious speck that got caught up in orbit.”

Ryan O'Neal

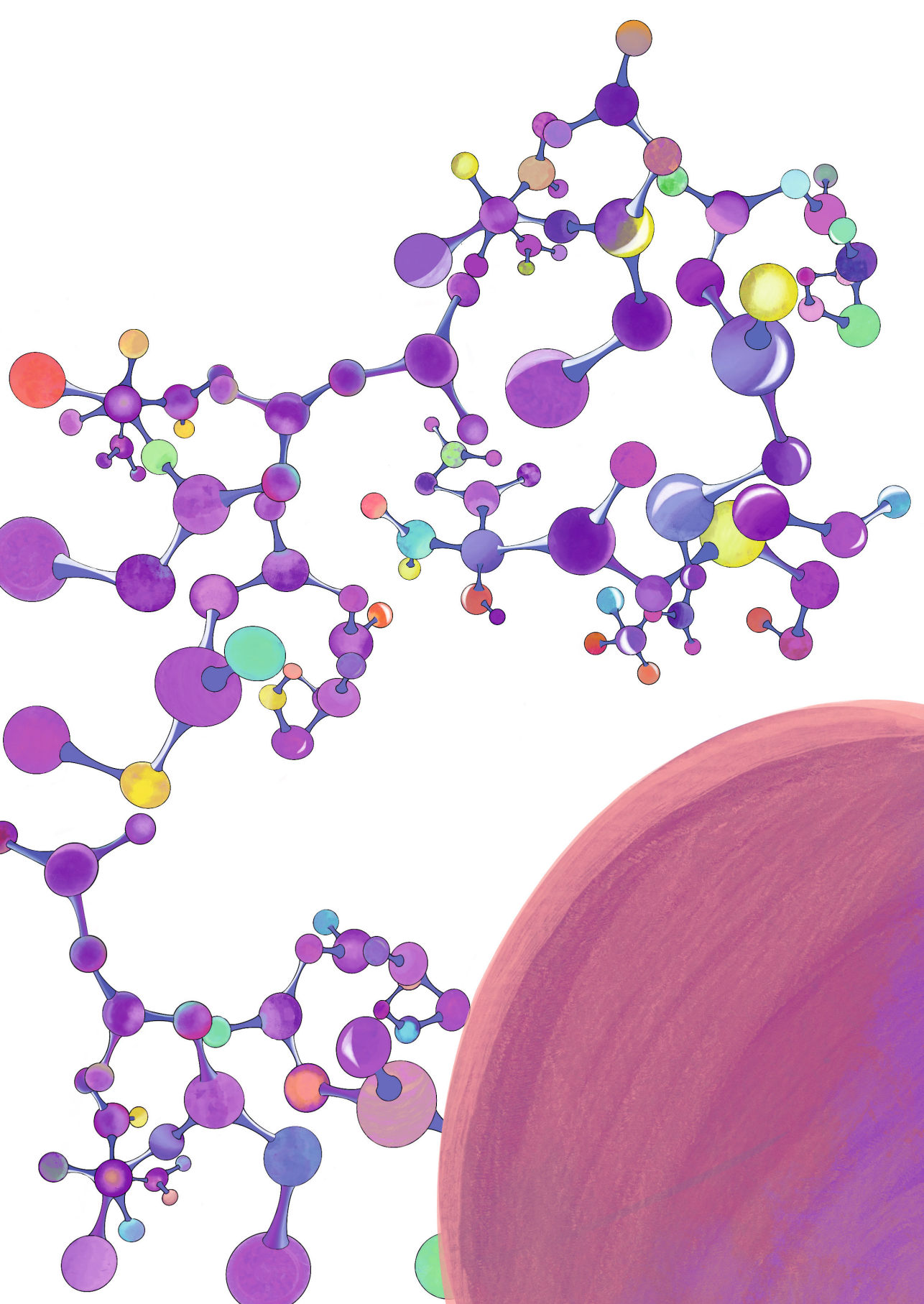

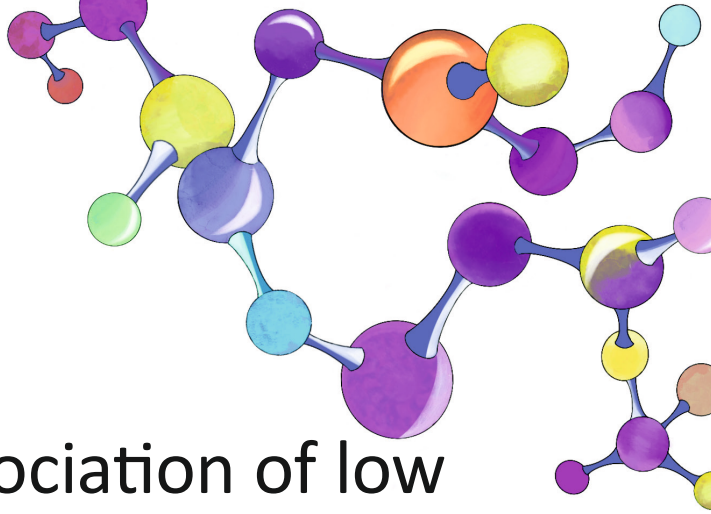

CHAPTER 6

Physical association of low density lipoprotein particles and extracellular vesicles unveiled by single particle analysis

Estefanía Lozano-Andrés [1,#], Agustin Enciso-Martinez [2], Abril Gijsbers [3], Sten F.W.M. Libregts [1], Cláudio Pinheiro [4,5,#], Guillaume Van Niel [6,7], An Hendrix [4,5,#], Peter J. Peters [3], Cees Otto [2], Ger J.A. Arkesteijn [1], Marca H.M. Wauben [1,#,*]

1 Department of Biomolecular Health Sciences, Faculty of Veterinary Medicine, Utrecht University, Utrecht, The Netherlands
2 Medical Cell Biophysics Group, University of Twente, Enschede, The Netherlands
3 Maastricht Multimodal Molecular Imaging Institute, Division of Nanoscopy, Maastricht University, Maastricht, The Netherlands
4 Laboratory of Experimental Cancer Research, Department of Human Structure and Repair Ghent University, Ghent, Belgium
5 Cancer Research Institute Ghent, Ghent, Belgium
6 Institute for Psychiatry and Neuroscience of Paris, Hopital Saint-Anne, Université Descartes, INSERM U1266, Paris 75014, France
7 GHU Paris Psychiatrie et Neurosciences, Hôpital Sainte Anne, Paris, France
TRAIN-EV Marie Skłodowska-Curie Action-Innovative Training Network, train-ev.eu
* Corresponding author

Under review for publication:
Lozano-Andrés E. et al., (2022). BioRxiv
https://doi.org/10.1101/2022.08.31.506022

ABSTRACT

Extracellular vesicles (EVs) in blood plasma are recognized as potential biomarkers for disease. Although blood plasma is easily obtainable, analysis of EVs at the single particle level is still challenging due to the biological complexity of this body fluid. Besides EVs, plasma contains different types of lipoproteins particles (LPPs), that outnumber EVs by orders of magnitude and which partially overlap in biophysical properties such as size, density and molecular makeup. Consequently, during EV isolation LPPs are often co-isolated. Furthermore, physical EV-LPP complexes have been observed in purified EV preparations. Since co-isolation or association of LPPs can impact single EV-based analysis and biomarker profiling, we investigated whether under physiological conditions LPPs and EVs can associate by using cryo-electron tomography, label-free synchronous Rayleigh and Raman scattering analysis of optically trapped particles and fluorescence-based high resolution single particle flow cytometric analysis. Furthermore, we evaluated the impact on flow cytometric analysis in the absence or presence of different types of LPPs using *in vitro* spike-in experiments of purified tumor cell line-derived EVs in different classes of purified human LPPs. Based on orthogonal single-particle analysis techniques we demonstrated that EV-LPP complexes can form under physiological conditions. Furthermore, we show that in fluorescence-based flow cytometric EV analysis staining of LPPs, as well as EV-LPP associations can influence EV analysis in a quantitative and qualitative manner. Our findings demonstrate that the biological colloidal matrix of the biofluid in which EVs reside impacts their buoyant density, size and/or refractive index (RI), which may have consequences for down-stream EV analysis.

Keywords: extracellular vesicles, exosomes, microvesicles, lipoprotein particles, blood, flow cytometry, single particle, rayleigh and raman scaterring, cryo-electron tomography, plasma, biomarker

INTRODUCTION

Extracellular vesicles (EVs) are a heterogeneous group of membrane enclosed vesicles that contain biological information from the cell of origin, such as lipids, nucleic acids, carbohydrates and proteins, and are involved in intercellular communication. EVs present in blood plasma can be obtained via minimally invasive methods and have been proposed to hold clinical potential as biomarkers for diagnosis and prognosis of diseases since their specific makeup reflects a unique signature of the cell of origin [1-3]. Next to small EVs (50-200nm), plasma contains large amounts of lipoprotein particles (LPPs). LPPs are heterogeneous particles enclosed by a single layer of phospholipids and are often categorized based on their density and protein/lipid composition. The major LPP-types are chylomicrons (CM), very low-density lipoprotein (VLDL) particles, low-density lipoprotein (LDL) particles and high-density lipoprotein (HDL) particles [4]. CM have a size range of 75-1200 nm in diameter, with varying concentration between individuals and (fatty) meal consumption. VLDL are derived from CM, with 30-80 nm in diameter, which can be further transformed into LDL particles, with a smaller size diameter range of 5-35 nm. These LPPs have a low density (< 0.930-1.063 g/cm3) and are reported to contain copies of ApoB proteins [4, 5]. HDL particles are even smaller in diameter (size range 5-12 nm), have a high density (1.063-1.210 g/cm3) and do not contain ApoB proteins but ApoAI proteins [4, 5]. Recent studies have shown that the presence of LPPs is expected to interfere with both EV isolation and analysis, as they not only outnumber EVs by several orders of magnitude but also partially overlap in biophysical properties such as size and density [6-10]. The most widely applied EV isolation methods, differential (ultra)centrifugation, size-exclusion chromatography (SEC) and density gradient centrifugation have been reported to be unable to efficiently separate EVs from LPPs and described the co-isolation or formation of co-precipitates in the final preparations [7-9, 11-13]. For example, SEC is currently applied frequently for the analysis of clinical samples and although SEC allows separation of EVs and smaller HDL particles, EV-enriched SEC fractions still contain similarly sized ApoB+ particles [10]. This is in agreement with recent studies showing co-isolation between EVs and LPPs in fresh and processed blood plasma samples [8, 9, 14]. It has been demonstrated that the combination of different EV isolation methods can strongly reduce the amount of LPPs and can be applied to obtain EVs from blood plasma with high purity, however such procedures may also result in the selection of certain subpopulations of EVs [10, 15-18]. Moreover, the implementation of such combined isolation methods, is currently limited in a clinical setting, because these procedures are elaborate, time-consuming and expensive. Importantly, the fact that EV-LPP complexes have been demonstrated in EV preparations should be taken into account, since EV characteristics will be influenced in such complexes [8, 9]. Currently, it is not known whether EV-LPP complexes are artefacts resulting from the EV isolation methods used, or also occur in a physiological situation. Interestingly, some studies using minimal sample processing reported the presence of LPPs in close proximity to the lipid bilayer of EVs, indicating that EV-LPP interactions

might indeed happen under physiological conditions [8, 9, 14]. Overall, this complex biological landscape complicates EV isolation and single EV-based analysis and limits the translation of EVs as biomarkers for diseases. Therefore, a better understanding on how the presence of distinct types of LPPs can affect the appearance of EVs is critical for the characterization of single EVs and their use as biomarkers in blood plasma. Techniques that allow for single particle analysis of heterogeneous populations are pivotal for this. Cryo-electron tomography (ET), although not being high-throughput, allows for the visualization of heterogeneous samples with great resolution and is able to distinguish between lipid bilayer EVs and single layer LPPs [19]. Label-free synchronous Rayleigh and Raman scattering analysis of optically trapped particles has been proposed as a feasible approach to detect and differentiate both EVs and LPPs based on their Raman spectrum and molecular composition with minimal need for sample processing [20]. Flow cytometry (FC) is a high-throughput multiparametric technique that is widely incorporated into clinical labs. However, detection of single EVs is challenging due to the resolution limit of most available instruments and the intrinsic features of EV, such as their small size and low refractive index (RI) [21, 22]. Previous studies have shown that the presence of LPPs in plasma can influence light scatter-triggered FC detection of EV [8, 23]. Fluorescence-triggered FC is an alternative for detection of EVs but depends on fluorescent staining procedures, e.g. staining with generic fluorescent dyes and/or incubation with fluorophore-conjugated antibodies against specific proteins [21, 22, 24-27]. We here used these three different analysis techniques to gain insight into the physiological interactions between LPPs and EVs. Furthermore, we evaluated the influence of LPPs on the quantitative and qualitative FC analysis of EVs and show the implications for EV-based biomarker profiling.

MATERIAL AND METHODS

Human lipoprotein particles. Purified human lipoprotein particles, i.e. human chylomicrons (0.89 mg/ml, catalog no. 7285-1000, Biovision Incorporated), human very-low-density and low-density lipoproteins (catalog no. 437647-5MG and 6 mg/ml, LP2-2MG, Merck Millipore, respectively) were purchased and stored according to the manufacturers' instructions. For experimental condition we used a fixed volume of 2 µl from each sample.

Human plasma. Blood samples from healthy human donors were collected in sodium citrate at a final concentration of 3.2% (0.105M). Platelet-depleted plasma (PDP) was obtained within 120 minutes after collection by two consecutive centrifugation steps at 2,500 x g for 15 minutes at room temperature. After each centrifugation step, the supernatant was transferred to a new sterile plastic tube and the pellet was discarded, after which depletion of platelets was verified with an hemato analyzer (0 x 10^4 plt/µL). Samples were then transferred to 1.5 mL tubes and stored at -80°C until used. Collection

of blood was approved by the Ethical Committee of Ghent University Hospital (approval EC/2014/0655). Participants provided written, informed consent.

Preparation of EVs. 4T1 murine mammary carcinoma cell line (American Type Culture Collection (ATCC), Manassas, VA) were used as a cellular source to obtain EVs. Cells were maintained in Dulbecco's minimal essential medium (DMEM) supplemented with 10% fetal bovine serum, 100 U/mL penicillin and 100 µg/mL streptomycin (Invitrogen, Carlsbad, CA). Every month cell cultures were tested for Mycoplasma contamination using MycoAlert Plus kit (Lonza, Verviers, Belgium). EVs were prepared from conditioned medium (CM) of the 4T1 cell culture as previously described [16, 28, 29]. Briefly, cells were washed once with DMEM, followed by two washing steps with DMEM supplemented with 0.5% EV-depleted fetal bovine serum. Cells were then incubated at 37 °C and 5% CO_2 with 15 mL DMEM containing 0.5% EV-depleted fetal bovine serum. After 24 h of culture and when cell confluency was > 70%, cell counting was performed with trypan blue staining to assess cell viability (>90%) using an automated cell counter (Countess™, Thermo Fisher Scientific). Conditioned medium was then collected and centrifuged for 10 min at 300 *g* and 4 °C. The supernatant was passed through a 0.45 µm cellulose acetate filter (Corning, New York, USA) and concentrated at 4 °C approximately 300 times using a 10 kDa Centricon Plus-70 centrifugal unit (Merck Millipore, Billerica, Massachusetts, USA). After filtration through a 0.22 µm filter (Whatman, Dassel, Germany), concentrated conditioned medium was used for Optiprep density gradient ultracentrifugation. EVs were characterized following the MISEV criteria [30]. Optiprep (Axis-Shield, Oslo, Norway) density gradients (ODG) were prepared as previously described [28]. In brief, a discontinuous iodixanol gradient was prepared by layering 4 mL of 40%, 4 mL of 20%, 4 mL of 10%, and 3.5 mL of 5% iodixanol in a 16.8 mL open top polyallomer tube (Beckman Coulter, Fullerton, California, USA). One milliliter of concentrated conditioned medium was pipetted on top of the gradient and samples were centrifuged for 18 h at 100,000 ×*g* and 4 °C using a SW 32.1 Ti rotor (Beckman Coulter, Fullerton, California, USA). Fractions of 1 mL were collected from the top and EV-rich fractions 9 and 10 (corresponding to a density of 1.10-1.12 g/mL) were pooled for additional purification. Size-exclusion chromatography (SEC) was performed by using a nylon net with 20 µm pore size (NY2002500, Merck Millipore, Billerica, Massachusetts, USA) was placed on the bottom of a 10 mL syringe (BD Biosciences, San Jose, California, USA), followed by stacking of 10 mL Sepharose CL-2B (GE Healthcare, Uppsala, Sweden). On top of the SEC column, 2 mL of sample was loaded and eluted with PBS. Fractions of 1 mL were collected and EV-containing eluates 4-7 were pooled together. Pooled eluates were then concentrated approximately 40 times using a centrifugal filter (Amicon Ultra-2 10k, UFC201024, Merck Millipore, Billerica, Massachusetts, USA) following the manufacturers' instructions. Concentrated EV-eluates were resuspended in PBS to a final volume of 100 µL and aliquoted in eppendorf tubes (20 µl each) and stored at -80 °C until further use.

Dot blot analysis. Samples were spotted onto a 0.22 µm pore size nitrocellulose membrane (GE Healthcare) and allowed to dry. Membranes were subsequently blocked with PBS containing 0.5% (w/v) fish gelatin (Sigma-Aldrich) and 0.1% Tween-20 and incubated overnight at 4°C in a humidified chamber with primary human anti-CD9 (Biolegend, catalog no. 312102, dilution 1:1000), human anti-CD63 (BD, catalog no. 556019, dilution 1:1000) or human anti-ApoB100 (R&D Systems, catalog no. AF3260, dilution 1:1000). After washing with 0.1% Tween-20 in PBS, membranes were probed with secondary goat anti-mouse Polyclonal (Jackson ImmunoResearch catalog no.115-035-044, 1:10000) or donkey anti-goat Polyclonal antibodies conjugated with HPR (Invitrogen, catalog no. A16005, dilution 1:5000) and detected using Supersignal West Dura Extended Duration chemiluminscent substrate (Thermo Fisher Scientific). Imaging was performed using a ChemiDoc MP system and data was visualized using Image Lab Software v5.1 (Bio-Rad, Hercules, CA, USA).

Electron Microscopy (TEM). Purified human lipoprotein particles were deposited on carbonated grids and fixed in 2% PFA in 0.1 M phosphate buffer, pH 7.4. The grids were then embedded in methyl-cellulose/Uranyl Acetate 0,4%. All samples were examined with a FEI Tecnai Spirit electron microscope (FEI Company), and digital acquisitions were made with a numeric camera (Quemesa; Soft Imaging System).

Synchronous Rayleigh and Raman scattering. For the optical setup measurements, and the characterization of single optically trapped particles, synchronous Rayleigh and Raman scattering acquisition was performed as described [20, 31] and briefly in Supporting Materials & Methods. The intensity and wavelength of the Rayleigh-Raman spectrometer were calibrated as described in [20] and briefly in Supporting Materials & Methods. Prior to the Rayleigh and Raman scattering measurements, all samples were diluted in PBS to prevent simultaneous trapping of multiple particles. Preparations of LPPs (CM, VLDL and LDLD), 4T1 EVs and EV-LPP mixtures were measured. For the LPP-EV mixtures, a fixed input volume of 5 mL of EVs, containing a nominal amount of 8.7E9 particles based on NTA analysis, were spiked with a fixed volume of 2 mL of LPPs (same as used from the samples analyzed in Figure 1a-c). The mixed samples were further diluted in PBS to a final volume of at least 300 µL and triplicates were measured alternating between sample types. For each sample type a volume of 50 µL was loaded in the well of a glass slide (BMS Microscopes; 1.0-1.2 mm thick), covered with a glass coverslip (VWR Ltd, thickness No. 1, diameter: 22 mm) and sealed with glue (EVO-STIK, Impact) to avoid evaporation. After the drying of the glue, each glass slide was placed under the microscope objective. The laser focal spot was focused inside the solution ~60 µm below the coverslip. In each cycle of 9.7 s, 256 Rayleigh-Raman spectra were acquired with an acquisition time of 38 ms per spectrum. The trapped particles were released from the laser focal spot by blocking the laser beam for 1 s. A total of 100 measurement cycles were acquired for each sample (n=13). Hence, a total of 332,800 Rayleigh-Raman spectra were acquired from which time traces were

computed to identify the time intervals corresponding to individual trapping events. A total of 510 individual trapping events were analyzed (72 on average per sample type). The computation, segmentation and analysis of the Rayleigh and Raman time traces is described in detail in [20] and briefly in Supporting Materials & Methods.

Cryo-electron tomography. The human lipoproteins were prepared in PBS/0.1% aggregate-depleted BSA, and BSA-gold 10 nm fiducials (OD_{600} 1). A volume of 2.5 µL was applied on glow-discharged UltrAuFoil Au200 R2/2 grids (Quantifoil), and excess liquid was removed by blotting for 3 s (blot force 5) using filter paper followed by plunge freezing in liquid ethane using a FEI Vitrobot Mark IV at 100% humidity at 4 °C. Electron tomography data were acquired with a 200-kV Tecnai Arctica transmission electron microscope (Thermo Fisher Scientific) equipped with a Falcon III direct electron detector. Movies were acquired at 53k× magnification using a stage tilt scheme of −60° to 60° in increments of 3° through a total electron dose of 120 e−/Å2 and a defocus target range of −3 to −5 µm. Tilt series were aligned and reconstructed with IMOD using gold-particles tracking and SIRT, respectively [32].

Fluorescent staining and labeling for high-resolution flow cytometric analysis. Generic staining of particles was performed as previously described [21] with some minor modifications indicated below. Briefly, 2 µL of CMs, VLDLs and LDLs or 5 µL of EVs were resuspended in 20 µL PBS/0.1% aggregate-depleted bovine serum album (BSA) prior to PKH67 staining (Sigma-Aldrich). The stock solution of aggregate-depleted BSA (5% w/v) was prepared by overnight centrifugation at 100,000 x *g* (SW28 rotor Beckman Coulter, Fullerton, California, USA; 4°C; κ-factor 334.2). For antibody labeling, samples were first resuspended in 20 µL PBS/0.1% aggregate-depleted BSA and incubated with 0.5 µg of Rat anti-mouse CD9-PE (Clone: KMC8, IgG2a, κ, Lot. no. 7268877, Becton Dickinson Biosciences) or matched Isotype antibodies (Rat IgG2a, κ, PE-conjugated, Lot. no. 8096525, Becton Dickinson Biosciences) for 1h at RT while protected from light exposure. After staining, samples were cleared from protein aggregates, unbound PKH67 dye and unbound antibodies by overnight bottom-up sucrose density gradient (SDG) ultracentrifugation at 192,000 *g* (SW40 rotor Beckman Coulter, Fullerton, California, USA; 4°C; κ-factor 144.5), according to the previously described protocol [21]. Gradient fractions of 1 mL were collected and densities were determined by using an Atago Illuminator (Japan) refractometer.

High-resolution flow cytometric analysis. High-resolution flow cytometric analysis was performed with a jet-in-air-based flow cytometer (BD Influx, Beckton Dickinson Biosciences, San Jose (CA)) that is modified and optimized for detection of submicron-sized particles, and which is fully described in detail previously [21]. Upon acquisition, all scatter and fluorescence parameters were set to a logarithmic scale. To ensure that each measurement was comparable, a workspace with predefined gates and optimal PMT settings for the detection of 100 and 200 nm yellow-green (505/515) FluoSphere beads

(Invitrogen, F8803 and F8848) was loaded. Upon aligning the fluid stream and lasers the 100 and 200 nm bead populations had to meet the criteria of pre-defined MFI and scatter values within these gates, where they displayed the smallest coefficient of variation (CV) for side scatter (SSC), reduced wide-angle forward scatter (rw-FSC) and FL-1 fluorescence. The trigger threshold level was set by running a clean PBS sample, thereby allowing an event rate ≤10-20 events/second. For detergent treatment of samples, 1% (v/v) triton X-100 (SERVA Electrophoresis GmbH, Heidelberg, Germany) was added to a final concentration of 0.1% triton X-100 and incubated for 30 seconds at RT prior re-analysis. When performing quantitative and qualitative analysis of submicron-sized particles, 50 mL of each fraction was diluted in 950 mL of PBS. Upon loading the sample, the sample was boosted into the flow cytometer until events appeared, after which the system was allowed to stabilize for 30 seconds. Measurements were then recorded for a fixed time of 30 seconds using BD FACS Sortware 1.01.654 (BD Biosciences). Particle concentrations were determined by measuring the flow rate of the instrument and correcting the number of detected particles for dilution and measured time. In between measurements of samples the sample line was washed subsequently with BD FACSRinse (BD Biosciences) and PBS for 5 seconds. Data analysis was performed using FlowJo Software version 10.0.8. Additional information according to the MIFlowCyt author checklist (Supplementary Table 1), MIFlowCyt-EV framework (Supplementary Table 2) and the calibration of the fluorescence axis (Supplementary Figure 1) using FlowJo Version 10.5.0 and FCMPASS Version v2.17 is provided in the Supplementary Material & Methods and described [33, 34].

Data availability. We have submitted relevant data of our experiments to the EV-TRACK knowledgebase (ID: EV190078) [35]. Flow cytometry data files are available upon request.

RESULTS

Fluorescence-triggered flow cytometry allows the detection of generic membrane-stained human LPPs in the absence or presence of EVs

To evaluate whether CMs, VLDLs and LDLs can be stained with generic membrane dyes and detected by fluorescence-triggered FC, we obtained commercially available purified human LPPs. To stain these LPPs, we used the lipophilic generic membrane dye PKH67, which has been successfully used for EV detection [21]. Based on its biochemical properties it is also expected that PKH67 can stain the single-layer enclosing the LPP particles. After incubation with PKH67 bottom-up sucrose density-gradient (SDG) ultracentrifugation was performed to evaluate the density at which the three types of LPPs could be detected. Fluorescence-triggered FC, showed for all LPP-types that the highest concentration of events was found in the lowest-density fraction (1.06 g/cm^3) of the gradient (Figure 1a). The increase in detected events in the low-density fractions was as expected strongest for the CMs, which are the biggest and least dense LPPs and thus more easily pass the fluorescent threshold as compared to the smaller VLDL/LDL particles. Also at higher densities, corresponding to typical EV-densities (1.11-1.16 g/cm^3), PKH67+ events could be detected, indicating that in the experimental set up used not all LPPs fully floated to their density equilibrium. Further analysis of the light scattering showed that the majority of CMs induced the strongest light scattering intensities (Figure 1b, upper panel), whereas LDLs, the smallest particles analyzed, induced the weakest light scattering intensities, with more than 50% of the particles displaying low light scattering signals (Figure 1b, bottom panel). Accordingly, VLDL particles, which fall in between CMs and LDLs in terms of size and heterogeneity, showed an intermediate light scattering profile (Figure 1b, middle panel). Although these observations are in agreement with the reported sizes of these LPPs, light scattering signals cannot be interpreted as a direct measurement of nanoparticle-size without appropriate calibration based on assumed RIs of these particles [36]. Interestingly, the LDL sample, and to a lesser extent the VLDL sample, showed a characteristic tail with increasing fluorescence, rw-FSC and SSC signals (Figure 1b, bottom and middle left panels), which can be generated by 'swarming' [37, 38] or by the presence of multi-particle LPP complexes.

Detergent lysis has been suggested as a control to confirm the detection of membrane enclosed EVs in samples and to rule out the detection of contaminants like protein complexes [39]. As LPPs display overlapping biochemical and biophysical features with EVs, we also evaluated the sensitivity of PKH67+ LPPs to detergent lysis. By incubating samples using triton X-100, a non-ionic detergent that has been reported to disrupt the lipid membrane of certain EV populations [39], we observed that upon re-analysis a great part of fluorescently stained LPPs, and/or their complexes disappeared upon triton X-100 lysis (Figure 1c). Indicating that these detergent lysis conditions cannot discriminate EVs and LPPs, which is consistent with previous reports also showing detergent lysis of LPPs under varying conditions (e.g. different staining and detection strategies) [6, 8]. After confirming

that LPPs can be stained and detected with PKH67, we next investigated whether the presence of different types of LPPs affects the generic staining and detection of EVs. For this we purified EVs from the 4T1 murine mammary carcinoma cell culture supernatant by a combination of ODG ultracentrifugation and SEC (Supplementary Figure 1a). After EV isolation, EVs were characterized by Western blot, which confirmed the presence of transmembrane protein markers (e.g. tetraspanins CD9 and CD63), and by Nanoparticle Tracking analysis (NTA), which indicated a relative concentration of ~1.8E12 particles/mL with a mean size distribution of ~125 nm (Supplementary Material & Methods, Supplementary Figure 2b-c). For FC analysis EVs were stained with PKH67, followed by SDG ultracentrifugation. Time-based quantification of all gradient fractions showed that the peak density fraction of 1.14 g/cm^3 contained the highest number of events for this 4T1EV preparation (Supplementary Figure 3a) and serial dilutions confirmed single EV detection (Supplementary Figure 3b). PKH67 fluorescence and light scattering signals from the EVs showed a clear and confined population (Supplementary Figure 3c).

After characterization of LPPs and EVs by FC, we next investigated how the simultaneous presence of LPPs and EVs in a preparation would affect the staining and/or detection. For this purpose we selected a fixed input volume of unstained 4T1 EVs (i.e., 5 mL containing a nominal amount of 8.7E9 particles based on NTA analysis) that was spiked with a fixed volume of LPPs (2 mL, similar as used in Figure 1a-c). Samples were next stained with PKH67 and fractionated by SDG ultracentrifugation for fluorescence-triggered FC analysis. The total number of PKH67+ events detected in all density fractions of interest, i.e. the sum of PKH67+ events in the range of 1.06 to 1.16 g/cm^3 corresponding to both EV enriched fractions (1.12-1.16 g/cm^3) and LPP-enriched fractions (1.06-1.10 g/cm^3), was increased in the presence of LPPs (Figure 1d). Spiking CM or VLDL particles did not affect the total number of PKH67+ events in the EV-rich fractions (1.12-1.16 g/cm^3), in contrast to spiking with LDL particles leading to an increase in the total number of PKH67+ events in these fractions (Figure 1e). Hence the presence of LDL particles affected fluorescence detection of EVs and thus quantitative EV analysis. In the LPP-rich fractions (1.06-1.10 g/cm3), the number of PKH67+ events increased in all spike-in samples (Figure 1f), whereas purified EVs displayed a very low number of events (Figure 1f), comparable to the procedural controls (Supplementary Figure 2c). Evaluation of the fluorescent and light scattering profiles of the EV-rich fractions revealed that LPPs also affect qualitative analysis by strongly increasing high light scattering signals in the spiked-in samples (Figure 1g). This was again most apparent in the presence of LDL particles. Overall, detected events in EV-LPP samples, in which multi-particle interactions might occur, exhibited higher fluorescent and light scattering intensity signals at different densities compared to EVs only. The PKH67 fluorescence and rw-FSC light scatter signals detected in the LPP-rich low-density fractions resembled the previously described PKH67+ LPP pattern (Figure 1b), while in the EV only sample very few events were detected in the low density fraction (Figure 1g, top row). Taken together, our findings demonstrate that the presence of CMs, VLDLs and LDLs in EV samples affects the quantitative and qualitative analysis of EVs.

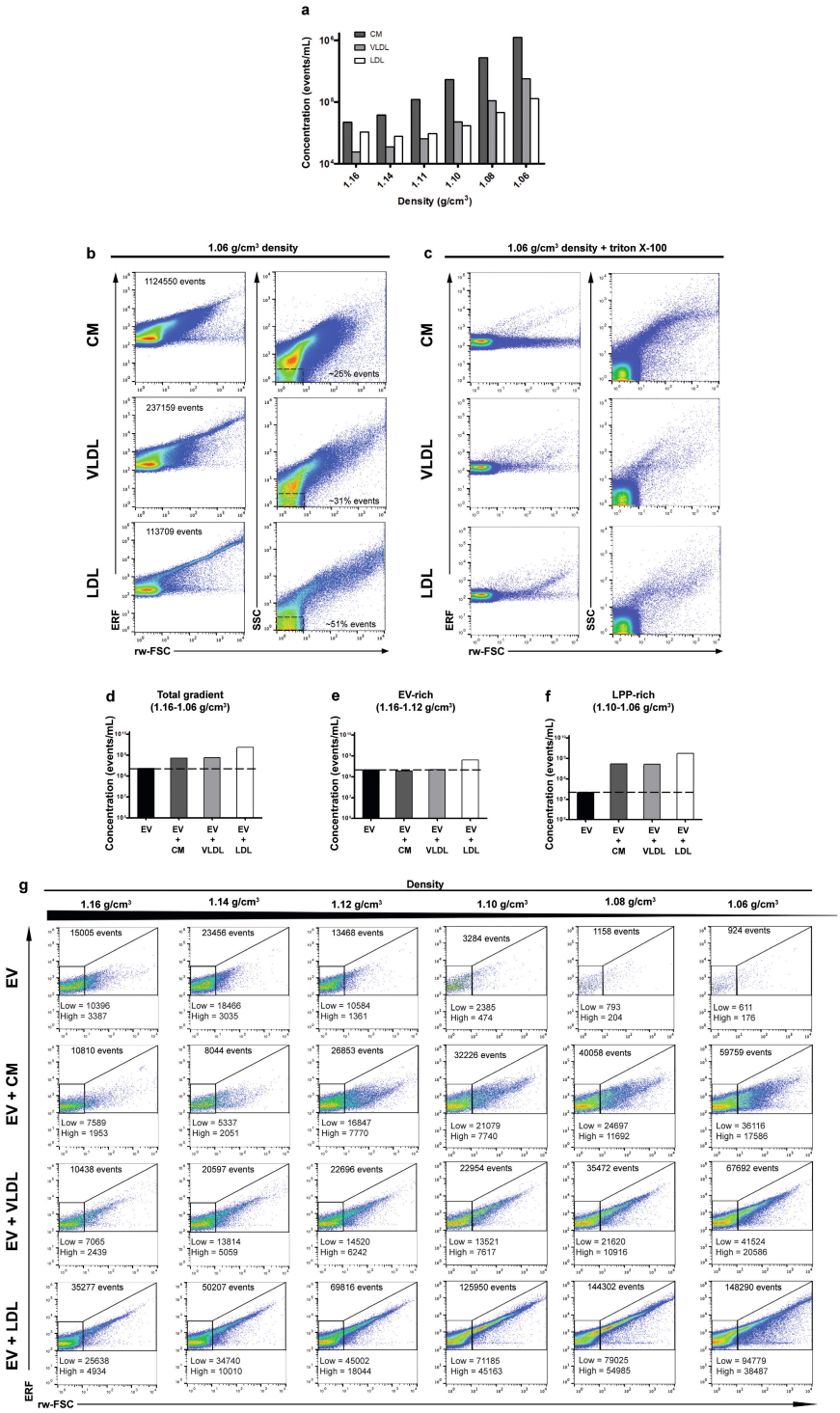
a
CM
VLDL
LDL
Concentration (events/mL)
Density (g/cm³)
1.16
1.14
1.11
1.10
1.08
1.06
b
1.06 g/cm³ density
c
1.06 g/cm³ density + triton X-100
CM
VLDL
LDL
1124550 events
~25% events
237159 events
~31% events
113709 events
~51% events
ERF
SSC
rw-FSC
d
Total gradient (1.16-1.06 g/cm³)
e
EV-rich (1.16-1.12 g/cm³)
f
LPP-rich (1.10-1.06 g/cm³)
Concentration (events/mL)
EV
EV + CM
EV + VLDL
EV + LDL
g
Density
1.16 g/cm³
1.14 g/cm³
1.12 g/cm³
1.10 g/cm³
1.08 g/cm³
1.06 g/cm³
EV
EV + CM
EV + VLDL
EV + LDL
15005 events
Low = 10396
High = 3387
23456 events
Low = 18466
High = 3035
13468 events
Low = 10584
High = 1361
3284 events
Low = 2385
High = 474
1158 events
Low = 793
High = 204
924 events
Low = 611
High = 176
10810 events
Low = 7589
High = 1953
8044 events
Low = 5337
High = 2051
26853 events
Low = 16847
High = 7770
32226 events
Low = 21079
High = 7740
40058 events
Low = 24697
High = 11692
59759 events
Low = 36116
High = 17586
10438 events
Low = 7065
High = 2439
20597 events
Low = 13814
High = 5059
22696 events
Low = 14520
High = 6242
22954 events
Low = 13521
High = 7617
35472 events
Low = 21620
High = 10916
67692 events
Low = 41524
High = 20586
35277 events
Low = 25638
High = 4934
50207 events
Low = 34740
High = 10010
69816 events
Low = 45002
High = 18044
125950 events
Low = 71185
High = 45163
144302 events
Low = 79025
High = 54985
148290 events
Low = 94779
High = 38467
ERF
rw-FSC

Figure 1. Analysis of generic fluorescence and light scattering profiles of commercial human LPP preparations and mouse EVs in presence or absence of LPPs. (a) Bar graph displaying the concentration of PKH67+ events in LPP, CM, VLDL and LDL preparations respectively, in each density fraction as determined using time-based flow cytometric analysis. (b) Representative dot plots displaying PKH67 fluorescence vs. reduced wide-angle FSC (rw-FSC) or SSC vs. rw-FSC of the low density fraction (1.06 g/cm^3) from CM, VLDL and LDL preparations, respectively. Percentage of the gated low SSC vs. rw-FSC events from the total population is indicated. (c) Representative dot plots displaying PKH67 fluorescence vs. reduced wide-angle FSC (rw-FSC) or SSC vs. rw-FSC of the low density fraction (1.06 g/cm^3) from LPPs after triton X-100 treatment (final concentration 0.1%). (d) Bar graph displaying total concentration of PKH67+ events in the density fractions of interest (1.06-1.16 g/cm^3) (e) Bar graph displaying the total concentration of PKH67+ events in the EV-rich density fractions (1.12-1.16 g/cm^3) or (f) in the LPP-rich density fractions (1.06-1.10 g/cm3) from the non-spiked, CM-, VLDL- or LDL-spiked EV samples, respectively. (g) Dot plots displaying PKH67 vs. rw-FSC of EV-rich density fractions (1.06-1.16 g/cm3) from the non-spiked, CM-, VLDL- or LDL-spiked EV samples, respectively. The total number of events for each plot is indicated on top of the plots. The number of the gated rw-FSC low or rw-FSC high populations is indicated within the plots.

Association between human LPPs and EVs in physiological samples revealed by immunoblotting and cryo-electron tomography

The profiles from the LPPs revealed by FC, together with previous literature reports showing co-isolation of LPPs and EVs in EV preparations from blood samples [8-10], prompted us to also characterize the commercial LPP preparations in detail. As indicated by the manufacturer these LPP samples obtained from healthy human plasma donors have a > 95% purity, which we confirmed with transmission electron microscopy (TEM) showing spheroidal-shaped LPP particles (Figure 2). As expected the CM preparation contained relatively large particles with a rather heterogeneous size range (Figure 2a, upper row), LDL-samples contained the smallest particles with a fairly homogeneous size range distribution of approximately 20 nm (Figure 2a, bottom row), whereas VLDL particles were found to have a size range in between CM and LDL particles (Figure 2a, middle row). To evaluate whether these preparations contain a small proportion of EVs, we next analysed the commercial LPP preparations also by immunoblot. We confirmed the presence of human Apolipoprotein B (ApoB), associated with these LPP types, in the stock solutions of the commercial LPPs and in a human platelet-depleted plasma (PDP) sample (Figure 2b). Since ApoB-48 is uniquely expressed in CM, whereas ApoB-100 is present in VLDL and LDL particles [4], the total ApoB signal cannot be used as an absolute measure for comparing these different samples. However, the volumetric-based analysis of the different preparations shows that the commercial LPP preparations contained less ApoB when compared to the physiological levels of ApoB detected in the PDP sample. Importantly, this indicates that the spike in effects of LPPs on FC analysis of EVs as observed in Figure 1, already occurred at relatively low LPP concentrations, and thus likely to happen as well in physiological blood plasma samples.

To detect the possible presence of EVs in the LPP preparations we used antibodies against two human tetraspanins present in plasma EVs (i.e., CD9 and CD63) for immunoblotting. As these tetraspanins are genuine transmembrane proteins, LPPs are negative for these proteins. However, a weak signal for human CD9 was detected in the commercial LDL preparation, but not in CM neither in VLDL preparations (Figure 2c). Based on the detection of this EV-marker in the LDL preparation we next used cryo-electron tomography to analyze possible EVs present in this preparation. With cryo-electron tomography single (i.e., LPPs) and double lipid layer (i.e., EVs) enclosed particles can be clearly distinguished. Besides the abundant present of LDL particles (~ 20 nm) (Figure 2d, red arrows) we also identified the presence of bigger sized double lipid layered particles resembling EVs (Figure 2d, yellow arrows). Remarkably, these EVs were not randomly distributed along the grid, but often in close proximity to LDL particles forming complexes of EV-LDL. Furthermore, we also observed the presence of multi-LDL complexes that were forming clusters as their layers were physically in contact (Figure 2d, right picture).

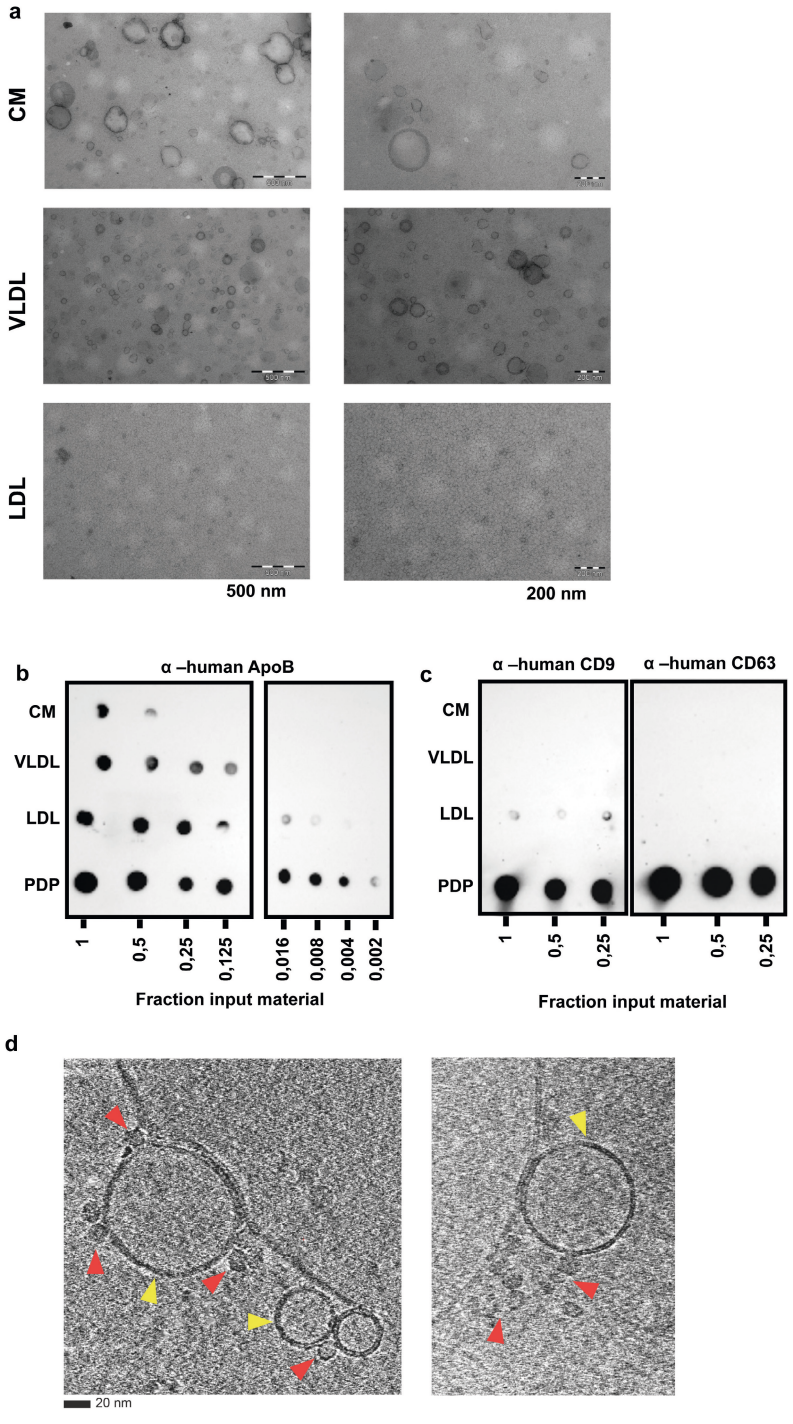
a
CM
VLDL
LDL
500 nm
200 nm
b
α –human ApoB
CM
VLDL
LDL
PDP
1
0,5
0,25
0,125
0,016
0,008
0,004
0,002
Fraction input material
c
α –human CD9
α –human CD63
CM
VLDL
LDL
PDP
1
0,5
0,25
1
0,5
0,25
Fraction input material
d
20 nm

Figure 2. Analysis of purified LPPs by TEM, immunoblotting and cryo-electron tomography. (a) Analysis of human LPPs by TEM. 4 µl from a 1/10 dilution of commercial preparations of CM (top row), VLDL (middle row) and LDL (bottom row) particles were loaded onto grids, negatively stained and visualized. Scale bars correspond to 500 nm and 200 nm for each column. (b) Dot blot immunodetection of the commercial LPPs next to human platelet depleted plasma (PDP). Serial dilutions were spotted starting from 1 µl LPP stock or PDP and analyzed for the presence of ApoB by using a specific anti-human antibody against -ApoB. (c) Immunoblot detection of human tetraspanins -CD9 and -CD63 present in commercial LPPs preparations and in human PDP from a healthy donor.(d) Cryo-electron tomography of particles present in the commercial LDL preparation Lipid bilayer enclosed structures (i.e., EVs) are indicated with yellow arrows, while smaller lipid monolayer structures (i.e., LDLs) are indicated with red arrows. Bars = 20 nm for both images.

Label-free single particle synchronous Rayleigh and Raman scattering analysis unveiled the physiological formation of EV-LDL complexes

To investigate whether EV-LPP complexes can form in solution, we performed optical trapping of particles in suspension and acquired both Rayleigh and Raman scattering signals to detect individual trapping events and to characterize the particles chemical composition, respectively [20, 31]. We evaluated the scattering profiles of optically trapped particles present in the LPP (i.e., LDL, VLDL and CM) and 4T1 EV preparations, as well as in mixtures of LPP and EV preparations.

Individual trapping events were identified as a step-wise increase of the Rayleigh signal when plotted over time. By segmenting individual trapping events a Raman spectrum per trapping event was obtained, which was corrected by background subtraction [20, 31]. To compare Raman spectra of trapped particles, principal component analysis (PCA) was performed on the 4T1 EV preparation, the different LPP preparations, and the EV-LPP mixtures (Figure 3a-c). Whereas, the particles trapped in the EV-CM mixture (Figure 3a) or in the EV-VLDL mixture (Figure 3b) clustered together with respectively CM or VLDL particles only, particles present in preparations of LDL, 4T1 EVs and a mixture of LDL and 4T1 EVs clustered in three separate groups (Figure 3c). Since particles clustering together have similar chemical composition, this indicates that we mainly trapped VLDL or CM particles in the EV-VLDL mixture and the EV-CM mixture, respectively. In contrast, particles in the EV-LDL mixture neither overlap with particles trapped in the LDL preparation, nor with particles trapped in the EV preparation, suggesting that the particles trapped in the mixed sample have a different chemical composition. As shown in Figure 3c, particles trapped in the EV-LDL mixture have PC1 scores >0 , similar to LDL particles, and also mainly PC2 scores >0, resembling the EV sample. This suggests that Raman features from both LDL and EVs contribute to the Raman spectrum of the particles trapped in the mixed sample. Since the difference between LDL and EVs was highest for PC1, we next analyzed the PC1 loading to identify the source of these differences. Figure 3d shows PC1 loading displaying positive and negative peaks at wavenumber positions that correspond to triglycerides (green lines) and cholesterol (red

lines), respectively. This means that particles with positive PC1 scores, such as particles trapped in the LDL preparation and in the LDL-EV mixture, have higher triglyceride and less cholesterol contributions to their Raman spectrum than particles with negative PC1 scores, such as particles trapped in the EV only preparation. Detailed analysis of the mean Raman spectrum between 1600 and 1700 cm^{-1}, shows that particles trapped in the EV preparation contain only cholesterol (1670 cm^{-1}), while particles present in the LDL preparation predominantly contain triglycerides (1657 cm^{-1}) (Figure 3e). The presence of cholesterol in the EV preparation was further confirmed by Raman bands associated to cholesterol in the high frequency region (2850, 2866, 2888 and 2932 cm^{-1}) (Supplementary Figure 4). Interestingly, particles trapped in the EV-LDL mixture showed clear contributions of both triglycerides and cholesterol in the Raman profile (Figure 3e). Importantly, these results show that EV-LPP associations are not only induced by isolation and/or staining procedures, but also form spontaneously in solution with label-free particles. Interestingly, LDL particles are more prone to form complexes with EVs than VLDL and CM.

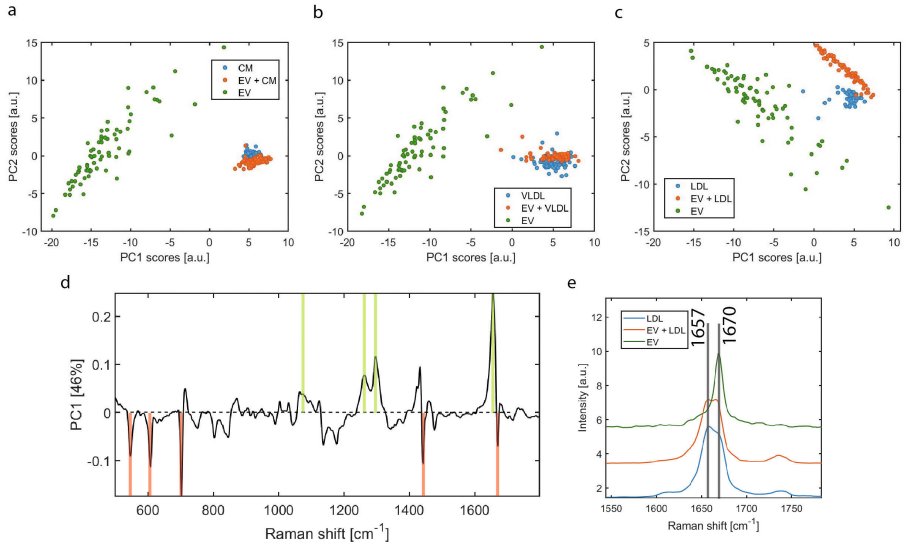

Figure 3. Principal component analysis (PCA) of LPP and EV preparations and mixed LPP and EV preparations. First and second principal component scores corresponding to the PCA of (a) CM, EV + CM and EV samples, (b) VLDL, EV + VLDL and EV, and (c) LDL, EV + LDL and EV (d) First principal component loading corresponding to the PCA of LDL, EV + LDL and EV. The green lines indicate triglyceride bands and the red lines indicate cholesterol bands. Particles with positive PC1 scores values in (c) are positively correlated with triglycerides, while negatively correlated with cholesterol. (e) Mean Raman spectrum per sample type (LDL, EV + LDL, EV) displaying a part of the Raman fingerprint region that shows triglyceride (1657) and cholesterol (1670) Raman bands.

EV-LPP associations can impact the identification and detection of specific EV markers
Since we found that EV-LPP associations can form spontaneously in solution, implicating that EV-LPP complexes are likely present in blood plasma, we further investigated whether such associations can impact the identification and detection of specific EV-markers by FC. Our experimental set-up in which mouse-derived 4T1 EVs were spiked-in human LPP preparations allowed the use of a murine-specific CD9 antibody to detect the EV-marker of interest. We confirmed the exclusive detection of murine CD9+ EVs without cross-reactivity in human LPP preparations by immunoblotting (Supplementary Figure 2d), thereby excluding the risk of the detection of human CD9+ EVs already present in the human LPP preparation, as shown before (Figure 2c). Specific FC detection of purified murine PKH67+CD9+ EVs was confirmed (Supplementary Figure 3), and the fluorescent intensity was calibrated (Supplementary Figure 1).

When equal numbers of murine EVs were stained for PKH67 and murine CD9 in the absence or presence of LPPs followed by density gradient centrifugation, different numbers of CD9+ events were detected in time-based quantitative EV measurements of the total density gradient fractions (1.06-1.16 g/cm^3) (Figure 4a). In the presence of LDL particles, the total number of CD9+ events was strongly increased, while no or marginal increase of the number of CD9+ events was observed in the presence of CM or VLDL particles, respectively (Figure 4a). In contrast, in the EV-rich density gradient fractions (1.12-1.16 g/cm3) the highest number of CD9+ EVs was detected in the EV sample in the absence of LPPs and the presence of CM and VLDL substantially reduced the number of CD9+ events(Figure 4b). Previously, we showed that the number of PKH67+ events in EV-rich densities were consistent for EVs in the absence or presence of CM or VLDL(Figure 1e). Hence, the detection of 2-fold less CD9+ EV in the presence of CM and VLDL (Figure 4b and 4d) indicates that CM and VLDL significantly affected the labelling and/or detection of CD9+ EVs. Although in the presence of LDL the number of CD9+ events was only marginally decreased (Figure 4b), the % reduction of CD9+ events was strongest (Figure 4d). This reduction in % CD9+ events is caused by the fact that in the presence of LDL the total number of PKH67+ events was increased in EV-rich fractions (Figure 1e), in contrast to the number of PKH67+ events of EVs in the presence of CM or VLDL that was similar to EVs only (Figure 1e).

Strikingly, a strong increase in the number of CD9+ events was observed in the LPP-rich densities (1.06-1.10 g/cm^3) when EVs were analyzed in the presence of LLPs, with the strongest effect in the presence of LDL (Figure 4c). Analysis of the corresponding dot plots revealed that CD9+ events, especially in the presence of LDL had a distinct profile (i.e., displaying higher PKH67+ and CD9+ intensities) (Figure 4d), which could be indicative for physical EV-LDL interactions. Altogether, these data demonstrate that the co-presence of LPPs in EV-samples, not only affects generic EV staining but can also impact the staining, enumeration and buoyant density of EV-subsets labeled for specific EV-markers.

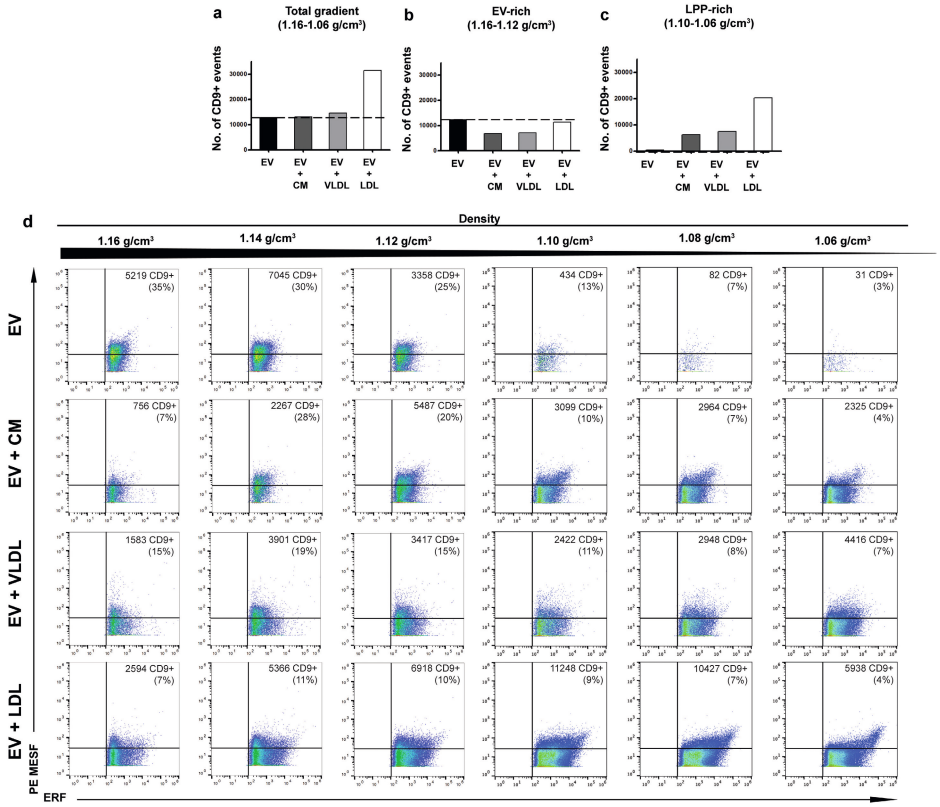

Figure 4. Detection of murine CD9+ EVs in the absence or presence of human CM, VLDL or LDL particles by fluorescence-triggered high-resolution flow cytometry. (a) Bar graphs displaying the number of PKH67+ CD9+ events in all density fractions of interest (1.16-1.06 g/cm^3), (b) Bar graphs displaying the number of PKH67+CD9+ events in EV-rich density fractions (1.16-1.12 g/cm^3) or (c) in the LPP-rich density fractions (1.10-1.06 g/cm3) from murine EVs in the absence or presence of CM, VLDL or LDL particles. (d) Dot plots displaying CD9+PE events in PE MESF units vs. PKH67+ events in ERF units from murine EVs in the absence or presence of CM, VLDL or LDL particles. The number of gated CD9+ events and its percentage from the total population is indicated for each plot.

DISCUSSION

To exploit the use of EV-based biomarkers in blood confounding effects of non-EV components, such as the abundant and variable presence of LPPs, need to be considered. Circulating EVs are often analyzed by FC and recent studies indicated confounding effects of LPPs present in EV preparations in flow cytometric EV analysis [6-8]. Based on the partially overlapping properties of EVs and LPPs, optimized sequential biophysical fractionation protocols were developed to separate LPPs from EVs [10, 15, 17]. However, in recent studies it has been indicated that also complexes of EV-LPP can be detected in EV samples [8, 9, 40].

We here explored whether such EV-LPP complexes can form in solution, or are merely a result of the EV isolation and/or labeling methods used. Furthermore, we analyzed how LPPs and EV-LPP complexes affect downstream EV analysis by FC. By using the generic membrane dye PKH67, known to be incorporated by a wide variety of lipid-containing components due to its lipophilic nature [41], we stained highly purified LPPs and EVs which resulted in partially overlapping fluorescent and light scattering signals as measured by FC. However the majority of fluorescent events was detected at different buoyant densities (i.e, LPP-rich density fractions (1.06-1.10 g/cm^3 and EV-rich density fractions (1.12-1.16 g/cm^3). Furthermore, in agreement with previous observations our data show that treatment with triton X-100 could not distinguish between LPPs and EVs, as both showed sensitivity to lysis under the exact same treatment conditions [8]. Previously, we optimized the PKH67 staining protocol for single EV-based FC and demonstrated the need of density gradient centrifugation to get rid of PKH-aggregates, which reside in high density gradient fractions excluded from our FC analysis [21]. Moreover, procedural controls were included to evaluate possible contributions of PKH67 artifacts. Using a fluorescence-based threshold triggering FC approach, the detection limit of particles depends on their generic fluorescent staining (PKH67) intensity, allowing only the detection of particles that exceed the set threshold, which in our instrument was calibrated to ~100 ERF units based on FITC MESF beads [42, 43]. Due to their size and refractive index, single VLDL and LDL particles are unlikely to be resolved at the single particle level with the settings that we used for FC analysis. However, their aggregates or multi-particle complexes can be detected by FC [8], and various reports have investigated and confirmed the formation of such physical LPP aggregates both *in vitro* and *in vivo* [44, 45]. Overall, our results clearly indicate the need for specific markers to attribute PKH67+ fluorescent events to LPPs or EVs, which is in accordance to previous observations [41, 46].

Our spike-in experiments using purified human LPPs and murine EVs were designed as a proof-of-principle study to address the knowledge gap on the impact of LPPs on EV analysis and to specifically investigate to formation of EV-LPP complexes [7]. To avoid artefacts resulting from too high concentrations of LPPs in these spike-in experiments, we intentionally used lower amounts of purified LPPs as compared to platelet depleted plasma samples (determined by immunoblotting for ApoB). Since we did not found a

reduction of the number of PKH67+ events in the EV-rich fractions, while a strong increase in PKH67+ events was observed in the LPP-rich fractions after EV-LPP spike-in, we do not have indications that the PKH dye was a limiting factor resulting in reduced staining efficiency of EVs in the EV-LPP sample. Importantly, the flow cytometric analysis of a specific EV marker (in our experimental set-up murine CD9) on EVs in the presence of LPPs clearly demonstrated the presence of murine EV- human LPP complexes in these samples. Consistent with our observations, also others have found EV-associated markers at lower densities as expected in blood plasma [10]. Furthermore, we detected in the purified human LDL preparation weak human CD9 signals by immunoblotting, and confirmed by cryo-ET the occurrence of EVs in this LDL preparation, decorated or surrounded by multiple LDL particles. Also others previously demonstrated the presence of CD9 in purified LPP preparations (i.e., purified HDL) [7]. Importantly, our findings are in line with recent reports showing that interactions between EVs and ApoB-containing LPPs can be observed using various isolation methods and detection techniques [11, 13]. However, since these previous experiments could not rule out that the formation of LPP-EV complexes was induced by the particle isolation, purification and/or staining methods used, we here explored the formation of EV-LPP complexes in solution. We demonstrate for the first time, by using label-free single particle synchronous Rayleigh and Raman scattering analysis of purified LPPs, purified EVs and their mixtures, that complexes between EVs and especially LDL particles form spontaneously in solution.

Follow-up studies are needed to address the amount of EV-LPP complexes in the blood circulation and to define EV and LPP subsets prone to form such complexes in health and disease conditions. For EV-based biomarker profiling in blood samples, our current findings demonstrate the importance of critical sample collection, preparation and experimental design, since the presence of EV-LPP complexes can impact the detection of EV markers, which can hamper but can also be exploited to identify EV-subsets of interest.

FUNDING SOURCES AND ACKNOWLEDGEMENTS

E.L.A. and C.P. are supported by the European Union's Horizon 2020 research and innovation programme under the Marie Skłodowska-Curie grant agreement No 722148 (TRAIN-EV). S.F.W.M.L. was supported by the Dutch Technology Foundation STW (Perspectief Program Cancer ID, project 14191), which is part of the Netherlands Organisation for Scientific Research (NWO), and which is partly funded by the Ministry of Economic Affairs. G.v.N. is supported by Fondation pour la Recherche Médicale (AJE20160635884) Institut National du Cancer (INCA N°2019-1033125 PLBIO19-059). We thank Laura Varela-Pinzon (Department of Biomolecular Health Sciences and Department of Clinical Sciences, Faculty of Veterinary Medicine, Utrecht University) for valuable discussions and lipidomic analysis of LPPs. E.L.A. and M.H.M.W greatly acknowledge the FACS Facility at the Faculty of Veterinary Medicine at Utrecht University and G.v.N. greatly acknowledge the Electron microscopy facility of the Institut Curie.

AUTHOR CONTRIBUTIONS

E.L.A. designed and performed experiments, analyzed data and wrote the original manuscript. A.E.M, A.G, S.F.W.M.L., C.P., and G.v.N. performed experiments, analyzed data and reviewed the manuscript. A.H., P.J.P and C.O. gave conceptual advice and reviewed the manuscript. G.J.A.A. supervised and designed the flow cytometric experiments and wrote the original manuscript. M.H.M.W. supervised the research, designed experiments and wrote the original manuscript. All authors critically reviewed and edited the manuscript.

COMPETING INTERESTS STATEMENT

During this study, the Wauben research group, Utrecht University, Faculty of Veterinary Medicine, Department of Biomolecular Health Sciences, had a collaborative research agreement with BD Biosciences Europe, Erembodegem, Belgium, to optimize analysis of EV using the BD Influx.

REFERENCES

1. Thery, C., M. Ostrowski, and E. Segura, *Membrane vesicles as conveyors of immune responses.* Nat Rev Immunol, 2009. **9**(8): p. 581-93.
2. Boukouris, S. and S. Mathivanan, *Exosomes in bodily fluids are a highly stable resource of disease biomarkers.* Proteomics Clin Appl, 2015. **9**(3-4): p. 358-67.
3. Fais, S., et al., *Evidence-Based Clinical Use of Nanoscale Extracellular Vesicles in Nanomedicine.* ACS Nano, 2016. **10**(4): p. 3886-99.
4. Feingold, K.R. and C. Grunfeld, *Introduction to Lipids and Lipoproteins*, in *Endotext*, K.R. Feingold, et al., Editors. 2000: South Dartmouth (MA).
5. Alonzi, T., et al., *Elucidation of lipoprotein particles structure by proteomic analysis.* Expert Rev Proteomics, 2008. **5**(1): p. 91-104.
6. Botha, J., A. Handberg, and J.B. Simonsen, *Lipid-based strategies used to identify extracellular vesicles in flow cytometry can be confounded by lipoproteins: Evaluations of annexin V, lactadherin, and detergent lysis.* J Extracell Vesicles, 2022. **11**(4): p. e12200.
7. Simonsen, J.B., *What Are We Looking At? Extracellular Vesicles, Lipoproteins, or Both?* Circ Res, 2017. **121**(8): p. 920-922.
8. Sodar, B.W., et al., *Low-density lipoprotein mimics blood plasma-derived exosomes and microvesicles during isolation and detection.* Sci Rep, 2016. **6**: p. 24316.
9. Yuana, Y., et al., *Co-isolation of extracellular vesicles and high-density lipoproteins using density gradient ultracentrifugation.* J Extracell Vesicles, 2014. **3**.
10. Karimi, N., et al., *Detailed analysis of the plasma extracellular vesicle proteome after separation from lipoproteins.* Cell Mol Life Sci, 2018. **75**(15): p. 2873-2886.
11. Linares, R., et al., *High-speed centrifugation induces aggregation of extracellular vesicles.* J Extracell Vesicles, 2015. **4**: p. 29509.
12. Baranyai, T., et al., *Isolation of Exosomes from Blood Plasma: Qualitative and Quantitative Comparison of Ultracentrifugation and Size Exclusion Chromatography Methods.* PLoS One, 2015. **10**(12): p. e0145686.
13. Takov, K., D.M. Yellon, and S.M. Davidson, *Comparison of small extracellular vesicles isolated from plasma by ultracentrifugation or size-exclusion chromatography: yield, purity and functional potential.* J Extracell Vesicles, 2019. **8**(1): p. 1560809.
14. Yuana, Y., et al., *Cryo-electron microscopy of extracellular vesicles in fresh plasma.* J Extracell Vesicles, 2013. **2**.
15. Onodi, Z., et al., *Isolation of High-Purity Extracellular Vesicles by the Combination of Iodixanol Density Gradient Ultracentrifugation and Bind-Elute Chromatography From Blood Plasma.* Front Physiol, 2018. **9**: p. 1479.
16. Vergauwen, G., et al., *Confounding factors of ultrafiltration and protein analysis in extracellular vesicle research.* Sci Rep, 2017. **7**(1): p. 2704.
17. Vergauwen, G., et al., *Robust sequential biophysical fractionation of blood plasma to study variations in the biomolecular landscape of systemically circulating extracellular vesicles across clinical conditions.* J Extracell Vesicles, 2021. **10**(10): p. e12122.
18. Tulkens, J., O. De Wever, and A. Hendrix, *Analyzing bacterial extracellular vesicles in human body fluids by orthogonal biophysical separation and biochemical characterization.* Nat Protoc, 2020. **15**(1): p. 40-67.
19. Cizmar, P. and Y. Yuana, *Detection and Characterization of Extracellular Vesicles by Transmission and Cryo-Transmission Electron Microscopy.* Methods Mol Biol, 2017. **1660**: p. 221-232.

20. Enciso-Martinez, A., et al., *Label-free identification and chemical characterisation of single extracellular vesicles and lipoproteins by synchronous Rayleigh and Raman scattering.* J Extracell Vesicles, 2020. **9**(1): p. 1730134.
21. van der Vlist, E.J., et al., *Fluorescent labeling of nano-sized vesicles released by cells and subsequent quantitative and qualitative analysis by high-resolution flow cytometry.* Nat Protoc, 2012. **7**(7): p. 1311-26.
22. Nolan, J.P., *Flow Cytometry of Extracellular Vesicles: Potential, Pitfalls, and Prospects.* Curr Protoc Cytom, 2015. **73**: p. 13 14 1-16.
23. van der Pol, E., et al., *Absolute sizing and label-free identification of extracellular vesicles by flow cytometry.* Nanomedicine, 2018. **14**(3): p. 801-810.
24. Shen, W., et al., *A Single Extracellular Vesicle (EV) Flow Cytometry Approach to Reveal EV Heterogeneity.* Angew Chem Int Ed Engl, 2018. **57**(48): p. 15675-15680.
25. Arraud, N., et al., *Fluorescence triggering: A general strategy for enumerating and phenotyping extracellular vesicles by flow cytometry.* Cytometry A, 2016. **89**(2): p. 184-95.
26. Morales-Kastresana, A., et al., *Labeling Extracellular Vesicles for Nanoscale Flow Cytometry.* Sci Rep, 2017. **7**(1): p. 1878.
27. Stoner, S.A., et al., *High sensitivity flow cytometry of membrane vesicles.* Cytometry A, 2016. **89**(2): p. 196-206.
28. Geeurickx, E., et al., *The generation and use of recombinant extracellular vesicles as biological reference material.* Nat Commun, 2019. **10**(1): p. 3288.
29. Van Deun, J., et al., *The impact of disparate isolation methods for extracellular vesicles on downstream RNA profiling.* J Extracell Vesicles, 2014. **3**.
30. Thery, C., et al., *Minimal information for studies of extracellular vesicles 2018 (MISEV2018): a position statement of the International Society for Extracellular Vesicles and update of the MISEV2014 guidelines.* J Extracell Vesicles, 2018. **7**(1): p. 1535750.
31. Enciso-Martinez, A., et al., *Synchronized Rayleigh and Raman scattering for the characterization of single optically trapped extracellular vesicles.* Nanomedicine, 2020. **24**: p. 102109.
32. Mastronarde, D.N. and S.R. Held, *Automated tilt series alignment and tomographic reconstruction in IMOD.* J Struct Biol, 2017. **197**(2): p. 102-113.
33. Welsh, J.A., et al., *MIFlowCyt-EV: a framework for standardized reporting of extracellular vesicle flow cytometry experiments.* J Extracell Vesicles, 2020. **9**(1): p. 1713526.
34. Welsh, J.A., et al., *FCMPASS Software Aids Extracellular Vesicle Light Scatter Standardization.* Cytometry A, 2020. **97**(6): p. 569-581.
35. Consortium, E.-T., et al., *EV-TRACK: transparent reporting and centralizing knowledge in extracellular vesicle research.* Nat Methods, 2017. **14**(3): p. 228-232.
36. Welsh, J.A., et al., *Extracellular Vesicle Flow Cytometry Analysis and Standardization.* Front Cell Dev Biol, 2017. **5**: p. 78.
37. Libregts, S., et al., *Flow cytometric analysis of extracellular vesicle subsets in plasma: impact of swarm by particles of non-interest.* J Thromb Haemost, 2018.
38. Groot Kormelink, T., et al., *Prerequisites for the analysis and sorting of extracellular vesicle subpopulations by high-resolution flow cytometry.* Cytometry A, 2016. **89**(2): p. 135-47.
39. Osteikoetxea, X., et al., *Differential detergent sensitivity of extracellular vesicle subpopulations.* Org Biomol Chem, 2015. **13**(38): p. 9775-82.
40. Busatto, S., et al., *Brain metastases-derived extracellular vesicles induce binding and aggregation of low-density lipoprotein.* J Nanobiotechnology, 2020. **18**(1): p. 162.
41. Simonsen, J.B., *Pitfalls associated with lipophilic fluorophore staining of extracellular vesicles for uptake studies.* J Extracell Vesicles, 2019. **8**(1): p. 1582237.

42. Arkesteijn, G.J.A., et al., *Improved Flow Cytometric Light Scatter Detection of Submicron-Sized Particles by Reduction of Optical Background Signals.* Cytometry A, 2020. **97**(6): p. 610-619.
43. Lozano-Andrés, E., et al., *Considerations for MESF-bead based assignment of absolute fluorescence values to nanoparticles and extracellular vesicles by flow cytometry.* bioRxiv, 2021: p. 2021.03.01.433358.
44. Lu, M. and O. Gursky, *Aggregation and fusion of low-density lipoproteins in vivo and in vitro.* Biomol Concepts, 2013. **4**(5): p. 501-18.
45. Ivanova, E.A., Y.V. Bobryshev, and A.N. Orekhov, *LDL electronegativity index: a potential novel index for predicting cardiovascular disease.* Vasc Health Risk Manag, 2015. **11**: p. 525-32.
46. Puzar Dominkus, P., et al., *PKH26 labeling of extracellular vesicles: Characterization and cellular internalization of contaminating PKH26 nanoparticles.* Biochim Biophys Acta Biomembr, 2018. **1860**(6): p. 1350-1361.

SUPPLEMENTARY INFORMATION

SUPPLEMENTARY MATERIAL & METHODS

Western blot analysis of EVs. Isolated EVs (1 µL or 4 µL) were resuspended in 3 µL PBS and 11 µL non-reducing SDS-PAGE sample buffer or 11 µL of non-reducing SDS-PAGE sample buffer, respectively. Samples were next separated on a 12.5% SDS-PAGE gel and transferred to a PVDF-membrane with a 0.45 mm pore size (Millipore, Amsterdam-Zuidoost, the Netherlands). Membranes were blocked for 1 hour using PBS containing 0.5% (w/v) fish gelatin (Sigma-Aldrich) and 0.1% Tween-20 and subsequently immunolabeled overnight at 4°C with primary antibody Rat anti-mouse CD9 (eBioscience, Thermo Fisher Scientific, Waltham, MA, USA; Clone KMC8, Lot #E028516, catalog #14-0091-85, 0.5 mg/ml, dilution 1:1000) or Rat anti-mouse CD63 (Biolegend, San Diego, CA, USA; Clone NVG-2, catalog #143902, dilution 1:500). After washing, membranes were incubated with a secondary antibody rabbit anti-rat PolyClonal conjugated to horseradish peroxidase (Jackson ImmunoResearch, Ely, Cambridgeshire, UK; 1:5000). Peroxidase was detected using Supersignal West Dura Extended Duration chemiluminscent substrate (Thermo Fisher Scientific). Imaging was performed using a ChemiDoc MP system and data was visualized using Image Lab Software v5.1 (Bio-Rad, Hercules, CA, USA).

Nanoparticle tracking analysis (NTA) of EVs. Size distribution and concentration of isolated EV were determined by measuring the rate of Brownian motion using a NanoSight LM10 system microscope (NanoSight Ltd, Amesbury, UK) equipped with a camera sCMOS and a 405 nm laser. An automatic pumping system was used for the injection of the sample. For each sample, 3 videos of 30 seconds were recorded and analysed with a detection threshold 3 and camera level 13. The measurements were performed and monitored at ambient temperature which did not exceed 25°C. Recorded videos were then analysed with NTA Software version 3.2. For optimal measurements, samples were diluted in PBS until particle concentration was within the dynamic range of NTA Software (between 3E8 and 5E9 particles/ml).

Fluorescence calibration. For calibration of the fluorescence axis, FITC MESF beads (custom made, lot MM2307#131-10; #131-8; #130-6; #130-5; 130-3, BD Biosciences, San Jose, CA) and PE MESF beads (Lot. No. 62981, BD Biosciences, San Jose, CA) were used according to the manufacturer's instructions. Calibration MESF beads were provided with assigned numbers of molecules of equivalent soluble fluorochrome (MESF) for each peak intensity. Briefly, each bead peak population was gated using FlowJo Version 10.5.0 and median fluorescence intensities (MFI) were obtained (Supplementary Figure 4). Next, FCMPASS Version v2.17 was used to perform a least-square linear regression analysis and generate the data displaying MESF calibrated axis.

Synchronous Rayleigh and Raman scattering. A Rayleigh-Raman spectrometer was used, which is based on a home-built Raman spectrometer integrated with the base of an upright optical microscope (Olympus BX41). For illuminating and trapping the particles, a single laser beam from a Coherent Innova 70C laser ($\boldsymbol{\lambda}_{exc}$=647.089 nm) was used. A cover glass corrected dry objective (Olympus, 40x, NA: 0.95) was used to collect the Rayleigh and Raman scattering, which was then separated in a homebuilt spectrometer and simultaneously detected with a single CCD camera (Andor Newton DU-970-BV). The average dispersion of the spectrometer was ~2.3 cm^{-1} (0.11 nm) wavenumber per pixel over the CCD camera surface with 1600 pixels along the dispersive axis and 200 pixels along the other axis. The laser power was measured underneath the objective and adjusted to 70 mW.

Calibration of the Rayleigh-Raman spectrometer. Both intensity and wavelength calibration were performed to convert the raw measured data from pixels vs relative counts to calibrated data in wavenumber (cm^{-1}) vs counts. The pixel-to-wave number conversion was performed by using the toluene spectrum and an argon-mercury lamp with narrow emission lines known with picometer accuracy. The intensity calibration was performed by acquiring a white light spectrum from a tungsten halogen light source (AvaLight-Hal; Avantes BV, Apeldoorn, The Netherlands) that resulted in the light detection efficiency per pixel for the entire setup. The offset of the detector was obtained from a measurement without any light falling onto the detector. To determine the background spectrum, the spectrum of the entire light path through the setup with the laser on, but without a sample, was acquired and subtracted from the measured data. All software was developed in-house with Matlab (2017b, MathWorks, USA).

Rayleigh-Raman data analysis. Rayleigh and Raman time traces were obtained by integrating the Rayleigh (-20 – 10 cm^{-1}) and lipid-protein Raman bands (2811 – 3023 cm^{-1}), respectively. The integrated Rayleigh and Raman values were concatenated and plotted against time to enable the selection of individual trapping events visualized as step-wise increases in the Rayleigh signal [1, 2]. These steps were manually segmented and their time intervals were used to obtain their corresponding Raman spectra. A Raman spectrum of a single particle was thereby acquired as the average Raman spectrum along the length of each segmented step. To remove the background contribution, e.g. water or soluble components, also present in the focal spot with each single trapped particle, the immediate previous segment to each step was segmented and its corresponding Raman spectrum was used for background subtraction using linear least squares fit. The mean Raman spectrum of each particle was interpolated to the same wavenumber axis and baseline correction and de-noising were performed on the full dataset using "Baseline Estimation And Denoising with Sparsity" [3]. Each Raman spectrum was then normalized to have a mean of zero and a standard deviation of one. Principal component analysis was performed in the Raman fingerprint spectral region (500 – 1800 cm^{-1}). All software was developed in-house in Matlab (2017, MathWorks, USA).

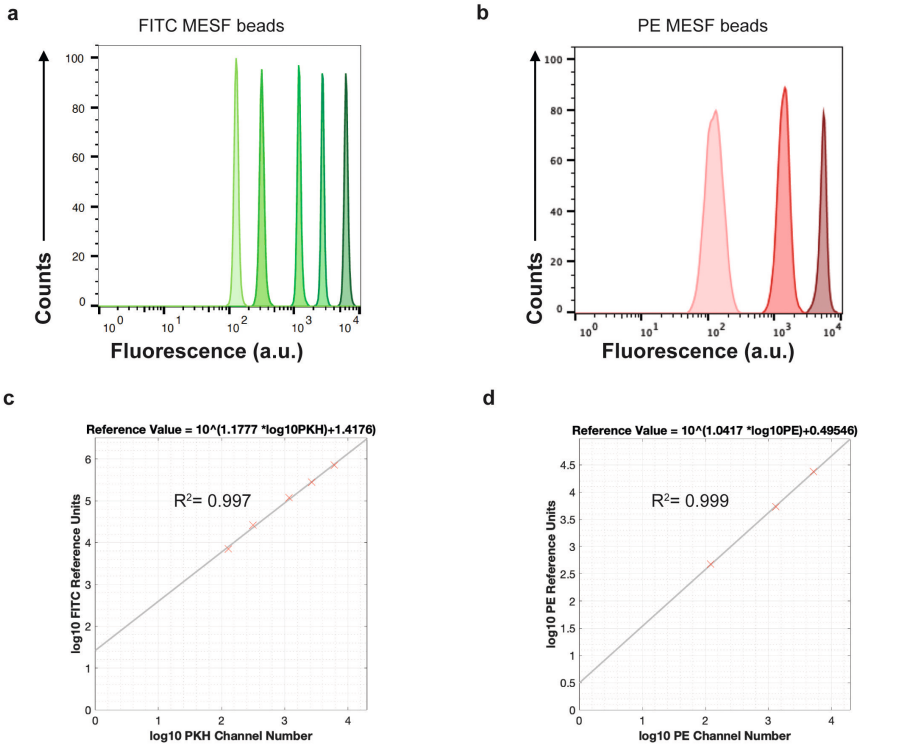

e

Peak	MFI	LogMFI	FITC MESF	LogFITC MESF
P1	129	2.1106	7094	3.8508
P2	317	2.5011	25910	4.4134
P3	1173	3.0693	118192	5.0725
P4	2684	3.4288	275288	5.4397
P5	6111	3.7861	715225	5.8544

f

Peak	MFI	LogMFI	PE MESF	LogPE MESF
P1	122	2.0863	474	2.6757
P2	1325	3.1222	5359	3.7290
P3	5186	3.7148	23843	4.3773

Supplementary Figure 1. Standardization of fluorescence intensities by using FITC and PE MESF calibration beads. (a) Histogram overlay of FITC-MESF beads and (b) PE-MESF beads. Axis is in arbitrary fluorescence units. (c) Relation between log10 fluorescence channel numbers and log10 FITC-MESF values or (d) PE-MESF values. (e) Characterization of the FITC-MESF beads and (f) PE-MESF beads. Shown are the respective peak numbers with their corresponding MFI as measured on the BD Influx, the log10 conversion thereof, the number of FITC-MESF or PE-MESF per bead and the log10 conversion thereof.

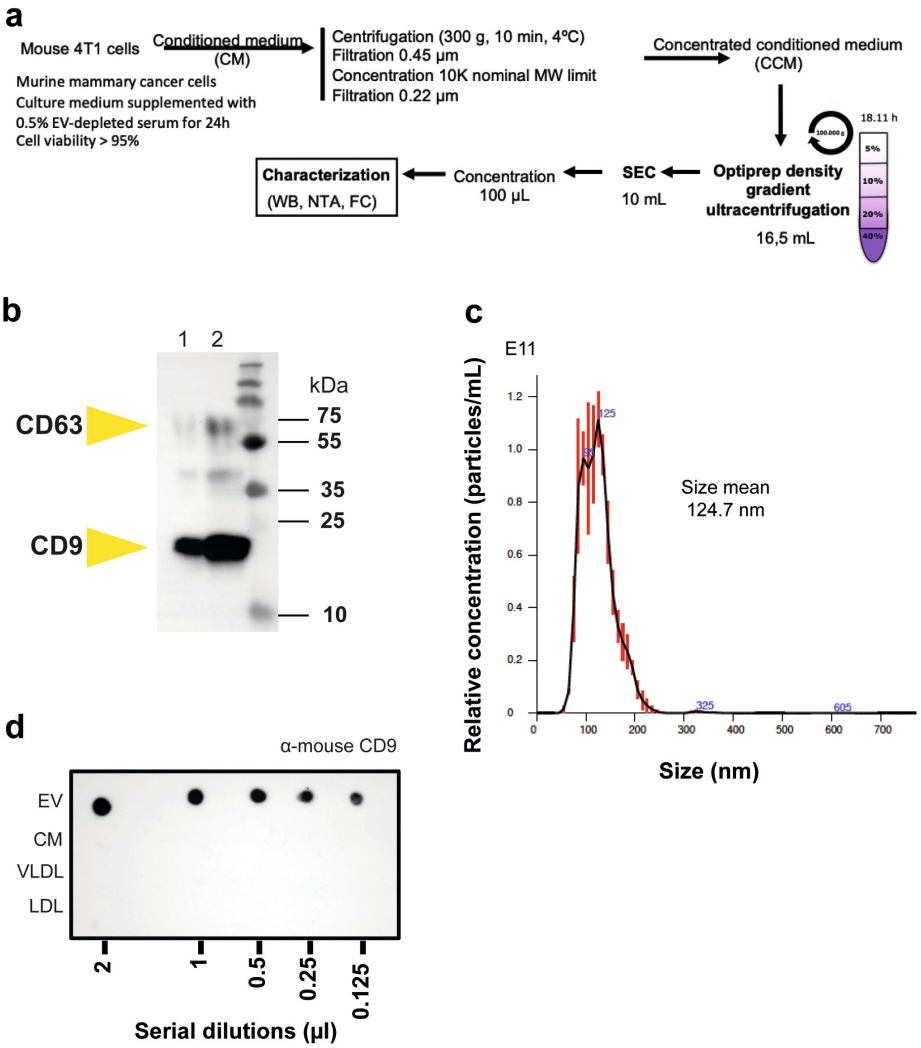

Supplementary Figure 2. Isolation, purification and characterization of mouse 4T1 EVs. (a) Schematic representation of mouse 4T1 EV isolation and purification methods. (b) Western blot analysis of purified EV. Samples were subjected to SDS-PAGE and detected by chemiluminescence using specific mAbs directed against mouse -CD9 (clone KMC8) and -CD63 (clone NVG-2). Lane 1 is a ¼ dilution from input in lane 2. (c) Nanoparticle tracking analysis (NTA) of purified EVs for size determination and quantification. (d) Side-by-side dot blot detection of mouse CD9 in mouse 4T1 EVs and commercial LPP samples.

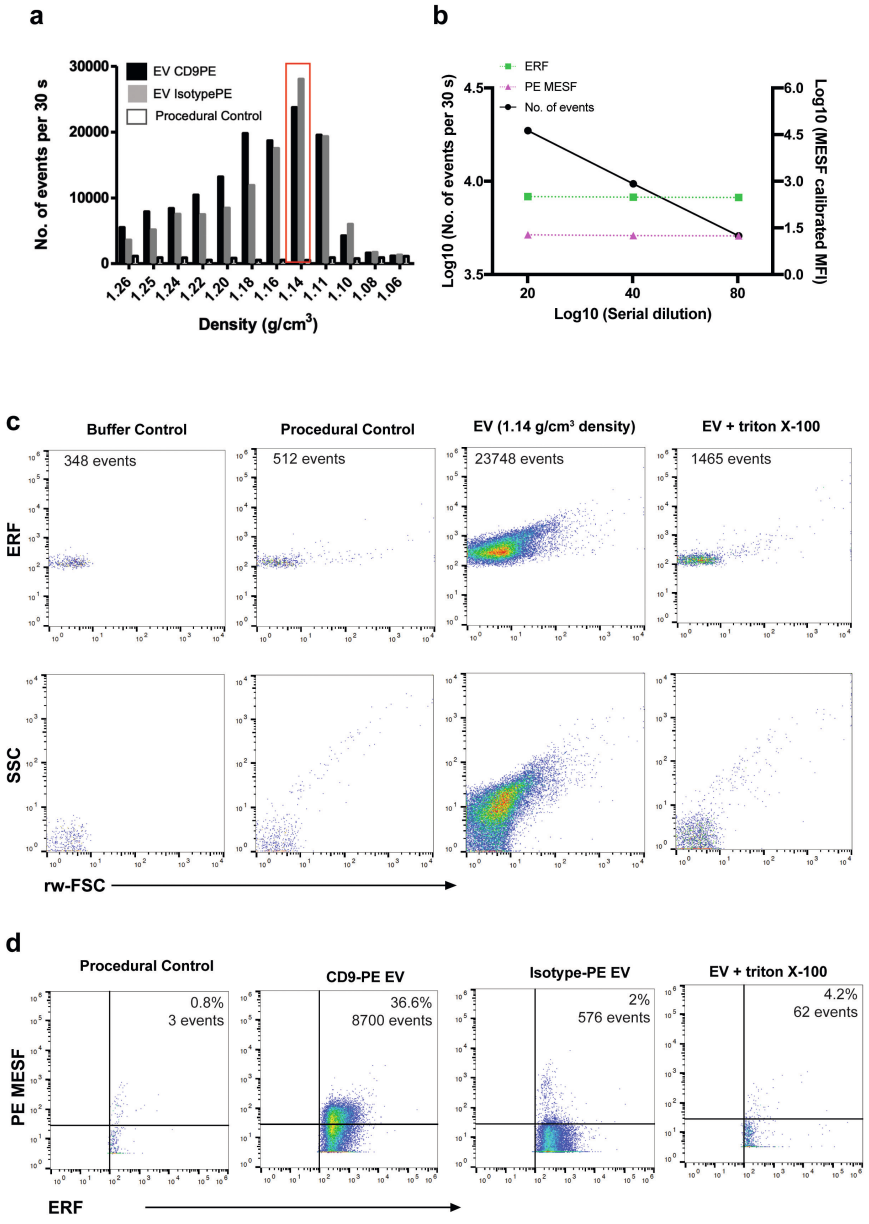

Supplementary Figure 3. Immunocharacterisation of mouse 4T1 EVs by high-resolution flow cytometry. (a) Bar graphs displaying the fractionation profile of stained EVs after sucrose density gradient floatation. The number of events in each density fraction is determined using time-based flow cytometric analysis (number of PKH67-positive events in 30 seconds). (b) Serial dilutions (1:20, 1:40, 1:80) of the fraction containing CD9 and PKH67 stained EV were analysed. Total number of events and MFI for FITC MESF and PE MESF are shown. (c) Dot plots of FITC MESF vs rw-FSC, SSC vs rw-FSC for experimental controls and the peak EV-fraction showing sensitivity of samples to detergent treatment (Triton X-100; final concentration of 0.1%). Respective total

number of events are shown in each plot. (d) Dot plots of PE MESF vs FITC MESF for relevant experimental controls and the peak EV-fraction.

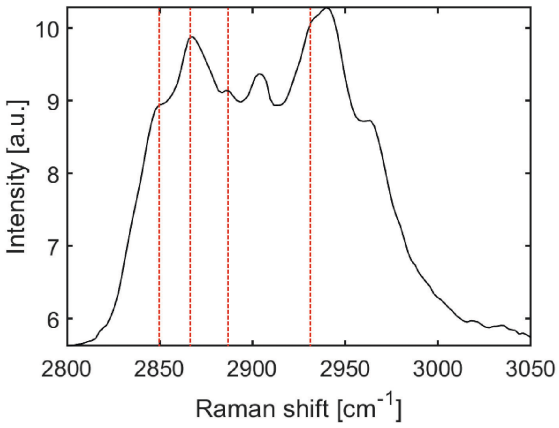

Supplementary Figure 4. High frequency region of the mean Raman spectrum of 4T1 EV. Red lines indicate Raman bands associated to cholesterol (2850, 2866, 2888 and 2932 cm-1).

Supplementary Table 1. Author Checklist: MIFlowCyt-Compliant Items.

Requirement	Please Include Requested Information
1.1. Purpose	Evaluate the influence of lipoprotein particles (LPP) for Extracellular Vesicle (EV) detection upon fluorescent threshold triggering by using the generic EV marker PKH67 upon fluorescence-based flow cytometry detection.
1.2. Keywords	extracellular vesicles, lipoprotein particles, flow cytometry, plasma, biomarker
1.3. Experiment variables	Different types of lipoprotein particles (Chylomicrons, VLDL and LDL)
1.4. Organization name and address	Department of Biochemistry & Cell Biology Faculty of Veterinary Sciences Utrecht University Yalelaan 2, 3584 CM Utrecht, The Netherlands
1.5. Primary contact name and email address	Prof. Dr. M.H.M. Wauben M.H.M.Wauben@uu.nl
1.6. Date or time period of experiment	March 2018 – September 2019

Supplementary Table 1. Continued

Requirement	Please Include Requested Information
1.7. Conclusions	LPP can be stained with PKH67 and detected upon fluorescence-based flow cytometry. The fluorescence and light scatter signals from stained LPP are in range to those of isolated and purified EV. Furthermore, when LPP were spiked-in presence of EV, the staining and detection of EV was affected. The detection of an EV-marker CD9 was influenced in presence of LPP, leading to an underestimation of the number of CD9+ EV.
1.8. Quality control measures	Procedural control for fluorescent stainings Matched isotype PE control Serial dilutions Detergent treatment control
2.1.1.1. (2.1.2.1., 2.1.3.1.) Sample description	EV isolated from 4T1 cell culture supernatant, Commercially available Lipoprotein Particles
2.1.1.2. Biological sample source description	Cell culture supernatant from the murine mammary carcinoma cell line 4T1 (ATCC, Manassas, VA) was used to isolate EV. Purified human lipoprotein particles: human chylomicrons (Catalog no. 7285-1000, Biovision Incorporated) human very-low-density (Catalog no. 437647-5MG, Merck Millipore) human low-density (Catalog no. LP2-2MG, Merck Millipore)
2.1.1.3. Biological sample source organism description	Mouse and human
2.1.2.2. Environmental sample location	
2.3. Sample treatment description	For detergent treatment control samples were treated with 0.1% (v/v) triton X-100 (SERVA Electrophoresis GmbH, Heidelberg, Germany) final concentration for 30 seconds before reanalysis.
2.4. Fluorescence reagent(s) description	PKH67 (Sigma-Aldrich) Rat anti-mouse CD9PE Clone: KMC8, IgG2a, k (Lot No. 7268877, Becton Dickinson Biosciences) Isotype Rat IgG2a, k PE (Lot. No. 8096525, Becton Dickinson Biosciences)
3.1. Instrument manufacturer	Becton Dickinson
3.2. Instrument model	BD Influx™ optimized instrument for detection of sub-micron sized particles as described previously.

Supplementary Table 1. Continued

Requirement	Please Include Requested Information
3.3. Instrument configuration and settings	BD Influx optimized to measure small particles. All configuration details can be found in van der Vlist, E. J., Nolte-'t Hoen, E. N., Stoorvogel, W., Arkesteijn, G. J., and Wauben, M. H. (2012) Fluorescent labeling of nano-sized vesicles released by cells and subsequent quantitative and qualitative analysis by high-resolution flow cytometry. Nat Protoc 7, 1311-1326. Briefly, samples were measured at a constant flow rate for 30 seconds using a fluorescence threshold on the 488 nm laser. Threshold level was set to detect 10-20 events per second when measuring a buffer control. PE signals obtained upon excitation with the 561 nm laser were collected in the 585/42 band pass filter.
4.1. List-mode data files	Are available upon request.
4.2. Compensation description	No compensation was required due to instrument configuration.
4.3. Data transformation details	No data transformation was applied.
4.4.1. Gate description	Gates were applied based on the controls or the matched isotype control for the specific staining with CD9 antibody (shown in Supplementary Material & Methods).
4.4.2. Gate statistics	The number of total events recorded in 30 seconds measurements are shown in the dot plots without any background correction. GeoMean of PE of the total number or gated events are shown and respectively described.
4.4.3. Gate boundaries	Images of the ungated and gated plots can be found in figures and supplementary data.

Supplementary Table 2. MIFlowCyt-EV framework.

1.1 Preanalytical variables conforming to MISEV guidelines	Yes, all relevant data has been submitted to EV-TRACK for transparent reporting and centralizing knowledge in extracellular vesicle research (EV-TRACK ID: EV190078).
1.2 Experimental design according to MIFlowCyt guidelines	Yes, MIFlowCyt checklist can be found as part of the supporting information of this manuscript.
2.1 Sample staining details	Yes, described in Materials and Methods.
2.2 Sample washing details	Yes, described in Materials and Methods.
2.3 Sample dilution details	Yes, described in Materials and Methods.
3.1 Buffer-only controls	Yes, relevant buffer controls were measure and are shown.
3.2 Buffer with reagent controls	Yes, see Figure S2c and S2d.
3.3 Unstained controls	N/A
3.4 Isotype controls	Yes, see Figure S2d.
3.5 Single-stained controls	N/A
3.6 Procedural controls	Yes, see Figure S2c and d.
3.7 Serial dilutions	Yes, serial dilutions were performed in previous characterization experiments to determine the ideal dilution used in this study. See Figure S2b.
3.8 Detergent-treated controls	Yes, sensitivity to triton X-100 was determined in previous characterization experiments. See Figure S2 c and d.
4.1 Trigger channel(s) and threshold(s)	Yes, all relevant details can be found in Materials and Methods.
4.2 Flow rate / volumetric quantification	Yes, low flow rate was kept constant and is described in Materials and Methods.
4.3 Fluorescence calibration	Yes
4.4 Scatter calibration	N/A
5.1 EV diameter/surface area/ volume approximation	N/A
5.2 EV refractive index approximation	N/A
5.3 EV epitope number approximation	N/A
6.1 Completion of MIFlowCyt checklist	Yes, see Table S1
6.2 Calibrated channel detection range	100 FITC MESF
6.3 EV number/concentration	Yes, see Figure 1.
6.4 EV brightness	Yes, reported in ERF or MESF, see Figure 4d.
7.1 Sharing of data to a public repository	Yes, all experimental details about the biological sample preparation can be found in EV-TRACK. All data files are available upon request

REFERENCES

1. Enciso-Martinez, A., et al., *Label-free identification and chemical characterisation of single extracellular vesicles and lipoproteins by synchronous Rayleigh and Raman scattering.* J Extracell Vesicles, 2020. **9**(1): p. 1730134.
2. Enciso-Martinez, A., et al., *Synchronized Rayleigh and Raman scattering for the characterization of single optically trapped extracellular vesicles.* Nanomedicine, 2020. **24**: p. 102109.
3. Ning, X., I.W. Selesnick, and L. Duval, *Chromatogram baseline estimation and denoising using sparsity (BEADS).* Chemometrics and Intelligent Laboratory Systems, 2014. **139**: p. 156-167.

“Embrace uncertainty.
Some of the most beautiful chapters in our lives won´t have a title until much later.”

Bob Goff

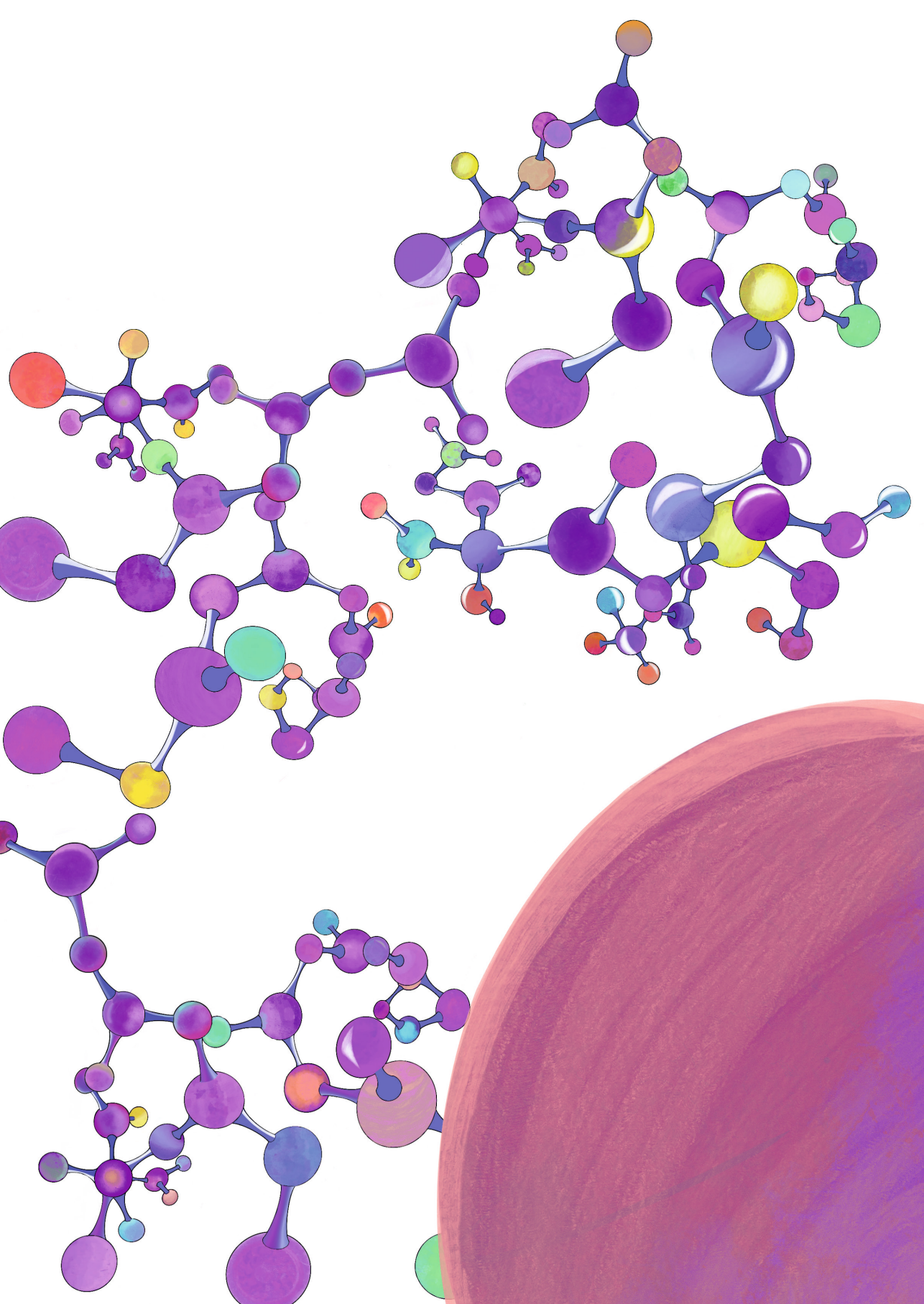

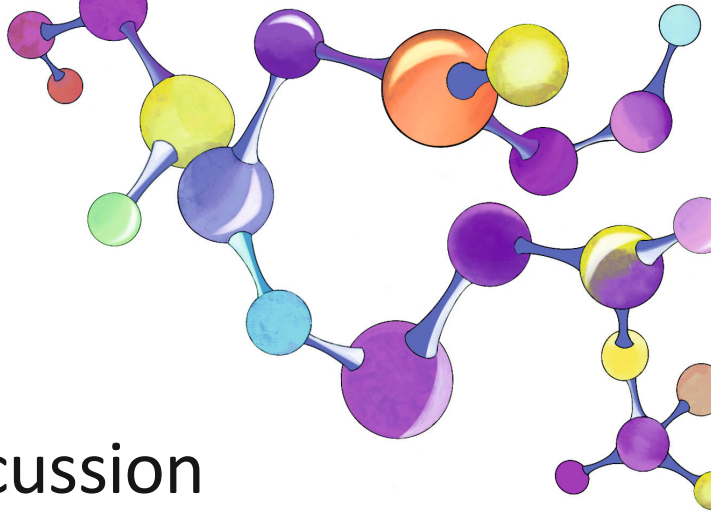

CHAPTER 7

General discussion

Estefanía Lozano-Andrés [1]

Division of Cell Biology, Metabolism & Cancer, Department of Biomolecular Health Sciences,
Faculty of Veterinary Medicine, Utrecht University, Utrecht, The Netherlands

This thesis deals with the currently existing hurdles that need to be taken for the reliable exploitation of EVs for biomarker profiling using flow cytometry. In the exponentially growing field of EV research, concerns have been raised about robustness and reproducibility. However, our understanding of EV biology is still evolving, together with the development and optimization of the technological tools needed to unveil EV complexity. Overcoming the hurdles in single EV-based analysis can aid to develop useful tools to continue the advancement of the field towards a successful clinical translation.

7.1. DEVELOPMENT OF SUITABLE REFERENCE MATERIALS FOR EV RESEARCH

Reference materials are important for method development, quality control and comparison of results across laboratories. The lack of suitable RM for EVs poses a significant hurdle to validate isolation and characterization methods [1]. In chapter 2 of this thesis, we designed a RM that shares EV biophysical properties, such as size distribution and RI. By modifying synthetic nanovesicles (niosomes) and decorating them with EV signature markers on the surface (i.e. CD9, CD63, CD81 tetraspanins), we were able to develop and characterize a novel RM that is compatible with a variety of bulk-based and single particle detection techniques. This RM is highly adaptable, as any biotinylated protein can be functionalized to the surface of the niosomes. In addition, antigen density can be modified by varying the amount of streptavidin that is present in the nanovesicles. Furthermore, the composition and properties of the niosomes themselves can be changed. Thus, different types of decorated nanovesicles can be re-designed for each specific purpose. Another interesting feature of this RM is the ability to use non-fluorescent and fluorescent niosomes, which can be exploited for different purposes, such as negative or positive controls for fluorescence-based detection. Because this RM is heterogeneous in size distribution and morphology, characterization by single particle detection techniques, such as NTA, cryo-EM or high-sensitivity flow cytometry, revealed signals that can resemble those from biological EVs, including the level of tetraspanin expression. In addition, a lower and different density was observed for the synthetic decorated nanovesicles when subjected to sucrose DGU compared to biological EVs, which can be exploited to separate RM from biological EVs during spike-in experiments using for example complex biofluids. Importantly, another peer-reviewed study has demonstrated the use of this RM in immunoassays, allowing for data normalization [2]. Complementary to the synthetic niosomes, other research groups have generated biological RM that aid in sample characterization and the optimization of detection settings [3, 4]. Although the RM presented in chapter 2 and other studies have been extensively characterized and proved helpful, the validation across laboratories is still lacking. Such follow-up studies would reinforce the value of these RM, while endorsing their implementation through standard operating procedures. Finally, the prospective use of RM will benefit clinical translation of EVs for biomarker profiling, so as to certify procedures and normalize data. As it has been pointed out by other peer-reviewed pub-

lications, few liquid biopsy tests are successfully translated into a pre-clinical stage [5]. The challenges reside in the low reproducibility, high impact of pre-analytical variables and the technological disparities [5]. New-generation developments would benefit from well-defined RM to identify sources of variation within clinical samples and control for reproducibility within isolation and detection methods.

7.2. ADVANCEMENT OF HIGH SENSITIVITY FLOW CYTOMETRY FOR THE DETECTION OF SINGLE EVS

Flow cytometry has earned its place at the core of many clinical laboratories and hospitals, enabling the diagnosis and prognosis of neoplastic and immunological diseases, among others [6, 7]. However, the reproducibility crisis that affects biomedical fields is raising questions about the robustness of scientific results [8], and FCM is not an exception. Guidelines, such as the minimum information about a flow cytometry experiment (MIFlowCyt), standards and validation protocols have been developed to deal with these issues [9-11]. However, the use of high resolution FCM (hFCM) for EV biomarker analysis entails particular challenges that are not specifically addressed in the available literature, including MIFlowCyt. Chapters 3, 4 and 5 of this thesis are dedicated to tackle current challenges in hFCM of EVs.

Reproducibility is key for clinical translation of any biological study. Therefore, to avoid an increment in the number of studies using unique isolation protocols [12], the use of guidelines and reporting tools is re-enforced [13]. Since the first publication of the MISEV guidelines in 2014, updates and community driven initiatives, such as the knowledge base EV-TRACK, have become available and gained a central place to ensure transparent reporting of sample preparation and analysis details [13, 14] [15]. The reporting framework MIFlowCyt-EV (Chapter 3), published as an ISEV position paper, is a product of the ISEV-ISAC-ISTH EV-Flow cytometry workgroup and aims to assist researchers into important aspects of experimental design, controls and technical settings that impact the interpretation of EV flow cytometry results. As a companion paper of MIFlowCyt-EV, the EV-Flow cytometry workgroup published a detailed compendium covering basic and specific aspects of hFCM [15]. Acceptance, dissemination and implementation of these guidelines and reporting tools will avoid ambiguity and ensure a body of literature with consistent and robust EV data. Considering the growing number of such initiatives, their implementation into centralized systems will guarantee successful utilization and maximize its positive impact.

As recommended in chapter 3, fluorescence calibration aids to compare data in standardized units. The method was developed for cell FCM and makes use of calibrators to which a MESF value is assigned. Thus, available calibrators are designed for cell measurements, whose signals are generally much brighter than those from EVs. Chapter 4 shows the results from an interdisciplinary study which we initiated between industry

partners (BD Biosciences, nanoFCM), a governmental agency (NIST) and academic institutions (Xiamen University, Utrecht University) to provide insights into the utilization of MESF-based fluorescence calibration for EVs. Using different calibrator sets showed an acceptable precision, making it possible to compare results across three different flow cytometers used in this study (BD Influx™, CytoFLEX LX™ and SORP BD FACSCelesta™), which is in line with another peer-reviewed article [16].

However, when we evaluated the accuracy of the method using these calibrator sets for silica nanoparticles containing six different fluorescent populations, we observed a tendency to increased variations into the dimmer populations (from ~27% to 76%). In addition, to provide insight into the use of this method for biological EVs, we analyzed the level of generic fluorescent EV staining with CFSE and the detection of the CD9 transmembrane protein on tumor derived EVs. CD9 has been proposed as a potential marker for biomarker profiling, as subpopulations of EVs carrying the CD9 molecule in prostate and breast cancer patients have been shown to hold clinical relevance for monitoring of the severity of disease (e.g. metastasis) and to decipher the phenotyping of subpopulations that co-express other cancer-related makers [17, 18]. In chapter 4, we showed that on tumor derived EVs, calibrated values varied ~79% and ~157% for generic CFSE ERF and for specific CD9 expression, respectively, depending on the two calibrator sets used for each parameter. Since fluorescence calibration using the available MESF beads designed for cell FCM relies on extrapolation, and assigned fluorescence values of calibrators have intrinsic uncertainties, variations in absolute fluorescence values assigned to dim fluorescent EVs are expected when different calibration bead sets are used. Our results revealed how undesired sources of variation (e.g. relative to the materials used) can impact the utility of EV calibration methods. To ensure robustness, the use of the same calibration bead sets is preferred in multi-center studies. Ideally, future research will build further on rigorous characterization of the calibration materials with defined precision and accuracy that allow to express intensity levels of an EV bearing certain biomarkers under healthy or disease conditions. These reference values should be expressed and quantified in standardized units, such as MESF, allowing to monitor patient samples and provide relevant clinical information, as has been done for cell FCM [19, 20].

As such, our observations concerning the accuracy of calibration presented in Chapter 4 can open up roads for the development and validation of calibration materials. At the same time, it highlights the importance of adequate reporting of both materials and methods used, as previously described in chapter 3. It would be very valuable that a level of uncertainty to each given value for a calibrator is also quantified and reported by manufactures. While researchers should implement fluorescence calibration, the use of well characterized calibration materials will ultimately facilitate EV data comparison across instruments and laboratories.

Technical advancements made in the last ten years and utilizing conventional flow cytometers as a groundwork have allowed improved detection of small particles and EVs [21]. However, limitations remain in the technology that is able to detect the full range of EVs. Scattered light is a valuable parameter that can confirm the presence of particles and also reveals information on physical properties such as shape and composition to distinguish between subpopulations. But since EVs scatter very dim signals, they end up overlapping with the background. As there are multiple sources of background when measuring EVs by hFCM, it is relevant to discriminate these sources and aim to reduce them, improving the sensitivity of EV detection. In chapter 5, we present an effective strategy to reduce optical background signals. By using a high-end and open-architecture BD Influx™, we tested a matrix of differently sized hardware components, including the pinhole and the obscuration bar. These two elements are essential for the collection of light scattering signals of interest into the reduced wide-angle FSC (rw-FSC) detector. We found that there was an optimal combination of these two components that reduced the detection of background events in buffer controls. As a result of the lower background, the light scatter-based trigger threshold level could be efficiently reduced. In comparison with a fluorescence-based trigger threshold, known to have lower background interference, we obtained similar detection sensitivities when measuring biological EVs stained with CFSE with both trigger threshold strategies. Few studies aim to use light scattering signals other than those collected by the SSC into an orthogonal direction. However, research studies of our own group have shown that relevant biological information is uniquely encrypted into rw-FSC signals [22]. Furthermore, the detection of light scattering signals collected by multiple detectors with different angles can further enhance the accuracy of estimates using advanced calibration methods that assess biophysical EV properties such as size, RI and composition [23], which puts in the spotlight the added value of investing in more than one sole light scatter parameter for EV hFCM detection. Recent peer-reviewed studies also addressed the effect of distinct diameters of pinhole and obscuration bars into both the forward and orthogonal direction using a conventional flow cytometer, finding analogous results to those presented in chapter 5 of this thesis [24]. Therefore, these technical adaptations provide useful lessons to be implemented into newer generations of instruments. Such instruments, with dedicated and improved detectors could aid to analyze the full range of light scattering signals from EVs [25].

7.3. INVESTIGATING THE ANALYSIS OF SINGLE EVS IN PRESENCE OF LIPOPROTEIN PARTICLES

In addition to the technological challenges, the biological matrix in which EVs reside presents a complex landscape for single EV detection. In chapter 6 we explored the detection of EVs in the presence of different types of lipoprotein particles (LPPs), which are known to outnumber EVs in plasma. Because LPPs and EVs share biophysical properties, such as size and density, it is extremely difficult to obtain pure EV preparations that

are completely devoid of LPPs. While the combination of different isolation methods has been proved useful, it is also very laborious and often requires for a large sample input. These prerequisites can restrict clinical translation, as patient material is often limited. Thus, to exploit circulating EVs in plasma for LB biomarker profiling, we need to investigate how co-isolated LPPs might affect single EV analysis.

To address this complex scenario, we acquired and characterized purified preparations of CMs, VLDL and LDL particles. After mixing purified tumor derived EVs with the LPPs, we observed the formation of EV-LPP complexes by using a combination of (1) unsupervised label-free synchronous Rayleigh and Raman scattering analysis of optically trapped particles and (2) supervised fluorescence-based high resolution single particle flow cytometric analysis. These two techniques complement each other by collecting information on the label-free signature of single trapped particles and characterizing the light scatter and fluorescence profiles of single particles in a suspension. Under the conditions described in chapter 6, we found that LDL particles are more prone to interact with tumor derived EVs than other LPP types such as CMs. Furthermore, the EV-LPP complexes can be formed under physiological conditions, in a label-free and minimally process environment. These EV-LPP complexes influence the analysis of EVs at the single particle level, showing distinct signature and profiles compared to those from the purified LPPs. Importantly, we found that the detection of an EV marker, the tetraspanin CD9, is influenced in presence of the LPPs, which has implications for biomarker profiling in circulating EVs.

A recent landmark study has demonstrated that a protein corona is formed around EVs in plasma [26]. Interestingly, the composition of the protein corona described in this study included apolipoproteins, which are common markers present on LPPs. Hence, these findings are in agreement with the results presented in chapter 6, suggesting the formation of EV-LPP complexes. Another interesting peer-reviewed study has described multiple functional roles assigned to the EV corona, including immunomodulation, angiogenesis and skin regeneration [27]. Therefore, these observations together with the results presented in chapter 6, may add a newer level of complexity to understand EV biology. Future studies might investigate the nature of these EV-LPP interactions in natural surroundings. Whether these interactions are specific (e.g. receptor mediated) or non-specific (e.g. attractive forces) might further advance the exploitation of plasma EVs as disease biomarkers. In addition, our findings are of interest for EVs obtained from other LPP containing sources different than plasma, such as cell culture medium, where these interactions could take place [28]. Another important study has shown how cancer EVs derived from brain metastases cells can induce the aggregation of LDL particles, accelerating immunomodulation [29]. While it is known that LDL particles have a role in the modulation of the immune response and can be used as circulating biomarkers to aid in the diagnosis of atherosclerotic and cardiovascular diseases [30, 31], not much attention has been paid to the potentially combined action of EV-LDL complexes.

Therefore, it is possible that the complexes of EV-LDL have emerging functions in health and disease than those from EV or LDL alone. Besides, it can also be speculated that the function of EVs as communication messengers towards the inner lining of blood vessels is hindered by binding to LDL particles. Thus, further investigations are needed to elucidate the potential roles of EVs upon interaction with LDL particles.

Thus, the results presented in chapter 6 may shed light into the interplay between EVs and other particles in the circulation, opening up new roads for the development of liquid biopsy EV biomarker profiling.

7.4. OUTLOOK AND FUTURE PERSPECTIVES

Overall, the field of high sensitivity FCM has improved with optimization of conventional flow cytometers that became more sensitive, specialized platforms with new capabilities and instruments dedicated to the nanometric scale becoming available [32, 33]. Other exciting technological developments include spectral flow cytometry, which might also find the way into advancing EV research in the coming years [34]. In response to these emerging specialized instruments, a next logical step would be to define the performance of these instruments while comparing their capabilities. The MIFlowCyt-EV framework presented in Chapter 3 can be used as a core element for future studies, where appropriate controls and reporting standards should be included and discussed. On top of this, the access to qualified RM will help to create awareness on the pitfalls and limitations of the technology [4]. Furthermore, solid developments are ongoing to estimate EV sizes, by assuming an EV effective refractive index and combining it with Mie theory modeling [23, 35]. Challenges remain however to assign an universal refractive index value to heterogeneous core-shell particles such as EVs, which is currently hardly attainable despite of some efforts [36]. Thus, critical data interpretation and reporting should remain a priority until these are extensively validated [37, 38]. Likewise, the combination of orthogonal detection methods that have been shown to complement each other represents an unique strength to reveal the complex interactions between EVs and other particles, as well as to validate EV-based biomarkers [39]. Though the methodology that enables the characterization of EVs is still evolving, the potential is enormous and well-worth investing in [40].

I hope that the advancement of the technology will be accompanied by an increase into reproducibility and standardization. Technological innovations will surely help to solve the biomedical puzzles that exist in our world. By combining efforts and building up bridges and strong networks I am confident that the promise of EV biomarker profiling can become a reality.

REFERENCES

1. Valkonen, S., et al., *Biological reference materials for extracellular vesicle studies.* Eur J Pharm Sci, 2017. **98**: p. 4-16.
2. Garcia-Manrique, P., et al., *Selected Tetraspanins Functionalized Niosomes as Potential Standards for Exosome Immunoassays.* Nanomaterials (Basel), 2020. **10**(5).
3. Geeurickx, E., et al., *The generation and use of recombinant extracellular vesicles as biological reference material.* Nat Commun, 2019. **10**(1): p. 3288.
4. Gorgens, A., et al., *Optimisation of imaging flow cytometry for the analysis of single extracellular vesicles by using fluorescence-tagged vesicles as biological reference material.* J Extracell Vesicles, 2019. **8**(1): p. 1587567.
5. Geeurickx, E. and A. Hendrix, *Targets, pitfalls and reference materials for liquid biopsy tests in cancer diagnostics.* Mol Aspects Med, 2020. **72**: p. 100828.
6. van de Loosdrecht, A.A., et al., *Clinical application of flow cytometry in patients with unexplained cytopenia and suspected myelodysplastic syndrome: A report of the European LeukemiaNet International MDS-Flow Cytometry Working Group.* Cytometry B Clin Cytom, 2023. **104**(1): p. 77-86.
7. Monneret, G., et al., *How Clinical Flow Cytometry Rebooted Sepsis Immunology.* Cytometry A, 2019. **95**(4): p. 431-441.
8. Plant, A.L., et al., *Improved reproducibility by assuring confidence in measurements in biomedical research.* Nat Methods, 2014. **11**(9): p. 895-8.
9. Cossarizza, A., et al., *Guidelines for the use of flow cytometry and cell sorting in immunological studies (third edition).* Eur J Immunol, 2021. **51**(12): p. 2708-3145.
10. Lee, J.A., et al., *MIFlowCyt: the minimum information about a Flow Cytometry Experiment.* Cytometry A, 2008. **73**(10): p. 926-30.
11. Selliah, N., et al., *Flow Cytometry Method Validation Protocols.* Curr Protoc Cytom, 2019. **87**(1): p. e53.
12. Van Deun, J., et al., *The impact of disparate isolation methods for extracellular vesicles on downstream RNA profiling.* J Extracell Vesicles, 2014. **3**.
13. Thery, C., et al., *Minimal information for studies of extracellular vesicles 2018 (MISEV2018): a position statement of the International Society for Extracellular Vesicles and update of the MISEV2014 guidelines.* J Extracell Vesicles, 2018. **7**(1): p. 1535750.
14. Witwer, K.W., et al., *Updating the MISEV minimal requirements for extracellular vesicle studies: building bridges to reproducibility.* J Extracell Vesicles, 2017. **6**(1): p. 1396823.
15. Welsh, J.A., et al., *A compendium of single extracellular vesicle flow cytometry.* J Extracell Vesicles, 2023. **12**(2): p. e12299.
16. Welsh, J.A., J.C. Jones, and V.A. Tang, *Fluorescence and Light Scatter Calibration Allow Comparisons of Small Particle Data in Standard Units across Different Flow Cytometry Platforms and Detector Settings.* Cytometry A, 2020. **97**(6): p. 592-601.
17. Soekmadji, C., et al., *Extracellular vesicles for personalized therapy decision support in advanced metastatic cancers and its potential impact for prostate cancer.* Prostate, 2017. **77**(14): p. 1416-1423.
18. Ekstrom, K., et al., *Characterization of surface markers on extracellular vesicles isolated from lymphatic exudate from patients with breast cancer.* BMC Cancer, 2022. **22**(1): p. 50.

19. Peng, B., et al., *Standardization of neutrophil CD64 and monocyte HLA-DR measurement and its application in immune monitoring in kidney transplantation.* Front Immunol, 2022. **13**: p. 1063957.
20. Coustan-Smith, E., et al., *Clinical relevance of BCL-2 overexpression in childhood acute lymphoblastic leukemia.* Blood, 1996. **87**(3): p. 1140-6.
21. Nolan, J.P., *Flow Cytometry of Extracellular Vesicles: Potential, Pitfalls, and Prospects.* Curr Protoc Cytom, 2015. **73**: p. 13 14 1-16.
22. van der Grein, S.G., et al., *Picornavirus infection induces temporal release of multiple extracellular vesicle subsets that differ in molecular composition and infectious potential.* PLoS Pathog, 2019. **15**(2): p. e1007594.
23. Welsh, J.A., et al., *FCMPASS Software Aids Extracellular Vesicle Light Scatter Standardization.* Cytometry A, 2020. **97**(6): p. 569-581.
24. de Rond, L., et al., *A Systematic Approach to Improve Scatter Sensitivity of a Flow Cytometer for Detection of Extracellular Vesicles.* Cytometry A, 2020.
25. Gorgens, A. and J.P. Nolan, *Aiming to Compare Apples to Apples: Analysis of Extracellular Vesicles and Other Nanosized Particles by Flow Cytometry.* Cytometry A, 2020. **97**(6): p. 566-568.
26. Toth, E.A., et al., *Formation of a protein corona on the surface of extracellular vesicles in blood plasma.* J Extracell Vesicles, 2021. **10**(11): p. e12140.
27. Wolf, M., et al., *A functional corona around extracellular vesicles enhances angiogenesis, skin regeneration and immunomodulation.* J Extracell Vesicles, 2022. **11**(4): p. e12207.
28. Busatto, S., et al., *Considerations for extracellular vesicle and lipoprotein interactions in cell culture assays.* J Extracell Vesicles, 2022. **11**(4): p. e12202.
29. Busatto, S., et al., *Brain metastases-derived extracellular vesicles induce binding and aggregation of low-density lipoprotein.* J Nanobiotechnology, 2020. **18**(1): p. 162.
30. Rhoads, J.P. and A.S. Major, *How Oxidized Low-Density Lipoprotein Activates Inflammatory Responses.* Crit Rev Immunol, 2018. **38**(4): p. 333-342.
31. Ishigaki, Y., Y. Oka, and H. Katagiri, *Circulating oxidized LDL: a biomarker and a pathogenic factor.* Curr Opin Lipidol, 2009. **20**(5): p. 363-9.
32. van der Vlist, E.J., et al., *Fluorescent labeling of nano-sized vesicles released by cells and subsequent quantitative and qualitative analysis by high-resolution flow cytometry.* Nat Protoc, 2012. **7**(7): p. 1311-26.
33. Zhang, W., et al., *Light-Scattering Sizing of Single Submicron Particles by High-Sensitivity Flow Cytometry.* Anal Chem, 2018. **90**(21): p. 12768-12775.
34. Nolan, J.P., *The evolution of spectral flow cytometry.* Cytometry A, 2022. **101**(10): p. 812-817.
35. de Rond, L., et al., *Deriving Extracellular Vesicle Size From Scatter Intensities Measured by Flow Cytometry.* Curr Protoc Cytom, 2018. **86**(1): p. e43.
36. Gardiner, C., et al., *Measurement of refractive index by nanoparticle tracking analysis reveals heterogeneity in extracellular vesicles.* J Extracell Vesicles, 2014. **3**: p. 25361.
37. Welsh, J.A., et al., *MIFlowCyt-EV: a framework for standardized reporting of extracellular vesicle flow cytometry experiments.* J Extracell Vesicles, 2020. **9**(1): p. 1713526.
38. Welsh, J.A., et al., *Extracellular Vesicle Flow Cytometry Analysis and Standardization.* Front Cell Dev Biol, 2017. **5**: p. 78.
39. Arab, T., et al., *Characterization of extracellular vesicles and synthetic nanoparticles with four orthogonal single-particle analysis platforms.* J Extracell Vesicles, 2021. **10**(6): p. e12079.
40. Lone, S.N., et al., *Liquid biopsy: a step closer to transform diagnosis, prognosis and future of cancer treatments.* Mol Cancer, 2022. **21**(1): p. 79.

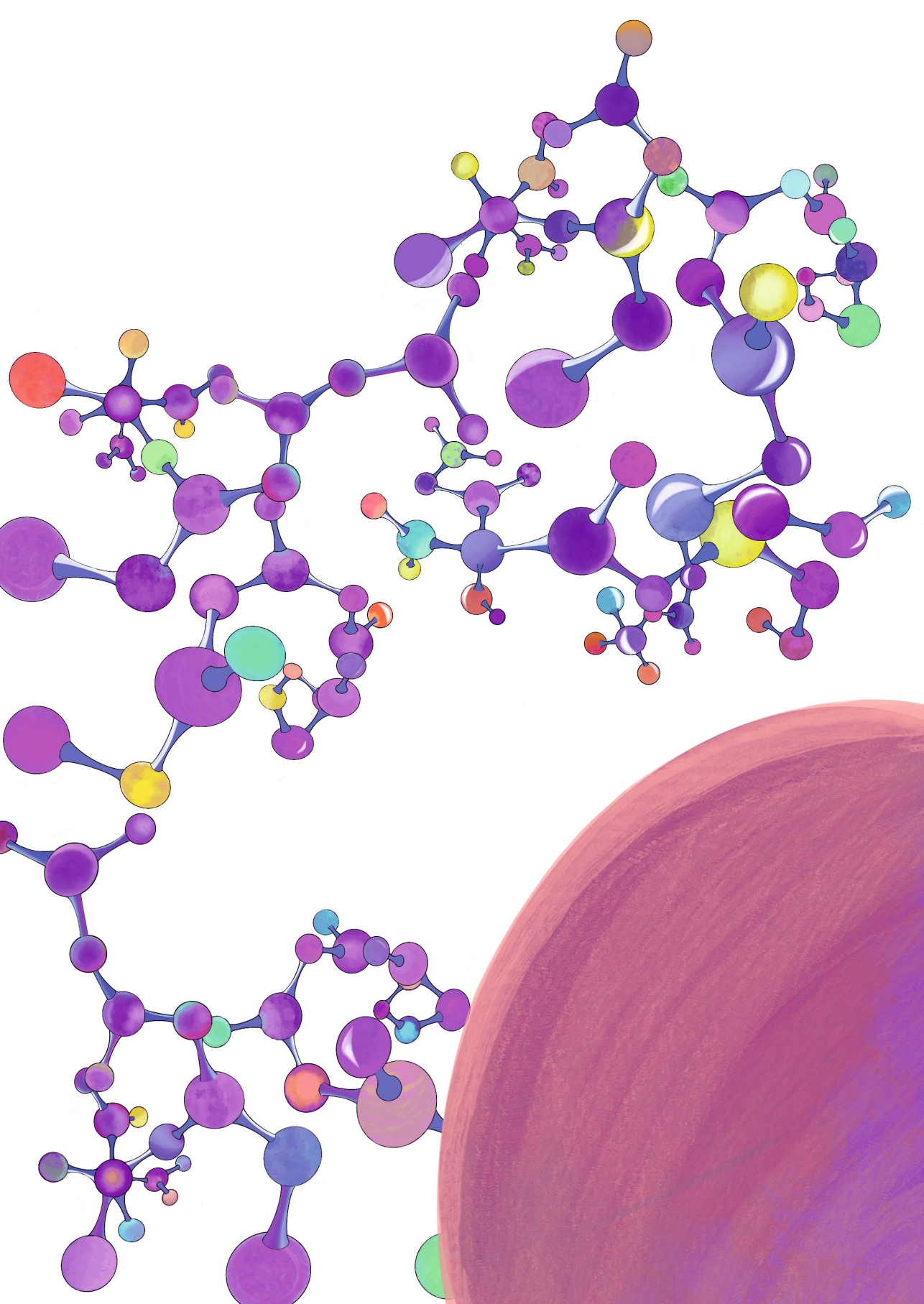

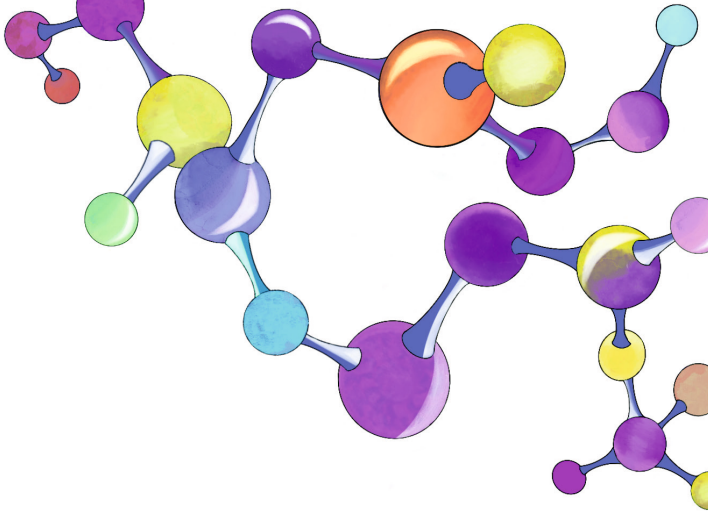

Appendices

AUTHORSHIP STATEMENT

Chapter 1. General introduction.
I proposed the general structure and wrote the original draft. I revised the text after comments from GJAA and MHMW.

Chapter 2. Tetraspanin-decorated extracellular vesicle-mimetics as a novel adaptable reference material.
I conducted research, analyzed data and prepared figures with lead supervision from MYM. I suggested experimental design along the project. I wrote original drafts and secured two grant applications, allocating funding into two external collaborations. I accomplished a short-term stay at the CIC bioGUNE (Bizkaia, Spain) to implement cryo-EM results and a secondment at Utrecht University (Utrecht, the Netherlands) to perform high-resolution flow cytometry. I wrote the original draft of the manuscript with revisions from MYM. The revised draft was reviewed and accepted by all the co-authors.

Chapter 3. MIFlowCyt-EV: a framework for standardized reporting of extracellular vesicle flow cytometry experiments.
I contributed to defining the scope of the manuscript. I participated in discussions and feedback rounds. I contributed to the writing of the original draft and provided comments, together with all the other co-authors.

Chapter 4. Intrinsic variability of current MESF calibrators impacts the assignment of absolute fluorescence values to nanoparticles and extracellular vesicles by flow cytometry.
I designed the study, conducted research and performed data analysis with input from GJAA and MHMW. I coordinated international collaborations with co-authors from industry, non-regulatory federal agency and academic institutions. I shared relevant data and files at the respective open sources (EV-TRACK knowledge base and flow repository). I wrote the original draft of the manuscript with revisions from GJAA and MHMW. I implemented input and comments from the other contributors. The revised draft was reviewed and accepted by all the co-authors. I uploaded the final version to BioRxiv.

Chapter 5. Improved Flow Cytometric Light Scatter Detection of Submicron-Sized Particles by Reduction of Optical Background Signals.
I conducted research and performed data analysis with GJAA. I suggested experimental design, commented on the original draft and prepared figures and shared relevant via the EV-TRACK knowledge base with lead supervision from GJAA and MHMW.

Chapter 6. Physical association of lipoprotein particles and extracellular vesicles unveiled by single particle analysis.
I designed the study, conducted research and analyzed results. I performed a secondment at Ghent University (Belgium) to prepare and analyze samples. I coordinated international collaborations with co-authors to obtain results using diverse advanced techniques. I wrote the original draft and prepared figures with input from GJAA and MHMW. I integrated input and comments from the other contributors. I curated and uploaded relevant data and raw files under the EV-TRACK knowledge base and the flow repository. The revised draft was reviewed and accepted by all the co-authors. I uploaded the final version to BioRxiv.

Chapter 7. General discussion.
I developed the set-up, conducted literature search and wrote the original draft. Therefore, the general discussion represents my point of view. The text was revised once with feedback from GJAA and MHMW.

ENGLISH SUMMARY

Extracellular vesicles (EVs) are cell-derived multicomponent messengers that participate in diverse intercellular communication processes regulating immune responses, cell survival and proliferation. However, EVs also play a role in disease processes like cancer. Since EVs contain biological information that reflects the status of the cell of origin, they might be used in liquid biopsies as disease biomarkers. The detection and characterization of EVs is a fundamental step towards EV-based biomarker profiling of pathological processes and is complicated due to their small size, heterogeneity and complex composition. Therefore, technological solutions that allow high throughput detection and analysis of single EVs are of utmost importance. Flow cytometry (FCM) is a promising technology for this purpose. However, traditional flow cytometers, designed for cells, lack the sensitivity for the detection of nano-sized EVs, whose signals are typically below or at the detection limit of conventional instruments.

In my PhD thesis I explored the limits of flow cytometry of single EVs, provide guidance for reproducible and robust EV FCM and address the challenges of EV analysis in body fluids. First, we developed and characterized a reference material for EV research. Next, we focused on high-sensitivity FCM for the detection of EVs and I present a reporting framework developed by the ISEV-ISAC-ISTH EV Flow cytometry workgroup to increase reproducibility of results. Since fluorescence calibration of EV signals is of importance for inter-instrument and inter-lab comparisons, we provide insights into the utilization of current calibrators and show that intrinsic variations related to these calibrators compromise accurate calibration of EV signals. In addition to the fluorescence, light scatter signals also contain valuable information that it is often lost within the background noise. By using an open-architecture flow cytometer, we optimized the configuration by combining differently sized hardware components to improve light scatter-based EV detection by reducing optical background signals. Lastly, we applied these technological advancements in the field of high-sensitivity FCM to investigate interactions between biological particles, namely EVs and lipoprotein particles (LPPs), which are known to co-isolate. Liquid biopsy EV-based biomarker profiling is complicated because LPPs in blood outnumber EVs by orders of magnitude and have biophysical overlapping properties with EVs, including size and density. We here demonstrate by high-sensitivity FCM, in combination with orthogonal methods; i.e., Rayleigh and Raman scattering and cryo-electron microscopy, that EV-LPP complexes can be formed and can impact EV-analysis in blood. Overall, the findings presented in my thesis can contribute to the development of robust liquid biopsy EV biomarker profiling by FCM and shed light on the complexity of single EV analysis in body fluids, which will ultimately help to a successful clinical translation of EVs as disease biomarkers.

Keywords: Extracellular vesicles, reference materials, reporting, , calibration, reproducibility, flow cytometry, biomarker, liquid biopsy, blood

NEDERLANDSE SAMENVATTING

Extracellulaire blaasjes (EVs) worden door cellen uitgescheiden en zijn samengesteld uit vele verschillende componenten. EVs nemen deel aan diverse intercellulaire communicatieprocessen die betrokken zijn bij celdeling, celoverleving en de regulatie van de immuunrespons.. EVs spelen echter ook een rol bij ziekteprocessen zoals kanker. Omdat EVs biologische informatie bevatten die de status van de cel van herkomst weerspiegelt, kunnen zij in vloeibare biopsieën worden gebruikt als biomarkers voor ziekten. De detectie en karakterisering van EVs is dus een fundamentele stap in de richting van EV-gebaseerde biomarker profilering van pathologische processen. De studie van EVs is echter ingewikkeld vanwege hun kleine omvang, heterogeniteit en complexe samenstelling. Daarom zijn technologische oplossingen die detectie en analyse van grote aantallen afzonderlijke EVs mogelijk maken zeer gewenst. Flow cytometrie (FCM) is hiervoor een veelbelovende technologie. Echter traditioneel ontworpen flow cytometers voor cellen missen de gevoeligheid voor de detectie van EVs van nanoformaat, waarvan de signalen meestal onder of op de detectiegrens van conventionele instrumenten liggen. In mijn proefschrift heb ik de grenzen van flow cytometrie van afzonderlijke EVs verkend, richtlijnen gegeven voor reproduceerbare en robuuste EV-FCM en de uitdagingen van EV-analyse in lichaamsvloeistoffen onderzocht. Eerst hebben we referentiemateriaal voor EV-onderzoek ontwikkeld en gekarakteriseerd. Vervolgens hebben we ons gericht op zeer gevoelige FCM voor de detectie van individuele EVs en presenteer ik richtlijnen voor de rapportage van EV-FCM experimenten die ontwikkeld zijn door de ISEV-ISAC-ISTH EV Flow cytometrie werkgroep om de reproduceerbaarheid te verbeteren. Aangezien fluorescentiekalibratie van EV-signalen van belang is voor vergelijkingen tussen instrumenten en laboratoria, hebben we de huidige kalibratoren voor FCM onderzocht en vastgesteld dat de intrinsieke variaties met betrekking tot deze kalibratoren een nauwkeurige kalibratie van EV-signalen belemmeren. Naast fluorescentie bevatten lichtverstrooiingssignalen ook waardevolle informatie over EVs die vaak verloren gaat in de achtergrondruis. Door gebruik te maken van een flow cytometer met een flexibele configuratie waren wij in staat om bepaalde hardwarecomponenten van verschillende grootte te combineren en de op lichtverstrooiing gebaseerde EV-detectie te verbeteren door optische achtergrondsignalen te verminderen. Ten slotte hebben we deze technologische verbeteringen toegepast om interacties te onderzoeken tussen biologische deeltjes, namelijk EVs en lipoproteïnedeeltjes (LPPs), waarvan bekend is dat ze co-isoleren. EV-gebaseerde biomarker profilering in vloeibare biopten is gecompliceerd omdat in bloed LPPs in veel grotere aantallen aanwezig zijn dan EVs en LPPs overlappende biofysische overlappende eigenschappen bezitten met EVs, inclusief grootte en dichtheid. Door middel van FCM met hoge gevoeligheid in combinatie met orthogonale methoden (Rayleigh- en Raman-verstrooiing en cryo-elektronenmicroscopie), tonen we hier aan dat EV-LPP complexen kunnen vormen en hierdoor EV-analyse in bloed kunnen beïnvloeden.

De bevindingen in mijn proefschrift dragen bijaan de ontwikkeling van robuuste EV-biomarker profilering in vloeibare biopten met behulp van FCM en werpen licht op de complexiteit van EV analyse in lichaamsvloeistoffen. Beiden aspecten zijn van belang voor eensuccesvolle klinische vertaling.

Trefwoorden: Extracellulaire blaasjes, referentiematerialen, rapportage, kalibratie, reproduceerbaarheid, flow cytometrie, biomarker, vloeibare biopsie, bloed

SCIENTIFIC OUTPUT

List of publications

Presented in this thesis:

1. **Lozano-Andrés E.**, Libregts S.F., Toribio V, Royo F., Morales S., López-Martín S., Valés-Gómez M., Reyburn H.T., Falcón-Pérez JM., Wauben M. H., Soto M. and Yáñez-Mó M. Tetraspanin-decorated extracellular vesicle-mimetics as a novel adaptable reference material. Journal of Extracellular Vesicles, 2019, 8:1, https://doi.org/10.1080/20013078.2019.1573052
2. Welsh J.A., Van Der Pol E., Arkesteijn G.J., Bremer M., Brisson A., Coumans F., Dignat-George F., Duggan E., Ghiran I., Giebel B., Görgens A., Hendrix A., Lacroix R., Lannigan J., Libregts S.F., **Lozano-Andrés E.**, Morales-Kastresana A., Robert S., De Rond L., Tertel T., Tigges J., De Wever O., Yan X., Nieuwland R., Wauben M.H., Nolan J.P. and Jones J.C. MIFlowCyt-EV: a framework for standardized reporting of extracellular vesicle flow cytometry experiments. Journal of Extracellular Vesicles, 2020 9: 1713526. https://doi.org/10.1080/20013078.2020.1713526
3. **Lozano-Andrés E.**, Van Den Broeck T., Wang L., Mehrpouyan M., Tian Y., Yan X., Wauben M.H.M., Arkesteijn G.J.A. Considerations for MESF-bead based assignment of absolute fluorescence values to nanoparticles and extracellular vesicles by flow cytometry. BioRxiv 2021; doi: https://doi.org/10.1101/2021.03.01.433358
4. Arkesteijn G.J.A., **Lozano-Andrés E.**, Libregts S.F.W.M. and Wauben M.H.M. Improved Flow Cytometric Light Scatter Detection of Submicron-Sized Particles by Reduction of Optical Background Signals. Cytometry part A. 2020, 97: 610-619. https://doi.org/10.1002/cyto.a.24036
5. **Lozano-Andrés E.**, Libregts, S.F.W.M., Pinheiro C., Gijsbers A., Enciso-Martinez A., Van Niel G., Hendrix A., Peters P.J., Otto C. , Arkesteijn G.J.A., Wauben M.H.M., Influence of lipoprotein particles in extracellular vesicle analysis by single particle flow cytometry. BioRxiv 2022; https://doi.org/10.1101/2022.08.31.506022 (Under review)

Other publications:

1. García-Manrique P., Serrano-Pertierra E., **Lozano-Andrés E.**, López-Martín S., Matos M., Gutiérrez G., Yáñez-Mó M., Blanco-López MC. (2020). Selected Tetraspanins Functionalized Niosomes as Potential Standards for Exosome Immunoassays. Nanomaterials. 10(5):971. https://doi.org/10.3390/nano10050971
2. Lak NSM., van der Kooi E.J., Enciso-Martinez A., **Lozano-Andrés E**., Otto C., Wauben M.H.M., Tytgat G.A.M. Extracellular Vesicles: A New Source of Biomarkers in Pediatric Solid Tumors? A Systematic Review. Front Oncol. 2022 May 24;12:887210. eCollection 2022. https://doi.org/10.3389/fonc.2022.887210

3. Welsh J.A., Arkesteijn G.J., Bremer M., Cimorelli M., Giebel B., Görgens A., Hendrix A., Kuiper M., Lacroix R., Lannigan J., **Lozano-Andrés E.**, Rao S., Robert S., De Rond L., Tertel T., De Wever O., Yan X., , Wauben M.H., Nolan J.P., Jones J.C., Nieuwland R. and Van Der Pol E., Educational compendium on flow cytometry experiments of single extracellular vesicles. Journal of Extracellular Vesicles, 2023, Feb;12(2):e12299. https://doi.org/10.1002/jev2.12299
4. **Lozano-Andrés E.**, Tian Y., Arkesteijn G.J.A., Libregts, S.F.W.M., Yan X., Wauben M.H.M., Towards Benchmarking flow cytometric analysis of nanoparticles: a cross-platform study for single extracellular vesicle detection. (In preparation)

Membership and institutional responsibilities

2020 – 2022 Student Network on Extracellular Vesicles (SNEV).
Co-founder and board member.
2019 – 2021 Prout (PhD Network Utrecht).
Representative for the Faculty of Veterinary Medicine.
2019 – 2022 Society of Spanish Scientists in the Netherlands (CENL-SWNL, non-profit association). Co-founder and board member.
Elected Director of Internal Affairs & Education.
2018 – now ISEV-ISAC-ISTH Extracellular Vesicle flow cytometry working group.
2018 – now International Society for Advancement of Cytometry (ISAC).
2018 – now International Society of Extracellular Vesicles (ISEV).
2016 – now Spanish Society for Innovation and Investigation in Extracellular Vesicles (GEIVEX).

Scientific outreach and media appearances

2021 – Spanish National Radio (RTVE) interview. I was invited for an interview at the section of 'Científicos en el Exterior' to talk about my scientific research and my experience of being a scientist abroad (in Spanish).
https://www.rtve.es/alacarta/audios/punto-de-enlace/punto-enlace-estefania-lozano-estudia-vesiculas-extracelulares-19-01-21/5765500/
2020 – EV Flow Seminar series. Lozano-Andrés E. Influence of lipoproteins in EV flow cytometry analysis. Virtual. September 2020 (oral presentation).
https://youtu.be/pY7FLeUBzKM
2020 – Research work was featured in Laser Focus World magazine. We received an invitation to feature our recent research work published in Cytometry Part A.
https://www.laserfocusworld.com/test-measurement/article/14181320/confocal-filtering-enables-submicron-detection-with-flow-cytometry
2019 – EMBL interview. I was invited for an interview by the European Molecular Biology Laboratory to share my experience as a trainer in the EMBO practical course ''Extracellular Vesicles: From Biology to Biomedical Applications''.
https://blogs.embl.org/events/2019/06/12/meet-the-trainer-estefania-lozano-andres/

Educational contributions

Supervision of Master, (visiting) PhD students and researchers.
Invited trainer at the EMBO practical course on Extracellular Vesicles: From Biology to Biomedical Applications.
Co-applicant and organizer of the CYTO2022 Workshop on Extracellular vesicle measurement by flow cytometry: practical examples of MIFlowCyt-EV.

Awards

2022 – I & I Scientific endeavor travel grant.
Honor issuer Infection & Immunity (Utrecht, the Netherlands).
2022 – Student travel award.
Honor issuer International Society for Advancement of Cytometry (Philadelphia, USA).
2020 – Outstanding Poster Presentation Award.
Honor issuer International Society for Extracellular Vesicles.
2019 – Student travel award.
Honor issuer International Society for Advancement of Cytometry (Vancouver, Canada).
2019 – Young Investigator Scholarship.
Honor issuer International Society for Extracellular Vesicles (Kyoto, Japan).
2017 – Autonomous University of Madrid Mobility Short-term Fellowship (Madrid, Spain).
2017 – GEIVEX Mobility Fellowship (Basque Country, Spain).

Conference contributions

Invited keynote speaker:

1. **Lozano-Andrés E.**, Detection of single Extracellular Vesicles Using Flow Cytometry. Technologic Innovation session. Grand-Ouest Extracellular Vesicle Network: Innovations for Health. Scheduled in Nantes (France) but held virtual due to COVID-19. 30 November 2020.
2. **Lozano-Andrés E.**, Analysis of tumor derived extracellular vesicles in presence of lipoprotein particles by flow cytometry. International Symposium ' Unravelling the role of extracellular vesicles in health and disease '. Virtual. 25-29 April 2022.

Accepted abstracts:

1. **Lozano-Andrés E.**, Enciso-Martinez A., Gijsbers A., Libregts, S.F.W.M., Pinheiro C., Van Niel G., Hendrix A., Peters P. J., Otto C., Arkesteijn G.J.A., Wauben M.H.M. Physical association of lipoprotein particles and extracellular vesicles unveiled by flow cytometry. 37th Congress of the International Society for Advancement of Cytometry. Philadelphia, USA, June 2022 (poster presentation, student travel award).
2. Monheim L., **Lozano-Andrés E.**, Dessing M., Meyer A., Schenkel T., Shi X., Van den Broeck T., Widmann S., Wauben M., Tyznik A. Good practice for analyzing extracellular vesicles using the BD FACSymphony™ A1 Cell Analyzer. 37th Congress of the International Society for Advancement of Cytometry. Philadelphia, USA, June 2022 (poster presentation).

3. Van den Broeck T., **Lozano-Andrés E.**, Dessing M., Meyer A., Schenkel T., Shi X., Monheim L., Widmann S., Wauben M., Tyznik A. Detection of extracellular vesicles using the BD FACSymphony™ A1 Cell Analyzer. 37th Congress of the International Society for Advancement of Cytometry. Philadelphia, USA, June 2022 (poster presentation).
4. **Lozano-Andrés E.**, Van den Broeck T., Wang L., Mehrpouyan M., Tian Y., Yan X., Wauben M.H.M., Arkesteijn G.J.A. Considerations towards the assignment of calibrated fluorescence values to nanoparticles and extracellular vesicles by using MESF beads by flow cytometry. Annual Meeting Netherlands Society for Extracellular Vesicles (NLSEV) Amsterdam, The Netherlands. November 2021 (poster presentation).
5. **Lozano-Andrés E.**, Van den Broeck T., Wang L., Mehrpouyan M., Tian Y., Yan X., Wauben M.H.M., Arkesteijn G.J.A. Calibration of fluorescence values to nanoparticles and extracellular vesicles by using MESF beads by flow cytometry. Science for Life Conference. Utrecht, The Netherlands. November 2021 (poster presentation).
6. **Lozano-Andrés E.**, Van den Broeck T., Wang L., Mehrpouyan M., Tian Y., Yan X., Wauben M.H.M., Arkesteijn G.J.A. Assignment of absolute MESF or ERF values to nanoparticles and extracellular vesicles by flow cytometry depends on the MESF-bead set used as calibrator. 36th Congress of the International Society for Advancement of Cytometry. Virtual. June 2021 (poster presentation).
7. **Lozano-Andrés E.**, Van den Broeck T., Wang L., Mehrpouyan M., Tian Y., Yan X., Wauben M.H.M., Arkesteijn G.J.A. Considerations towards flow cytometric calibration of fluorescent signals from nanoparticles and extracellular vesicles by using MESF-bead based calibrators. Annual Meeting International Society for Extracellular Vesicles (ISEV). Virtual. May 2021 (poster presentation).
8. **Lozano-Andrés E.**, Libregts, S.F.W.M., Pinheiro C., Van Niel G., Hendrix A., Arkesteijn G.J.A., Wauben M.H.M. Interference of lipoprotein particles during flow cytometric analysis of single extracellular vesicles in plasma. Science for Life Conference. Virtual. November 2020 (poster presentation).
9. **Lozano-Andrés E.**, Arkesteijn G.J.A., Wauben M.H.M. Considerations in MESF-bead based assignment of absolute fluorescence values of nanoparticles and extracellular vesicles by flow cytometry. Veterinary Science Day Utrecht University. Virtual. November 2020 (poster presentation).
10. **Lozano-Andrés E.**, Tian Y., Arkesteijn G.J.A., Libregts, S.F.W.M., Yan X., Wauben M.H.M. Towards benchmarking flow cytometric analysis of sub-micron sized particles: a cross-platform study for single extracellular vesicles. 35th Congress of the International Society for Advancement of Cytometry. Virtual. August 2020 (poster presentation).

11. **Lozano-Andrés E.**, Tian Y., Arkesteijn G.J.A., Libregts, S.F.W.M., Yan X., Wauben M.H.M. Benchmarking flow cytometric analysis of nanoparticles: a cross-platform study for single extracellular vesicle detection. Annual Meeting International Society for Extracellular Vesicles (ISEV). Virtual. July 2020 (poster presentation, outstanding presentation award).
12. **Lozano-Andrés E.**, Tian Y., Arkesteijn G.J.A., Libregts, S.F.W.M., Yan X., Wauben M.H.M. Benchmarking Analysis of sub-micron sized particles: a cross-platform study for single extracellular vesicle flow cytometric characterization. ISEV workshop: Open, transparent and reproducible EV research. Ghent University, Belgium. December 2019 (poster presentation).
13. **Lozano-Andrés E.**, Libregts, S.F.W.M., Pinheiro C., Van Niel G., Hendrix A., Arkesteijn G.J.A., Wauben M.H.M. The presence of lipoprotein particles in plasma interferes with labeling and fluorescence-based flow cytometric analysis of extracellular vesicles. Veterinary Science Day Utrecht University, The Netherlands. November 2019 (poster presentation).
14. **Lozano-Andrés E.**, Libregts, S.F.W.M., Pinheiro C., Van Niel G., Hendrix A., Arkesteijn G.J.A., Wauben M.H.M. Lipoprotein particles can influence extracellular vesicle labeling and fluorescence based detection by flow cytometry. 3rd Annual Meeting Netherlands Society for Extracellular Vesicles (NLSEV) Utrecht, The Netherlands. November 2019 (oral presentation).
15. Arkesteijn G.J.A., **Lozano-Andrés E.**, Libregts S.F.W.M. and Wauben M.H.M., Improved scatter based flow cytometric detection of particles in the 100 nm range by reduction of optical background signals. 3rd Annual Meeting Netherlands Society for Extracellular Vesicles (NLSEV) Utrecht, The Netherlands. November 2019 (poster presentation).
16. **Lozano-Andrés E.**, Libregts, S.F.W.M., Pinheiro C., Van Niel G., Hendrix A., Arkesteijn G.J.A., Wauben M.H.M., Lipoprotein Particles can Interfere in Fluorescent-Based Single Extracellular Vesicle Analysis by Flow Cytometry. 34th Congress of the International Society for Advancement of Cytometry. Vancouver, Canada. June 2019 (poster presentation, student travel award).
17. **Lozano-Andrés E.**, Optimization of EV characterisation by Flow Cytometry. TRAIN-EV Mid-term evaluation, Research Executive European Agency. Brussels, Belgium. June 2019 (oral presentation).
18. **Lozano-Andrés E.**, Libregts, S.F.W.M., Pinheiro C., Van Niel G., Hendrix A., Arkesteijn G.J.A., Wauben M.H.M., Influence of lipoprotein particles in extracellular vesicle analysis by single particle flow cytometry. Annual Meeting International Society for Extracellular Vesicles (ISEV). Kyoto, Japan. April 2019 (oral presentation).
19. **Lozano-Andrés E.**, Optimization of EV characterisation by Flow Cytometry. 3rd TRAIN-EV Meeting and workshop on Extracellular Vesicles Isolation. Semmelweis University, Hungary. April 2019 (oral presentation).

20. **Lozano-Andrés E.**, Libregts, S.F.W.M., Arkesteijn G.J.A., Wauben M.H.M. Optimization of the generic labelling of extracellular vesicles in human plasma for single particle analysis by flow cytometry. 2nd Annual Meeting Netherlands Society for Extracellular Vesicles (NLSEV) Amsterdam, The Netherlands. November 2018 (poster presentation).
21. **Lozano-Andrés E.**, Libregts, S.F.W.M., Arkesteijn G.J.A., Wauben M.H.M. Generic labelling of human plasma Extracellular Vesicles for single particle analysis by flow cytometry. Infection & Immunity 25 years Symposium. Utrecht University, The Netherlands. October 2018 (poster presentation).
22. **Lozano-Andrés E.**, Optimization of EV characterisation by Flow Cytometry. 2nd TRAIN-EV Meeting and workshop on Extracellular Vesicles Isolation. Tallinn, Estonia. October 2018 (oral presentation).
23. **Lozano-Andrés E.**, Libregts S.F., Royo F., Morales S., López-Martín S., Valés-Gómez M., Reyburn H.T., Falcón-Pérez JM., Wauben M. H., Soto M. and Yáñez-Mó M. Bioengineered nanovesicles as Extracellular Vesicle-Mimetics: A novel Standard for Extracellular Vesicle analysis. Annual Meeting International Society for Extracellular Vesicles (ISEV) Barcelona, Spain. May 2018 (oral presentation).
24. **Lozano-Andrés E.**, Defined EV-subset analysis in blood by flow cytometry. 1st TRAIN-EV Meeting: For benefit in Health and Disease. Dublin, Ireland. April 2018 (oral presentation).
25. **Lozano-Andrés E.**, Synthetic nanoparticles decorated with recombinant tetraspanins as EV mimetics for biotechnological applications. CNIC PhD Day. Spanish National Cardiovascular Research Center (CNIC) Madrid, Spain. November 2016 (poster presentation).
26. **Lozano-Andrés E.**, Manrique P., Morales-López S., López-Martín S., Blanco C., Yáñez-Mó M. Synthetic nanoparticles decorated with recombinant tetraspanins as a standard for EV analysis by flow cytometry. 3er International Symposium on Therapeutic applications of extracellular vesicles. Grupo Español de Inovación e Investigación en Vesículas Extracelulares (GEIVEX). San Sebastián, Spain. September 2016 (poster presentation, creative design award).
27. **Lozano-Andrés E.**, Manrique P., Morales-López S., López-Martín S., Blanco C., Yáñez-Mó M. Synthetic nanoparticles functionalized with recombinant tetraspanins as a standard for EV analysis techniques. Advance Course on Extracellular Vesicles: from Biology to Biomedical Applications. European Molecular Biology Laboratory (EMBL). Heidelberg, Germany. September 2016 (poster presentation).

ACKNOWLEDGMENTS

All the gratitude that I felt and continue to feel over the course of this incredible journey of seven years can hardly be contained in this section. But, as always, I will try my best to express how deeply my appreciation goes for all the support in science and life that I have received. I always say that my curiosity naturally led me to doing a PhD in biomolecular sciences and I can say that looking back now, I would gladly do it all over again. My heart is full with joy and gratitude for this experience and for the amazing individuals that I got to meet thought the years.

Marca, you inspired me since I first met you almost seven years ago in Heidelberg. Your talk on EV flow cytometry was fascinating. Little did I know at that time that, one year later, life would present me with an opportunity to visit your lab for three months. And how much did I enjoy every second of those three months in Utrecht. I was truly captivated by the research environment that you had built and amazed at all the knowledge that I was only able to grasp at the time. I felt that I had found a research topic that could keep me triggered for decades to come and that I would be thrilled if I could join your group. So I decided to follow my heart and made a decision that was not easy but I knew it was right. Shortly after, I moved countries and joined your lab to continue my PhD studies at Utrecht University, and I can never thank you enough for giving me this opportunity (I know there were many candidates for this position). I only have words of gratitude and admiration for you. During the past five years you have been my promotor, my mentor, my inspiration, my confident and one of my biggest supports. I am forever grateful for your invaluable advices, for your guidance and for always giving me the space to grow and explore those ideas that seemed a bit crazy but were too exciting to not try. Also know that your role was essential for my 'dreams come true' moments over these years. I will never forget 2019 when I received two awards from ISEV and CYTO that made possible to travel to Japan and Canada, presenting my work in front of thousands of people was one of the highlights of my PhD. But I also have to thank you for your shared enthusiasm and dedication. Thank you for teaching me how to think critically while being creative and flexible, for showing the great value of negative results and for helping me to build a resilience that will never fade away. Working on multiple projects simultaneously from the beginning was a challenge but I learned a lot from it, and now I can say how much I enjoyed working at the interface of multidisciplinary projects. I would love to continue working together with you to share the ongoing projects that still need to be finished with the rest of the world and to keep building new amazing research lines, for years to come.

Ger, thank you for your teachings and guidance. I am grateful for all the knowledge that you took the time to share with me over the years. We both know that the Influx is not an easy instrument but I have always enjoyed a good challenge and I had the best

mentor to guide me through the troubleshooting moments. You always knew what to do when a problem came up, which never ceased to amaze me. I think that you behind the Influx is what makes this technology so special and unique in the world, which had a major contribution in my decision to move countries. You built a technology that allows to push the limits of detection (and knowledge). And I will always continue to be grateful to you, the chapters in my thesis would look very different without you. Thank you for also helping me to cultivate patience, for being a great listener and for showing me the benefits of setting boundaries. I could not have asked for a better mentor to learn all the ins and outs of flow cytometry. Please know that it has been an incredible honour to take over your role running the flow cytometry facility and that I will do my best to keep your legacy alive while advancing the field of EV flow cytometry.

Dear committee members, prof. dr. E. I. Buzas, prof. dr. G.W. Jenster, dr. R. Nieuwland, prof. dr. R.M. Schiffelers and prof. dr. M.A. Tryfonidou, thank you for accepting to be in my committee and for your time to review my thesis.

To my paranymphs and friends, Maya and Laura. You both know how close to my heart you have become during the past 5 years. Thank you for always being there, during the highs and the lows. **Maya**, thanks for your kindness and support. For all the bunny and horse therapy moments and birthday celebrations together with board game nights. For cheering me when I was driving my first boat around Giethoorn and for always having my back. Also thanks to Martijn for being such a great company during Kings day celebrations and dinners. I hope to keep sharing many more unforgettable experiences together the coming years. **Laura**, gracias por aparecer en Utrecht y cambiar mi vida. Desde el primer día que decidimos ir a un concierto de Yann Tiersen juntas supe que te ibas a convertir en una de mis mejores amigas. Gracias por todo, todo, todo. Por la visita a Heidelberg cargada con una caja de mis muestras, por los viajes a Bloemendaal aan Zee, Sassenheim, Maastricht, Londres, etc. También a Ricardo, con quién me alegro infinitamente de que estés compartiendo tu vida rodeados de gatetes preciosos. Eres mi persona favorita con quién celebrar el fin de los veintitodos y empezar el salto a los 30. Espero que tengamos muchos más saltos de años y décadas juntas.

Of course, seven years of PhD across countries gave me plenty of time to travel and live abroad, getting to work in multiple laboratories. These fruitful collaborations do not go unnoticed and I truly appreciate both the professional and personal opportunities that came with moving into new cities to do one of the things I love the most: science! **María**, muchas gracias por tu supervisión y tus enseñanzas durante los dos primeros años de mi tesis doctoral. La oportunidad de venir a Utrecht durante esos tres primeros meses definitivamente cambió mi vida... y siempre te estaré agradecida por apoyarme con la decisión de formar parte del TRAIN-EV. Recuerdo con cariño esos dos años trabajando en Madrid, con mudanza de laboratorio incluida. También gracias a mis compañeros **Soraya**, **Henar** y **Víctor**, por los buenos momentos que compartimos.

Y a mi querida amiga **Carla**, muchísimas gracias por compartir esa visión de la vida tan bonita que tienes. Gracias por acogerme en Boston y por hacer mi 31 cumpleaños un día muy especial. Espero que la vida nos vuelva a cruzar pronto y os deseo todo lo mejor.

Juanma, **David**, **Félix** y **Esperanza**, gracias por recibirme en Bilbao y por vuestra ayuda, me quedo con todo lo que aprendí sobre microscopía electrónica y que llevo conmigo allá adónde voy. **An**, thank you for welcoming me in Ghent, I arrived with loads of things to do and a few months to accomplish them but it was a pleasure to work in your lab and to get to know Ghent, which has become one of my favourite cities in the world. **Tina**, thank you for all your support, which made chapter 4 possible and gave me the opportunity to collaborate with BD Biosciences over the years. Visiting you in Erembodegem to learn about a leader company building flow cytometers has been a dream, thanks so much for sharing your passion for EVs and for always being helpful. Also thanks to **Mark**, **Tim** and **Annette**, for the fantastic weeks I got to spent working in Heidelberg. Testing a new generation small particle flow cytometer was surely a lot of fun, next to talking all things flow cytometry made the perfect combination. I hope that we can find a way to keep working together. **Agustin**, **Abril**, **Guillaume**, **Cees** and **Peter**, thanks for your invaluable help with the experiments presented in chapter 6 and for your shared enthusiasm about this exciting project. To all my collaborators, thanks for everything.

Martijn, thanks for the great advices and for always lending a listening ear. **Tom**, thanks for the positive vibes around the lab and for sharing that passion for science that feels addictive. **Liz,** thanks for being such a cheerleader and a fantastic supervisor- I look forward to visiting you in Australia. **Marije**, thank you for all the things that you do in the lab. From training people, to making sure things run smoothly and always being there- even for late evening calls when we unfortunately had some freezer emergencies. You are a superwoman. **Sten**, thank you for supervising my secondment in Utrecht during those three months. I learnt a lot from you and this truly had an impact in all the pages presented in this thesis. **Marthe**, it was very nice to share the office with you, thanks for sending me that house ad that became my home for almost 2 years. **Xiaogang**, thanks for your company during the weekends in the lab and for showing me a taste of how your future Chinese restaurant will be. **Richard**, **Esther** and **Willem**, thank you for all the feedback during presentations to help me improve both my work and my communication skills. I am always amazed by all the incredible suggestions and invaluable points of view that you add during our meetings. **Susanne**, **Alberta**, **Kyra**, **Xinyi** and **Marije K**, thanks for always lending a helping hand and for the fun moments we shared. It has been a pleasure to share this journey with you and observe you become incredible scientists.

Nafiseh, **JC**, **Ziying**, **Min**, **Thi**, **María**, **Martijn** and all colleagues, thank you for everything! **Bernd**, **Celia**, **Esther**, **Dora**, **Bart**, **Petra**, **Martin**, **Chris**, **Bas**, **Jeroen**, **Iris**, **Ruud**, **Theo**, **Jillis** thanks for the interesting ideas, for always being helpful and for the nice conversations around the coffee table!

Femke, thank you for your support and guidance during the last year of my PhD thesis while I was transitioning into a new exciting job at the flow cytometry facility. I really appreciate your understanding and help, especially during the last few months when I was finalizing the writing of these chapters. I hope that we can grow our flow cytometry facility into a great knowledge center and I look forward to work with you in the coming years. Also to my new colleagues from Immunology. **Edwin**, thank you for always having a nice word. I really like our green plant-based office and enjoy sharing the office with you. **Irene, Daniëlle**, **Ema**, **Elise**, **Ali**, **Adil**, **Fenne**, **Arjan**, **Deja** and all my new colleagues, thank you for the great atmosphere that you create in the lab. I am looking forward to the coming years working together.

To my colleagues and friends from TRAIN-EV. I will be forever grateful for the opportunity to continue my PhD within such an amazing network of researchers and experts. I genuinely enjoyed all of our meetings and have very fond memories from our meetings in Dublin, Budapest, Estonia, etc. **Claudio**, I have a vivid memory from the kick-off meeting and us talking all things science until the last minute of the dinner, it was meant to be we would be working together in Ghent, Utrecht and even Heidelberg. I really enjoyed learning, teaching and laughing with you all these years. Thanks for all the help and the good vibes. Also thanks to **Elena**, **Tanmay**, **Federico**, **Quentin**, **Dela**, **Delva** and everyone, thanks for being a great company during the PhD. I wish you all the best.

To the members and flow cytometry experts from the EV FCM WG, it has been an honour to contribute to this group during the last five years. Especially thanks to **Joanne**, **Josh**, **John**, **Edwin** and **André**, for the insightful conversations and for always being available to help. Also thanks to the people from SNEV, especially to **Amir** and **Sara**, for giving me the opportunity to be part of such an exciting international network. También agradecer a mi gente de CENL, especialmente a **Noelia, Rodrigo**, **Andrea** y **Elena**, gracias por crear un espacio tan maravilloso y por darme energía durante la tesis con vuestra ilusión, sin duda formar CENL ha sido una parte importante de mi aventura como científica en Utrecht.

Miriam, te conocí gracias a CENL y te has convertido en parte de mi Utrecht family. Gracias por todos los momentos que hemos compartido y por dejarme cuidar de tu bebé **Chupi**, al que adoro y que también me ha ayudado con su amor perruno. Y también a **Hans** por ser una gran compañía durante cenas y eventos. **Fabienne**, thanks for becoming one of my dearest friends in this city. We really just hit it off like Miriam predicted

and shared many moments from self-care to running, birthdays and also frustrations over the PhD journey. You deserve all the happiness and I will be there to celebrate with you the highs and the lows. **Aina**, mi vecinita, moltes gràcies por todos los consejos, los paseos, las conversaciones filosóficas y las fiestas. Eres mi persona favorita para ir a conciertos y me alegro muchísimo de haber conocido la persona tan increíble que eres.

También a mis amigos que me han acompañado a lo largo del tiempo y del espacio. De los años y de la distancia. **Eduardo**, solo tengo gratitud y cariño por todas las cosas que hemos compartido y los ánimos que me has dado todos estos años. A mis compis de la carrera en la UAH: **Aitor**, gracias por acompañarme desde hace más de una década en esta aventura de la tesis doctoral, desde los viajes en coche hasta las visitas en Sagunto compartiendo una buena paella con mi familia. **Cris** y **Aroa**, gracias por vuestra autenticidad y por todas las tardes que pasamos estudiando fisiología vegetal, y por las fiestas en Alcalá y por muchos encuentros más en navidades y verano. **Estela**, con todos los momentos que hemos vivido juntas desde hace más de veinte años siempre que nos reencontramos parece que el tiempo pasa de otra manera, gracias por seguir ahí y acogerme siempre que te he visitado en UK. **Elena**, mi pava favorita. Gracias por escucharme y por animarme siempre, se me llena el corazón de felicidad cuando te escucho hablar de citometría de flujo y de la amiga pava que es científica con tanto amor y orgullo.

To the city that felt like love at first sight, **Utrecht**. I will always remember the feeling of not being ready to leave you back in December 2017. At the time, I had just spent three very cold, rainy, snowy and windy months here and I loved every second of it to my core. And I did not know how to say goodbye so I left wishing it would just be a 'see you soon'. Stars aligned, those three months transformed into three years. Then I found that I love you during all the seasons of the year and it never stopped surprising me how I keep falling in love with you. I know that you will never read this but thank you for feeling like home, I had to come back to you. It is not easy to put into words what makes you so special but my love for you just keeps growing.

Cas, thank you for being the amazing person (aka flying bean) that you are. I am forever grateful for all the peaceful vibes that you sent my way when I needed them the most. I am also grateful for your kindness and for all the incredible things you embody. You showed me a whole new level of experiencing life that is full of brightness, happiness and love. I thank the universe for making our paths cross and you for becoming one of my greatest supports in life. I love us and I look forward to our next adventures together.

Por último, a mi querida familia. **Pinky**, gracias por haber formado parte de mi vida, siempre estás conmigo y yo sin ti… no sería. **Cristina**, mi querida hermana, gracias por ser mi meji y llegar a este mundo. Millones de gracias por acompañarme toda la vida, tu corazón no tiene límites y me siento muy afortunada y orgullosa de la persona que eres. También gracias por los maravillosos diseños que me has hecho, me llena de felicidad que un pedacito de tu arte forme parte de mi tesis doctoral. A mis padres, **Alfredo** y **Esperanza**, las palabras siempre se quedarán cortas para todo lo que tengo que agradeceros. Gracias por siempre saber darme el espacio que he necesitado para crecer como persona, y como científica. Es difícil tener esta distancia, que duele pero no separa. Si acaso ha hecho nuestros lazos más fuertes. Sin vosotros, esta tesis doctoral no existiría. Sin vosotros, yo no existiría. Gracias infinitas. Habéis sido, sois y seréis mi mayor inspiración, mi mayor motivación y mi mayor apoyo.

ABOUT THE AUTHOR

Estefanía Lozano Andrés was born on the 12th of June 1991 in Guadalajara, Spain. She pursued her interest in understanding the science of life and accomplished a Bachelor degree in Molecular Biology at the University of Alcalá de Henarés in 2014. Estefanía performed her Bachelor thesis at the Hospital of Guadalajara under the supervision of dr. Dolores Subirá and dr. Jorge Monserrat. Her thesis work titled *The immunodiagnosis of hematological malignancies by multiparametric flow cytometry* received a summa cum laude mention and the invitation for an oral presentation at the 10th National Congress on Health Sciences. Her interest in flow cytometry and immunology led her to obtain a Master of Science in Immunology Research at the Complutense University of Madrid. Her Master thesis was titled *Immune system analysis of the P-selectin glycoprotein ligand-1 (PSGL-1) deficient mice by multiparametric flow cytometry* and performed under the supervision of dr. Ana Urzainqui. In 2015, Estefanía received an award from the faculty of Medicine due to her outstanding performance, achieving the top 5% academical grades at the Complutense University of Madrid.

In January 2016, Estefanía joined the lab of dr. María Yañez-Mó to start her PhD research at the Autonomous University of Madrid. Her work focused on EV-mimetics for biotechnological and biomedical applications. During this time, Estefanía was awarded two scholarships to perform scientific stays at the labs of prof. dr. Juan Manuel Falcón at the CIC bioGUNE (Bizkaia, Spain) and prof. dr. Marca Wauben at Utrecht University (the Netherlands). Fascinated by the potential of single particle flow cytometry to investigate EVs, Estefanía applied for a PhD position under the Innovative Training Network in Extracellular vesicles: for benefit in health and disease. In March 2018, Estefanía moved to Utrecht to continue her PhD and pursue a career in flow cytometry under the supervision of dr. Ger Arkesteijn and prof. dr. Marca Wauben. The results of her PhD research are described in this thesis. Furthermore, Estefanía promoted the collaboration between institutions in Spain, Belgium, Germany, China, USA and the Netherlands to advance multidisciplinary projects. She participated in international meetings obtaining awards (GEIVEX2016, ISEV2019, CYTO2019, ISEV2020, CYTO2022). Throughout her PhD, Estefanía was also a founder member in associations such as CENL and SNEV. She co-organized two international conferences (TRAIN-EV2021 and SNEV2021) and received invitations as chair at international meetings (ISEV2019 and ISEV2020), as a keynote speaker (GOEV2020 and LABNALCIT2022), and as a trainer (EMBL2019, CYTO2022, and EMBL2023).

Since July 2022, Estefanía is running the flow cytometry facility at the Faculty of Veterinary Medicine, Utrecht University. Here she continues to share her passion for flow cytometry as a wonderful technology to resolve challenging questions, as well as helping others and advancing knowledge.

“Learn from yesterday, live for today, hope for tomorrow.
The important thing is not to stop questioning.
Curiosity has its own reason for existing.”

Albert Einstein

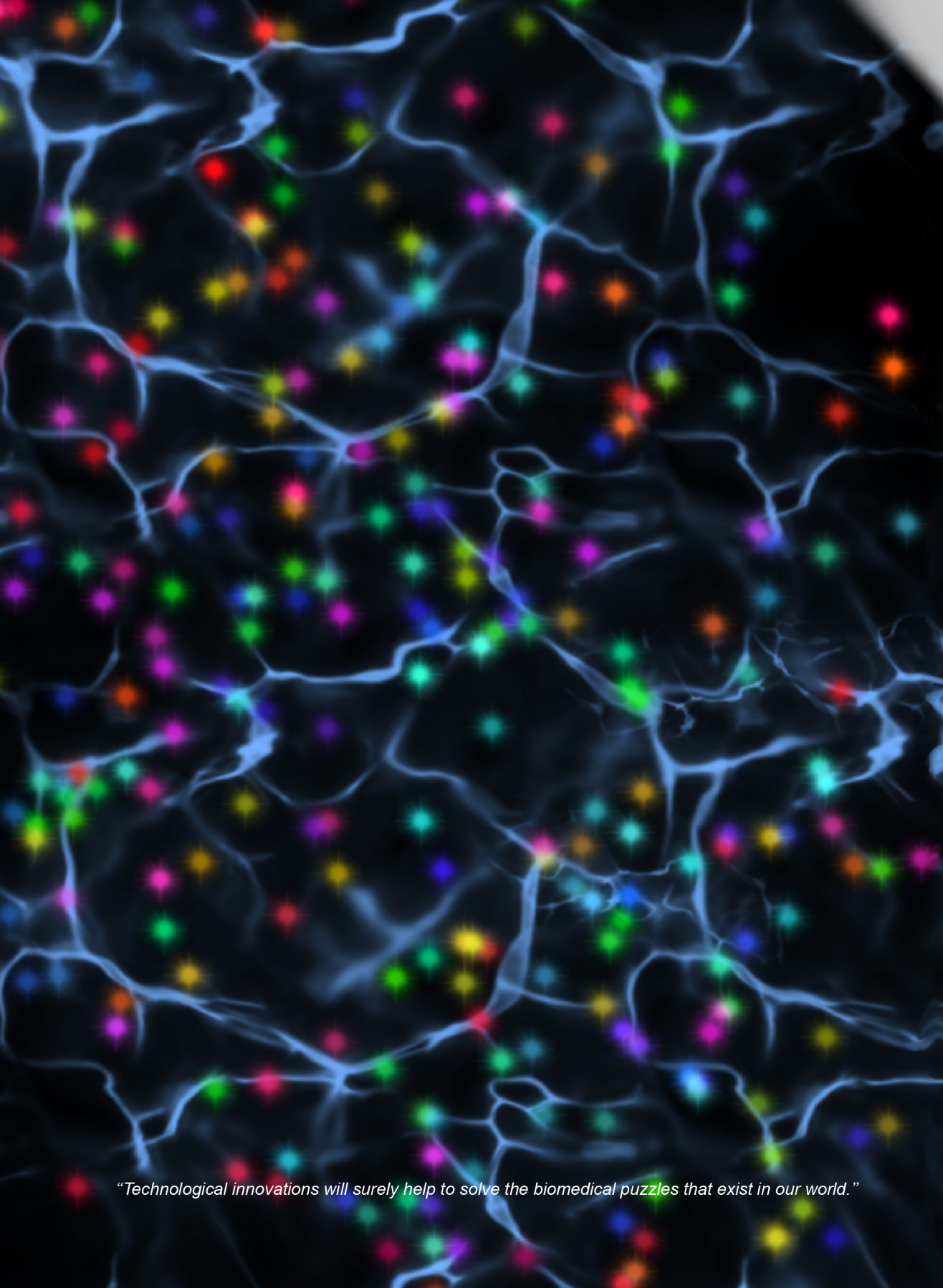

“Technological innovations will surely help to solve the biomedical puzzles that exist in our world.”